

# **EEG Analysis to Decode Perceptual Ability of Human Subjects**

*Thesis submitted by*

**Anuradha Saha**

*Doctor of Philosophy (Engineering)*

*Artificial Intelligence Laboratory  
Department of Electronics and Tele-Communication Engineering  
Faculty Council of Engineering and Technology  
Jadavpur University  
Kolkata-700032, India*

2017

**JADAVPUR UNIVERSITY  
KOLKATA-700032, INDIA**

**INDEX NO.: 259/14/E**

**1. Title of the thesis: EEG Analysis to Decode Perceptual Ability of Human Subjects**

**2. Supervisor Name: Dr. Amit Konar, FNAE**

Designation: **Professor, Dept. of Electronics & Telecommunication Engineering**

Institution: **Jadavpur University, Kolkata**

**3. List of Publications:**

***I. Journal Publications***

- [1] **Anuradha Saha**, Amit Konar, Amita Chatterjee, Anca L. Ralescu and Atulya K. Nagar, "EEG Analysis for Olfactory Perceptual-ability Measurement Using a Recurrent Neural Classifier," *In IEEE Transactions on Human-Machine Systems*, vol. 44, no. 6, pp. 717-730, December, 2014.
- [2] **Anuradha Saha**, Amit Konar and Atulya Nagar, "EEG-Induced Cognitive Failure Detection in Driving Using Type-2 Fuzzy Classifiers," *In IEEE Transactions on Emerging Topics in Computational Intelligence*, accepted, 2018 (*to appear*).

***II. Book Chapters***

- [1] **Anuradha Saha** and Amit Konar, "A Cyber-Physical System Approach to Cognitive Failure Detection in Driving Using EEG and EMG Artifacts," *Cyber Physical Systems – A Computational Perspective*, CRC Press, Taylor & Francis Group, LLC, Florida, USA, 2016.
- [2] **Anuradha Saha** and Amit Konar, "EEG-Analysis to Decode Tactile Sensory Perception Using Neural Techniques," *Handbook of Research on Applied Computational Intelligence in Engineering*, IGI Global, Hershey PA, USA, 2017.

***III. Conference Publications***

- [1] Mainak Dan, **Anuradha Saha**, Amit Konar, Anca L. Ralescu and Atulya K. Nagar, "A Type-2 Fuzzy Approach Towards Cognitive Load Detection Using fNIRS Signals," *in the Proceedings of IEEE International Conference on Fuzzy Systems (FUZZ-IEEE 2016)*, Vancouver, Canada, July 24-29, 2016.
- [2] Snehalika Lal, **Anuradha Saha**, Amit Konar, Mousumi Laha, Anca L. Ralescu, Kalyan Kumar Mallik and Atulya K. Nagar, "EEG-based Mind Driven Type Writer by Fuzzy Radial Basis Function Neural Classifier" *in the Proceedings of IEEE International Joint Conference on Neural Networks (IJCNN)*, Vancouver, Canada, July 24-29, 2016.
- [3] Sriparna Saha, Amit Konar, **Anuradha Saha**, Arup Kumar Sadhu, Bonny Banerjee and Atulya K. Nagar, "EEG Based Gesture Mimicking by An Artificial Limb Using Cascade-

- Correlation Learning Architecture,” in the *Proceedings of IEEE International Joint Conference on Neural Networks (IJCNN)*, Vancouver, Canada, pp. 4680-4687, July 24-29, 2016.
- [4] **Anuradha Saha**, Amit Konar, Pratyusha Das, Basabdatta Sen Bhattacharya and Atulya K. Nagar, “Data-point and Feature Selection of Motor Imagery EEG Signals for Neural Classification of Cognitive Tasks in Car- Driving,” in the *Proceedings of IEEE International Joint Conference on Neural Networks (IJCNN)*, Killarney, Ireland, July 12-17, 2015.
- [5] **Anuradha Saha**, Amit Konar, Basabdatta Sen Bhattacharya and Atulya K. Nagar, “EEG Classification to Determine the Degree of Pleasure Levels in Touch Perception of Human Subjects,” in the *Proceedings of IEEE International Joint Conference on Neural Networks (IJCNN)*, Killarney, Ireland, July 12-17, 2015.
- [6] **Anuradha Saha**, Amit Konar, Mainak Dan and Sudipta Ghosh, “Decoding of Motor Imagery Potentials in Driving Using DE-Induced Fuzzy-Neural Classifier,” in the *Proceedings of IEEE (RETIS)*, Kolkata, India, pp. 416 – 421, July 9-11, 2015.
- [7] Amit Konar, **Anuradha Saha**, Reshma Kar, Aruna Chakraborty, “Brain-computer interfacing for bio-perceptive and rehabilitative applications,” in the *Proceedings of IEEE Third International Conference on Computer, Communication, Control and Information Technology (C3IT)*, pp.1-8, Hoogly, India, February 7-8, 2015.
- [8] **Anuradha Saha**, Amit Konar, Ritambhar Burman and Atulya K. Nagar, “EEG Analysis for Cognitive Failure Detection in Driving Using Neuro-Evolutionary Synergism,” in the *Proceedings of IEEE International Joint Conference on Neural Networks (IJCNN)*, pp. 2108-2115, Beijing, China, July 7-11, 2014.
- [9] **Anuradha Saha**, Sayan Basu Roy, Amit Konar and Ramadoss Jonarthanan, “An EEG-based Cognitive Failure Detection in Driving Using Two-stage Motor Intension Classifier”, in the *Proceedings of IEEE International Conference on Control, Instrumentation, Energy & Communication (CIEC)*, pp. 277-281, Kolkata, India, January 31-February 2, 2014.
- [10] **Anuradha Saha**, Amit Konar, Pratyusha Rakshit, Anca L. Ralescu and Atulya K. Nagar, “Olfaction recognition by EEG analysis using differential evolution induced Hopfield neural net”, in the *Proceedings of IEEE International Joint Conference on Neural Networks (IJCNN)*, pp. 1-8, Dallas, August 4-9, 2013.
- [11] Shreyasi Datta, **Anuradha Saha** and Amit Konar, “Perceptual Basis of Texture Classification from Tactile Stimulus by EEG Analysis”, *National Conference on Brain and Consciousness (NCBC)*, Kolkata, September 21, 2013.
- [12] Reshma Kar, Aruna Chakraborty, **Anuradha Saha** and Amit Konar, “Detection of True Emotion or Pretention: A Brain-Computer Interface Approach”, *National Conference on Brain and Consciousness (NCBC)*, Kolkata, September 21, 2013.

#### 4. List of Patents: NIL

## **5. List of Presentations in International Conferences**

- [1] In the “International Conference on Recent Trends in Information System (RETIS),” IEEE, 2015, held in Kolkata, India on 10<sup>th</sup> July, 2015.
- [2] In the “International Conference on Control, Instrumentation, Energy & Communication (CIEC),” IEEE, 2014, held in Kolkata, India on 31<sup>st</sup> January, 2014.

## CERTIFICATE FROM THE SUPERVISOR

*This is to certify that the thesis entitled “**EEG Analysis to Decode Perceptual Ability of Human Subjects**” submitted by **Smt. Anuradha Saha**, who got her name registered on **03/01/2014** for the award of **Ph.D. (Engineering)** degree of Jadavpur University is absolutely based upon her own work under the supervision of **Prof. Amit Konar** and that neither her thesis nor any part of it has been submitted for any Degree/Diploma or any other academic award anywhere before.*

.....  
Signature of the Supervisor  
and date with Official seal

**THE THESIS IS DEDICATED TO**  
*My parents*

## Preface

The word “Perception” is synonymous with the act of perceiving. However, perception has a wider meaning in cognitive neuroscience. It refers to the biological process of acquiring information from the external world using our sense organs and also understanding the message carried therein. Perception, in general, is a vast and unexplored research arena, and there exists ample scope of research opportunity for its underlying importance.

The current research on perception revolves around the structural and functional aspects of different brain modules and their interconnections. Apparently, a perceptual process, such as olfaction, is localized as it involves only the pre-frontal and temporal lobes of the brain. The localized activity involved in a perceptual process offers primitive interpretation carried by the percept. For instance, the pre-frontal lobe processes the olfactory stimuli to recognize the stimuli. However, if the aroma perceived is associated with one or more additional events, such as association of a person with a perfume, the brain employs multiple lobes to understand the true meaning (here, the presence of the person carrying the aroma) of the stimulus. Thus, perception in a bigger sense includes higher level cognition, triggered with external stimuli.

The thesis aims at understanding the biological basis of perception by analyzing the brain signals acquired from the scalp of the subjects during excitation of the brain with external stimuli. Electroencephalography (EEG) offers the temporal activity of the human brain during stimuli acquisition and understanding. This inspires researchers to understand the biological processes involved in perception from the time-domain, frequency-domain and time-frequency correlated characteristics of the acquired brain signals. Although there are several brain-signaling and imaging techniques to uncover the mystery behind the underlying perceptual processes, EEG is preferred to its competitors for its spontaneous (having good temporal resolution) response, portability and non-invasive characteristics. This justifies our choice of EEG for the present research.

Although there is an immense scope of research on understanding the biological basis of perception using EEG signal analysis, we have restricted our research into three main heads. The restriction is apparent due to limited time duration of the Ph.D. research and non-availability of the suitable subjects in a non-hospital environment. The first problem is concerned with subjective perceptual-ability detection and ranking when stimulated with aromatic substance. The problem has importance in diverse domains of applications,

including selection of tea-tasters from a list of candidates, testing perceptual-ability of the early Alzheimer's patients and determining the degree of Alzheimer from the estimation of their perceptual-ability etc. The second problem deals with a very interesting subject concerning cognitive-failure detection in driving. The importance of the second problem is apparent for its application in safety-critical driving. The third problem is targeted to detect the tactile perceptual-ability of psychologically retarded people and/or patients suffering from Schizophrenia and other brain-related diseases.

The thesis includes five chapters. Chapter 1 provides a thorough review of the EEG-based research undertaken on perception. It begins with a definition of perception and perceptual-ability and also explores different brain signalling/imaging techniques including EEG, Positron Emission Tomography (PET), functional Magnetic Resonance Imaging (fMRI) and functional Near-Infrared Spectroscopy (fNIRs). The later part of the chapter covers well-known brain signals and their association with different cognitive processes. Special emphasis is given to single and multi-modal BCI problems. The Later part of the chapter deals with standard techniques of problem-solving, such as pre-processing and artifact removal, feature extraction, feature selection and classification. Next, the chapter provides a discussion on the current research directions associated with the problems undertaken in the thesis. The scope of the thesis is also appended at the end of the chapter.

Chapter 2, 3 and 4 are original contributions of the thesis. Here, the candidate provides three distinct problems in perception engineering and offers solutions to these problems by extending the traditional techniques of pattern recognition. Although the problems have their own diversity, the commonality of the problems lies in utilizing and extending computational intelligence techniques adopted for pattern recognition. The other common aspect of the problems undertaken and the approaches adopted include that the analysis of all the problems are performed in real time. Naturally, time required for execution of the algorithms here play a vital role for their amenability in real world systems.

Chapter 2 addresses one interesting problem on olfactory perceptual-ability detection of human subjects, where the motivation is to detect the individual perceptual-ability of the subject and rank them in descending order. These subjective ranks offer the user the relative merits in decoding aromatic substance. Traditional supervised learning techniques, such as support vector machines (SVMs), back-propagation learning etc. could have been used to solve the problem. However, the existing techniques are appropriate for small class size and thus unsuitable for the present application, requiring large (equals to 10) class-size, and that too in real time. To alleviate the present problem,



we employed a Hopfield-like recurrent neural classifier, the stability of which is ensured at multiple optima of a selected Lyapunov energy surface. In the classification of aromatic stimuli from the pre-frontal EEG response of a subject, we first need to map the EEG-features of the individual olfactory stimulus to one of the local optima in the Lyapunov energy function of the energy-surface. This mapping is done automatically by the selection of the weight matrix of the Hopfield-like dynamics with an aim to minimize the selected Lyapunov energy function for the dynamics. In the present context, we develop an alternative formulation, where a multi-modal high dimensional Rastrigin function is used as the Lyapunov energy surface. Thus for the selected energy surface, we construct a Hopfield-like dynamics, which essentially ensures mapping of the olfactory stimuli to the local optima.

Once the weight matrix of the Hopfield dynamics is ready, we can use it as a classifier. This is done in a tricky way. Suppose we measure the feature vector of an unknown olfactory stimulus. The feature vector is mapped onto the Lyapunov energy surface. We initialize the Hopfield-like dynamics at the mapped location of the energy surface, and solve the differential equation until it converges at one of the nearest optima. Since each optimum is earmarked with one smell class, we declare the smell class associated with the optimum as the target class. Experiments undertaken confirm that the proposed technique of classifying olfactory perceptual-ability of subjects outperforms traditional techniques by a good margin.

Existing literature in driving primarily focuses attention to physiological aspects of the drivers and the failures related to gestural/postural aspects in driving. However, online detection of cognitive failures from the brain signals is yet a virgin arena of research in traffic engineering. The thesis introduced an interesting approach to design a set-up for on-line cognitive failure detection of the drivers from three fundamental aspects. These are i) visual alertness failure detection, ii) motor planning failure detection and iii) motor-execution failure detection.

In Chapter 3, the candidate proposes a novel scheme of cognitive failure detection in driving using brain signals. Although there exist different types of cognitive inability responsible for driving failures, we here adopt three possible cognitive failures, called visual attention failures (VAF), motor planning failures (MPF) and motor execution failures (MEF). VAF refers to cognitive failures due to lack of visual perception. Primarily, in driving context, visual attention failure takes place when the driver is not visually attentive. In case the driver is visually attentive, we test any possible failure in motor planning by the subject. The failures involved in motor planning include possible

mistakes in executing braking, acceleration and/or steering control. Occasionally it is noticed that the driver planned his motor activities correctly and timely but failed in executing the planned task. This is generally due to muscle fatigue and/or poor health condition and/or stray situations on part of the driver. The third test adopted is detection of cognitive failures in motor execution.

Testing of cognitive failures has been accomplished by acquiring the EEG signals from three distinct brain lobes. To detect VAF, we acquire EEG signal from the pre-frontal, frontal and occipital lobes. MPF detection requires examining brain signals from the parietal lobe and motor cortex, while MEF is detected from the EEG acquired from the motor cortex region only. These electrical signals are pre-processed using Independent Component Analysis (ICA) to eliminate artifacts, and then passed through band-pass filters of specific frequency bands for individual cognitive tasks. For instance, the EEG acquired for VAF detection is filtered in the alpha band (8-13 Hz), while the EEG signal acquired in motor planning and execution is filtered in the mu-beta bands (8-30 Hz). Next the filtered signals are processed to extract certain signal features. For the VAF detection problem, we extract adaptive autoregressive (AAR) parameters and for MPF and MEF detection we extract power spectral density (PSD) and discrete wavelet transform (DWT). The feature dimension, usually being moderately high (of dimension = 78) for MPF and MEF, we reduce it by a novel evolutionary feature selection algorithm. The algorithm autonomously generates a set of fixed dimensional features from the total list of features, and examines the best set of features for which the intra-class distance is minimized and inter-class distance is maximized. This is done by measuring fitness of the individual trial solutions, where the fitness measure indicates the degree of maximization of inter-class distance and minimization of intra-class distance jointly. The evolutionary process generates expectedly improved trial solutions over the program iterations, and thus when the terminating condition is reached, the best-fit candidate solution represents the highest degree of satisfaction of both the said criteria.

The main research component of the work lies in designing a suitable classifier, capable of classifying VAF into two classes: visually attentive or non-attentive, MPF into four classes: braking failure, acceleration failure, steering control failure and no failure, and MEF into three classes: braking, acceleration and steering control execution failures. Each of the above three classes is again classified into two sub-classes: brake pressed or not pressed and the like. The classifiers are supplied with extracted features for the respective cognitive failure, and the classifier response is the detected class. Apparently, any traditional supervised learning classifiers could serve the purpose. However, because

of parallel brain activations and stochastic noise associated with eye blinking and other muscle movements, the features are often found noisy. The creeping of noise in the features makes the traditional classifiers unsuitable for the MPF detection. For the VAF and MEF, however, support vector machine (SVM) classifier has acceptable performance.

The fundamental problem in the present research thus is to design a classifier worthwhile for classification of motor planning classes in presence of stochastic noise in the EEG features. Fuzzy sets, in general, and type-2 fuzzy sets in particular, have inherent characteristics to take precise decisions in presence of noisy measurements. While classical (type-1) fuzzy sets can capture the noise due to the randomness of the measurement, type-2 fuzzy sets can capture intra- and inter-personal level uncertainty that might appear in a decision-making system because of the randomness in the assignment of memberships within and across experimental subjects respectively. Here, we propose two distinct models of type-2 fuzzy classification, one realized with interval type-2 fuzzy sets (IT2FS) and the other with general type-2 fuzzy sets (GT2FS). The IT2FS-induced classifier determines the average degree of membership of a data point (by taking the average of the upper and lower membership functions at the given measurement point) in a given class, and declares the class with the highest membership as the class for the given data point. The GT2FS-induced classification employs secondary grades as additional input to tune the primary membership function in each class to determine the degree of membership of a data point in a given class. The class with the highest secondary grade induced primary membership for a given data point is declared as the winning class. A thorough comparison of the IT2FS- and GT2FS-induced classifiers is provided in the chapter to examine the relative merits of GT2FS-based classifier over its counterpart.

The fourth chapter is concerned with touch perception, where the motivation is to classify the touch nourishment received by psychological patients from different nurses in a hospital environment. The objective is to select the right nurse by individual patient for their highest degree of pleasure during the phase of mental treatment. Touch perception is primarily active in the somato-sensory cortex. The nearest electrodes available are frontal and parietal electrodes and the motor cortex region. EEG signals acquired from the above electrodes of the patients are first pre-processed and filtered from artifacts. The processed signals are then fed to a classifier to recognize the pleasure levels received by the patients.

The classifier design is given primary consideration in the present work. We adopted radial basis function (RBF) induced back-propagation neural networks to classify the pleasure level of the patients. The RBF-neural network selects specific touch nourishments, such as soft touch, rubbing, messaging and embracing. Next, for a given touch nourishment we select a back-propagation neural network to classify the individual touch nourishment into three classes: pleasant, acceptable and unpleasant. Experiment undertaken reveals that the proposed neural architecture outperforms its competitors with respect to classification accuracy. To test statistical validation of the proposed classifier performance, McNemar's test is employed. The proposed scheme has successfully been realized to select appropriate nurses by Schizophrenic patients based on the degree of qualitative touch perceived by them across nurses.

The thesis ends with a concluding chapter dealing with the self-review of the works undertaken in chapters 2, 3 and 4 and also possible future research directions.

Artificial Intelligence Laboratory

Department of Electronics and Tele-Communication Engineering,

Jadavpur University.

Anuradha Saha

# Acknowledgement

I owe sincere and earnest thankfulness to my supervisor Prof. Amit Konar for his relentless inspiration to strive for the best of knowledge and to excel in research. His presence was the enormous value-add in the field of Perception Engineering using Brain-Computer Interfacing. It has always been a privilege to me to have his guidance throughout all the time of research and writing of this dissertation. I am also thankful to him for morally supporting me during my time of crisis period.

I also reckon it as a great boon to be backed with support from the present Head of the Department, Prof. P. Venkateshwaran, and past Head of the Department, Prof. Iti Saha Mishra. It was also a pleasure to express my gratitude to Prof. Suranjan Das, the Vice-Chancellor, for his valuable inputs. I would also like to thank University Grants Commission (UGC), India, University with Potential for Excellence Program (Phase II) in Cognitive Science, Jadavpur University for the financial support.

The realization of this practical work would not have been possible without the whole-hearted co-operation from fellow researchers and students in our lab for making my stay enjoyable and memorable. I am grateful to put on record the contribution of Dr. Pratyusha Rakshit, Dr. Sanchita Ghosh, Dr. Anisha Halder, Dr. Sumantra Chakraborty, Dr. Diptendu Bhattacharya, Dr. Saugat Bhattacharyya, Dr. Anwesha Khasnobish, Ms. Reshma Kar, Mr. Arup K. Sadhu, Ms. Archana Chowdhury, Ms. Sriparna Saha, Mr. R. Janarthanan, Mr. Abhishek Ghosh Roy, Ms. Pratyusha Das, Ms. Rimita Lahiri, Mr. Mainak Dan, Ms. Lidia Ghosh, Ms. Moushumi Laha, Mr. Arnab Rakshit, Ms. Tanuka Bhattacharjee, Ms. Anwesha Banerjee and Ms. Snehalika Lal in this regard.

I extend my gratitude to Ex-Prof. D. R. Poddar, Dr. Shibani Das and Dr. Sudipta Nath of Jadavpur University for motivating me to pursue my Ph.D. I am also thankful to Prof. T. K. Maiti, Prof. A. K. Ghosh, and Dr. Hirikesh Mondal of Netaji Subhash Engineering College for inspiring me to complete my thesis. Heartfelt thanks to my colleagues Ms. Priyadarshiny Dhar, Ms. Swatilekha Das, Ms. Manideepa Pal, Mr. Sumitesh Majumder, Mr. Aritra Dasgupta and Mr. Animesh Bhattacharya for all their encouragement during the course of my research work. I should not forget to mention the name of my childhood friends Moumita Duttgupta, Purbita Sen Chowdhuri, Pamela Bhattacharya and Paramita Chakraborty, whose unfathomable love and affection keeps me motivated to complete my thesis.

The thesis could hardly be completed without constant support of my mother, Smt. Anita Saha, whose encouragement and love made me progress in my journey to complete the thesis both qualitatively and timely. I would especially like to dedicate this thesis to my father, Late Bijan Behari Saha, who could not live long to see the journey of my Ph.D., but always remained my source of inspiration amidst hardship and distresses. I must also mention the encouragement and active cooperation from my mother-in-law, Mrs. Shanta Karmakar and my father-in-law, Mr. Bimal Karmakar in making me free to pursue this work. I also remember the happy faces of my beloved nephews Anubhav and Bishwatanu, whose love helped me continuing my research in difficult period of my research. In addition, the unplumbed love, affection and

support from my very dear friend and husband, Anirban Karmakar always kept me happy instead of having diverse complexity of our lives.

Finally, I thank all my reviewers for their suggestions to improve the quality of my paper, my well-wishers who have contributed directly and indirectly towards the completion of this work and the almighty GOD for everything.

Artificial Intelligence Laboratory

Department of Electronics and Tele-Communication Engineering,  
Jadavpur University.

Anuradha Saha

# TABLE OF CONTENTS

Preface, **vii**

Acknowledgment, **xiii**

List of Figures, **xviii**

List of Tables, **xx**

## **Chapter 1: An Introduction to EEG Analysis in Decoding Human Perception**

- 1.1 Defining Perception, **2**
- 1.2 Brain Map and Brain-Imaging Techniques, **3**
  - 1.2.1 Brain-Imaging Techniques, **4**
  - 1.2.2 EEG Electrodes, **7**
- 1.3 Brain Signals, **8**
  - 1.3.1 P300 Event-Related Potential, **9**
  - 1.3.2 Event-Related De-synchronization/Synchronization (ERD/ERS), **10**
  - 1.3.3 Other Signals, **12**
- 1.4 Real World Problem Solving Using EEG Signals, **15**
  - 1.4.1 Problem Solving with Single EEG Signal, **15**
    - A. *P300/SSVEP signal-Based BCI Speller*, **15**
    - B. *SCP or ERD/ERS (Sensorimotor) signal-based Cursor Control*, **17**
  - 1.4.2 Problem Solving with Mixed EEG Signals, **18**
    - A. *Multi-modal BCI Speller*, **18**
    - B. *Multi-modal Cursor Control*, **20**
    - C. *Multi-modal Wheelchair/Vehicle Destination Control*, **22**
    - D. *Multi-modal Artificial Limb Control*, **25**
- 1.5 Components of a Brain-Computer Interfacing System, **27**
  - 1.5.1 EEG Signal Preprocessing, **28**
  - 1.5.2 EEG Feature Extraction Techniques, **29**
    - A. *Discrete Wavelet Transform*, **30**
    - B. *Power Spectral Density*, **31**
    - C. *Adaptive Autoregressive Parameters*, **31**
    - D. *Hjorth Parameters*, **32**
    - E. *Common Spatial Pattern*, **32**
  - 1.5.3 EEG Feature and Data-point Selection, **33**
  - 1.5.4 EEG Classification, **34**
    - A. *Fisher's Linear Discriminant Analysis (FLDA)*, **36**
    - B. *Quadratic Discriminant Analysis (QDA)*, **37**
    - C. *Support Vector Machine (SVM)*, **38**
    - D. *k-Nearest Neighbor (k-NN)*, **39**
    - E. *Multi-Layer Perceptron (MLP)*, **40**
    - F. *Hidden Markov Model (HMM)*, **41**
    - G. *Naïve Bayes Classifier*, **41**
- 1.6 Performance Analysis in EEG-BCI Research, **42**

1.7 Current Research Directions in Sensory Perception, Motor Imagery and Alertness,	<b>43</b>
1.7.1 Decoding of Sensory Perception,	<b>43</b>
1.7.2 Decoding of Motor Imagery,	<b>46</b>
1.7.3 Decoding of Alertness,	<b>48</b>
1.8 Scope of the Thesis,	<b>49</b>
1.9 Summary,	<b>53</b>
References,	<b>53</b>

## **Chapter 2: Olfactory Perceptual Ability Measurement Using a Recurrent Neural Classifier**

2.1 Introduction,	<b>73</b>
2.2 Lyapunov Stability Analysis,	<b>75</b>
2.3 System Overview and Design,	<b>76</b>
2.3.1 Feature Extraction,	<b>77</b>
2.3.2 Feature Selection,	<b>78</b>
2.3.3 Data Reduction Using PCA,	<b>80</b>
2.3.4 Classification,	<b>80</b>
2.4 Perceptual-Ability Measure,	<b>83</b>
2.5 Physiological Signal Processing and Classification Experiments,	<b>84</b>
2.5.1 Experimental Framework,	<b>85</b>
2.5.2 Experiment 1(Selection of Active Brain Regions),	<b>85</b>
2.5.3 Experiment 2(Frequency Band and Type Selection of Filters in Preprocessing),	<b>86</b>
2.5.4 Experiment 3(Selection of EEG Features),	<b>87</b>
2.5.5 Experiment 4(Noisy Stimulus Discrimination),	<b>90</b>
2.6 Classifier Validation and Performance,	<b>90</b>
2.6.1 Individual Class Performance during Training,	<b>91</b>
2.6.2 Overall Performance during Testing Phase,	<b>91</b>
2.6.3 Performance Analysis with/without Data-Point Reduction,	<b>92</b>
2.6.4 Relative Performance Analysis,	<b>93</b>
2.7 Application in Simulated Tea-Taster Selection,	<b>94</b>
2.8 Conclusion,	<b>96</b>
Appendix,	<b>97</b>
References,	<b>100</b>

## **Chapter 3: Cognitive Failure Detection in Driving Using Type-2 Fuzzy Classifiers**

3.1 Introduction,	<b>106</b>
3.2 System Design and Integration,	<b>109</b>
3.3 Feature Selection,	<b>112</b>
3.4 Classifier Selection and Design,	<b>113</b>
3.4.1 Preliminaries on Interval-Valued, IT2FS and GT2FS,	<b>114</b>
3.4.2 IT2FS-Based Classifier Design,	<b>116</b>
3.4.3 GT2FS-Based Classifier Design,	<b>118</b>
A. <i>Secondary Membership Evaluation,</i>	<b>119</b>
B. <i>GT2FS-Based Classification,</i>	<b>120</b>



3.4.4 Complexity Analysis,	121
3.4.5 The KSVM Classifiers,	122
3.5 Psycho-Physiological Experiments,	123
3.5.1 Experimental Set-up,	123
3.5.2 Participants,	124
3.5.3 The Training Session,	124
A. Stimuli Preparation,	125
B. EEG Electrodes and Signal Acquisition,	126
C. Pre-processing and Filtering,	127
D. EEG Feature Selection,	129
3.5.4 The Test Session,	132
3.6 Performance Analysis,	133
3.6.1 Performance Analysis of VAFD Classifier,	133
3.6.2 Performance Analysis of Type-2 MPFD Classifiers,	135
3.6.3 Performance Analysis of MEFD Classifier,	137
3.6.4 Lead-time Estimation,	138
3.6.5 Objective Performance of the Proposed CFD System,	140
3.7 Classifier Validation Using Statistical Test,	141
3.8 Conclusions,	143
Appendix,	144
References,	145

## **Chapter 4: Tactile Perception of Human Subjects Using Radial Basis Function-Induced Back-Propagation Neural Net Classifier**

4.1 Introduction,	151
4.2 System Overview and Touch Classification,	152
4.2.1 Feature Extraction,	153
4.2.2 Data-Point Reduction and Feature Selection Using PCA,	153
4.2.3 Classification,	153
4.3 Degree of Perceived Pleasure,	155
4.4 Experiments and Results,	155
4.4.1 Experiment 1: Acquisition of EEG Signals within Bands of Interest,	156
4.4.2 Experiment 2: Selection of EEG Features,	158
4.4.3 Experiment 3: Validation of Subject-Defined Class Labels,	160
4.4.4 Experiment 4: Ranking of Nurses Based on EEG Feature Performance,	161
4.4.5 Experiment 5: Classifier Performance and Validation,	161
4.5 Conclusions,	162
References,	163

## **Chapter 5: Conclusions and Future Directions**

5.1 Self-Review of the Thesis,	168
5.2 Future Research Directions,	170
References,	171

## LIST OF FIGURES

<b>Fig. No.</b>	<b>Description</b>	<b>Page No.</b>
<b>1.1</b>	Different brain lobes and their association with their cognitive abilities	<b>4</b>
<b>Fig. 1.2</b>	EEG devices used for the experiments performed for decoding cognitive tasks from brain signals	<b>7</b>
<b>1.2 (a)</b>	24-channel EEG data acquisition system	<b>7</b>
<b>1.2 (b)</b>	14-channel wireless EEG headset	<b>7</b>
<b>1.3</b>	10-20 electrode placement system for 21-channel EEG device	<b>9</b>
<b>1.4</b>	The origin and nature of P300 signal	<b>10</b>
<b>1.5</b>	The origin and nature of ERD/ERS signal	<b>11</b>
<b>1.6</b>	Hybrid BCI speller using P300 and SSVEP signals jointly	<b>20</b>
<b>1.7</b>	Artificial limb control using ERD/ERS and SSVEP signals jointly	<b>26</b>
<b>1.8</b>	Components of a brain-computer interfacing system	<b>27</b>
<b>1.9</b>	Generation of approximation and detail coefficients by Discrete Wavelet Transform	<b>30</b>
<b>1.10</b>	Linear two-class classification scheme	<b>35</b>
<b>1.11</b>	Linear multi-class classification scheme	<b>36</b>
<b>1.12</b>	Non-linear multi-class classification scheme	<b>36</b>
<b>1.13</b>	Design of hyper-plane for Quadratic discriminant analysis classifier	<b>38</b>
<b>1.14 (a)</b>	Design of hyper-plane for Support vector machine classifier	<b>38</b>
<b>1.14 (b)</b>	Estimation of weight vector <b>W</b>	
<b>1.15</b>	Mapping of linearly non-separable data-points using Kernel function	<b>39</b>
<b>1.16</b>	$k$ -NN classification of feature vectors in three classes	<b>40</b>
<b>2.1</b>	A schematic architecture of smell-stimuli classification	<b>77</b>
<b>2.2</b>	An example trial vector	<b>79</b>
<b>2.3</b>	The plot of a two-dimensional Rastrigin function with dimension=2	<b>81</b>
<b>2.4</b>	An experimental trial, having a subject experiencing an unknown smell stimulus for olfactory recognition	<b>85</b>
<b>2.5</b>	Component epoch maps of 14-channel Emotiv headset	<b>86</b>
<b>2.6</b>	Frequency spectra of four stimuli: the theta (3-7Hz) and alpha (8-13Hz) bands are proven as the desired band of interest	<b>87</b>
<b>2.7</b>	Frequency response of a Butterworth, Chebyshev-I, Chebyshev-II and Elliptic band pass filter with a pass band and stop band attenuation	<b>88</b>
<b>2.8</b>	Approximate wavelet coefficient $A_3$ extracted from AF3 electrode to discriminate four selected stimuli	<b>89</b>
<b>2.9</b>	Power spectral density extracted from AF3 electrode to discriminate four selected stimuli	<b>89</b>
<b>2.10</b>	Power spectral density extracted from AF3 electrode to discriminate five Indian spices	<b>89</b>
<b>2.11</b>	Approximate wavelet coefficient $A_3$ extracted from AF3 electrode to discriminate five Indian spices	<b>90</b>
<b>2.12</b>	Average percentage shift in optimum versus percentage of noise amplitude injected	<b>91</b>
<b>2.13</b>	Feature level discrimination of best two selected features for both noisy (contaminated) and noise free (ideal) tea-samples	<b>97</b>
<b>3.1</b>	Proposed psychological model of cognitive failure detection in driving to appropriately alert the driver with different audio alarms	<b>109</b>
<b>3.2</b>	Basic classifier architecture for CFD	<b>111</b>
<b>3.3</b>	Complete architecture of IT2FS induced planning failure detection in driving	<b>112</b>

<b>Fig. No.</b>	<b>Description</b>	<b>Page No.</b>
<b>3.4</b>	Construction of IT2FS <sub>1</sub> for feature $f_j$ from 10 Gaussians for 10 subjects in braking	<b>116</b>
<b>3.5</b>	Architecture of the an IT2FS neuron $r$	<b>117</b>
<b>3.6(a)</b>	The structure of a neuron	<b>117</b>
<b>3.6(b)</b>	Architecture of the proposed IT2FS- induced classifier to classify motor-planning classes	<b>117</b>
<b>3.7</b>	Architecture of the proposed GT2FS-induced neuron	<b>120</b>
<b>3.8</b>	Experimental set-up for acquisition of EEG and EMG signals from a subject driving a virtual driving simulator	<b>123</b>
<b>3.9</b>	The tree representing 43 EEG data-samples for 43 stimuli per subject per training session	<b>124</b>
<b>3.10</b>	Structure of the stimulus used and timings	<b>124</b>
<b>3.11</b>	10-20 electrode placement system for 21-channel EEG device	<b>127</b>
<b>3.12</b>	Frequency response of Filters: Butterworth, Chebyshev-I, Chebyshev-II and Elliptic filters of order 4	<b>128</b>
<b>3.13</b>	Pass band (7-13 Hz) selection of the elliptic filter for occipital EEG for four stimuli	<b>128</b>
<b>3.14</b>	Pass band (13-30 Hz) selection of the elliptic filter during execution of four motor actions for four stimuli	<b>129</b>
<b>3.15</b>	ICA scalp components from 19 EEG electrodes. Here, red color denotes the highest activation, whereas, blue color represents the lowest activation	<b>129</b>
<b>3.16</b>	AAR parameter discrimination from occipital EEG of a subject during four different types of stimuli	<b>130</b>
<b>3.17</b>	PSD feature discriminations from motor imagery response of a subject during ACC, BR, STR control and NOP planning	<b>130</b>
<b>3.18</b>	DWT feature discriminations from motor imagery response of a subject during ACC, BR, STR control and NOP planning	<b>130</b>
<b>3.19</b>	Audio alarm generation and lead-time for a braking instance	<b>139</b>
<b>3.20</b>	Audio alarm generation and lead-time for an acceleration instance	<b>140</b>
<b>3.21</b>	Audio alarm generation and lead-time for a steering control instance	<b>140</b>
<b>4.1</b>	An overview of touch perception by EEG analysis	<b>152</b>
<b>4.2</b>	A schematic representation of classification scheme	<b>154</b>
<b>4.3</b>	Change in brain-map patterns of one healthy subject and one patient for one specific touch class (here, soft touch)	<b>156</b>
<b>4.4</b>	Frequency response of a Butterworth, Chebyshev-I, Chebyshev-II and Elliptic band pass filter with a pass band and stop band attenuation	<b>157</b>
<b>4.5</b>	Raw EEG signals for two touch nourishments: soft touch and massage	<b>157</b>
<b>4.6</b>	Filtered EEG response for two touch nourishments: console and massage	<b>158</b>
<b>4.7</b>	PSD features extracted for five distinct touch nourishments: console, massage, rubbing, soft touch and embracing	<b>159</b>
<b>4.8(a)</b>	Approximate wavelet coefficient features extracted for four distinct touch nourishments: massage, rubbing, soft touch and embracing	<b>159</b>
<b>4.8(b)</b>	Detail wavelet coefficient features extracted for four distinct touch nourishments: massage, rubbing, soft touch and embrace	<b>159</b>

## LIST OF TABLES

<b>Table No.</b>	<b>Description</b>	<b>Page No.</b>
<b>1.1</b>	Frequency bands with their associated brain regions and cognitive activities	<b>6</b>
<b>1.2</b>	EEG channels and associated brain regions for different cognitive functionalities	<b>8</b>
<b>1.3</b>	Origin, latency and use of well-known EEG signals	<b>13</b>
<b>1.4</b>	Basis of selection of EEG signals for BCI speller	<b>16</b>
<b>1.5</b>	Basis of selection of EEG signals for cursor control	<b>18</b>
<b>1.6</b>	Average classification accuracy and control time for MI-P300 wheelchair control	<b>24</b>
<b>2.1</b>	Average Training Accuracy of 25 Subjects for 10 Stimuli across Different Genres	<b>91</b>
<b>2.2</b>	Average Training Accuracy of 25 Subjects for 5 Stimuli within A Same Genre	<b>92</b>
<b>2.3</b>	Confusion Matrix of Ten Smell Classes of Different genres Using DE-Recurrent NN classifier Along with PSD and Wavelet Coefficient Features	<b>92</b>
<b>2.4</b>	Confusion Matrix of Five Intra-genre Smell Classes Using DE-Recurrent NN Classifier Along with PSD and Wavelet Coefficient Features	<b>92</b>
<b>2.5</b>	Average Classifier Accuracy Along with True Positive, True Negative, False Positive and False Negative Rates Using PCA	<b>93</b>
<b>2.6</b>	Average Classifier Accuracy Along with True Positive, True Negative, False Positive and False Negative Rates Without Using PCA	<b>93</b>
<b>2.7</b>	Mean Classifier Accuracy and Standard Deviation (within Parenthesis) of Inter-Genre Testing Data Using DE Feature Selection Algorithm along with False Positive Rate ( $\alpha$ ) and False Negative Rate ( $\beta$ )	<b>94</b>
<b>2.8</b>	Statistical Comparison of Classifiers using McNemar's Test	<b>95</b>
<b>2.9</b>	Recognition-Ability of Subjects Based on Classification Accuracy	<b>95</b>
<b>2.10</b>	Ranking of Perceptual-Ability of 10 Subjects	<b>96</b>
<b>3.1</b>	Experimental Procedure for the Training Session	<b>125</b>
<b>3.2</b>	List of Stimuli and Required Motor Intension	<b>126</b>
<b>3.3</b>	Activation of Scalp Maps for Different Cognitive Modalities at Different Frequency Bands	<b>128</b>
<b>3.4</b>	Confusion Matrices of Four Motor-Planning Classes Using PCA and DE-Induced Feature Selection Algorithm	<b>131</b>
<b>3.5</b>	Classification Accuracy of KSVM-RBF Classifier for Varied C and $\sigma$	<b>132</b>
<b>3.6</b>	Classification Accuracy of KSVM-Linear and Polynomial Classifier for Varied C and $d$	<b>132</b>
<b>3.7</b>	Experimental Procedure for the Test Session	<b>133</b>
<b>3.8</b>	Run-Time and Mean Percentage VAFD Classification Accuracies (standard deviation in percentage) by Different Classifiers	<b>134</b>
<b>3.9</b>	Mean Percentage Classification Accuracy of IT2FS-NN (GT2FS-NN) Against Standard Classifiers for Traffic Instances Plus Without (With) Phone Calls	<b>135</b>
<b>3.10</b>	Run-Time of IT2FS-NN and Other Competitive Classifiers	<b>136</b>
<b>3.11</b>	Comparative Studies of Percentage TP, TN, FP and FN Measures (%) of the Proposed Classifiers With Existing IT2FS Classifiers	<b>136</b>

<b>Table No.</b>	<b>Description</b>	<b>Page No.</b>
<b>3.12</b>	Comparative Studies of TP, TN, FP and FN Measures With/Without Phone Calls for IT2FS-NN (GT2FS-NN) Classifier across 10 Subjects	<b>137</b>
<b>3.13</b>	Mean Percentage Accuracies of KSVM-RBF and Other Standard Classifiers EEG-Based MEFD Classification	<b>138</b>
<b>3.14</b>	Mean Percentage Accuracies of KSVM-RBF and Other Standard Classifiers for EMG-Based MEFD Classification	<b>138</b>
<b>3.15</b>	Average Estimate of Lead-Time for Seven Different Stimuli for Driving Speed=64km/hr	<b>139</b>
<b>3.16</b>	Number of Failures Corrected in Presence of the Proposed CFD System	<b>141</b>
<b>3.17</b>	Percentages of TP, Tn, FP, FN rates of the proposed CFD system	<b>141</b>
<b>3.18</b>	Statistical Validation of Classifiers Using McNemar's Test during MPFD Phase	<b>142</b>
<b>3.19</b>	Statistical Validation of Classifiers Using McNemar's Test during VAFD and MEFD Phase	<b>143</b>
<b>4.1</b>	True Positive, True Negative, False Positive and False Negative rates along with average classification accuracy over 2400 trials without using PCA	<b>160</b>
<b>4.2</b>	True Positive, True Negative, False Positive and False Negative rates along with average classification accuracy over 2400 trials using PCA	<b>160</b>
<b>4.3</b>	Touch nourishment classifications by averaging over 5 nurses	<b>161</b>
<b>4.4</b>	Ranking of nurses based on degree of pleasure perceived from pleasant touch nourishment	<b>161</b>
<b>4.5</b>	Mean classifier accuracy and statistical significance of testing data using PCA algorithm along with feature sets	<b>162</b>
<b>4.6</b>	Statistical comparison of classifiers using McNemar's test	<b>163</b>

# Chapter 1

## An Introduction to EEG Analysis in Decoding Human Perception

*This chapter provides a general introduction to EEG signal analysis to understand the biological basis of perception. It also aims at classifying the perceptual stimuli based on the characteristics of the acquired EEG signal. The chapter begins with the definition of perception, and gradually progresses through different modalities of brain signaling/imaging techniques. The next part of the chapter includes major brain signals including P300 event-related potential, event-related desynchronization/synchronization, slow cortical potential, steady-state visual evoked potential, olfactory event-related potential and error-related potential. Special emphasis is given to problem solving schemes for the selection of single and mixed signals. The later part of the chapter gives an overview of EEG signal processing, such as filtering, artifact removal, and low level feature extraction, such as discrete wavelet transforms, power-spectral density, adaptive autoregressive parameters, Hjorth parameters, and common spatial patterns. The chapter provides a discussion on EEG signal classification to decode cognitive activities. The list of classifiers includes Linear Discriminant Analysis (LDA), Support Vector Machine (SVM), Multi-layer Perceptron (MLP), Hidden Markov Model (HMM), k-nearest neighbor (kNN) algorithm and Naïve Bayes' classifier. An outline to well-known performance analysis metrics is also included. The chapter comes to an end with a brief review of current research directions and the scope of EEG signals in sensory-motor perception and decoding of motor imagery and alertness.*

## 1.1 DEFINING PERCEPTION

Perception refers to the process of acquisition and understanding of external stimuli. Humans use their sense organs to acquire information from the external world and utilize their brain to understand the stimuli. Depending on the sensory modality used, perception can be broadly divided into five categories: visual, auditory, tactile and olfactory/taste. Among the above modalities, the olfactory and tactile perceptions are considered as primitive as these are extensively used by animals in their daily lives. Animals normally use olfactory perception for hunting, food-source localization and also mate-selection. Tactile perceptual modality is generally used by animals/humans to have ideas about object shape and size, texture, and elastic/deformable characteristics. Visual and auditory perceptions generally require higher cognitive functionalities and thus are limitedly used by lower class animals. For instance, most of the animals do not have 3D perception of their world like the human being. Further, animals cannot recognize natural languages like the humans.

The phrase “cognition” is sometimes synonymously used with “perception”. However, cognition involves almost all mental processes at different levels of functionality. At the lowest level, cognition includes perception, memory and attention. At higher levels, it deals with reasoning, learning, planning, motor control and sensory-motor coordination. Thus perception is treated as a basic cognitive process and in that sense it appears as a subset of cognition.

Human nervous (and also endocrine) systems play a major role in sensory perception. Sensory stimuli received by our sense organs are transferred to the sensory-motor cortex through a complex process of chemical modulation and demodulation. For example, olfactory stimuli acquired by the nose are passed on to the olfactory epithelium, where the receptor proteins interact with the molecules of the aromatic substance to form a protein-complex. This is referred to as biological modulation. Unique set of protein-complexes is formed for encoding a particular olfactory stimulus while odor is sensed by one (or fewer) of several hundred receptor neurons. Neurons responsible for sensing similar protein-complex are distributed across a specific epithelium cortex [1], from where response of the fired neurons is collected by one of several glomeruli of olfactory bulbs [2]. In this manner, composite signal is synthesized to get transferred to the *piriform cortex*, which is then transferred to the sensory-motor cortex for decoding. Similarly, the visual stimuli acquired by our eyes are processed at different layers inside the eyes and the electrical response to visual stimuli is collected by the optic nerve from the retina for transfer to the visual cortex. Complete understanding of the biology of the perceptual processes still remains a mystery.

The thesis is primarily concerned with olfactory and tactile perception with little indigenous experiments on visual perception, particularly in subjective alertness detection. It

includes interesting experiments to detect visual alertness in driving environments, olfactory perceptual-ability of human subjects in tea-taster selection and tactile perceptual-ability of patients in the selection of nurses based on their quality of touch-nourishments.

## **1.2 BRAIN MAP AND BRAIN-IMAGING TECHNIQUES**

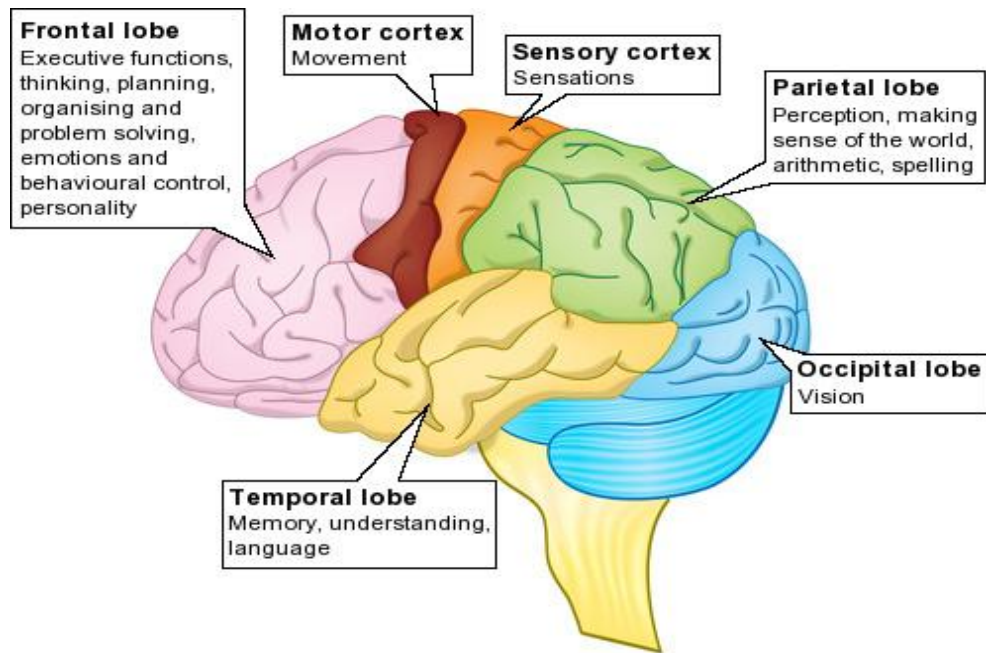
The human brain comprises several 100 billions of nerve cells, called neurons, which individually/in groups are responsible for executing complex mental tasks like interpretation of stimuli, memory encoding and recall, motor planning /execution and coordination of multi-sensory/sensory-motor interactions. Apart from this, the human brain is also involved to control most of our biological activities, including respiration rate, cardiac activity, muscular activity, and many others. The neurons in the brain and also in the rest of our nervous system act partly electrically and partly chemically for stimuli processing, signal transduction and motor activity. A look inside the neuron reveals that the cell-body of the neuron yields a linear combination of the received electrical stimuli for transfer to the pre-synaptic region. The accumulated electrical stimuli next trigger the synapse to synthesize the neurotransmitters for transfer of information from the pre-synaptic region to the post-synaptic region. Thus communication of information inside a neuron is performed by both electrical and chemical means.

The brain is divided into three main modules, called cerebrum, cerebellum and Pons. The cerebrum is the largest part of the human brain with highest functionality. The second part of the brain, called cerebellum is the area of the hindbrain. The third part called pones is the portion of brain stem, which is located above the medulla oblongata and below the midbrain. The cerebrum is covered with a cortical layer having convoluted topography, called the cerebral cortex. It looks like a sheet of neural tissue that includes a large surface area within the skull by folding itself. Cerebral cortex is divided into almost symmetrical right and left hemispheres. Each hemisphere consists of different lobes such as frontal, parietal, temporal and occipital lobes. Besides the four lobes, neocortical areas of the brain including primary motor and sensorimotor cortices play major role during motor-planning/execution and tactile perception respectively. Figure 1.1 shows the different brain lobes and their association with their cognitive abilities, which is briefly described in this section.

1. The frontal lobe is one of the important lobes of cerebral hemisphere. It is located in the frontal part of the brain. Central sulcus separates the frontal lobe from the parietal lobe whereas sylvian sulcus separates the frontal lobe from the temporal lobe. The frontal lobe and its pre-frontal region are responsible for problem solving tasks, physical reaction, abstract thinking, planning, short term memory task and motivation [3]. The anterior



portion of frontal lobe is known as pre-frontal area, which is associated with olfaction recognition [4], [5] and emotion recognition [6], [7].



**Fig. 1.1** Different brain lobes and their association with their cognitive abilities

2. The parietal lobe extends from the central sulcus nearly to the occipital lobe and is situated on the postcentral gyrus, which is responsible for processing all tactile and proprioceptive sensory information from the contralateral side of the body [8]. This lobe is also used for planning/navigation and spatial sense.
3. The temporal lobe, which is the largest brain lobe (containing approximately 17% of the cerebral cortex) [9], is situated below the frontal lobe, and is separated from the frontal lobe by sylvian sulcus [10]. The temporal lobe controls auditory and olfactory information processing, semantic memory, and perception of spoken or written language [10].
4. The occipital lobe is the smallest lobe in the brain. It is situated behind the parietal lobe. The main function of this lobe is visual reception, colour recognition and visuo-spatial processing [11].

### 1.2.1 Brain-Imaging Techniques

Over the last two decades, communications between humans and machines through brain signals have been the most fascinating topic in *brain compute interfacing* (BCI). The large amount of research work in cognitive neuroscience has resulted in serious progress to make direct interfacing with the human brain by means of various sensors. The sensors measure

electrical impulses due to neuronal firing inside the brain and relate to the specific action that reflects users' intent. The above process provides an alternative channel of communication between the humans and external environment by analyzing the brain rhythms in a number of cognitive tasks such as cursor control [12], wheelchair movement control [13], alphabet selection [14], prosthetic limb movement [15], drowsiness [16] and fatigue detection [17] of drivers, emotion recognition [18], haptic perception [19], computer gaming [20], olfactory perception [21] and so on. To perform these cognitive tasks, communication between the human brain and a computer is necessary with an aim to control brain-states using artificially generated stimuli and/or to decode brain-states involving attention, perception, motor imagination or any other cognitive functioning. Decoding of brain states requires the analysis of brain rhythms either by invasive or non-invasive means.

The invasive way of recording brain signals includes the implementation of single or multi-electrode array directly on or within the brain, whereas the non-invasive technique offers the measurement of brain activity with the help of externally placed electrodes over the scalp. *Electrocorticogram* (ECoG), being an invasive recording technology, provides wider frequency range, higher topographical resolution and better signal quality than non-invasive technologies. However, it often covers very small regions of the brain and once implanted, it cannot be moved to measure different regions of the brain. Furthermore, it requires some surgical procedures that often lead to medical complications including risk of tissue damage and infection [22], [23]. Among the lists of non-invasive technologies, *electroencephalography* (EEG), *magneto-encephalography* (MEG), *functional magnetic resonance imaging* (fMRI) and *functional near infra-red spectroscopy* (fNIRS) are few of the well-known methods required for measuring brain activities [24]-[29]. EEG measures the weak (5-100 $\mu$ V) electrical potentials generated due to neuronal firing inside the brain. The Ag-AgCl electrodes are carefully placed over the scalp to record the brain activity and provide superior temporal resolution (tens or hundreds of milliseconds). EEG is the preferred technique for most BCI researchers because of its superior temporal resolution [30], non-invasiveness [31], [32] portability, cost effectiveness and easy availability, and also the main concern of our present study. MEG measures magnetic fields generated by electrical activity of the brain, which is proven to be more sensitive than EEG. It offers higher spatial resolution than EEG [33] and has been used in rehabilitation of stroke patient [34], [35]. fMRI deals with magnetic properties of blood to measure blood oxygenation from *blood oxygen level dependent* (BOLD) response, which has been found in correlation with neural activity inside the brain [36], [37]. fMRI provides high spatial resolution (approx. 1millimeter-1centimeter) and produces satisfactory result in real-time robotic arm control through motor imagery task [38], [39]. However, MEG and fMRIs are bulky and expensive due to presence of superconducting magnets. On the other hand, portable brain imaging instrument such as

fNIRs works by projecting near infra red light having the range of 700-1000 nanometer [40] into the brain from the surface of the scalp to determine changes in tissue oxygenation and by measuring optical changes at various wavelengths when the light is reflected back. Unlike MEG and fMRI, fNIRs is inexpensive and portable along with the merit of non-invasiveness [41] and is considered to be a promising tool in near-future use. A brief overview of EEG acquisition device is provided below.

EEG acquisition device noninvasively records the signals from human scalp by using metal electrodes, preferably made of Ag/Ag-Cl. The amplitude of the recorded signal is found 100  $\mu$ V when measured on the scalp. The sampling rate at which EEG captures brain signal lies between 200 and 2000 Hz for clinical and research purposes; however, modern EEG devices are capable of recording at sampling rates above 20,000 Hz if desired. EEG signal can be further sub-divided into a number of specific frequency bands including i) delta (1-4Hz), ii) theta (4-7Hz), iii) alpha (8-12Hz), iv) mu (8-13Hz), v) beta (12-30Hz) and vi) gamma bands (25-100Hz) [42]. Table 1.1 provides source of origin, bands of frequency and cognitive tasks associated with different sub-bands.

**Table 1.1** Frequency bands with their associated brain regions and cognitive activities

<b>Band Name</b>	<b>Frequency</b>	<b>Source of Origin</b>	<b>Cognitive Activity/task</b>
Delta	1-4 Hz	Deep cortex	Analysis of sleep stages
Theta	4-7 Hz	Thalamus	Deep meditation, emotion recognition, olfactory perception
Alpha	8-12 Hz	Visual cortex	Drowsiness detection, determination of eye-closed relax condition
Mu	8-13 Hz	Sensorimotor cortex	Determination of physically rest condition
Beta	12-30 Hz	Motor cortex	Motor activity
Gamma	25-100 Hz	Somatosensory cortex	Visual perception, learning, attention, memory

In this thesis, we have used two different kinds of EEG acquisition devices. The first one is the expandable EEG-1200 model from NIHON KOHDEN, which is well-equipped for all in-patient/human-subject EEG-diagnostic applications, and the second is 14-channel wireless EEG headset, called EMOTIV. EEG-1200 provides the ideal customized configuration, which is applicable for both the collection of routine EEG data and long-term monitoring of intracranial activities. This particular model consists of 32 channel amplifier, of which 24 channels are dedicated to measure EEG signals and the remaining 8 channels are dedicated for SpO<sub>2</sub>, EtCO<sub>2</sub> and DC. This device has successfully been utilized in the experimental

procedures involved in cognitive failure detection of the vehicle drivers (described in chapter 3) and tactile perception of human subjects (described in chapter 4). EMOTIV is a wireless headset version of the stand-alone device, which is used to decode olfactory perceptual-ability of human subjects (described in chapter 2). Fig. 1.2 (a) and (b) present both the 24-channel EEG data acquisition system and the wireless 14-channel EEG headset, which are available in the Artificial Intelligence Laboratory, Jadavpur University.



(a)



(b)

**Fig. 1.2(a)-(b)** EEG devices used for the experiments performed for decoding cognitive tasks from brain signals. (a): 24-channel EEG data acquisition system, (b): 14-channel wireless EEG headset

### 1.2.2 EEG Electrodes

Accurate decoding of EEG signals for different cognitive tasks requires the correct placement of EEG electrodes or channels on the human scalp. The possible use of EEG electrodes for both stand-alone and wireless EEG systems and associated brain lobes/regions for different cognitive functionalities are presented in Table 1.2. The placement of EEG electrodes at the corresponding brain regions/lobes (as referred to the Table 1.2) is followed by internationally standardized 10-20 electrode placement system [43]. This system is based on the relationship between the location of an electrode and the underlying area of cerebral cortex. The “10” and “20” refer to the fact that the actual distances between adjacent electrodes are either 10% or 20% of the total span between the nasion to the inion regions over the scalp. Nasion is the intersection between the forehead and the nose, and the inion is the lowest point of the skull on the back just above the neck.

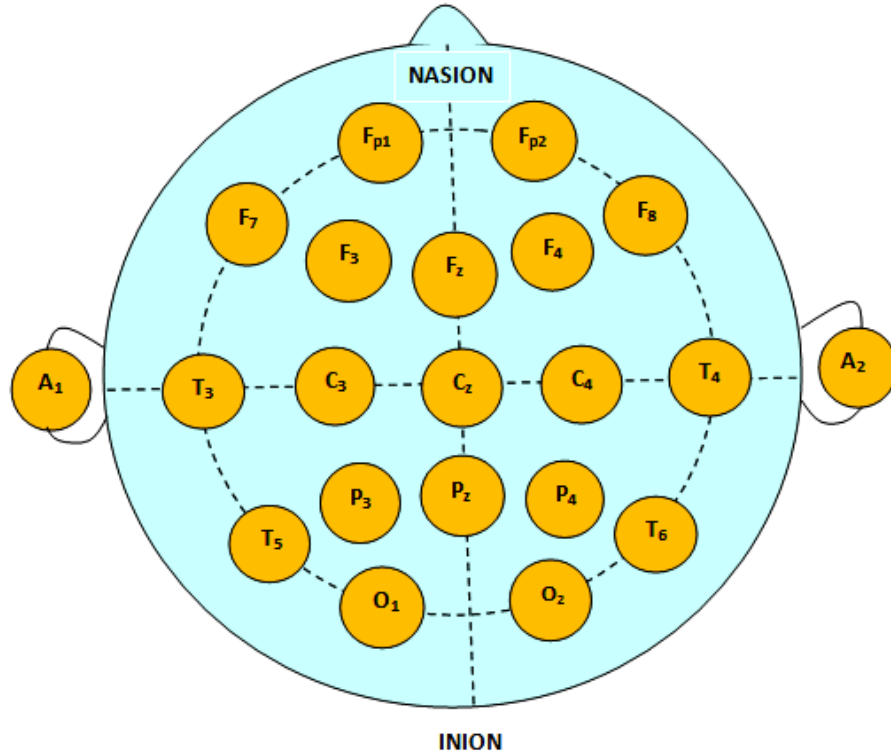
**Table 1.2** EEG channels and associated brain regions for different cognitive functionalities

Cognitive Functionalities	Brain	EEG Electrode Positions from	
	Lobes/ Regions	21-Channel EEG System	14-Channel EEG System
Emotion, olfactory recognition	Pre-frontal	Fp <sub>1</sub> , Fp <sub>2</sub>	AF <sub>3</sub> , AF <sub>4</sub>
Thinking, problem solving, reasoning, planning, higher level cognition	Frontal	F <sub>3</sub> , F <sub>4</sub> , F <sub>z</sub> , F <sub>7</sub> , F <sub>8</sub>	F <sub>7</sub> , F <sub>8</sub> , F <sub>3</sub> , F <sub>4</sub>
Understanding spatial relationship, verbal memory, processing tactile and sensory information	Parietal	P <sub>3</sub> , P <sub>4</sub> , P <sub>z</sub>	P <sub>7</sub> , P <sub>8</sub>
Vision	Occipital	O <sub>1</sub> , O <sub>2</sub>	O <sub>1</sub> , O <sub>2</sub>
Motor imagery and motor-execution	Motor cortex	C <sub>3</sub> , C <sub>4</sub> , C <sub>z</sub>	FC <sub>5</sub> , FC <sub>6</sub>
Language skills, speech perception, behavior, memory, hearing	Temporal	T <sub>1</sub> , T <sub>2</sub> , T <sub>3</sub> , T <sub>4</sub> , T <sub>5</sub> , T <sub>6</sub>	T <sub>7</sub> , T <sub>8</sub>

Fig. 1.3 shows the International 10-20 electrode placement system on the cerebral cortex, where the first letter of each brain region refers to identify the lobe of electrode placement and a number to identify the hemisphere location. The “C” letter is only used for identification purposes only, since no central lobe exists. Usually, electrodes positions in 10-20 system are encoded in decimal number, where even numbers are assigned to electrodes in the right hemisphere and odd numbers in the left hemisphere. It is important to mention here, among 24 electrodes used in our present (Nihon-Cohden) EEG stand-alone system, two reference and one ground electrode are reserved for placement on the ear-lobe or mastoid, and hence only 21 channels are distributed across the scalp to acquire brain signals.

### 1.3 BRAIN SIGNALS

During execution of different cognitive tasks, EEG signals released by the brain indicate certain special characteristics, which can be detected from the temporal changes in signal wave shapes. An EEG signal, if elicited in response to specific events or stimuli is referred to as *Event-related Potential* (ERP) [44]. Certain ERPs liberated in response to sensory stimuli with relevant discrete phase-locked events are referred to as *Evoked potential* (EP) [45]. EPs are best described by their polarity (positive or negative) and latency counted from the onset of stimuli.



**Fig. 1.3** 10-20 electrode placement system for 21-channel EEG device.

F: Frontal, F<sub>p</sub>: Pre-frontal, C: Motor cortex, T: Temporal, P: Parietal and O: Occipital

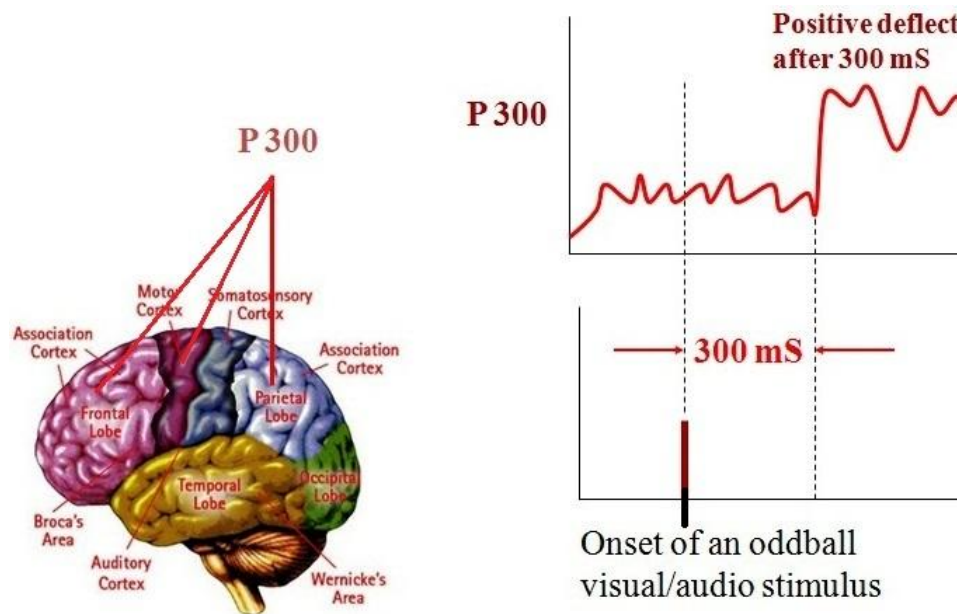
Among the EPs, *N100*, *P200*, *N200*, *P300* [46], [47], *Slow cortical potential* (SCP) [48] and *Error-related potential* (ErrP) [49] need special mention. One special type of EP, which exhibits natural responses to visual stimulations at specific frequencies, is referred to as *Steady-state visual-evoked* (SSVEP) [48] response. Besides, certain EEG signals are induced spontaneously as a response to specific cognitive tasks without any stimuli. These ERPs liberated in absence of any stimuli represent frequency-specific changes and are generally referred to as *non-phase locked ERPs* [50]. A well-known example of such ERPs is *Event-related de-synchronization/synchronization* (ERD/ERS) [51], where an event-related decrease in power is noticed at the onset of motor imagery/execution. This phase of the signal is referred to as Event Related De-synchronization (ERD). After the motor imagination/execution is over, the signal-power continues increasing until the original signal power is restored. The latter phase of the signal is referred to as ERS. This section provides a detailed description of P300 and ERD/ERS signals, which play significant roles in this thesis and also a brief overview of other well-known EEG signals popularly used in decoding cognitive tasks.

### 1.3.1 P300 Event-Related Potential

The most extensively studied ERP is the P300 wave, which is characterized by a positive deflection after 300 millisecond counted from the onset of the stimulus (Fig. 1.4). It

represents the transfer of information to consciousness. P300 wave is generated as a response to recognition of rarely occurring/meaningful *oddball* stimuli [52]. In most BCI studies concerning P300, the subject is asked to recognize a “target” stimulus from a regular set of stimuli.

P300 is a positive going wave with an expected large amplitude (possibly the largest amplitude) at the P<sub>z</sub> electrode (of the parietal lobe), a very small amplitude at the F<sub>z</sub> electrode (of the frontal lobe) and of moderate amplitude at the C<sub>z</sub> electrode (of the motor cortex region) [53]. The functional areas of the brain related to P300 generation and their corresponding EEG electrode locations are shown in Fig. 1.4.



**Fig. 1.4** The origin and nature of P300 signal

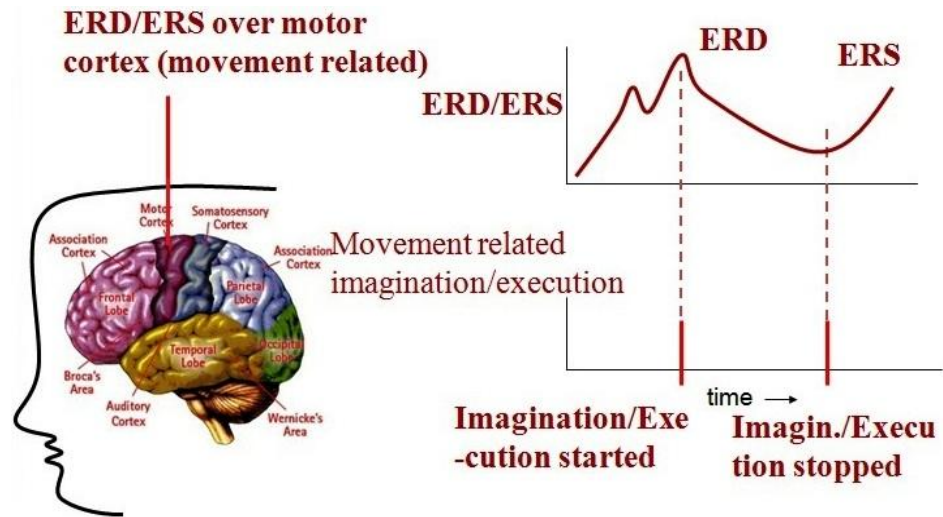
During the dual task performance, it has been observed that the amplitude of the P300 is sensitive to the amount of attention-related resources [46], in fact, it decreases with the increase in difficulty involved in primary task, regardless of the other factors related to the primary task [54], [55]. For cognitively impaired individuals, the amplitude of the P300 wave is smaller than for age-matched healthy subjects.

### 1.3.2 Event-Related De-synchronization/Synchronization (ERD/ERS)

The ERD/ERS signal carries a typical signature of motor imagery (MI) and/or motor execution (ME) tasks, and hence this signature can be used to recognize the movement-related cognitive activity performed by the subject. It has been experimentally been found that there is association between ERD/ERS signals with motor imagery, active and passive proprioception (with and without muscle contraction) as well as active and passive motor movement (with and without voluntary effort) [56]. The ERD represents a decrease in EEG



power while the ERS represents an increase in EEG power [51]. It is apparent from Fig. 1.5 that at the onset of MI/ME, there is a drastic negative going change in signal amplitude representing de-synchronization, with a subsequent synchronization with original EEG.



**Fig. 1.5** The origin and nature of ERD/ERS signal

In [57], Pfurtscheller and Neuper confirmed that a voluntary movement experiment may experience the existence of three different types of ERD oscillation at the same electrode position over the sensorimotor (SMR) area. The mu-rhythm ERD, having frequency ranges from 10Hz to 12Hz, starts 2.5sec before the onset of movement, reaches maximum de-synchronization shortly after the onset of the movement and finally attains the baseline level after few seconds. The central beta-rhythm ERD (14-18 Hz), in contrast, displays a shorter lasting ERD during the initiation of movement followed by a maximum ERS with post movement. Lastly, gamma-rhythm ERD, which has frequency ranges from 36Hz to 40Hz and rarely exists in human EEG-related experiment, exhibits sharp power increase shortly before the onset of the movement. Pfurtscheller, further along with Lopes Da Silva [58] and Neuper [59], also categorized the association of various ERD/ERS pattern with active or self-paced movement-related task in the following way: i) pre-movement ERD, which appears as contra-lateral SMR rhythm in the alpha and beta ERD, ii) ERD during motor execution, which appears as bilateral symmetrical alpha and beta ERD, and iii) post-movement ERD, which appears as contra-lateral-dominant beta-rebound or beta-ERS within the first second after the offset of the movement.



### 1.3.3 Other Signals

Besides P300 and ERD/ERS, a few more signals that need special mention are outlined below. SCP is used to modulate ERPs with electrically positive or negative shifts that last from a few hundred milliseconds up to several seconds [60]. During active or self-paced movements, two independent components of SCP can be observed: i) potential occurring while the subjects intend or anticipate an upcoming movement [61], and ii) potential occurring at the time of motor execution [62]. Another unique brain signal that is available in literature [63]-[65], is acquired by EEG system to detect errors while either a BCI delivers erroneous feedback [66], [67] or human subjects recognize that error [68]. This pattern is observed while the brain elicits a sharp negative-going signal (Error-related negativity or ERN), followed by a small positivity, followed by a negativity again from fronto-central and centro-parietal lobes, referred to as ErrP, which is also further utilized to correct the erroneous action [64], [69]. The frontal and central EEG electrode locations exhibit the largest ERN response and it is sensitive to the intention and motivation of the participant. ERN latencies can also be manipulated through rapid feedback where subjects show shorter ERN peak latencies during incorrect responses. This signature can provide a clear indication of errors during the motor-imagery BCI experiments and hence can be employed in the BCI control system as an error feedback [63]-[69]. Unlike P300, an increase in EEG response, termed as SSVEP is visible around the frequency of a visual stimulus when the stimulus is modulated periodically as a function of time [70] at that frequency. It is observed that in most research associated with SSVEP, the frequency of the stimulus is considered above 8-10Hz because of the nearly sinusoidal nature of SSVEP signal above 10Hz. Besides the above well-known signals, we need to draw readers' attention to a special kind of ERP, called *olfactory event-related potentials* (OERP), which offers high sensitivity to olfactory function in cortical response to olfactory stimuli [71]. It has also been reported that patients suffering from multiple sclerosis or Alzheimer's disease usually experience olfactory disorder [72], [73]. Table 1.3 summarizes the list of the origin, latency and use of the well-known EEG signals that have been mentioned in this section.

**Table 1.3** Origin, latency and use of well-known EEG signals

<b>EEG Signals</b>	<b>Origin</b>	<b>Latency</b>	<b>Use</b>
N100 [74]	Significantly at Cz electrode position	Negative deflection between 80-200ms after the onset of stimulus	Detection of unexpected stimulus
N200 [75]	N2a or mismatch negativity: anterior-cortical region [76]; N2b: central-cortical region; N2c: frontally and centrally [77]; N2pc: occipital-temporal region of contra-lateral cortex [78]	180-325ms after the onset of visual or auditory stimulus [79]	Detection of- N2a: disparity between deviating stimulus and a sensory-memory representation of standard stimulus [80]; N2b: selective attention to deviation in oddball paradigms; N2c: classification task, N2pc: attention-related shift
P200	Significantly at Cz electrode position [81]	Positive peak between 100 - 250 ms after the onset of stimulus [74]	Attention to the tones [82]
P300	Fronto-centro-parietal region (Fz-Cz-Pz electrode position) [53]	Positive peak between 250 to 400 ms after the onset of stimulus [74]	Detection of oddball paradigm for visual and auditory stimuli
N400/P600	Centro-parietal region	Negative/positive peak between 300-600ms after the onset of stimulus [74]	Detection of syntactic violation during language processing
OERP	Orbitofrontal cortex [5], parainsular cortex and superior temporal sulcus [83]	Less than 50msec after the onset of stimulus [84]	Odor threshold, odor identification and odor discrimination [85]
ERD/ERS [57]-	Sensorimotor (SMR) region	Ranges from 2.5s before the onset to 1s after	Motor imagery, active and passive motor movement

EEG Signals	Origin	Latency	Use
[59]		the offset of stimulus	
SSVEP	Media occipital lobe [70]	Periodically appears with flickering stimulus	Selection of target stimulus
SCP	Significantly at Cz electrode position [86]	0.5-10s [87]	Detection of intended or anticipated upcoming movement
ErrP	Fronto-central and centro-parietal lobes [63], Early Pe: fronto-central lobe; Late Pe: centro-parietal lobe	ERN (Ne): Negative peak between 50-100ms after erroneous response [88], [89]; Early Pe: positive peak directly after ERN; Late Pe: 200-400ms after error [90]	Detection of erroneous feedback by human subjects or BCI and correction of that error

## 1.4 REAL-WORLD PROBLEM-SOLVING USING EEG SIGNALS

Design of a BCI problem to reach a fixed target using standard brain signals is of great interest to the BCI-research community. The challenge here lies in optimal formulation of the problem to solve the target objective accurately within a given time limit. Until now, there is no well-known approach to address the above issues. We here illustrate the problem formulation strategies for a few selected target problems.

### 1.4.1 Problem-Solving with Single EEG Signal

We here address two problems. The first one is concerned with BCI speller, while the second one deals with cursor position control with a single BCI signal.

#### *A. P300/SSVEP Signal-based BCI-Speller*

BCI spellers are useful media of communication for people with neuromuscular disability. Here, the subject can perform mental selection of letters/numbers from a two-dimensional array of alphanumeric characters in sequence to construct words/sentences for communication to a computer [91], [92]. The BCI signals that are popularly used for BCI speller are SSVEP or P300.

To utilize the oddball paradigm of P300, four different techniques of BCI design are popularly used. The most popular approach, called the Row-Column (RC) selection approach involves flashing individual rows/columns, so that a row/column containing the target character can be selected [92] from P300 evoked response. The second alternative but tedious approach is to allow users to select single character (SC) with a delay between flashes [93] by oddball paradigm, perhaps, is to flash individual characters randomly on the array [94]. The third approach, called region-based (RB) approach [94] flashes a region of same characters jointly to help users easily apply oddball paradigm without mistake to select the flashing character. The last approach, called checkerboard (CB) speller [93], [95] is an extension of the RC approach, to eliminate possible ambiguity in selecting two consecutive flashing characters on the same row/column by fixing them on consecutive black and white tiles as in a checkerboard. In this way, CB speller reduces the inherent noise due to row/column association [93] as well as enhances information transfer rate (ITR) [96].

The principle of selecting characters in SSVEP based BCI speller is similar to SC/RC-based BCI, except the fact that the characters or row/columns are flickered at specific frequency to elicit SSVEP. When the periodic presentation (flicker) of a character or row/column is significantly high ( $>6$  Hz), a steady-state signal, called SSVEP is elicited that resonates at the flickering rate of the character or row/column and its multipliers.

Now, to select the right EEG signal for BCI-speller, a user needs to compare the relative merits of BCI design using P300 and SSVEP and the user-friendliness of the individual modalities as well. We here introduce three metrics to examine the relative merits of the two

signals. These are i) training time (TT), ii) classification accuracy (CA) and iii) information transfer rate (ITR). TT is a measure of absolute training time required to enable the subject to use the BCI-speller. ITR of a BCI system, as given by (1.1) [97], depends on i) the number of cognitive samples recognized per second, ii) number of cognitive trials and iii) classification accuracy.

$$ITR = N_t \left[ \log_2 N + C \log_2 C + (1-C) \log_2 \frac{1-C}{N-1} \right] \quad (1.1)$$

where,  $N_t$  is number of cognitive samples/second,  $N$  is number of cognitive trials and  $C$  is classification accuracy.

Table 1.4 offers a comparative framework of SSVEP and P300 based BCI speller.

**Table 1.4** Basis of selection of EEG signals for BCI speller

<b>Problem</b>	<b>EEG Signals</b>	<b>Use of EEG Signals</b>	<b>TT in Month</b>	<b>%CA</b>	<b>ITR in bits/min</b>	<b>Basis of selection of EEG Signal</b>
BCI Speller	P300	Oddball paradigm	No training	86	~35/10-25 (for healthy/ disabled )	SSVEP, because of higher %CA and ITR
	SSVEP	Brain signal modulation	No training	91.35	58-166	

TT fortunately is zero for both the signals. The average classification accuracy (CA) of P300-RC speller using linear discriminant analysis (LDA) classifier varies from 86% for healthy person in dynamic environment, whereas the average accuracy is dropped to 62% when experiments conducted on persons having motor impairments and suffering from locked-in syndrome [98]. In another study [99], mean classification accuracy of P300 speller using a list of standard classifiers including LDA and its variants, support vector machines (SVMs) and its variant, and neural network is found 62% to 72%, when experiments performed on disabled persons, particularly amyotrophic lateral sclerosis (ALS), middle cerebral artery stroke, and hemorrhage patients, who are suffering from motor and speech disabilities. Besides P300 speller, depending on i) stimulus preparation, ii) multiple target coding, and iii) target identification, mean classification accuracy of the SSVEP speller is found 91.35% [100] using canonical correlation analysis (CCA). According to ITR analysis, SSVEP outperforms P300 with an average ITR up to 58 bits/min [101] and can reach up to of ~166 bits/min [100], whereas P300 provides much lower ITR of ~35 bits/min [100], which is further reduced to 10-25 bits/min for disabled subjects [102]. Therefore, it can be concluded that SSVEP proves to be better modality for using BCI spelling in terms of CA and high ITR, if proper design strategies will be implemented to make the system more familiar to the patients suffering from multiple sclerosis.

### *B. SCP or ERD/ERS (Sensorimotor) signal-based Cursor Control*

Cursor control is a well-known BCI application, where users suffering from multiple sclerosis intend to move a cursor only by means of brain activity towards a target appeared on the monitor. To accomplish this, different types of control strategies are considered: one-dimensional, two-dimensional and four-dimensional. However, one- and two-dimensional cursor control problems are more popular than their four-dimensional counterpart because of its low average classification accuracy (51-60%) [103]. One-dimensional control strategy provides cursor movement in either vertical or horizontal direction, whereas two-dimensional control strategy includes the both. The cursor control employs the use of well-known BCI signals including ERD/ERS or sensorimotor (SMR) rhythm and SCP. ERD/ERS response is elicited when users perform left/right/forward/backward hand motor imagery in association with left/right/top/bottom cursor movement. A clear discrimination between low-amplitude beta-ERD and high-amplitude beta-ERS responses is utilized to identify successful completion of cursor movement. The distance between cursor and the target is divided into predefined steps, where in each step users perform the above motor imagery task to bring the cursor closer to the target. As soon as the cursor reaches the target, users stop to plan the intended motor imagery for cursor movement, and hence no further beta-ERS is generated.

Besides ERD/ERS or SMR rhythm, SCP is used to control the movement of a cursor using user's amplitude shifts. Positive shifts in amplitude ensure the cursor movement into the upper half, whereas negative shifts provide the direction of cursor in lower half of the computer screen. A trial is rejected (regarded as invalid), if either SCP changes remain below  $0.5 \mu\text{V}$  (no response) or the SCP shift exceeds  $200 \mu\text{V}$  (artifact caused by involuntary movements). Here, in both the cases, subjects are instructed to self-regulate or control the amplitude of their SCP or ERD/ERS (SMR rhythm) to control the movement of the cursor either at the top or the bottom of the computer screen (for one-dimensional control), where the vertical movement is controlled by the amplitude of SCP or SMR.

Here too, selection of right signal for cursor control is performed by comparing their performances across the three metrics, as mentioned before. Successful completion of target reach is reinforced by an animated face on the computer screen and a chime, which helps to evaluate the classifier performance. TT for both is significantly high, especially from several months to 1 year. The classification accuracy (CA) of controlling the cursor in one dimension, such as either vertical or horizontal by using SCP is found around 70-80% [104]. On the other hand, control of the cursor movement using SMR or ERD/ERS is achieved with average classification accuracies of ~81% [105] (for one-dimensional control) and 80% [103], [106] (for two-dimensional control). There. Too exists mention of higher classification accuracy (>95%) for one-dimensional cursor movement by controlling SMR rhythm [107], [108]. From the system realization point of view, processing of SCP response makes the system relatively

slower, which is by ITR of 15-20 bits/min [105], as given in Table 1.5. Besides, ERD/ERS attains a higher ITR of 20-25 bits/min [109]. Although both modalities need significant training time, we conclude that ERD/ERS serves better online control for cursor movement because of its relatively higher ITR.

**Table 1.5** Basis of selection of EEG signals for cursor control

<b>Problem</b>	<b>EEG Signals</b>	<b>Use of EEG Signals</b>	<b>TT in Month</b>	<b>%CA</b>	<b>ITR in bits/min</b>	<b>Basis of selection of EEG Signal</b>
Cursor Control	SCP	Slow positive/negative amplitude shifts	Several months to 1 year	70-80	15-20	ERD/ERS for its higher CA and ITR
	ERD/ERS (SMR)	High amplitude beta-ERS synchronized to motor imagination	Several months to 1 year	80- >95	20-25	

#### 1.4.2 Problem Solving with Mixed EEG Signals

The limitations in using single EEG signal are eliminated by incorporating two or more signals jointly in order to perform a specific cognitive task. BCI system using mixed signals is known as multi-modal or hybrid BCI system. This section provides some well-known BCI applications using mixed signals that are already prevalent in the existing literature.

##### *A. Multi-modal BCI speller*

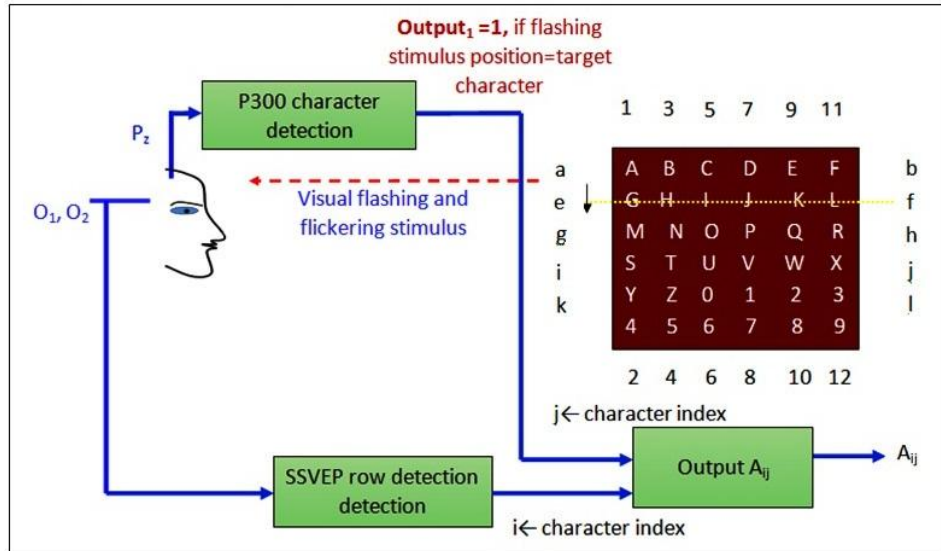
The use of P300 and SSVEP in BCI speller single-handedly includes few limitations, which has already been discussed in this section. By keeping this in mind, an attempt has been taken to design an asynchronous BCI speller by combining SSVEP with P300 potential in order to reduce the error exhibited by P300 in presence of target character at the same row or column [110]. The random flashes and flickers of P300 and SSVEP respectively, in general, are utilized to select row/column and target characters. In a particular speller [110], row/column-wise target selection using P300 can be performed once control state is detected by SSVEP. Control state detection is achieved by eliciting SSVEP response when the user gazes at the screen, thus confirming that the user intends to send a command. Besides row/column selection, sub-area wise target selection by 2-D coordinate is also an alternative choice [111], where SSVEP response, after elicited by a particular flickering frequency is used to select a sub-area of user's choice. P300 here is used to select the target character present on the chosen area by superimposing the character onto the periodic flickering. The blocking state of SSVEP, called SSVEP-blocking response is proven equally useful, in which change in

luminance of target character from light to dark state during target selection dismisses the natural SSVEP response. In contrast to P300-SSVEP BCI, ErrP can be used in conjunction with the P300 speller to automatically detect the error during spelling task [112], [113], [69]. In this scheme, user utilizes the elicited ErrP to cancel a character selected by his P300 response, or alternatively, to select the second most possible character according to the elicited P300 response [92].

Like single signal selection, here too, selection of composite/mixed signals for a hybrid-BCI is an important issue. Sometimes, BCI researchers evaluate some pre-defined metrics for both unimodal and multi-modal BCI for determining whether hybrid BCI outperforms its single-modal counterparts. For both P300-SSVEP and P300-ErrP-based hybrid BCI speller, the previous three aspects need to be discussed again: i) training time (TT), ii) classification accuracy (CA) and iii) information transfer rate (ITR). The former hybrid BCI speller has the advantage of high ITR and almost no or zero training time, which is already proven merits of both P300 and SSVEP independently. It is observed that use of SSVEP signals to evoke P300 potentials enhances overall speed and accuracy of the hybrid speller [111], [114], [115], when compared with that of the speller using P300 or SSVEP only. The hybrid P300-SSVEP speller, as specified earlier, is capable of transferring information at a rate of 30.81 bits/min with an average classification accuracy of 94.44% [110]. Although the ITR of the hybrid P300-SSVEP speller is not quite impressive in comparison to its unimodal counterpart, it has been improved by changing the pattern of SSVEP stimulus. In particular, with the changed SSVEP stimulus, the corresponding ITR of sub-area/location (SL) mode speller and row-column (RC) mode speller have been increased to 44.70 bits/min and 53.06 bits/min respectively [111].

On the other hand, for P300-ErrP hybrid speller, user requires more training time because of the liberation of ErrP signal correctly when needed. Well-known evolutionary approach, such as, genetic algorithm (GA) is utilized to detect P300 and ErrP online and at the preliminary level, the average classification accuracy has been found roughly 90% and 60% respectively [112]. Literature [116] also reveals that P300-ErrP provides the ITR of 19.56 bits/min, when multi-dimensional Gaussian classifier is used for classification with mean and standard deviation of each of the two Gaussians as model parameters. From the above discussion, it may be suggested to select P300-SSVEP mixed signal for hybrid BCI speller because of no training time, and higher classification accuracy and ITR, as compared with P300-ErrP speller. Fig. 1.6 provides a general scheme of P300-SSVEP speller during the row and character selection using SSVEP and P300 responses respectively.





**Fig. 1.6** Hybrid BCI speller using P300 and SSVEP signals jointly

### B. Multi-modal Cursor Control

The use of mixed modality in 2-D BCI cursor control is of four kinds: i) P300 and ERD/ERS, ii) P300 and SSVEP, and iii) ERD/ERS and SSVEP, iii), and iv) ERD/ERS and ErrP. Initially, in the first case [117], vertical movement of the cursor is controlled by user's P300 response, by utilizing which user can select any of the given vertical movements including a) moving upward, b) moving downward or c) no vertical movement. On the other hand, ERD/ERS, as elicited from the scalp of the user, is translated into a continuous value that determines the direction and velocity of the horizontal movement. This system not only provides two independent control signals that are based on P300 and ERD/ERS, but also offers cursor movement from any arbitrary position to an arbitrary target position. Later, the earlier work is extended by hybrid task-based approach for target selection [118]. Here, once the cursor hits the target, user gets a chance to decide whether the target is correct or incorrect. The correct or incorrect target appears on the computer screen as green or blue squares respectively. The user has a choice of focusing on a pre-defined flashing button if the target is corrected one, otherwise performing left/right hand motor imagery (MI) without focusing on any button to ensure the rejection of the target. The user maintains an idle state of MI while focusing on the flashing button in order to select the correct target, and thus belonging to one class: the idle state of MI with P300. The second class of this two-class classification problem is MI without P300 during the rejection of target.

The second hybrid BCI paradigm provides a novel 2-D cursor control system by using SSVEP and P300 to the users, who are unable to liberate ERD/ERS well, but can generate SSVEP and P300. In this case [119], users are instructed to utilize their EEG response to control the direction and speed of the cursor instead of controlling horizontal and vertical movement of the cursor. Here, an SSVEP response corresponding to a specific direction

(left/right) is recognized by users' attention, which results in turning of the cursor either counterclockwise or clockwise. Similarly, the cursor gets accelerated or decelerated when P300 potential in association with top or bottom flashing stimulus is elicited by counting its flashing time. A novel use of SSVEP response in cursor control includes the confirmation of reach to the target by the cursor. This is estimated by calculating the distance between the center of the cursor and the center of any target. The reach is confirmed if the above distance is shorter than  $\frac{1}{2}$  times the sum of the diagonal side lengths of the target and cursor plus a preset threshold.

The third kind, the SSVEP-ERD/ERS-based cursor control follows similar approach like P300-ERD/ERS based cursor control, such as, utilizing SSVEP to control one dimension of movement, while ERD/ERS to control another dimension [120]. In general, SSVEP and ERD responses are simultaneously elicited, when the users keep their visual attention for controlling cursor movement in the horizontal direction and simultaneously perform motor imagery for controlling the vertical position of a virtual ball.

In the last multi-modal BCI approach, ERD/ERS and ErrP signals are jointly used to control one-dimensional step-wise movement of a cursor [67], [121]. Here, ERD/ERS potential evoked by cursor movement is decoded to indicate correct or erroneous movement. The cursor is returned to the previous position if the movement is found erroneous.

Now, to select right combination of mixed signal for cursor control is a challenging one, since the performance of cursor control depends on the task assigned to the subjects, where the task combinations, as designed in different literature [117]-[121], vary across the subjects. Besides, the performance also depends on various factors including training time, literacy rate, timeout interval, number of electrodes, target size as percent of workspace and movement time [67]. Based on these factors, existing literature refer a number of metrics to evaluate the performance of their control algorithms. Success rate or hit rate in terms of average percentage classification accuracy and the average control time to complete each trial are the two most important measures among these. The success rate is usually referred to describe the degree of accomplishment of the task (here, cursor control), and in the present case, is calculated by the number of the targets hit successfully over the number of all targets required to finish. The average control time or task completion time is often referred to the time taken from the cursor getting moved to hitting the desired target, including the confirmation time.

The average success rate of P300-ERD/ERS based cursor control scheme is 90.75%, whereas average control time of each trial is 28 sec, when Fisher's linear discriminant (FLD), step-wise linear discriminant analysis (SWLDA) and linear support vector machines (L-SVMs) are considered as classifiers. The reason behind the large control time is relatively small-sized cursor and target, and large time consumed for triggering and detecting P300

response [117]. In [118], the average success rate is increased to 93.99%, whereas, task completion time also reduces to 18.19 sec, when experimented using L-SVM classifier with common spatial pattern (CSP) features. For P300-SSVEP-based cursor control [119], the performance of the paradigm depends on the success rate for three control schemes: (i) average success rate of turning the cursor in clockwise and anti-clockwise direction using SSVEP (direction control), (ii) average success rate of non-turning command for the cursor, and only changing speed of the cursor using P300 (speed control), and (iii) average success rate of acceptance and rejection of the final target position using SSVEP (confirmation of reach). It is found that the average success rates for (i), (ii) and (iii) are 95%, 70% and >96%, whereas the over-all average success rate of cursor control across all subjects is 95.88% with a clear indication that direction control and confirmation of reach using SSVEP outperforms the speed control using P300. It is also indicated in [119] that the average task completion time is 36.53 sec, which is quite larger because of the inclusion of three control schemes. For ERD-SSVEP-based and ErrP-ERD/ERS-based cursor control, average success rate is found quite lower than the previous two paradigms, and is reported as 60% [120] and 73.1% [121] respectively. During ERD-SSVEP based cursor control, motor imagery (MI) using ERD is classified by selecting CSP and LDA as feature-classifier combination, whereas, SSVEP classification is done by taking logarithmic band power as feature in conjunction with LDA. On the contrary, EEG electrodes and frequency are considered as features for controlling cursor movement using ErrP and ERD/ERS [121]. This discussion comes to an end with a special mention that higher classification accuracy of 80% is reported for ErrP recognition in [121], when used to indicate correct or erroneous trial, and also reduces MI decoding error from about 30% to less than 9%.

### *C. Multi-modal Wheelchair/Vehicle Destination Control*

Wheelchair/vehicle destination control is another well-known BCI application, which provides an interface for severely disabled individuals to move their wheelchair or vehicle at a desired destination. Two types of mixed signals including i) P300 and Mu-Beta and ii) P300 and SSVEP can be used to serve the above purpose. Usually in the first case, discrete decisions, such as, selection of one out of different control options are made by using P300 response, whereas, continuous decisions including control of the movement of the wheelchair are performed by using mu-beta rhythm [122]. Therefore, wheelchair control includes various control commands: i) destination selection, ii) navigation and iii) stopping command [123]. The destination of the wheelchair motion, as mentioned earlier, is fixed by selecting one of the items among a list of destinations using P300 modality. Once the destination is selected, an autonomous motion control is introduced. During navigation, the motion of the wheelchair is followed by virtual guiding paths, where a proximity sensor, mounted in front of the wheelchair protects the wheelchair from any frontal collision [123], [124]. The controller automatically stops the wheelchair in presence of any obstacle within 50cm. Now, to generate

stopping command on the reach of wheelchair at the destination, two approaches are available in the literature [123], [124]. One approach considers a fast P300 algorithm instead of the regular P300 response, since the regular P300 response, as elicited from the same panel where other command buttons are present fails to stop the wheelchair in a decent time [124]. Therefore, an improved algorithm is designed to make the users to concentrate on one single button, labeled “STOP” to generate faster P300 response. Although it reduces the reaction time, however, generates very high false acceptance (around 2.5%), which makes this approach inapplicable. The second approach implements mu-beta rhythm, which is liberated from the imagination of arm movement [123]. To accomplish this, a cursor movement is controlled on the screen by performing arm motor imagery and the position of the cursor is considered for presenting visual feedback for mu-beta-based system. This approach holds same response time as the previous approach, however, a rate of zero false acceptance is also occurred, which makes the second approach is more reliable for wheelchair control application. In [125], navigation of the wheelchair is controlled using left and right hand motor imagery (MI), and the stopping command is generated by using P300 response. Every time when the navigation command updates the current position of the wheelchair, this update, in turn, triggers a detector, which detects whether the current position falls into areas corresponding to device control state. If detected, then controller stops MI detection and switches to the device control state. In this state, the control panel is presented to the subject to elicit P300 response as oddball paradigm. The system again reverts to the navigation state once the subject selects the ‘quit’ command from the control panel, and the loop continues. It is important to mention here that the controller automatically switches the system state if ‘quit’ is not detected even after six commands.

Although the response of MI-based stopping command is fast, it is often used to control direction of the wheelchair [125, 126]. This motivates the researchers to develop a new hybrid system for wheelchair control using P300 and SSVEP [127], [128]. In [127], four groups of buttons, one large button in the middle and eight small buttons surrounding it, are displayed on computer screen, where, all buttons in each group flicker at a fixed frequency. For example, 6.0Hz, 6.67Hz, 7.5Hz and 8.75Hz frequencies are selected for the four groups and SSVEP is evoked at frequency related the given frequency of a particular group. At the same time, four large buttons of the four groups flashes randomly to evoke P300 response. The system detects the target group if both SSVEP and P300 occur in the same group of buttons, thereby enabling the user to elicit SSVEP and P300 simultaneously while focusing on one group of buttons. This approach is utilized to produce “go/stop” command for controlling wheelchair movement. A slightly different approach is found in [128], which includes two components: one is selection components based on P300 response, and the other is confirmation component based on SSVEP response. Here, the desired destination of a vehicle is selected using P300 response from a 3×3 matrix of characters, each character representing a

predefined destination. Once the selection is over, SSVEP response associated to two flickering checkerboards confirms the acceptance (12Hz)/rejection (13Hz) of the desired destination.

Selection of right composite signals for wheelchair/vehicle destination control here depends on a number of performance metrics including average percentage classification accuracy and control time. Study [125] reveals that the average classification accuracy as well the control time for MI (P300) varies from around 81-88% (around 76-84%) and around 40-71secs (around 48-78secs) respectively across all subjects when the wheelchair navigates 90°, 180° and 360°, which is presented in Table 1.6.

**Table 1.6** Average classification accuracy and control time for MI-P300 wheelchair control [125]

Degree of Navigation	Average Classification Accuracy (%)		Control time (seconds)	
	Hybrid Control using MI	Hybrid Control using P300	Hybrid Control using MI	Hybrid Control using P300
90° in the left	81.07%	84.67%	40.3	50
180° in the right	84.47%	76.25%	71.3	48.8
360°	88.09%	84.13%	64.5	78.8

On the other hand, using P300 and SSVEP signals, the average classification accuracies of vehicle control in the laboratory and real driving environment are found 99.07% and 98.93% respectively, with average control time of ~24secs and ~25secs respectively [128]. The proposed scheme, as compared to previous study [129], improves the accuracy of destination selection in comparison to the P300-based selection system, particularly for those participants who may have a relative low accuracy in using P300 BCI. Furthermore, it is more useful than other motor-imagery based selection system for those persons who suffered from severe neuromuscular disorders such as the ALS, multiple sclerosis, brainstem stroke and cerebral palsy. In [a hybrid bci], there is also an indication of improved response time (5.28secs) to generate a ‘go/stop’ command in motion-condition, which is quite significant. It is also important to mention that this hybrid system outperforms its competitors [130], [14] by attaining comparatively lower false acceptance rate of 0.52/min and a higher ITR of 22.11bits/min. Based on the existing results, it can be concluded that P300-SSVEP-based hybrid control is more advantageous for its higher average classification accuracy, lesser command time, and a high ITR, if efforts are taken by the researchers to reduce its false positive rate.

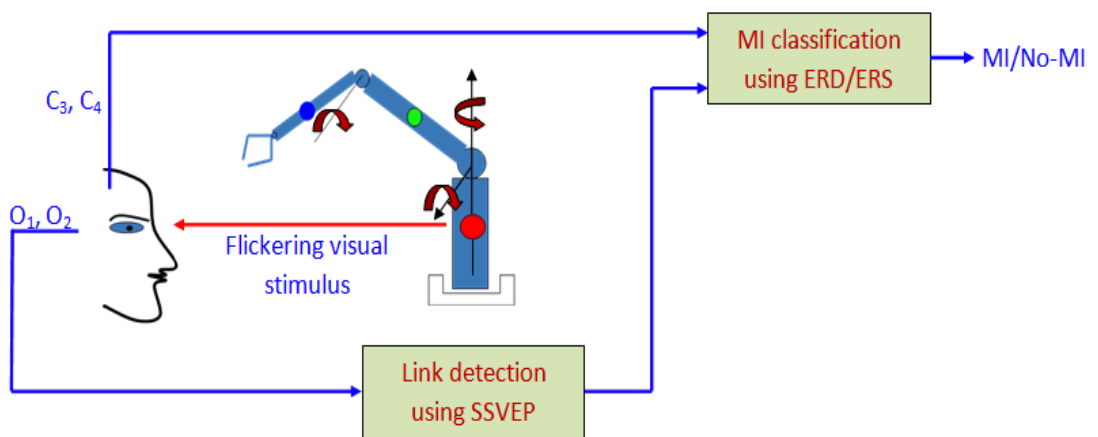
#### *D. Multi-modal Artificial Limb Control*

Artificial limb control using mixed signals includes three combinations of composite signals: i) ERD/ERS and SSVEP, ii) MI, P300 and ErrP and iii) MI and ErrP. Each modality has its merits and limitations. Here, we discuss each hybrid modality and its performance one by one. There exist ample amount of use of ERD/ERS and SSVEP for controlling the movement of artificial limb/prosthetic arm and is available in [131]-[137]. In [131], authors use a hybrid interfacing system to control a two-degree of freedom robotic arm, where SSVEP is applied to control the elbow function using a binary classification, while ERD/ERS using imagined brisk feet movement for opening and closing of a gripper. The authors have made intelligent use of the SSVEP/ERD combination by using imagined feet movement rather than left/right hand movement, because hand movement (real or imagined) causes activation mainly in the contralateral hemisphere of the brain, but still causes activity in the lateral hemisphere, which can lead to increase in false positive rates. Furthermore, using ERDs from feet movement only creates two possible states (movement/idle), which when compared to the three states for hand movement (left/right/idle) also increases the chance of false positive rates. The overall offline accuracy of MI and SSVEP is found around 87% and 91% respectively, which is a good result however average time needed to complete SSVEP control during online is ~14.7secs.

In [136], authors propose a hybrid interfacing system using ERD-SSVEP as composite modality for hand-orthosis control. During the ERD-based task, two arrows appear on the screen. When the left arrow appears, subjects are instructed to imagine opening and closing their left hand. For the right arrow, subjects are instructed to imagine opening and closing the corresponding hand. In the SSVEP task, subjects are instructed to gaze at either left (8Hz) or right (13Hz) LED depending on which cue appeared. In the hybrid task, when the left arrow is showed, subjects are instructed to imagine the left hand opening and closing while gazing at the left LED simultaneously. The task is similar for the right arrow. Result shows that the average accuracy of ~87.9% for hybrid feedback paradigm, which is quite higher than the normal feedback paradigm, as reported by ~71.4%.

An inverse approach is considered [137] for orthosis control application, where, SSVEP-based BCI has been utilized for opening the orthosis at the activating stage and an ERS-based BCI has been used as a switch to deactivate the LEDs that were mounted on the orthosis for SSVEP generation in the resting stage. The SSVEP-based stage entails four steps for opening and closing the orthosis completely. Frequencies 8 and 13Hz LEDs are used for the opening and closing tasks, respectively. During training sessions, subjects are instructed to close the brain switch. Then, they are instructed to open and close the orthosis by gazing at the LEDs mounted on the orthosis. In the next stage, the SSVEP-based BCI is turned off by opening the brain switch. This switch is kept open during the resting period. At the end of the resting

period, the brain switch is closed, and SSVEP task is repeated. During the activity period, the true positive rate and false positive rates are measured, whereas during resting period, the false positive rate is measured. It has been shown that false positive rate is reduced by more than 50% when hybrid BCI is utilized and the average classification accuracy is found 85%. Besides, the trial time during control experiment is obtained 292secs, whereas, the trial time during brain-switch and SSVEP experiment is reported 430secs, which is slightly higher. A general overview of artificial limb control using well-known SSVEP and MI-based hybrid approach is presented in Fig. 1.7.



**Fig. 1.7** Artificial limb control using ERD/ERS and SSVEP signals jointly

In [138], motor imagery (MI), P300 and ErrP signals are used to control the movement of a robotic arm. This scheme aims at position control of a robot arm by decoding motor imagery signals to control the direction of movement of the robot. After reaching the target position, the subject stops the movement of the robot arm by eliciting P300 response. Here, the errors may exist for two reasons: i) due to misinterpretation of brain signal by the classifier, and ii) because of crossing the target by the robot arm and then it stops. On detection of the first form of error, the movement of the robot arm is stopped immediately and it is made travel back to its previous position. On detection of the second form of error, the robot arm is re-aligned to the target by an offset which is experimentally determined during the training of the subjects. The average classification accuracy for hybrid MI, P300 and ErrP are found 71.2%, 89.5% and 80.1% respectively with average ITR of 22.12 bits/min, 23.83 bits/min and 23.47bits/min.

In [139], the movement of each link of the robot arm is controlled in a fixed pre-defined order by using MI and ErrP signals. This scheme is much simpler than the scheme described in [138]; however, it requires a considerable switching effort between activation of two links. This scheme controls the movement of each link by using motor imagery signals and each links are activated at a fixed interval of time. The motor imagination detector for an individual

link classifies the desired movement of the link and the decoded task concerning the desired movement is executed until a visually inspired positional error is detected by an error-related potential classifier. The error-related potential signal is generated after the robotic link crosses the desired target position. Naturally, after the error is decoded, the actuator is commanded to stop further movement, and the robotic link is turned in reverse direction by a fixed experimentally determined offset before to commence planning for the movement of the next link in sequence. The process is repeated for each link in a fixed order to align the robot end-effector with the desired target position. Adaptive autoregressive parameters and moving averages are extracted as features for motor imagery and ErRP signals respectively. A support vector machine classifier is used for decoding of motor imagination and error-related potential with high classification accuracy above 80% for all the decoders with average ITR of 21.65bits/min (for link 1), 14.94bits/min (for link 2 and 3) and 22.65bits/min (for ErrP detection). The average time taken by the proposed scheme for decoding and execution of control intentions for the complete movement of three links of a robot is above 50 seconds.

### 1.5 COMPONENTS OF A BRAIN-COMPUTER INTERFACING SYSTEM

The main aim of an electroencephalographic-brain computer interfacing (EEG-BCI) system is to create a communication channel between the user's intention and an external device (e.g. computers, prosthesis) without any muscular intervention. Unfortunately, while executing an assigned task, the human brain occasionally undertakes parallel thoughts, which might appear as the cross-talk to the acquired EEG signals recorded to examine the targeted task. In case, the frequency band of the EEG signals for the non-targeted parallel tasks do not overlap with those of the targeted task, the frequency band for the targeted task can be separated from the parallel thoughts by filtering. The EEG signal being of very low frequency and pass bands for individual tasks being too narrow, we go for digital filtering rather than conventional analog filtering. Fig. 1.8 presents all steps of BCI.

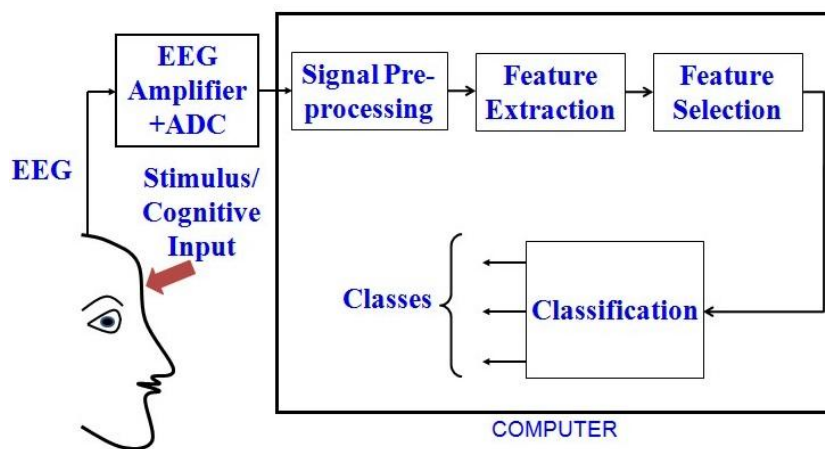


Fig. 1.8 Components of a brain-computer interfacing system



The next step that follows digital filtering is feature extraction. Feature extraction involves determining the most appropriate features of the acquired EEG that best resembles the EEG signal for a given task. In other words, true features of an EEG signal are those, which directly/indirectly can help in reconstruction of the EEG signal. Unfortunately, there is no standard technique to extract the true features of an EEG for a given task. The usual practice thus is to determine a set of standard features that can capture one or more characteristics of the EEG signal. If the list of features is too long, we need to select a fewer of the features. In fact, there is an extensive literature on feature selection. A few of these that deserve mentioning includes forward search, backward search, and evolutionary search algorithms [140], [141]. The motivation of these algorithms is to identify a subset of features from its entirety so that they best represent the EEG signals at the sampled time-points. Most of BCI techniques terminate with a classification algorithm that aims at classifying the target task/class from the rest. Usually, most of the BCI problems are formulated as a two-class classification problem, unless the problem by nature is a multi-class classification problem. In a two-class classification task, the classifier produces a binary output, one for the target class and zero for the rest. A multi-class classification problem, such as classification of aroma from EEG signatures, is again solved usually as a sequence of two-class classification problem. For example, A, B and C are three classes. We use binary classifiers to classify the features into A and non-A. Then the non-A class is again classified into class B and C. Had there been more than three classes, the classification tree would have a longer length but that too has to follow the above principle.

Occasionally, a few BCI systems require additional steps to realize a controller to execute specific control tasks based on the results of classification. For example, suppose, if the classifier response is class A, we may need to turn a motor on. If it is class B, we may turn it off. More sophisticated control logic is also adopted in recent BCI systems [140], where the motor is activated based on the classification of subjective motor imagery, and stopped based on the occurrence of error when the motor-shaft passes the fixed target position.

### **1.5.1 EEG Signal Preprocessing**

In this step of the BCI system, the raw EEG signals are filtered in the desired frequency bands, where the information pertaining to the user intention is dominant. It also serves the purpose of eliminating noise emerging from the environment, muscle movement and power line interference (in 50 or 60 Hz). The filters implemented in BCI research is broadly classified into two categories: a) Spectral filters, and b) Spatial filters.

Spectral filter consists of Finite and Infinite Impulse Response Filter (FIR and IIR) [142] and Fourier Filters [143]. Researchers have widely used Butterworth [144], Chebyshev [144] and elliptical filters [144] to extract information in a given frequency range. IIR filters

produce a steeper slope for a much lower order than FIR filters but the former filter tends to be more unstable than the latter one.

Spatial filters are used to get a more localized signals corresponding to a single source. Bipolar filters [145], Common Average Referencing filters [146] and Laplacian Filters [145] are commonly used spatial filters found in BCI literature. Bipolar filters determine the voltage difference between two electrode pairs, such as C<sub>3</sub>-C<sub>4</sub>. This technique reduces the effect of spatial smearing and emphasizes on local activity while attenuating the effect of distant sources. In common average referencing, the mean of all EEG electrodes is subtracted from each individual electrodes which reduces the influence of far field sources but may contribute to spatial smearing. More localized signals are determined from Laplacian filtering which removes the influence of neighboring electrodes from an individual one.

Sometimes special techniques such as principal component analysis (PCA) [147], independent component analysis (ICA) [148], common spatial patterns (CSP) [149] and adaptive filters [150] are designed by researchers to perform noise removal from the raw EEG data.

### **1.5.2 EEG Feature Extraction Techniques**

After the brain signals are pre-processed, these are subjected to further processing involving one or more than one feature extraction methods. This step aims at extracting relevant characteristics of the signals corresponding to the different mental states of the user. Feature extraction methods include processing in the time-domain (such as Hjorth parameter [151], Auto-regressive parameter [152]), frequency-domain (such as Power Spectral Density Estimates [153]), spatial-domain (such as Common Spatial Patterns [149]), non-linear-domain (such as Fractal Dimensions [154], Approximate Entropy [155]) and time-frequency-correlated domain (like Discrete Wavelet Transforms [156] and Adaptive Autoregressive Parameters [157]).

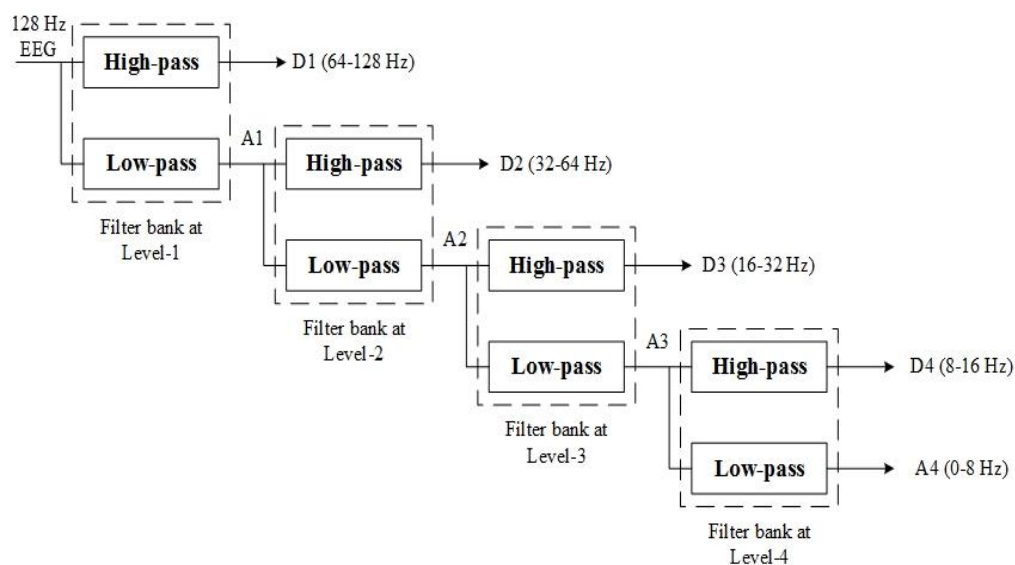
Among the conventional techniques, discrete wavelet transforms and common spatial patterns (CSP) are the most widely used feature extraction techniques employed by BCI researchers across the globe. Several variants, such as, Common Sparse Spectral Spatial Pattern [158], Sub-band CSP (SBCSP) [158], Filter bank CSP (FBCSP) [159], Discriminative FBCSP (DFBCSP) [160], Sliding Window Discriminative CSP [160] are designed to improve the discrimination-ability among various mental states.

Because of the intrinsic non-stationarity of EEG, the discriminative capability of statistical or non-linear features like Hjorth parameter, Auto-regressive parameters are not efficient. On the contrary, non-linear features like Empirical Mode Decomposition [161], Common Spatial Patterns [149], Multi-fractal Detrended Fluctuation Analysis [162] yield good results at the expense of the high computational cost. Thus, researchers are attempting to design an optimal

feature extractor which would exhibit high discriminative capability and low computational complexity. Some of these features are Adaptive Auto-regressive Parameters, time-varying Hjorth Parameters, Extreme Energy Ratio [163] and Extreme Energy Difference [164].

### A. Discrete Wavelet Transform

In the past several years, wavelet transform is proven as one of the well-known feature extraction methods for classifying different cognitive tasks from the acquired EEG signals. Discrete Wavelet Transform (DWT) [156] has its proven merits over techniques based on time-domain (such as, Time domain parameters) or frequency-domain (like Fourier transforms). Standard Frequency based techniques lack the ability to deal with non-stationary signals because of their inability to deal with non-stationary signals. Time-domain parameters are also unable to quantify frequency related information, whereas, Fourier transform is unable to quantify time related information. Besides, Fourier transform misses to identify the local changes in high frequency components since it considers the whole time domain. All the drawbacks are overcome by using discrete wavelet transforms (DWT) by providing localized frequency related information at a given time. The discrete wavelet transforms (DWT) analyzes the signals by decomposing the signal into coarse approximation and detail information. Each level includes two digital filters and two down-samplers by 2. The down-sampled outputs of the first high-pass and low-pass filters provide the detail D1 and approximation A1, respectively. The first approximation is further decomposed and the process is continued, until the desired level of decomposition is obtained. Fig. 1.9 provides the generation of approximation and detail coefficients by DWT, where the detail coefficient indicates alpha and low beta band (8-16 Hz) and the approximation coefficient indicates delta and theta band (0-8 Hz).



**Fig. 1.9** Generation of approximation and detail coefficients by Discrete Wavelet Transform

### B. Power Spectral Density

Power spectral density (PSD) [165], one of the most popular time-domain features, is defined as a mode of describing the power distribution contained in the signal. PSD is used to evaluate the power density for filtered EEG recordings. Typically, a band pass infinite impulse response (IIR) filter having pass band of 0.5-70 Hz (depending of the activation of EEG in the frequency spectrum) is used for pre-processing the raw data before the application of PSD extraction algorithms. PSD finds signal power contained in these frequency ranges by computing Fourier Transform of the autocorrelation sequence of the time series  $eeg(t)$ , which is given in (1.2) and (1.3).

$$EEG(f) = \int_{t_1}^{t_2} eeg(t) e^{-2\pi ft} dt \quad (1.2)$$

$$PSD(f) = 2 \frac{\|EEG(f)\|^2}{(t_2 - t_1)} \quad (1.3)$$

where, time segment  $(t_2-t_1)$  is the duration over which EEG is acquired.

### C. Adaptive Autoregressive Parameters

The time-varying characteristics of autoregressive (AR) parameters can be classically estimated with the help of segmentation based approach [152]. In this approach, the information is divided into short segments and the AR parameters are predicted from each segment. The segment length determines the accuracy of the estimated parameters. Therefore, for the AR model, the shorter the segment length, the higher is the time resolution. However, this may increase error of the AR estimates. To overcome this problem, adaptive autoregressive (AAR) algorithm is used which has the advantage of less computational effort and no buffering. This model has the following form, as given in (1.4):

$$y_k = a_{1,k}y_k + \dots + a_{p,k}y_{k-p} + \varepsilon_k \quad (1.4)$$

Here,  $y_k$  is EEG time series,  $a_{1,k}, \dots, a_{p,k}$  are time-variant autoregressive parameters,  $p$  is the model order and  $\varepsilon_k$  is a noise process. Least mean squares (LMS) [166] and recursive least squares (RLS) [167] are the two popular approaches for estimating AAR parameters. These algorithms are well suited for online analysis due to the advantages of AAR model. AAR models often utilize a Kalman filter algorithm for feature extraction process from the raw EEG data [168], [169]. Usually, two types of evaluation schemes are generally used. First, a cross-validation procedure is implemented on each of the two sessions available for each subject. Second, analysis of the session-to-session transfer process is performed by observing the results from unseen data.

#### D. Hjorth Parameter

The parameters introduced by Hjorth are popularly known as Hjorth parameters, which are time domain parameters, having three features [151], and is defined in (1.5), (1.6) and (1.7).

$$\text{Activity} = \text{var}(x(t)) , \text{ the signal power} \quad (1.5)$$

$$\text{Mobility} = \sqrt{\frac{\text{Activity}\left(\frac{dx(t)}{dt}\right)}{\text{Activity}(x(t))}} , \text{ the mean frequency} \quad (1.6)$$

$$\text{Complexity} = \frac{\text{Mobility}\left(\frac{dx(t)}{dt}\right)}{\text{Mobility}(x(t))} \quad (1.7)$$

The merit of Hjorth parameters lies in checking whether different number of derivatives of the signal can enhance the classification performance and hence, the number of derivatives calculated,  $p$  is needed as parameter of  $p_i$ .

$$p_i(t) = \text{var}\left(\frac{d^i x(t)}{dt^i}\right) , i = 0, \dots, p. \quad (1.8)$$

#### E. Common Spatial Pattern

Common spatial pattern (CSP) is applied to extract useful features from each channel by using a unique projection matrix. CSP aims at finding a linear subspace for which the variance of one projected class is maximized while the variance of the other class is minimized, the rows of the transformed matrix being the indication of the weights of each channel. The formation of the above matrix is made possible by combined diagonalization of two covariance matrices obtained from the two classes of the EEG signals. The normalized covariance matrix of a single trial EEG signal is given by (1.9):

$$R = \frac{XX'}{\text{trace}(XX')} . \quad (1.9)$$

Here,  $X$  is represented as an  $n \times d$  matrix,  $n$  being the number of channels and  $d$  being the number of samples in the time interval of interest. The average of covariance matrices from trials within two classes, i.e., from class  $a$  and class  $b$  is summed to produce a composite covariance matrix, given by (1.10):

$$R_c = R_a + R_b = U_{eg} \sum U_{eg}^T . \quad (1.10)$$

Here,  $U_{eg}$  is the matrix comprising few chosen Eigenvectors ( $U_{eg1}, \dots, U_{egn}$ ) such that when class  $a$  and  $b$  are both projected onto the first Eigenvector  $U_{eg1}$ , then class  $a$  yields the maximal variance and class  $b$  the minimal variance, and when the classes are projected onto the last Eigenvector  $U_{egn}$ , then class  $a$  yields the minimal variance and class  $b$  the maximal variance.  $\Sigma$  is the diagonal matrix. The final projection matrix is given by (1.11):

$$P = \sum^{-1/2} U_{eg}^T \quad (1.11)$$

with average transformed matrices (from  $R_a$  and  $R_b$  respectively):

$$S_a = PR_a P^T \quad \text{and} \quad S_b = PR_b P^T. \quad (1.12)$$

These two matrices  $S_a$  and  $S_b$  shares common Eigenvectors so that the diagonal matrices  $\Sigma_a$  and  $\Sigma_b$  of corresponding matrices are always one.

The projection matrix  $W$  is given as:

$$W = U^T P \quad (1.13)$$

where,  $U$  is a common orthogonal Eigenvectors, and EEG trial is transformed as:

$$Z = WX. \quad (1.14)$$

From Eq. 1.14, we extract CSP features as the variance of  $Z$ , given as:

$$F_m = \text{var}(Z_m) \quad (1.15)$$

where,  $m$  ( $m=1, \dots, 2p$ ) is the reduced dimension of the original signal.

### 1.5.3 EEG Feature and Data-point Selection

The features, sometimes extracted from the filtered EEG, may have high dimensionality, which may result in two major drawbacks: (a) increase in computational overhead of the classifier [170], and (b) poor signal-to-noise ratio [171] of the EEG signal. During the past few decades, researchers have included a feature selection stage before the classification stage [172]-[174]. This stage selects a subset of features from the original feature set having an enhanced discriminative power. Principal Component Analysis (PCA), Maximum Relevance Minimum Redundancy (mRmR) [175], Sequential Forward Search (SFS) [176], Sequential Floating Forward Search (SFFS) [176] are few of the well-known statistical feature selectors used by BCI researchers.

Existing approaches in feature selection suffer from a few major drawbacks. First, sometimes, even if the variances are found good among components, they still provide low classification performance. It may be due to the fact that the feature selection algorithm failed to remove the redundant features. Determination and removal of redundant features is not possible simply by inspection of the feature set. Second, many of the popular feature extraction techniques perform a linear transformation of the original feature set to a vector of low dimensionality for consideration in the classifier stage, because of which the reduced features in most cases become a linear transformation of the original feature set. Therefore, even if the feature set used in the classifier stage is reduced, the original features still need to be measured. Lastly, the optimal number of reduced features to be considered in the classifier stage after dimensions reduction is determined by cumbersome experimental validations. The above problems can be solved by designing an algorithm to choose an optimal set of features from the

original feature set itself and thus cumbersome experimental validations are avoided. For this, a simple run of the optimizer is sufficient, which also optimizes the classifier performance. Selectors based on Differential Evolution (DE) [177], Particle Swarm Optimization (PSO) [178] and Genetic Algorithms (GE) [179] are few of the most frequently used evolutionary techniques in brain-computer interfacing research. Here in subsequent chapters, we design novel feature selection techniques using DE to classify several stimuli or cognitive actions/tasks performed by subject and validate their better performances with respect to traditional feature selection technique.

Besides feature selection, sometimes it is necessary to select one representative data-point or trial from a large set of data-points (trials) in a particular class in order to find stable optimum of that class. For example, in chapter 2, we select class-representatives for various olfactory stimuli to find the stable optima of different smell classes, where input stimuli is fed to a recurrent neural network classifier for olfactory recognition. One way to achieve this is the novel use of traditional feature selection algorithm for data-point selection instead of feature selection.

#### **1.5.4 EEG Classification**

Classification of the acquired brain signals is the most important step in electroencephalographic-based brain computer interfacing (EEG-BCI) system. The output of a classifier is used as control signals to operate an external device. In BCI research, the classification algorithms are used to identify the different brain activity based on their signature features. Before applying the BCI system in the real world, the classifier of the system needs to be trained on the required mental states. Thus, for optimal functioning of the BCI system, the training of the classifier must be optimal. The different types of classifier are available which can be used for BCI research.

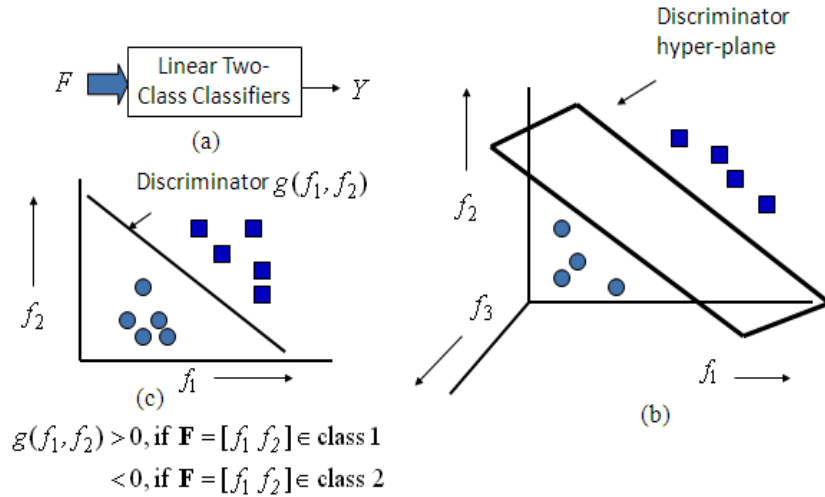
*i. Generative and Discriminative:* Generative classifiers (like Bayes Quadratic) compute the likelihood of each class and select the most likely one based on a criterion. Discriminative classifier (such as, Support Vector Machines) learns the class membership of each class to decode a feature vector directly.

*ii. Static and Dynamic:* Static classifiers (like Multilayer Perceptrons) classify only a single feature vector and cannot take into the temporal information of the incoming signal. Dynamic classifiers (such as, Hidden Markov Model) can work on the temporal dynamics of the system and thus, can classify a sequence of feature vectors.

*iii. Stable and Unstable:* Stable classifiers (like Linear Discriminant Analysis) are those whose performances are not affected small variation in the training set and thus, they have low complexity. Unstable classifiers (such as, Multilayer Perceptron) have high complexity and their performance is affected by small variations in the training set.

iv. *Regularized*: Regularized classifier control the complexity of the classifier and thus, prevents overtraining in the process. It has a good generalization performance and is more robust as compared to the standard classifiers.

A number of classifiers have been used in BCI research and. In practice, we are more familiar in selecting suitable classifiers for classifying EEG features in two or more classes that are linear or non-linearly separable. Linear two-class classification can be best explained from Fig. 1.10 as shown below.



**Fig. 1.10** Linear two-class classification scheme

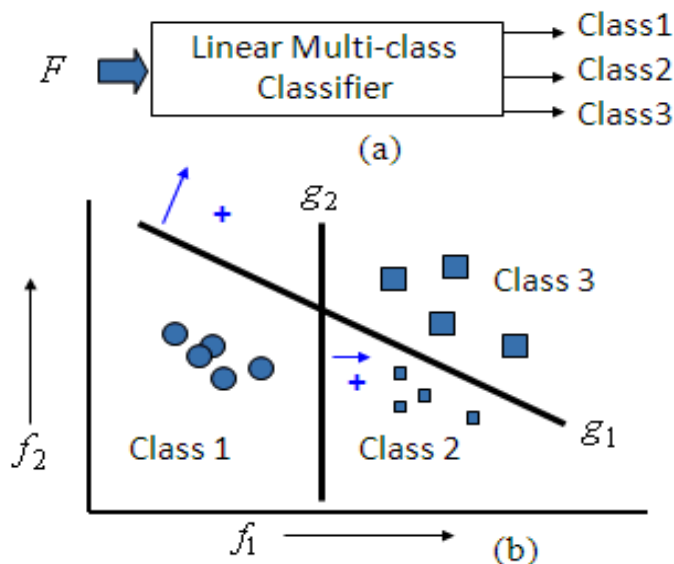
Fig. 1.10(a) shows basic building block of two-class classification problem, where,  $F$  is the input feature vector and  $Y$  is the output score. The decision boundary between two classes here forms a hyper-plane in the high-dimensional input space, where points (in blue squares) lying in the positive side of hyper-plane are classified as class 1, while points (in blue dots) lying in the negative side are classified as class 2 (Fig. 1.10(b)). In fig. 1.10(c), discriminator  $g(f_1, f_2)$  clearly separates both the classes (i.e., points in blue dots and points in blue squares) at its furthest.

On the contrary, linear multiclass classification (See fig. 1.11(a)) involves a classification problem with more than two classes, where each sample lies in one and only one class. Linear multiclass classification forms a hyper-plane or set of hyper-planes in a high dimensional space (Fig. 1.11(b)), whereas better separation is achieved by the hyper-plane that has the largest distance to the nearest training data-point of any class. Some popular linear multi-class classification techniques are linear Discriminant analysis, multivariate linear regression analysis, multiple logistic regression, support vector machines, and perceptron model.

Besides linear classification of two or more class classification, non-linear classification involves classification of data-points that are not linearly separable. Fig 1.12 (a) and (b) presents the basic architecture of non-linear classifiers and its non-linear decision boundaries

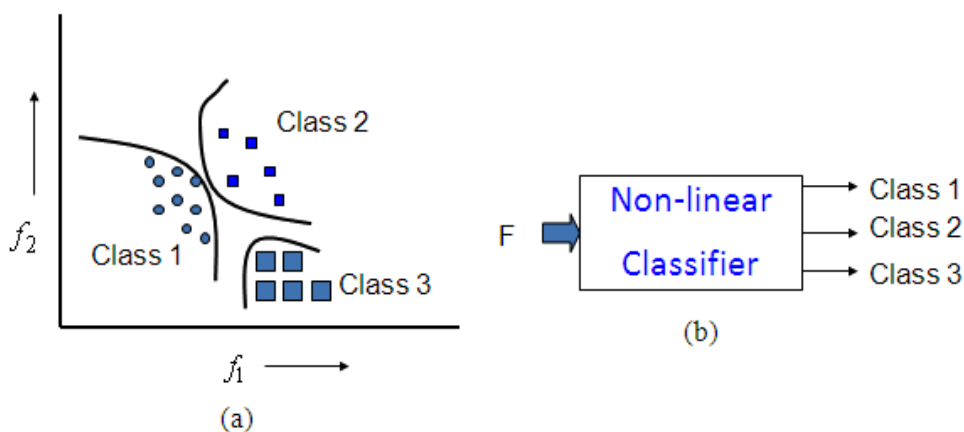


for a three-class classification problem. Now, this section provides a brief summary of few linear and non-linear classifiers often used for cognitive task classification in subsequent chapters.



If  $g_1(f_1, f_2) < 0$  and  $g_2(f_1, f_2) < 0$ , then  $\mathbf{F} = [f_1 \ f_2] \in \text{class 1}$ .  
 If  $g_1(f_1, f_2) < 0$  and  $g_2(f_1, f_2) > 0$ , then  $\mathbf{F} = [f_1 \ f_2] \in \text{class 2}$ .  
 If  $g_1(f_1, f_2) > 0$  and  $g_2(f_1, f_2) > 0$ , then  $\mathbf{F} = [f_1 \ f_2] \in \text{class 3}$ .

**Fig. 1.11** Linear multi-class classification scheme



**Fig. 1.12** Non-linear multi-class classification scheme

### A. Fisher's Linear Discriminant Analysis (FLDA)

Linear discriminant analysis (LDA) [180] aims at separating the data representing different classes by constructing a hyperplane. The class of an observation depends on which side of the hyperplane the feature vector falls. The separating hyperplane is a projection that maximizes the distance between two class means and minimizes the inter-class variance by

assuming normal distribution of a data with equal covariance matrix for all classes.

This technique is suitable for an online BCI system for its simplicity in algorithm and low computational speed. It is successfully used several motor imagery based BCI problems and BCI speller. The main disadvantage of LDA classifier lies in poor while dealing with non-stationary nature of the EEG signal.

For FLDA classification technique, let,  $X_i = \{X_1, X_2, \dots, X_n\}$  be the set of  $n$  data-points having  $m$  dimensions for  $i$ -th trial, representing a specific cognitive task and  $\mu_i$  be the mean of the data-points for the same task. For two-class classification, Fisher's criterion, as given in (1.16) for an unknown weight vector  $\mathbf{W}$  needs to be maximized.

$$z = \frac{(\mathbf{W}^T S_b \mathbf{W})}{(\mathbf{W}^T S_w \mathbf{W})} \quad (1.16)$$

Here,  $S_b = (\mu_1 - \mu_2)(\mu_1 - \mu_2)^T$  is *between-class scatter matrix* and

$$S_w = Cov_1 + Cov_2 \text{ is } \textit{within-class scatter matrix}.$$

It is important to mention here that scatter matrices are proportional to covariance matrices, which are given in (1.17) and (1.18).

$$\text{Covariance matrices } Cov_1 = E[(X_1 - \mu_1)(X_1 - \mu_1)^T] \quad (1.17)$$

$$\text{and } Cov_2 = E[(X_2 - \mu_2)(X_2 - \mu_2)^T] \quad (1.18)$$

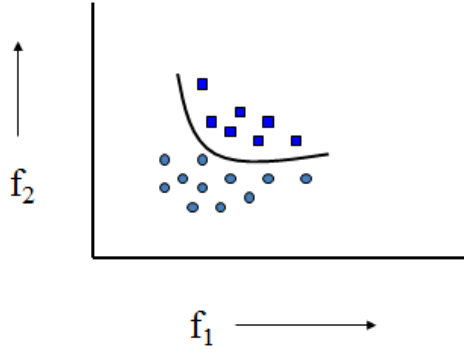
Solving the above equations using linear algebra, we obtain optimal solution of  $\mathbf{W}$ , as given in (1.19).

$$\mathbf{W} = S_w^{-1} (\mu_1 - \mu_2) \quad (1.19)$$

### B. Quadratic Discriminant Analysis (QDA)

QDA classifier is referred to as the closest cousin of the well-known FLDA [181]. The only difference between these two is FLDA can learn only linear boundaries, whereas QDA can learn quadratic boundaries, and hence much more flexible, which is presented in Fig. 1.13. For QDA, separate covariance matrix needs to be estimated for different classes. Although QDA minimizes the misclassification rate, it is not as widely used as LDA. The requirement of much larger training sets may be one of the reasons. The quadratic discriminant function is given by (1.20).

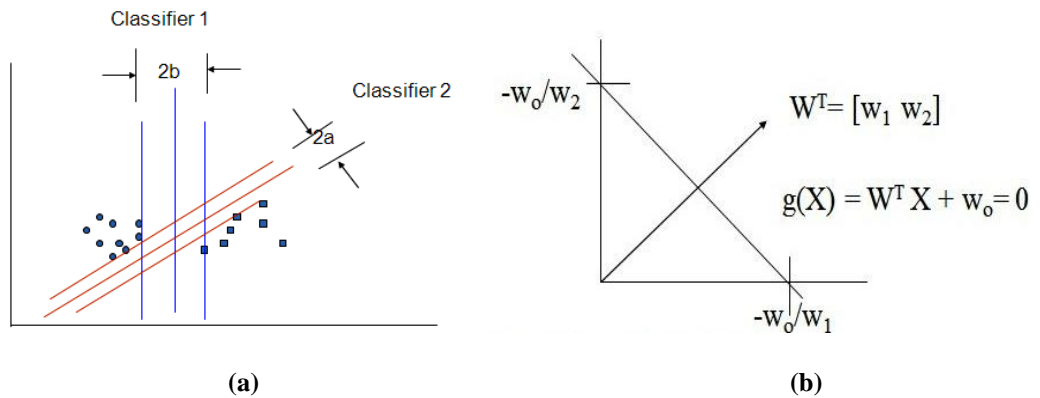
$$g(F) = F^T \mathbf{W} F + w' F + w_0 \quad (1.20)$$



**Fig. 1.13** Design of hyper-plane for Quadratic discriminant analysis classifier

### C. Support Vector Machine (SVM)

An SVM [182], similar to FLDA is one of the most widely used classifiers in BCI research. To classify EEG features using SVM, along with the construction of an optimized hyperplane, two separate margins are also required on both sides of the hyperplane (Fig. 1.14) from the nearest training points, which is known as support vectors. Maximizing this margin increases the generalization capability of the classifier and a regularization parameter allows error on the training set. Literature reveals that the performance of SVM classifier is insensitive to overtraining and curse-of-dimensionality for its good generalization property. Usually, a linear decision boundary enables the SVM to perform classification and it provides good performance while decoding mental states in BCI problem. For any two data-points  $X_1$  and  $X_2$ , SVM holds the relation, which is given in (1.21) and (1.22).



**Fig. 1.14** (a) Design of hyper-plane for Support vector machine classifier (b) Estimation of weight vector  $\mathbf{W}$

$$\mathbf{W}^T X_1 + w_0 = \mathbf{W}^T X_2 + w_0 = 0 \quad (1.21)$$

$$\text{or, } \mathbf{W}^T (X_1 - X_2) = 0 \quad (1.22)$$

Eqn. (1.22) indicates the condition for  $\mathbf{W}$  to be orthogonal to the hyper-plane as

$(X_1 - X_2)$  is along the plane. Our goal in SVM classifier is to determine its weights so as to maximize the margin. This is done to obtain  $\mathbf{W}$  so as to:

Minimize  $J(\mathbf{W}, w_0) = \frac{1}{2} \|\mathbf{W}\|^2$ , subject to

$$y_i(\mathbf{W}^T X_i + w_0) \geq 1, i = 1, 2.$$

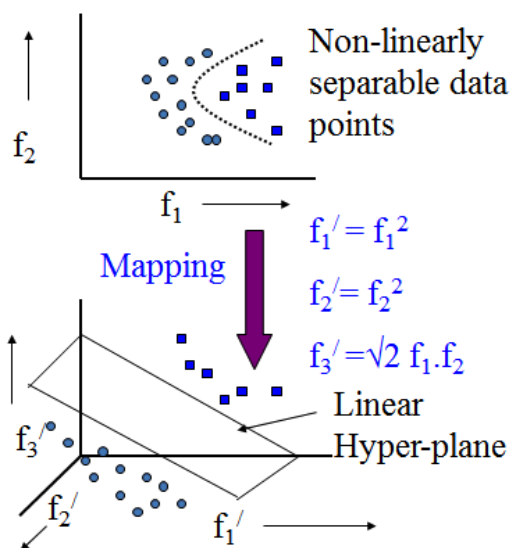
where,

$y_i = 1$  for data point lying above the hyper-plane

$= -1$  for data points below the hyper-plane.

This can be solved using Lagrange multiplier technique [183].

One can also employ non-linear decision boundaries by using kernel functions such as, Radial Basis Function (RBF), Multi-layered Perceptron (MLP), Polynomial and Quadratic functions. In Kernelized SVM, a Kernel function is used to map linearly non-separable data points into a high dimension using a Kernel function to make the mapped data points linearly separable, which is depicted in Fig. 1.15. For a mapping function  $\Phi(X)$ , it can be shown that,  $\Phi^T(X_i) \Phi^T(X_j) = K(X_i, X_j)$ , where,  $K$  being the kernel. In this way, the computation involved in  $\Phi^T(X_i) \Phi^T(X_j)$  is reduced.

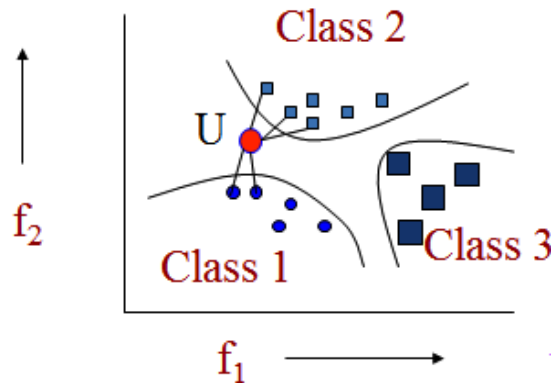


**Fig. 1.15** Mapping of linearly non-separable data-points using Kernel function

#### D. *k*-Nearest Neighbor (*k*-NN)

*k*-NN [184] is a non-parametric classifier, which refers to one of the simplest classifiers available in pattern recognition, machine learning and BCI research.

Here, all feature vectors from the training set are plotted in a feature space. A feature vector belonging to the test data is classified according to the class of majority of  $k$ -nearest neighbors located in the feature space. The performance of this classifier depends on the distance metric and the  $k$ -parameter, which controls the volume of the neighborhood. Euclidean distance metric is the most common distance function among the BCI researchers. Fig. 1.16 provides an example of  $k$ -NN classification of EEG features, where, number of classes is three.



**Fig. 1.16**  $k$ -NN classification of feature vectors in three classes

The algorithm of  $k$ -NN classifier is presented below.

1. Identifying  $k$ -nearest neighbors of the unknown data-point  $U$  (training instance) out of  $N$  data-points, regardless of the class labels.
2. Identifying the number of nearest neighbors  $k_i$  falling in class  $i$ , for  $i=1$  to  $M$  classes (here,  $M=3$ ).
3. Assigning the unknown data-point  $U$  to the class  $C_i$  having the maximum number of  $k_i$  samples.

Therefore, from Fig. 1.15, it can be concluded that  $U$  falls in class 2, since  $k_1=2$ ,  $k_2=3$  and  $k_3=0$ .

Although  $k$ -NN provides fair classification accuracy in comparison with multi-layer perceptron (MLP) and SVM, it is not as popular as MLP and SVM in the BCI community for its high sensitivity to curse of dimensionality [185], and hence it fails during the realization of real-time BCI problems. Further, it is highly susceptible to changes in the local distribution of feature vectors, which too makes it unsuitable for EEG problems.

#### *E. Multi-Layer Perceptron (MLP)*

An MLP is made of several layers of neurons, which are i) an input layer, ii) one or several hidden layers, and iii) an output layer. The input of each neuron is connected with the output of the previous layer's neuron [186]. The input and output nodes have linear activation functions, whereas each hidden unit node has non-linear activation functions. Besides, the

input node has no threshold, whereas each hidden node and output node have thresholds in addition to the weights associated with them. These classifiers are universal approximator, which means that they can approximate any continuous function provided they are supplied with enough neurons and layers. Further, they can classify any number of classes, which makes it very flexible for multi-class problems.

MLPs have been widely used for binary [187] and multiclass [188], [189] and synchronous [190] and asynchronous [191] BCI problems. These classifiers are sensitive to overtraining, especially for noisy and non-stationary data like EEG. Therefore, careful regularization and architecture selection is required.

#### *F. Hidden Markov Model (HMM)*

An HMM [191] is a well-known dynamic classifier which provides the probability of observing a given sequence of feature vectors and is often used for time-series [192], text [193] and speech [192] classification problems. Each state of the classifier can construct a model of observation for each feature vector. In BCI research, Gaussian Mixture Models are generally used for estimating the probability. HMM finds acceptance in BCI research because it can be applied to the classification of temporal sequence of BCI features, even classifying from raw EEG data.

For BCI research, a variant of HMM known as Input-Output HMM (IOHMM) [191] has been designed. The main advantage of this classifier is that one IOHMM can discriminate between various classes, whereas in the conventional method, one HMM is required for each class to achieve the same operation.

#### *G. Naïve Bayes Classifier*

The Naïve Bayes classifier assigns the most likely class labels to problem instances, represented as feature vectors [194], where the class labels are derived from some finite set. It works with the principle that each feature-value of a particular data-point is independent of other feature-values, and for this data-point to belong to a class, the contribution of each feature-value independently is considered by the classifier, regardless of any possible correlation of all feature-values. The algorithm is explained below.

Let,

$F = [f_1 f_2 f_3 \dots f_n]$  be the feature vector, where  $f_i$  lies in  $\{0,1\}$ , and

$C_i$  = Cognitive task for class  $i$ .

Then, by Bayes theorem, the probability

$P(C_i|F)$

$$\begin{aligned}
&= P(F | C_i) \cdot P(C_i) \\
&= P(f_1, f_2, \dots, f_n | C_i) \cdot P(C_i) \\
&= P(f_1 | C_i) \cdot P(f_2 | C_i) \dots P(f_n | C_i) \cdot P(C_i) \\
&= \prod_{i=1}^m p_i^{f_i} (1 - p_i)^{1 - f_i} \cdot P(C_i), \text{ where } p_i = P(f_i | C_i)
\end{aligned} \tag{1.23}$$

Similarly for class  $j$ ,

$$P(C_j | F) = \prod_{i=1}^m q_i^{f_i} (1 - q_i)^{1 - f_i} \cdot P(C_j), \text{ where } q_i = P(f_i | C_j) \tag{1.24}$$

Discriminator:

$$\begin{aligned}
g(F) &= \ln\{P(C_i | F) | P(C_j | F)\} \\
&= \sum_{i=1}^m \{f_i \ln(p_i | q_i) + (1 - f_i) \ln\{(1 - p_i) | (1 - q_i)\} + \ln\{P(C_i) | P(C_j)\}\}
\end{aligned} \tag{1.25}$$

Comparing,  $g(F) = \mathbf{W}^T X + w_0$  with above, we obtain  $W = [w_1 \ w_2 \ \dots \ w_m]$ .

## 1.6 PERFORMANCE ANALYSIS IN EEG-BCI RESEARCH

The performance of a EEG-BCI system is analyzed using a number of performance metrics. This section discusses on few of them, which are frequently used in the subsequent chapters.

*i. Confusion Matrix:* The confusion matrix is a tabular representation which the relationship between the desired class intended by the user and the actual classes predicted by the classifier [195], [196].

*ii. Classification Accuracy:* It is the most widely used evaluation criterion in BCI research because it is easy to calculate and interpret. It is defined as the ratio of the number of correct observations made by the classifier to the total number of observations [197].

*iii. Type-I and Type-II Error Rate:* A type I error ( $\alpha$ ) represents the rate of incorrect rejection of a true null hypothesis, and hence known as false positive rate. The error of the second kind, i.e., a type II error ( $\beta$ ) refers to the rate of failure to reject a false null hypothesis., and hence known as false negative rate [198].

*iv. Information Transfer Rate:* Information Transfer Rate ( $B_t$ ) represents the bit rate of the BCI system [199]. Its representation in bits/min is given as

$$B_t = \left( \log_2 N + P \log_2 P + (1 - P) \log_2 \frac{1 - P}{N - 1} \right) \times \frac{60}{T} \tag{1.1}$$

where,  $N$  represents the number of possible states and  $P$  represents the classification accuracy between 0 and 1.  $T$  is the time needed to convey each action in second/symbol i.e., time interval from the issue of a command to the classified output of the same.

v. *Statistical Hypothesis Testing*: Statistical hypothesis testing [198] is required to ensure that the experimental data are correctly interpreted; the apparent relationship between them is significant or meaningful and does not occur by chance. There exist a number of well-known statistical tests, which can be classified into four main categories namely, i) correlational (such as, Pearson correlation [200] and Spearman correlation [201]), ii) comparison of means (such as, Paired t-test [201] and ANNOVA [202]), iii) regression [201] (such as, Simple regression and Multiple regression) and non-parametric (such as, McNemar's test [203], Friedman's test [204], Wilcoxon rank-sum test [205] and Wilcoxon signed-rank test [206]). The selection of right statistical test depends on the type of data, distribution of data, and number of data-points and observations available.

## **1.7 Current Research Directions in Sensory-Perception, Motor Imagery and Alertness**

In this section, we describe current research directions undertaken by BCI researchers in recent years to decode sensory perception, motor imagery tasks and alertness.

### **1.7.1 Decoding of Sensory-Perception**

In recent years, decoding of sensory perception has become an interesting research arena in BCI domain. Researchers showed keen interest to explore the perceived response using various sensory modality including vision, audio, touch and olfactory and also the involvement of fronto-parietal brain regions in mediating conscious sensory experience. The previous research in decoding sensory perception also helps to study whether there exists any neural correlation between two modalities for similar conscious perception. Hovland and McCarragher in [207] propose a new method for controlling sensory perception, which is based on stochastic dynamic programming and is set in a discrete event control framework. First, the dynamic programming evaluates all possible orderings of process monitors, which are then stored in a lookup table. Later, this look-up table is used by a real-time sensory perception controller (SPC), which increases the average recognition rate while keeping the average monitoring cost low. The process of controlling sensory perception has two primary objectives: 1) collection of perceptual information to identify discrete events with high levels of confidence and 2) keeping the sensing costs low. The authors in [208] demonstrated two applications including robotic assembly and mobile navigation, which prove the benefits of sensory perception control. In [209], authors address the problem of controlling sensory input and perception for mobile navigation application, and also propose solutions that offer several advantages compared to existing methods in the literature. This includes design of a i) real-time SPC by solving a constrained optimization approach, ii) unique task-independent discrete event model of mobile navigation for a wide range of navigation problems and iii) unique approach to online discrete event identification.



Ishikawa *et al.* in [210] addresses certain possible clues for sensory perception of an unexpected sudden change in floor level during human gait. It can be discrepancies in the time of heel contact, location of force application point or center of pressure in the sole at the heel contact and subsequent stance period from the ones prescribed prior to the gait execution prepared for the normal level gait, if they exist. Participants are asked to perform a psychophysical experiment during gait on a walk with a small, unexpected and sudden change in the floor level in order to get insight for this perception mechanism. The subjects here are instructed to answer among step-down, flat, and step-up immediately after the walk. During the gait, the measured foot pressure distribution (FPD), electromyogram (EMG) of the ankle muscles, and gait trajectory (GT) quantify accuracy of the perception.

Kerren *et al.* in [211] conduct a different perception-based experiment on a wide range of wines from different parts of the worlds. This research involves interactive visualization techniques that help in linguistic exploration and comparisons of visual, olfactory, gustatory and textual properties of all the different wines from different grape varieties, or from different vintages. It also supports the immediate creation of visual profiles for descriptions of sensory perceptions for exploratory purposes as well as for purposes of confirmatory investigations of linguistic patterns in text and discourse and their correlations to metadata variables.

The spatio-temporal oscillations in EEG signals are proven as an indicative measure of sensory and cognitive processing. Brockmeier *et al.* in [212] propose a method that aims at determining the spatial amplitude patterns of a time-limited waveform across multiple EEG channels. It includes a single iteration of multichannel matching pursuit, where the base waveform is obtained via the Hilbert transform of a time-limited tone. The vector of extracted amplitudes across channels is utilized for classification, from which the effect of deviation in temporal alignment of the waveform on classification performance is analyzed. The result of the proposed method is found comparable with existing result for a previously published dataset.

Recent research [213] suggested by Mathias *et al.* confirm the strong interrelation between perception and action. The findings also reveal that here is an evidence for distinct time courses of sensory, schematic, and motoric influences within the same recognition task and association between auditory-motor responses to out-of-key pitches. The skilled pianists are given a set of novel melodies to investigate the role of motor experience in auditory memory recognition processes. EEG signals are recorded during an auditory memory recognition test with or without an out-of-key pitch alteration. A comparatively larger N2 ERP component is elicited with each altered pitch in comparison to the original pitches from the cortical motor planning regions. Early sensory (N1) and later cognitive (P3a) components are also elicited which gives a prediction of sensory echoic and schematic tonality models, respectively.

Vecchiato *et al.* in [214] during music perception, further attempt to investigate the similarity between cerebral signs of pleasantness in healthy child and in monolateral and/or bilateral cochlear implanted users. Experiments reveal significant differences in cortical activities in alpha band between a healthy child and the patients during the fruition of a musical cartoon. In particular, the alpha EEG asymmetry patterns observed in a healthy child and that of a bilateral cochlear implanted patient are congruent with the approach-withdrawal theory, which states that there exist correlation between variations of the frontal EEG alpha activity and the perceived pleasantness of the sensory stimulation received. For a monolateral cochlear implanted patient, the difference of scalp topographic distribution of EEG power spectra in the alpha band from that of the healthy child or bilateral cochlear implanted patient confirms that the former perceives the music in a less pleasant way when compared to the later ones.

Khasnobish *et al.* in [215] uses tactile stimulus, visuo-tactile stimulus, as well as audio-tactile stimulus separately to study the basis of object shape recognition from EEG signals acquired from the scalp of the human brain. Adaptive auto-regressive parameters with different model orders and power spectral density are selected as EEG features for classification, where Support Vector Machine classifier with Radial Basis Function kernel is used to recognize ten different object shapes. The classifier performance is evaluated in terms of classification accuracy, sensitivity, specificity and computation times where, the average recognition rate of 88.02% over all features is indicated in [215].

A lot of research has been performed to advance technologies that can improve spatial perception of blind and partially sighted persons. Twardon *et al.* in [216] attempt a common approach to enhance or substitute vision by audition with a proposed system for gaze-contingent auditory substitution of spatial vision. It helps immensely to a visually impaired mobile helper in his everyday life. The prototype of the proposed system includes the combination of eye-tracking with depth measuring and sonification techniques. EEG experiments reveal that as a result of neuroplasticity, the blind and visually impaired persons might learn to perceive gaze-dependent sound visually, since gaze-contingent sensory substitution is found to permit depth perception, which leads to intermodal (audio-visual) processing in untrained subjects.

Chaumon and Busch in [217] record EEG signals while participants performed a visual detection task with stimuli having different contrast intensities. The authors aim at comparing psychometric functions obtained under different levels of ongoing alpha power and evaluating the inhibitory effect of ongoing alpha oscillations in terms of contrast or response gain models. The experiments undertaken reveal a number of interesting observations. First, the ongoing alpha activity affects subject's visual performance. Second, there exist strong pre-

stimulus occipital alpha oscillations, however, not so strong anterior mu oscillations. Lastly, the performance is reduced for the highest intensity-based stimuli.

### 1.7.2 Decoding of Motor Imagery

Motor imagery, as mentioned earlier, is one of the most widely researched brain signals among BCI researchers. Cososchi *et al.* in [218] propose an approach that uses self-organizing fuzzy neural network based time series predictor to classify between left and right motor imagery. A single fuzzy neural network is used for each electrode to extract their corresponding features in time domain. Features are constructed from the mean squared error of the predictions by means of a sliding window. The architecture of the two-organizing fuzzy neural networks is composed of multiple inputs and a single output. The reasoning behind the usage of an auto-organizing fuzzy neural network is that it can adapt itself to each individual's EEG signals with very little prior knowledge of the subject or parameter selection. The algorithm is designed to perform in real-time environment where continuous learning and continuous adaptation of the dynamics of each individual's EEG is present. The algorithm was tested on 300 trials obtained from two subjects and an accuracy of more than 75% was obtained in approximately 3-4 seconds.

Zhou *et al.* in [219] aims at developing a wavelet packet-based independent component analysis (WPICA) to extract the ERD/ERS patterns from different frequency bands during complex lower limb movement imagery. In WPICA processing no imaginary part appears that removes the effect of frequency permutation. It also transforms the original signal into sparse distribution, which emphasizes on the non-Gaussian nature of the observed signal. In this study, EEG data are recorded during three complex imagery movements, which are, standing up and left/right movement combined with homolateral hand movement. Then, the independent components of each characteristic frequency band are extracted by WPICA and the principal ones containing the most ERD/ERS information are projected back to the time-frequency domain of its corresponding electrodes. The proposed technique is tested on 10 subjects and an accuracy of about 80% is obtained for WPICA, which is higher than the traditional ICA method (72.3%) and non-spatial filtering condition (68.34%). This method is an effective technique to recognize ERD/ERS patterns and it improves the pattern classification performance of complex mental tasks.

Corralejo *et al.* in [220] use Genetic Algorithm as a feature selection method to classify between two classes of motor imagery data. The features used in this study are a combination of spectral features, continuous wavelet transform using Morlet mother wavelet, discrete wavelet transform, autoregressive model and  $\mu$  rhythm matched filter. From this large set of features, the best relevant set is selected using Genetic Algorithm. The proposed technique was applied to the dataset IIB of the BCI competition IV and it achieved a kappa coefficient of

0.613.

Common Spatial Pattern (CSP) is well suited to discriminate mental states characterized by ERD/ERS patterns. Several variants of CSP have come forward for extracting discriminative patterns from the EEG. In one approach [149], time delay embedding is utilized in order to extend the CSP algorithm to the state space. This form of CSP has been seen to outperform the classical CSP in classification accuracy as well as its generalization ability. Another algorithm uses incremental learning method for adaptive computation of CSP [221]. This rule extracts the first CSP component and minor components are estimated using an online deflation procedure. This method has lower computational cost compared to retraining the whole data, and makes it more suitable for development of online BCI system. Sub-band CSP (SBCSP) uses a fixed filter bank of 9 equal bandwidth Chebyshev type 2 IIR filter on the EEG signal followed by CSP feature extraction on each frequency bands [222]. Filter bank CSP (FBCSP) was proposed to select the best frequency bands by computing the mutual information between the CSP features with the class label [160]. The Discriminative FBCSP (DFBCSP) [160] was proposed to obtain subject specific discriminative FB based on comparing the fisher ratio of filtered EEG signal from channels C3 or C4. The Sliding Window Discriminative CSP (SWDCSP) filters the raw EEG data at a set of overlapping frequency bands using sliding window and then uses an unsupervised algorithm called affinity propagation (AP) to select discriminative feature set [160].

Liyanage *et al.* in [223] devised an Evolutionary Artificial Neural Network (EANN) for classification of motor imagery signals. Genetic Algorithm (GA) and Particle Swarm Optimization (PSO) were used to evolve the architecture of the ANN by tuning their parameters in this study. CSP is selected as a feature vector and the PSO based approach showed a reduction of 28% in the execution time when compared to the classical approach and an average of 78% accuracy was obtained, which was comparable to the best result while using the classical approach. Khushaba *et al.* in [224] proposed a Differential Evolution (DE) based feature selection (FS) technique which outperformed GA and PSO based FS technique. It was also seen that DEFS required smaller memory and yielded a reduced computational cost.

In the works of Wang and Makeig [225], the EEG information generated in the parietal cortex was derived in the form of subject-specific time- and frequency-domain parameters. To optimize the latency and frequency, a sliding window was used and then a low pass filter was used to extract the frequency components. Then the normalized amplitudes were selected for each time window. The feature vector was concatenated and then used as input in a SVM classifier using RBF as a kernel. The resulting classification was found to be 80.25%.

In a study carried out by Pfurtscheller et al [226], a Linear Vector Quantization (LVQ) was used for online classification. The features that were taken for the classifier were extracted

from a 1 sec epoch from two channels, four band power estimates, each representing a time interval of 250 ms, per EEG channel and frequency range. Based on these 16 features per trial, the LVQ classifier derives a classification plus a measure that describes the certainty of this classification. The result for the online classification varied from 10% to 38.12% error, the mean being 21.9% +/-6.40.

Obermaier *et al.* in [227] employed two HMMs, one to represent left motor imagery and the other right motor imagery as classifiers. They were trained using the trials recorded during their corresponding motor imagery. Hjorth Parameters were used as feature vector set in this case. In another work by Lee *et al.* [228], two methods of classification were studied: 1) PCA + HMM (HMM1), and 2) PCA+HMM+SVM (HMM2). It is observed that HMM1 had an accuracy of 75.70% using PCA while an accuracy of 60.63% was obtained for the raw data. Similar increase was obtained for HMM2 whereas it also had higher accuracy to HMM1. Thus, hybrid classifiers are also possible for classification of motor imagery.

Recently, Lu *et al.* in [229] propose a novel deep learning scheme based on restricted Boltzmann machine (RBM) for motor imagery tasks, particularly control of prosthetic limb movement. Frequency domain representations of EEG signals obtained from fast Fourier transform (FFT) and wavelet package decomposition (WPD) are considered as features and used to train three RBMs. These RBMs along with an extra output layer are stacked up to form a four-layer neural network, called the frequential deep belief network (FDBN). The softmax regression is used by the output layer for classification, whereas the conjugate gradient method and back-propagation algorithm are applied to fine tune the FDBN. Experiments undertaken on public benchmark datasets reveal the significant outperformance of FDBN over other selected state-of-the-art methods.

### 1.7.3 Decoding of Alertness

Decoding of alertness in BCI-EEG domain has always been an interesting research topic, particularly in mental state classification [230]-[ ]. Classification of mental states of a person, more specifically, of a driver during driving is very crucial, since driving for longer hours may cause fatigue and drowsiness. Therefore, a few significant researches on estimating human alertness is presented here, since it relates to our very own problem of cognitive failure detection in driving, as presented in chapter 3. To estimate human alertness, researchers have taken keen interest to design EEG-based monitoring system that can estimate human alertness. One such effort has taken by Jung *et al.* in [230], where authors have shown that EEG signals, after acquiring from the scalp of human brain and processing through a combination of power spectrum estimation, PCA and artificial neural network, can estimate human alertness in real-time. Auditory task is proven a significant stimulus in this case [230], [231], using which changes in normalized EEG cross-spectrum in conjunction with feed-forward neural network,

are also used in monitoring alertness. Further, research reveals that the loss of alertness during auditory detection task is highly associated with the extent, topography and frequency content of spectral coherence in several frequency bands and EEG channel pairs [231]. Begum *et al.* in [232] aims at designing a real-time alarm system to alert about one's mental states by classifying EEG-wavelet features using a neuro-fuzzy classifier. Besides neuro-fuzzy approach, Vezard *et al.* in [233] utilize a CSP-coupled LDA classifier to decode the mental alertness, while EEG signal is acquired from optimally selected EEG electrodes using Genetic algorithm. Fusion-based approach is also taken care to quantify the level of alertness during various cognitive tasks. Sengupta *et al.* in [234] attempts to fuse the information from EEG signal, high-speed image sequence and speech data in order to compute a metric that can indicate the level of alertness. The performance of the proposed system has been validated by using standard neuro-physiological tests including visual response test (VRT), auditory response test (ART), letter counting (LC) and stroop test; and also by using standard statistical measures such as multivariate linear regression and ANOVA. Car and flight simulators are also significantly used by researchers to experimentally monitor and provide the solutions to the lack of mental alertness for car-drivers and flight operators [235], [236].

## **1.8 SCOPE OF THE THESIS**

The thesis includes five chapters. Chapter 1 provides a thorough review of the EEG-based research undertaken on perception. It begins with a definition of perception and perceptual-ability and also explores different brain signaling/ imaging techniques including EEG, PET, fMRI and fNIRs. The chapter also covers well-known brain signals and their association with different cognitive processes. Special emphasis is given to single and multi-modal BCI problems. The later part of the chapter deals with standard techniques of problem-solving, such as pre-processing and artifact removal, feature extraction, feature selection and classification. Next the chapter provides a discussion on the current research directions associated with the problems undertaken in the thesis. The scope of the thesis is also appended at the end of the chapter.

Chapter 2, 3 and 4 are original contributions of the thesis. Here, the candidate provides three distinct problems in perception engineering and offers solutions to these problems by extending the traditional techniques of pattern recognition. Although the problems have their own diversity, the commonality of the problems lies in utilizing and extending computational intelligence techniques adopted for pattern recognition. The other common aspect of the problems undertaken and the approaches adopted include that the analysis of all the problems are performed in real time. Naturally, time required for execution of the algorithms here play a vital role for their amenability in real world systems.

Chapter 2 addresses one interesting problem on olfactory perceptual-ability detection of human subjects, where the motivation is to detect the individual perceptual-ability of the subject and rank them in descending order. These subjective ranks offer the user the relative merits in decoding aromatic substance. Traditional supervised learning techniques, such as support vector machines (SVMs), back-propagation learning etc. could have been used to solve the problem. However, the existing techniques are appropriate for small class size and thus unsuitable for the present application, requiring large (over 10) class-size, and that too in real time. To alleviate the present problem, we employed a Hopfield-like recurrent neural classifier, the stability of which is ensured at multiple optima of a selected Lyapunov energy surface. In the classification of aromatic stimuli from the pre-frontal EEG response of a subject, we first need to map the EEG-features of the individual olfactory stimulus to one of the local optima in the Lyapunov energy function of the energy-surface. This mapping is done automatically by the selection of the weight matrix of the Hopfield-like dynamics with an aim to minimize the selected Lyapunov energy function for the dynamics. In the present context, we develop an alternative formulation, where a multi-modal high dimensional Rastrigin function is used as the Lyapunov energy surface. Thus for the selected energy surface, we construct a Hopfield-like dynamics, which essentially ensures mapping of the olfactory stimuli to the local optima.

Once the weight matrix of the Hopfield dynamics is ready, we can use it as a classifier. This is done in a tricky way. Suppose we measure the feature vector of an unknown olfactory stimulus. The feature vector is mapped onto the Lyapunov energy surface. We initialize the Hopfield-like dynamics at the mapped location of the energy surface, and solve the differential equation until it converges at one of the nearest optima. Since each optimum is earmarked with one smell class, we declare the smell class associated with the optimum as the target class. Experiments undertaken confirm that the proposed technique of classifying olfactory perceptual-ability of subjects outperforms traditional techniques by a good margin.

Existing literature in driving primarily focuses attention to physiological aspects of the drivers and the failures related to gestural/postural aspects in driving. However, online detection of cognitive failures from the brain signals is yet a virgin arena of research in traffic engineering. The thesis introduced an interesting approach to design a set-up for on-line cognitive failure detection of the drivers from three fundamental aspects. These are i) visual alertness failure detection, ii) motor planning failure detection and iii) motor-execution failure detection.

In Chapter 3, the candidate proposes a novel scheme of cognitive failure detection in driving using brain signals. Although there exists different types of cognitive inability responsible for driving failures, we here adopt three possible cognitive failures, called visual attention failures (VAF), motor planning failures (MPF) and motor execution failures (MEF).

VAF refers to cognitive failures due to lack of visual perception. Primarily, in driving context, visual attention failure takes place when the driver is not visually attentive. In case the driver is visually attentive, we test any possible failure in motor planning by the subject. The failures involved in motor planning include possible mistakes in executing braking, acceleration and/or steering control. Occasionally it is noticed that the driver planned his motor activities correctly and timely but failed in executing the planned task. This is generally due to muscle fatigue and/or poor health condition and/or stray situations on part of the driver. The third test adopted is detection of cognitive failures in motor execution.

Testing of cognitive failures has been accomplished by acquiring the EEG signals from three distinct brain lobes. To detect VAF, we acquire EEG signal from the pre-frontal, frontal and occipital lobes. MPF detection requires examining brain signals from the parietal lobe and motor cortex, while MEF is detected from the EEG acquired from the motor cortex region only. These electrical signals are pre-processed using Independent Component Analysis (ICA) to eliminate artifacts, and then passed through band-pass filters of specific frequency bands for individual cognitive tasks. For instance, the EEG acquired for VAF detection is filtered in the alpha band (8-13 Hz), while the EEG signal acquired in motor planning and execution is filtered in the mu-beta bands (8-30 Hz). Next the filtered signals are processed to extract certain signal features. For the VAF detection problem, we extract adaptive autoregressive (AAR) parameters and for MPF and MEF detection we extract power spectral density (PSD) and discrete wavelet transform (DWT). The feature dimension, usually being moderately high (of dimension= 78) for MPF and MEF, we reduce it by a novel evolutionary feature selection algorithm. The algorithm autonomously generates a set of fixed dimensional features from the total list of features, and examines the best set of features for which the intra-class distance is minimized and inter-class distance is maximized. This is done by measuring fitness of the individual trial solutions, where the fitness measure indicates the degree of maximization of inter-class distance and minimization of intra-class distance jointly. The evolutionary process generates expectedly improved trial solutions over the program iterations, and thus when the terminating condition is reached, the best-fit candidate solution represents the highest degree of satisfaction of both the said criteria.

The main research component of the work lies in designing a suitable classifier, capable of classifying VAF into two classes: visually attentive or non-attentive, MPF into four classes: braking failure, acceleration failure, steering control failure and no failure, and MEF into three classes: braking, acceleration and steering control execution failures. Each of the above three classes are again classified into two sub-classes: brake pressed or not pressed and the like. The classifiers are supplied with extracted features for the respective cognitive failure, and the classifier response is the detected class. Apparently, any traditional supervised learning classifiers could serve the purpose. However, because of parallel brain activations and stochastic noise associated with eye blinking and other muscle movements, the features



are often found noisy. The creeping of noise in the features makes the traditional classifiers unsuitable for the MPF detection. For the VAF and MEF, however, support vector machine (SVM) classifier has acceptable performance.

The fundamental problem in the present research thus is to design a classifier worthwhile for classification of motor planning classes in presence of stochastic noise in the EEG features. Fuzzy sets, in general, and type-2 fuzzy sets in particular, have inherent characteristics to take precise decisions in presence of noisy measurements. While classical (type-1) fuzzy sets can capture the noise due to the randomness of the measurement, type-2 fuzzy sets can capture intra- and inter-personal level uncertainty that might appear in a decision-making system because of the randomness in the assignment of memberships within and across experimental subjects respectively. Here, we propose two distinct models of type-2 fuzzy classification, one realized with interval type-2 fuzzy sets (IT2FS) and the other with general type-2 fuzzy sets (GT2FS). The IT2FS-induced classifier determines the average degree of membership of a data point (by taking the average of the upper and lower membership functions at the given measurement point) in a given class, and declares the class with the highest membership as the class for the given data point. The GT2FS-induced classification employs secondary grades as additional input to tune the primary membership function in each class to determine the degree of membership of a data point in a given class. The class with the highest secondary grade induced primary membership for a given data point is declared as the winning class. A thorough comparison of the IT2FS- and GT2FS-induced classifiers is provided in the chapter to examine the relative merits of GT2FS-based classifier over its counterpart.

The fourth chapter is concerned with touch perception, where the motivation is to classify the touch nourishment received by psychological patients from different nurses in a hospital environment. The objective is to select the right nurse by individual patient for their highest degree of pleasure during the phase of mental treatment. Touch perception is primarily active in the somato-sensory cortex. The nearest electrodes available are frontal and parietal electrodes and the motor cortex region. EEG signals acquired from the above electrodes of the patients are first pre-processed and filtered from artifacts. The processed signals are then fed to a classifier to recognize the pleasure levels received by the patients.

The classifier design is given primary consideration in the present work. We adopted radial basis function (RBF) induced back-propagation neural networks to classify the pleasure level of the patients. The RBF-neural network selects specific touch nourishments, such as soft touch, rubbing, messaging and embracing. Next, for a given touch nourishment we select a back-propagation neural network to classify the individual touch nourishment into three classes: pleasant, acceptable and unpleasant. Experiment undertaken reveals that the proposed neural architecture outperforms its competitors with respect to classification accuracy. To test

statistical validation of the proposed classifier performance, McNemar's test is employed. The proposed scheme has successfully been realized to select appropriate nurses by Schizophrenic patients based on the degree of qualitative touch perceived by them across nurses.

The thesis ends with a concluding chapter dealing with the self-review of the works undertaken in chapters 2, 3 and 4 and also possible future research directions.

## 1.9 SUMMARY

This chapter provides a general introduction to EEG signal analysis to understand the biological basis of perception. It also gives an overview of different modalities of brain signaling/imaging techniques and major brain signals used in the subsequent chapters. Special emphasis is given to problem solving schemes for the selection of single and mixed signals. The later part of the chapter provides a discussion on EEG signal processing, low level feature extraction techniques and classification algorithms to decode cognitive activities. An outline to well-known performance analysis metrics is also included. The chapter comes to an end with a brief review of current research directions and the scope of EEG signals in sensory-motor perception and decoding of motor imagery and alertness.

## References

1. D. Purves, R. Cabeza, S. A. Huettel, K. S. LaBar, M. L. Platt and M. G. Woldorff, *Principles of Cognitive Neuroscience-Second Edition*, Sinauer Associates, Inc. Publishers, Sunderland, MA, USA, 2008.
2. S. Firestein, "How the olfactory system makes sense of scents," *Nature*, vol. 413, no. 6852, pp. 211–218, 2001.
3. S. M. Courtney, L. Petit, J. V. Haxby and L. G. Ungerleider, "The role of prefrontal cortex in working memory: examining the contents of consciousness," *Philosophical Transactions of the Royal Society B: Biological Sciences*, vol. 353, no. 1377, pp. 1819-1828, 1998.
4. W. L. Zhou, P. Yan, J. P. Wuskell, L. M. Loew and S. D. Antic, "Dynamics of action potential backpropagation in basal dendrites of prefrontal cortical pyramidal neurons," *European Journal of Neuroscience*, vol. 27, no. 4, pp. 923–936, 2008.
5. E. T. Rolls, "The orbitofrontal cortex and reward," *Cerebral cortex*, vol. 10, no. 3, pp. 284-294, 2000.
6. J. M. Spielberg, J. L. Stewart, R. L. Levin, G. A. Miller and W. Heller, "Prefrontal cortex, emotion, and approach/withdrawal motivation," *Social and Personality Psychology Compass*, vol. 2, no. 1, pp. 135-153, 2008.
7. C. D. Salzman and S. Fusi, "Emotion, cognition, and mental state representation in amygdala and prefrontal cortex," *Annual Review of Neuroscience*, vol. 33, pp. 173-202, 2010.

8. M. Shoykhet and R. S. B. Clark, "Structure, Function, and Development of the Nervous System," ed. B. P. Fuhrman, J. J. Zimmerman, J. A. Carcillo, R. S. B. Clark, M. Relvas, A. T. Rotta, A. E. Thompson and J. D. Tobias, in *Pediatric Critical Care (Fourth Edition)*, Elsevier, pp. 783-804, 2011.
9. J. G. Mai, G. Paxinos, and T. Voss, *Atlas of the Human Brain*, Elsevier, Amsterdam, The Netherlands, 3rd edition, 2008.
10. J. A. Kiernan, "Anatomy of the Temporal Lobe," *Epilepsy Research and Treatment*, Hindwai Publishing, pp. 1-12, 2012.
11. E. Lugaresi, F. Cirignotta and P. Montagna, "Occipital lobe epilepsy with scotosensitive seizures: the role of central vision," *Epilepsia*, vol. 25, no. 1, pp. 115-120, 1984.
12. J. R. Wolpaw, D. J. McFarland, G. W. Neat and C. A. Forneris, "An EEG-based brain-computer interface for cursor control," *Electroencephalography and Clinical Neurophysiology*, vol. 78, no. 3, pp. 252-259, 1991.
13. B. Rebsamen, E. Burdet, Q. Zheng, H. Zhang, M. Ang, C. L. Teo, C. Guan and C. Laugier, "Hybrid P300 and Mu Beta Brain Computer Interface to Operate a Brain-Controlled Wheelchair," in *Proc.2<sup>nd</sup> International Convention on Rehabilitation Engineering and Assistive Technology*, pp. 51-55, 2008.
14. R. C. Panicker, S. Puthusserypady and Y. Sun, "An Asynchronous P300 BCI with SSVEP-Based Control State Detection," *IEEE Transactions on Biomedical Engineering*, vol. 58, no. 6, pp. 1781-1788, 2011.
15. G. R. Muller-Putz, R. Scherer, G. Pfurtscheller and R. Rupp, "Brain-Computer Interfaces for Control of Neuroprosthesis: From Synchronous to Asynchronous Mode of Operation," *Biomedizinische Technik/Biomedical Eng.*, pp. 57-63, 2006.
16. C. T. Lin, C. J. Chang, B. S. Lin, S. H. Hung, C. F. Chao and I. J. Wang, "A real-time wireless brain-computer interface system for drowsiness detection," *IEEE Trans. Biomedical Circuits and Systems*, vol. 4, no. 4, pp. 214-222, 2010.
17. S. Kar, M. Bhagat and A. Routray, "EEG Signal Analysis for the Assessment and Quantification of Driver's Fatigue," *Transportation Research Part F*, vol. 13, pp. 297-306, 2010.
18. R. J. Davidson, "Anterior Cerebral Asymmetry and the Nature of Emotion," *Brain Cogn*, vol. 20, no. 1, pp. 125-151, 1992.
19. M. Grunwald, T. Weiss, W. Krause, L. Beyer, R. Rost, I. Gutberlet and H. J. Gertz, "Power of theta waves in the EEG of human subjects increases during recall of haptic information," *Neuroscience Letters*, vol. 260, no. 3, pp. 189-192, 1999.
20. N. Chumerin, N. V. Manyakov, M. van Vliet, A. Robben, A. Combaz and M. M. Van Hulle, "Steady-state visual evoked potential-based computer gaming on a consumer-grade EEG

- device” *IEEE Trans. on Computational Intelligence and AI in Games*, vol. 5, no. 2, pp. 100-110, 2013.
21. L. A. Dade, R. J. Zatorre and M. J. Gotman, “Olfactory learning: Convergent findings from lesion and brain imaging studies in humans,” *Brain*, vol. 125, no. 1, pp. 86–101, 2002.
  22. G. Buzsáki, C. A. Anastassiou and C. Koch, “The origin of extracellular fields and currents—EEG, ECoG, LFP and spikes,” *Nature Reviews Neuroscience*, vol. 13, no. 6, pp. 407-420, 2012.
  23. G. Buccheri, D. Ferrigno and M. Tamburini, “Karnofsky and ECOG performance status scoring in lung cancer: a prospective, longitudinal study of 536 patients from a single institution,” *European Journal of Cancer*, vol. 32, no. 7, pp. 1135-1141, 1996.
  24. G. Pourtois, R. Vocat, K. N’diaye, L. Spinelli, M. Seeck and P. Vuilleumier, “Errors recruit both cognitive and emotional monitoring systems: simultaneous intracranial recordings in the dorsal anterior cingulate gyrus and amygdala combined with fMRI,” *Neuropsychologia*, vol 48, no. 4, pp.1144-1159, 2010.
  25. S. Ahn, T. Nguyen, H. Jang, J.G.Kim and S. C. Jun, “Exploring neuro-physiological correlates of drivers' mental fatigue caused by sleep deprivation using simultaneous EEG, ECG, and fNIRS data,” *Frontiers in human neuroscience*, vol. 10, 2016.
  26. I. Maidan, H. Bernad-Elazari, E. Gazit, N. Giladi, J. M. Hausdorff and A. Mirelman, “Changes in oxygenated hemoglobin link freezing of gait to frontal activation in patients with Parkinson disease: an fNIRS study of transient motor-cognitive failures,” *Journal of neurology*, vol. 262, no. 4, pp.899-908, 2015.
  27. C. T. Lin, I. F. Chung, L. W. Ko, Y. C. Chen, S. F. Liang and J. R. Duann, “EEG-based assessment of driver cognitive responses in a dynamic virtual-reality driving environment,” *IEEE Trans. on Biomedical Engineering*, vol. 54, no. 7, pp. 1349-1352, 2007.
  28. C. T. Lin, L. W. Ko, I. F. Chung, T. Y. Huang, Y. C. Chen, T. P. Jung and S. F. Liang, “Adaptive EEG-based alertness estimation system by using ICA-based fuzzy neural networks,” *IEEE Trans. Circuits and Systems I: Regular Papers*, vol. 53, no. 11, pp. 2469-2476, 2006.
  29. C. J. Stam, “Use of magnetoencephalography (MEG) to study functional brain networks in neurodegenerative disorders,” *Journal of the Neurological Sciences*, vol. 289, no. 1, pp. 128-134, 2010.
  30. A. M. Dale and M. I. Sereno, “Improved localization of cortical activity by combining EEG and MEG with MRI cortical surface reconstruction: a linear approach,” *Journal of cognitive neuroscience*, vol. 5, no. 2, pp. 162-176, 1993.
  31. F. Babiloni, D. Mattia, S. Bufalari, F. Aloise, A. Tocci, L. Astolfi, F. D. V. Fallani, S. Gao, S. Salinari, M. G. Marciani and F. Cincotti, “Non invasive EEG-based brain computer interface for communication and control,” *International Journal of Bioelectromagnetism*, vol. 9, no. 1, pp. 17-18, 2007.

32. T. Ball, M. Kerna, I. Mutschler, A. Aertsenb and A. Schulze-Bonhage, "Signal quality of simultaneously recorded invasive and non-invasive EEG," *Neuroimage*, vol. 46, no. 3, pp. 708-716, 2009.
33. F. Tadel, S. Baillet, J. C. Mosher, D. Pantazis and R. M. Leahy, "Brainstorm: a user-friendly application for MEG/EEG analysis," *Computational Intelligence and Neuroscience*, vol. 8, 2011.
34. S. L. Morris, K. J. Dodd and M. E. Morris, "Outcomes of progressive resistance strength training following stroke: a systematic review," *Clinical Rehabilitation*, vol. 18, no. 1, pp. 27-39, 2004.
35. N. F. Gordon, M. Gulanick, F. Costa, G. Fletcher, B. A. Franklin, E. J. Roth and T. Shephard, "Physical activity and exercise recommendations for stroke survivors," *Stroke*, vol. 35, no. 5, pp. 1230-1240, 2004.
36. A. L. Vazquez and D. C. Noll, "Nonlinear aspects of the BOLD response in functional MRI," *NeuroImage*, vol. 7, no. 2, pp. 108-118, 1998.
37. G. H. Glover, "Deconvolution of impulse response in event-related bold fmri 1," *Neuroimage*, vol. 9, no. 4, pp. 416-429, 1999.
38. R. Leeb, L. Tonin, M. Rohm, L. Desideri, T. Carlson and J. D. R. Millán, "Towards independence: a BCI telepresence robot for people with severe motor disabilities," *Proceedings of the IEEE*, vol. 103, no. 6, pp. 969-982, 2015.
39. R. Leeb, R. Chavarriaga and J. D. R. Millán, "10 Brain-Machine Symbiosis," *Human Computer Confluence Transforming Human Experience Through Symbiotic Technologies*, pp. 175-197, 2016.
40. L. D. Liao, V. Tsytsarev, I. Delgado-Martínez, M. L. Li, R. Erzurumlu, A. Vipin, J. Orellana, Y. R. Lin, H. Y. Lai, Y. Y. Chen and N. V. Thakor, "Neurovascular coupling: in vivo optical techniques for functional brain imaging," *Biomedical Engineering Online*, vol. 12, no. 1, pp 38-58, 2013.
41. A. Pellicer and M. del Carmen Bravo, "Near-infrared spectroscopy: a methodology-focused review," *In Seminars in Fetal and Neonatal Medicine*, WB Saunders, vol. 16, no. 1, pp. 42-49, 2011.
42. S. Amiri, A. Rabbi and L. Azinfar, "A review of P300 SSVEP and hybrid P300/SSVEP brain-computer interface systems," *Brain-Computer Interface Systems—Recent Progress and Future Prospects*, pp. 195-213, 2013.
43. R. W. Homan, J. Herman and P. Purdy, "Cerebral location of international 10–20 system electrode placement," *Electroencephalography and Clinical Neurophysiology*, vol. 66, no. 4, pp. 376-382, 1987.
44. K. C. Squires, C. Wickens, N. K. Squires and E. Donchin, "The effect of stimulus sequence on the waveform of the cortical event-related potential," *Science*, vol. 193, no. 4258, pp. 1142-1146, 1976.

45. S. Sutton, M. Braren, J. Zubin and E. R. John, "Evoked-potential correlates of stimulus uncertainty," *Science*, vol. 150, no. 3700, pp. 1187-1188, 1965.
46. J. Polich, "Updating P300: An integrative theory of P3a and P3b," *Clinical Neurophysiology*, vol. 118, pp. 2128-2148, 2007.
47. Y. Miyazato and C. Ogura, "Abnormalities in Event-Related Potentials: N100, N200 and P300 Topography in Alcoholics," *Psychiatry and Clinical Neurosciences*, vol. 47, no. 4, pp. 853-862, 1993.
48. B. Z. Allison, J. Faller and C. Neuper, "BCIs that use steady-state visual evoked potentials or slow cortical potentials," *Brain-Computer Interfaces: Principles and Practice*, vol. 14, pp. 241-249, 2012.
49. N. Yeung, M. M. Botvinick and J. D. Cohen, "The neural basis of error detection: conflict monitoring and the error-related negativity," *Psychological Review*, vol. 111, no. 4, pp. 931-959, 2004.
50. A. Mouraux, J. M. Guerit and L. Plaghki, "Non-phase locked electroencephalogram (EEG) responses to CO<sub>2</sub> laser skin stimulations may reflect central interactions between A $\delta$ - and C-fibre afferent volleys," *Clinical Neurophysiology*, vol. 114, no. 4, pp. 710-722, 2003.
51. G. Pfurtscheller and FH Lopes Da Silva, "Event-related EEG/MEG synchronization and desynchronization: basic principles," *Clinical neurophysiology*, vol. 110, no.11, pp. 1842-1857, 1999.
52. E. W. Sellers, Y. Arbel and E. Donchin, "BCIs that use P300 event-related potentials," *Brain-Computer Interfaces: Principles and Practice*, Ed. J. Wolpaw and E. W. Wolpaw, Oxford University Press, 2012.
53. R. Johnson, "On the neural generators of the P300 component of the event-related potential," *Psychophysiology*, vol. 30, pp.90-90, 1993.
54. J. B. Isreal, G. L. Chesney, C. D. Wickens and E. Donchin, "P300 and tracking difficulty: Evidence for multiple resources in dual-task performance," *Psychophysiology*, vol. 17, no. 3, pp. 259-273, 1980.
55. A. F. Kramer, C. D. Wickens and E. Donchin, "Processing of stimulus properties: evidence for dual-task integrality," *Journal of Experimental Psychology: Human Perception and Performance*, vol. 11, no. 4, p. 393, 1985.
56. A. Ramos-Murguialday and N. Birbaumer, "Brain oscillatory signatures of motor tasks," *Journal of Neurophysiology*, vol. 113, no.10, pp. 3663-3682, 2015.
57. G. Pfurtscheller and C. Neuper, "Motor imagery and direct brain-computer communication," *in Proceedings of the IEEE*, vol. 89, no. 7, pp. 1123-1134, 2001.

58. G. Pfurtscheller and FH. Lopes da Silva, "Event-related desynchronization," *In Handbook of Electroencephalography and Clinical Neurophysiology*, vol. 6, Eds. G. Pfurtscheller and FH. Lopes da Silva, Elsevier, pp. 51–66, Amsterdam, Netherlands, 1999.
59. G. Pfurtscheller and C. Neuper, "Future prospects of ERD/ERS in the context of brain–computer interface (BCI) developments," *Progress in Brain Research*, vol. 159, pp. 433-437, 2006.
60. H. Gevensleben, B. Albrecht, H. Lütcke, T. Auer, W. I. Dewiputri, R. Schweizer, G. Moll, H. Heinrich and A. Rothenberger, "Neurofeedback of slow cortical potentials: neural mechanisms and feasibility of a placebo-controlled design in healthy adults," *Frontiers in Human Neuroscience*, vol. 8, pp. 1-13, 2014.
61. G. Barrett, H. Shibasaki and R. Neshige, "Cortical potentials preceding voluntary movement: evidence for three periods of preparation in man," *Electroencephalography and Clinical Neurophysiology*, vol. 63, no.4, pp. 327-339, 1986.
62. L. Deecke, P. Scheid and H. H. Kornhuber, "Distribution of readiness potential, pre-motion positivity, and motor potential of the human cerebral cortex preceding voluntary finger movements," *Experimental Brain Research*, vol. 7, no. 2, pp. 158-168, 1969.
63. M. Spüler and C. Niethammer, "Error-related potentials during continuous feedback: using EEG to detect errors of different type and severity," *Frontiers in Human Neuroscience*, vol. 9, no. 155, pp. 1-10, 2015.
64. N. M. Schmidt, B. Blankertz and M. S. Treder, "Online detection of error-related potentials boosts the performance of mental typewriters," *BMC Neuroscience*, vol. 13, no.1 pp. 1-13, 2012.
65. M. Falkenstein, J. Hohnsbein, J. Hoormann and L. Blanke, "Effects of errors in choice reaction tasks on the ERP under focused and divided attention," *Psychophysiological Brain Research*, vol. 1, pp. 192-195, 1990.
66. P. W. Ferrez and J. R. Millán, "Error-related EEG potentials generated during simulated brain–computer interaction," *IEEE Trans. on Biomedical Engineering*, vol. 55, no.3, pp. 923-929, 2008.
67. R. Chavarriaga, A. Sobolewski and J. R. Millán, "Errare machinale est: the use of error-related potentials in brain-machine interfaces," *Frontiers in Human Neuroscience*, vol. 8, no. 208, pp. 53-65, 2014.
68. M. Falkenstein, J. Hoormann, S. Christ and J. Hohnsbein, "Erp components on reaction errors and their functional significance: a tutorial," *Biol. Psychol*, vol. 51, pp. 87–107, 2000.
69. M. Spüler, M. Bensch, S. Kleih, W. Rosenstiel, M. Bogdan, and A. Kübler, "Online use of error-related potentials in healthy users and people with severe motor impairment increases performance of a P300-BC," *Clin. Neurophysiol*, vol. 123, pp. 1328–1337, 2012.
70. A. M. Norcia, L. G. Appelbaum, J. M. Ales, B. R. Cottreau and B. Rossion, "The steady-state visual evoked potential in vision research: a review," *Journal of Vision*, vol. 15, no. 6, pp. 1-46, 2015.

71. W. J. Evans, L. Cui and A. Starr, 'Olfactory event-related potentials in normal human subjects: effects of age and gender,' *Electroencephalography and Clinical Neurophysiology*, vol. 95, no. 4, pp. 293-301, 1995.
72. F. Caminiti, S. De Salvo, M. C. De Cola, M. Russo, P. Bramanti, S. Marino and R. Ciurleo, "Detection of olfactory dysfunction using olfactory event related potentials in young patients with multiple sclerosis," *PloS One*, vol. 9, no. 7, pp. 1-7, 2014.
73. C. D. Morgan and C. Murphy, "Olfactory event-related potentials in Alzheimer's disease," *Journal of the International Neuropsychological Society*, vol. 8, no. 6, pp. 753-763, 2002.
74. S. Sur and V. K. Sinha, "Event-related potential: An overview," *Industrial Psychiatry Journal*, vol. 18, no. 1, pp. 70-73, 2009.
75. R. Näätänen and T. W. Picton, "N2 and automatic versus controlled processes," *Cerebral Psychophysiology: Studies in Event-Related Potentials (EEG Suppl. 38)*, Eds. W. C. McCallum, R. Zappoli and F. Denoth, Elsevier Science Publishers, pp. 169-186, 1986.
76. R. Näätänen, "The role of attention in auditory information processing as revealed by event-related potentials and other brain measures of cognitive function," *Behavioral and Brain Sciences*, vol. 13, no. 2, pp. 201-233, 1990.
77. W. S. Pritchard, S. A. Shappell and M. E. Brandt, "Psychophysiology of N200/N400: A review and classification scheme," *Advances in Psychophysiology*, vol. 4, pp. 43-106, 1991.
78. S. J. Luck, M. Girelli, M. T. McDermott and M. A. Ford, "Bridging the gap between monkey neurophysiology and human perception: An ambiguity resolution theory of visual selective attention," *Cognitive Psychology*, vol. 33, no. 1, pp. 64-87, 1997.
79. S. H. Patel and P. N. Azzam, "Characterization of N200 and P300: selected studies of the event-related potential," *Int J Medical Sciences*, vol. 2, no. 4, pp. 147-154, 2005.
80. K. Alho, "Cerebral generators of mismatch negativity (MMN) and its magnetic counterpart (MMNm) elicited by sound changes," *Ear and Hearing*, vol. 16, no. 1, pp. 38-51, 1995.
81. M. Lijffijt, F. G. Moeller, N. N. Boutros, J. L. Steinberg, S. L. Meier, S. D. Lane and A. C. Swann, "Diminished P50, N100 and P200 auditory sensory gating in bipolar I disorder," *Psychiatry Research*, vol. 167, no. 3, pp. 191-201, 2009.
82. N. Kumar, S. Sood and M. Singh, "Effect of acute moderate exercise on cognitive event-related potentials N100, P200, N200, and interpeak latencies," *Indian Journal of Psychological Medicine*, vol. 32, no. 2, pp. 131-135, 2010.
83. B. Kettenmann, C. Hummel, H. Stefan and G. Kobal, "Multiple olfactory activity in the human neocortex identified by magnetic source imaging," *Chemical Senses*, vol. 22, pp. 493-502, 1997.
84. J. Kayser, C. E. Tenke, D. Malaspina, C. J. Kropfmann, J. D. Schaller, A. Deptula, N. A. Gates, J. M. Harkavy-Friedman, R. Gil and G. E. Bruder, "Neuronal generator patterns of olfactory



- event-related brain potentials in schizophrenia,” *Psychophysiology*, vol. 47, no. 6, pp. 1075-1086, 2010.
85. J. Löttsch and T. Hummel, “The clinical significance of electrophysiological measures of olfactory function,” *Behavioral Brain Research*, vol. 170, pp. 78–83, 2006.
  86. T. Hinterberger, S. Schmidt, N. Neumann, J. Mellinger, B. Blankertz, G. Curio, and N. Birbaumer, “Brain-computer communication and slow cortical potentials,” *IEEE Trans. on Biomedical Engineering*, vol. 51, no. 6, pp. 1011-1018, 2004.
  87. F. Beverina, G. Palmas, S. Silvoni, F. Piccione and S. Giove, “User adaptive BCIs: SSVEP and P300 based interfaces,” *PsychNology Journal*, vol. 1, no. 4, pp. 331-354, 2003.
  88. M. Falkenstein, J. Hohnsbei, J. Hoormann and L. Blanke, “Effects of crossmodal divided attention on late erp components. ii. error processing in choice reaction tasks,” *Electroencephalogr. Clin. Neurophysiol*, vol. 78, pp. 447–455, 1991.
  89. W. J. Gehring, B. Goss, M. G. Coles, D. E. Meyer and E. Donchin, “A neural system for error detection and compensation,” *Psychol. Sci*, vol. 4, pp. 385–390, 1993.
  90. M. Ullsperger, A. G. Fischer, R. Nigbur and T. Endrass, “Neural mechanisms and temporal dynamics of performance monitoring,” *Trends Cogn. Sci.* vol. 18, pp. 259–267, 2014.
  91. E. Donchin, K. Spence and R. Wijeshinge, “The mental prosthesis: assessing the speed of P300-based brain-computer interface,” *IEEE Transactions on Rehabilitation Engineering*, vol. 8, no. 2, pp. 174–179, 2000.
  92. L. A. Farwell and E. Donchin, “Talking off the top of your head: toward a mental prosthesis utilizing event-related brain potentials,” *Electroencephalography and Clinical Neurophysiology*, vol. 70, no. 6, pp. 510–523, 1988.
  93. R. Fazel-Rezai, B. Z. Allison, C. Guger, E. W. Sellers, S. C. Kleih and A. Kübler, “P300 brain computer interface: current challenges and emerging trends,” *Frontiers in Neuroengineering*, vol. 5, no. 14, pp. 1-14, 2012.
  94. J. Pan, Y. Li, Z. Gu, and Z. Yu, “A comparison study of two P300 speller paradigms for brain-computer interface,” *Cognitive Neurodynamics*, vol. 7, no. 6, pp. 523-529, 2013.
  95. G. Townsend, BK. LaPallo, CB. Boulay, DJ. Krusienski, GE. Frye, CK. Hauser, NE. Schwartz, TM. Vaughan, JR. Wolpaw and EW. Sellers, “A novel P300-based brain-computer interface stimulus presentation paradigm: moving beyond rows and columns,” *Clinical Neurophysiology*, vol. 121, pp. 1109–1120, 2010.
  96. D. B. Ryan, G. E. Frye, G. Townsend, D. R. Berry, G. S. Mesa, N. A. Gates, and E. W. Sellers, “Predictive spelling with a P300-based brain-computer interface: increasing the rate of communication,” *Intl. Journal of Human-Computer Interaction*, vol. 27, no. 1, pp. 69-84, 2010.
  97. J. Kronegg, S. Voloshynovskyy and T Pun, “Information-transfer rate modelling of EEG-based synchronized brain-computer interfaces,” *Technical Report*, Universite De Geneve, pp. 1-7, 2005.

98. R. Ortner, R. Prueckl, V. Putz, J. Scharinger, M. Bruckner, A. Schnuerer and C. Guger, "Accuracy of a P300 Speller for different conditions: A comparison," in *Proc. of the 5th International Brain-Computer Interface Conference*, pp. 1-4, Graz, Austria, 2011.
99. N. V. Manyakov, N. Chumerin, A. Combaz and M. M. Van Hulle, "Comparison of classification methods for P300 brain-computer interface on disabled subjects," *Computational Intelligence and Neuroscience*, vol. 2, pp. 1-12, 2011.
100. M. Nakanishi, Y. Wang, Y. T. Wang, Y. Mitsukura and T. P. Jung, "A high-speed brain speller using steady-state visual evoked potentials," *International Journal of Neural Systems*, vol. 24, no. 6, 2014.
101. G. Bin, X. Gao, Z. Yan, B. Hong, and S. Gao, "An online multi-channel SSVEP-based brain-computer interface using a canonical correlation analysis method," *Journal of Neural Engineering*, vol. 6, no. 4, 2009.
102. U. Hoffmann, J. M. Vesin, T. Ebrahimi, T and K. Diserens, K. "An efficient P300-based brain-computer interface for disabled subjects," *Journal of Neuroscience methods*, vol. 167, no. 1, 115-125, 2008.
103. O. Bai, P. Lin, D. Huang, D. Y. Fei and M. K. Floeter, "Towards a user-friendly brain-computer interface: initial tests in ALS and PLS patients," *Clinical Neurophysiology*, vol. 121, no.8, pp. 1293-1303, 2010.
104. A. Kübler, B. Kotchoubey, T. Hinterberger, N. Ghanayim, J. Perelmouter, M. Schauer, C. Fritsch, E. Taub and N. Birbaumer, "The thought translation device: a neurophysiological approach to communication in total motor paralysis," *Experimental Brain Research*, vol. 124, no. 2, pp.223-232, 1999.
105. T. Hinterberger, F. Nijboer, A. Kübler, T. Matuz, A. Furdea, U. Mochty, M. Jordan, T. N. Lal, N. J. Hill, J. Mellinger and M. Bensch, "Brain-computer interfaces for communication in paralysis: A clinical experimental approach," *Towards Brain-Computer Interfacing*, pp.43-64, 2007.
106. O. Bai, P. Lin, S. Vorbach, M. K. Floeter, N. Hattori and M. Hallett, "A high performance sensorimotor beta rhythm-based brain-computer interface associated with human natural motor behavior" *Journal of Neural Engineering*, vol. 5, no. 1, p. 24, 2007.
107. L. A. Miner, D. J. McFarland and J. R. Wolpaw, "Answering questions with an electroencephalogram-based brain-computer interface," *Archives of Physical Medicine and Rehabilitation*, vol. 79, no.9, pp.1029-1033, 1998.
108. J. R. Wolpaw, H. Ramoser, D. J. McFarland and G. Pfurtscheller, "EEG-based communication: improved accuracy by response verification," *IEEE Trans Rehabil Eng*, vol. 6, pp. 326-333, 1998.
109. D. J. McFarland, W. A. Sarnacki, T. M. Vaughn and J. R. Wolpaw, "EEG-based brain-computer interface communication effect of target number and trial length on information transfer rate," *Soc Neurosci Abstr*, vol. 26, p. 1228, 2000.

110. R. C. Panicker, S. Puthusserypady and Y. Sun, "An asynchronous P300 BCI with SSVEP-based control state detection," *IEEE Transactions on Biomedical Engineering*, vol. 58, no. 6, pp. 1781-1788, 2011.
111. E. Yin, Z. Zhou, J. Jiang, F. Chen, Y. Liu and D. Hu, "A speedy hybrid BCI spelling approach combining P300 and SSVEP," *IEEE Transactions on Biomedical Engineering*, vol. 61, no. 2, pp. 473-483, 2014.
112. B. Dal Seno, M. Matteucci and L. Mainardi, "Online detection of P300 and error potentials in a BCI speller," *Computational Intelligence and Neuroscience*, vol. 2010, no. 11, 2010.
113. A. Combaz, N. Chumerin, N. Manyakov, A. Robben, J. Suykens and M. V. Hulle, "Towards the detection of error-related potentials and its integration in the context of a P300 speller brain-computer interface," *Neurocomputing*, vol. 80, pp. 73-82, 2012.
114. E. Yin, Z. Zhou, J. Jiang, F. Chen, Y. Liu and D. Hu, "A novel hybrid BCI speller based on the incorporation of SSVEP into the P300 paradigm," *Journal of Neural Engineering*, vol. 10, no. 2, 2013.
115. M. Wang, I. Daly, B. Z. Allison, J. Jin, Y. Zhang, L. Chen and X. Wang, "A new hybrid BCI paradigm based on P300 and SSVEP," *Journal of Neuroscience Methods*, vol. 244, pp. 16-25, 2015.
116. P. Margaux, M. Emmanuel, D. Sébastien, B. Olivier and M. Jérémie, "Objective and subjective evaluation of online error correction during P300-based spelling," *Advances in Human-Computer Interaction*, vol. 4, 2012.
117. Y. Li, J. Long, T. Yu, Z. Yu, C. Wang, H. Zhang and C. Guan, "An EEG-based BCI system for 2-D cursor control by combining Mu/Beta rhythm and P300 potential," *IEEE Transactions on Biomedical Engineering*, vol. 57, no. 10, pp. 2495-2505, 2010.
118. J. Long, Y. Li, T. Yu and Z. Gu, "Target selection with hybrid feature for BCI-based 2-D cursor control," *IEEE Transactions on Biomedical Engineering*, vol. 59, no. 1, pp. 132-140, 2012.
119. L. Bi, J. Lian, K. Jie, R. Lai and Y. Liu, Y, "A speed and direction-based cursor control system with P300 and SSVEP," *Biomedical Signal Processing and Control*, vol. 14, pp. 126-133, 2014.
120. B. Z. Allison, C. Brunner, C. Altstätter, I. C., Wagner, S. Grissmann and C. Neuper, "A hybrid ERD/SSVEP BCI for continuous simultaneous two dimensional cursor control," *Journal of Neuroscience Methods*, vol. 209, no. 2, pp. 299-307, 2012.
121. P. W. Ferrez and J. D. R. Millán, "Simultaneous real-time detection of motor imagery and error-related potentials for improved BCI accuracy," *In Proceedings of the 4th international brain-computer interface workshop and training course*, pp. 197-202, 2008.
122. H. Riechmann, N. Hachmeister, H. Ritter and A. Finke, "Asynchronous, parallel on-line classification of P300 and ERD for an efficient hybrid BCI," *In Proc. of 5th International IEEE/EMBS Conference on Neural Engineering (NER)*, (pp. 412-415), 2011.

123. S. Amiri, R. Fazel-Rezai and V. Asadpour, "A review of hybrid brain-computer interface systems," *Advances in Human-Computer Interaction*, vol. 2013, pp. 1-8, 2013.
124. B. Rebsamen, E. Burdet, Q. Zeng, H. Zhang, M. Ang, C. L. Teo, C. Guan and C. Laugier, "Hybrid P300 and Mu-Beta brain computer interface to operate a brain controlled wheelchair," *In Proceedings of the 2nd International Convention on Rehabilitation Engineering & Assistive Technology*, Singapore Therapeutic, Assistive & Rehabilitative Technologies (START) Centre, pp. 51-55, 2008.
125. Y. Su, Y. Qi, J. Luo, B. Wu, F. Yang, Y. Li, Y. T. Zhuang, X. X. Zheng and W. D. Chen, "A hybrid brain-computer interface control strategy in a virtual environment," *Journal of Zhejiang University SCIENCE C*, vol. 12, no. 5, pp. 351-361, 2011.
126. J. Long, Y. Li, H. Wang, T. Yu, J. Pan and F. Li, "A hybrid brain computer interface to control the direction and speed of a simulated or real wheelchair," *IEEE Transactions on Neural Systems and Rehabilitation Engineering*, vol. 20, no. 5, pp. 720-729, 2012.
127. Y. Li, J. Pan, F. Wang Z. Yu, "A hybrid BCI system combining P300 and SSVEP and its application to wheelchair control," *IEEE Transactions on Biomedical Engineering*, vol. 60, no. 11, pp. 3156-3166, 2013.
128. X. A. Fan, L. Bi, T. Teng, H. Ding and Y. Liu, "A brain-computer interface-based vehicle destination selection system using P300 and SSVEP signals," *IEEE Transactions on Intelligent Transportation Systems*, vol. 16, no. 1, pp. 274-283, 2015.
129. L. Bi, X. A. Fan, N. Luo, K. Jie, Y. Li and Y. Liu, "A head-up display-based P300 brain-computer interface for destination selection," *IEEE Transactions on Intelligent Transportation Systems*, vol. 14, no. 4, pp. 1996-2001, 2013.
130. H. Zhang, C. Guan and C. Wang, "Asynchronous P300-based brain-computer interfaces: A computational approach with statistical models," *IEEE Transactions on Biomedical Engineering*, vol. 55, no. 6, pp. 1754-1763, 2008.
131. P. Horki, T. Solis-Escalante, C. Neuper and G. Müller-Putz, "Combined motor imagery and SSVEP based BCI control of a 2 DoF artificial upper limb," *Medical & Biological Engineering & Computing*, vol. 49, no. 5, pp. 567-577, 2011.
132. C. Brunner, B. Z. Allison, C. Altstätter and C. Neuper, "A comparison of three brain-computer interfaces based on event-related desynchronization, steady state visual evoked potentials, or a hybrid approach using both signals," *Journal of Neural Engineering*, vol. 8, no. 2, pp. 1-7, 2011.
133. B. Z. Allison, C. Brunner, V. Kaiser, G. R. Müller-Putz, C. Neuper and G. Pfurtscheller, "Toward a hybrid brain-computer interface based on imagined movement and visual attention," *Journal of Neural Engineering*, vol. 7, no. 2, pp. 1-9, 2010.
134. C. Brunner, B. Z. Allison, D. J. Krusienski, V. Kaiser, G. R. Müller-Putz, G. Pfurtscheller and C. Neuper, "Improved signal processing approaches in an offline simulation of a hybrid brain-computer interface," *Journal of Neuroscience Methods*, vol. 188, no. 1, pp. 165-173, 2010.

135. F. Duan, D. Lin, W. Li and Z. Zhang, "Design of a multimodal EEG-based hybrid BCI system with visual servo module," *IEEE Trans. on Autonomous Mental Development*, vol. 7, no. 4, pp. 332-341, 2015.
136. T. Yu, J. Xiao, F. Wang, R. Zhang, Z. Gu, A. Cichocki and Y. Li, "Enhanced motor imagery training using a hybrid BCI with feedback," *IEEE Trans. on Biomedical Engineering*, vol. 62, no. 7, pp. 1706-1717, 2015.
137. G. Pfurtscheller, T. Solis-Escalante, R. Ortner, P. Linortner and G. R. Muller-Putz, "Self-paced operation of an SSVEP-Based orthosis with and without an imagery-based "brain switch:" a feasibility study towards a hybrid BCI," *IEEE Trans. on Neural Systems and Rehabilitation Engineering*, vol. 18, no. 4, pp. 409-414, 2010.
138. S. Bhattacharyya, A. Konar and D. N. Tibarewala, "Motor imagery, P300 and error-related EEG-based robot arm movement control for rehabilitation purpose," *Medical & Biological Engineering & Computing*, vol. 52, no. 12, pp. 1007-1017, 2014.
139. S. Bhattacharyya, A. Konar and D. N. Tibarewala, "Motor imagery and error-related potential induced position control of a robotic arm," *IEEE CAA J. of Automatica Sinica*, 2017 (to appear).
140. K. G. Dy, and C. E. Brodley, "Feature selection for unsupervised learning," *Journal of Machine Learning Research*, vol. 5, pp. 845-889, 2004.
141. Y. Kim, W. N. Street and F. Menczer, "Feature selection in unsupervised learning via evolutionary search," *In Proceedings of the Sixth ACM SIGKDD International Conference on Knowledge Discovery and Data Mining*, pp. 365-369, 2000.
142. M. Weeks and B. Wang, "A hybrid infinite/finite impulse response (HIR) filter," *In Proc. of IEEE 2002 45th Midwest Symposium on Circuits and Systems*, vol. 2, 2002.
143. N. Beaudoin and S. S. Beauchemin, "A new numerical Fourier transform in d-dimensions. *IEEE Trans. on Signal Processing*," vol. 51, no. 5, pp. 1422-1430, 2003.
144. P. Podder, M. M. Hasan, M. R. Islam and M. Sayeed, "Design and Implementation of Butterworth, Chebyshev-I and Elliptic Filter for Speech Signal Analysis," *International Journal of Computer Applications*, vol. 98, no. 7, pp. 12-18, 2014.
145. F. Lotte, "A tutorial on EEG signal-processing techniques for mental-state recognition in brain-computer interfaces," *In Guide to Brain-Computer Music Interfacing*, Springer, London, pp. 133-161, 2014.
146. M. J. Alhaddad, "Common average reference (car) improves p300 speller," *International Journal of Engineering and Technology*, vol. 2, no. 3, p. 452-467, 2012.
147. F. Lee, R. Scherer, R. Leeb, A. Schlögl, H. Bischof and G. Pfurtscheller, "Feature mapping using PCA, locally linear embedding and isometric feature mapping for EEG-based brain computer interface," 2014.
148. A. Hyvärinen, "Survey on independent component analysis," 1999.

149. F. Lotte, and C. Guan, "Regularizing common spatial patterns to improve BCI designs: unified theory and new algorithms," *IEEE Trans. on Biomedical Engineering*, vol. 58, no. 2, pp. 355-362, 2011.
150. R. G. Soumya, N. Naveen and M. J. Lal, "Application of adaptive filter using adaptive line enhancer techniques," *In Proc. of IEEE Third International Conference on Advances in Computing and Communications (ICACC)*, pp. 165-168, 2013.
151. C. Vidaurre, N. Krämer, B. Blankertz and A. Schlögl, "Time domain parameters as a feature for EEG-based brain-computer interfaces," *Neural Networks*, vol. 22, no. 9, pp. 1313-1319, 2009.
152. A. O. Argunsah and M. Cetin, "AR-PCA-HMM approach for sensorimotor task classification in EEG-based brain-computer interfaces," *In Proc. of 20th IEEE International Conference on Pattern Recognition (ICPR)*, pp. 113-116, 2010.
153. R. T. Mina, A. Atiya, M. I. Owis and Y. M. Kadah, "Brain-Computer Interface Based on Classification of Statistical and Power Spectral Density Features," *In Proc. of Cairo International Biomedical Engineering Conference*, pp. 1-4, 2006.
154. Y. Bao, G. Yu, H. Sun and D. Wang, "Performance optimization of fractal dimension based feature selection algorithm," *In Proc. of International Conference on Web-Age Information Management, Springer Berlin Heidelberg*, pp. 739-744, 2004.
155. J. T. Cavanaugh, V. S. Mercer and N. Stergiou, "Approximate entropy detects the effect of a secondary cognitive task on postural control in healthy young adults: a methodological report," *Journal of Neuroengineering and Rehabilitation*, vol. 4, no. 1, pp. 1-7, 2007.
156. L. Ming-Ai, W. Rui, H. Dong-Mei and Y. Jin-Fu, "Feature extraction and classification of mental eeg for motor imagery," *In Proc. of Fifth IEEE International Conference on Natural Computation*, vol. 2, pp. 139-143, 2009.
157. S. Hengstler, S. Sand and A. H. Costa, "Adaptive autoregressive modeling for time-frequency analysis," *In Proceedings of the Third International Conference on Information, Communications & Signal Processing*, pp. 241-244, 2001.
158. Y. Liu, H. Zhang, Q. Zhao and L. Zhang, "Common Spatial-spectral boosting pattern for brain-computer interface," *In Proc. of the Twenty-first European Conference on Artificial Intelligence, IOS Press*, pp. 537-542, 2014.
159. K. K. Ang, Z. Y. Chin, H. Zhang and C. Guan, "Filter bank common spatial pattern (FBCSP) in brain-computer interface. *In proc. IEEE International Joint Conference on World Congress on Computational Intelligence Neural Networks*, pp. 2390-2397, 2008.
160. F. Jamaloo and M. Mikaeili, "Discriminative Common Spatial Pattern Sub-bands Weighting Based on Distinction Sensitive Learning Vector Quantization Method in Motor Imagery Based Brain-computer Interface," *Journal of Medical Signals and Sensors*, vol. 5, no. 3, pp. 1-16, 2015.

161. N. V. Davis, "Feature extraction using empirical modedecomposition of speech signal," *Int. J. Eng. Trend. Technology*, vol. 3, no. 2, 2012.
162. E. A. Ihlen, "Introduction to multifractal detrended fluctuation analysis in Matlab," *Fractal Anal*, vol. 3, 97.
163. S. Sun, "The extreme energy ratio criterion for EEG feature extraction," *In Proc. of International Conference on Artificial Neural Networks, Springer Berlin Heidelberg*, pp. 919-928, 2008.
164. S. Sun, 2010, "Extreme energy difference for feature extraction of EEG signals," *Expert Systems with Applications*, vol. 37, no. 6, pp. 4350-4357, 2010.
165. R. Martin, "Noise power spectral density estimation based on optimal smoothing and minimum statistics," *IEEE Trans. on Sspeech and Audio Processing*, vol. 9, no. 5, pp. 504-512, 2001.
166. A. Schlögl, K. Lugger and G. Pfurtscheller, "Using adaptive autoregressive parameters for a brain-computer-interface experiment," *In Proc. of the 19th IEEE Annual International Conference of Engineering in Medicine and Biology Society*, vol. 4, pp. 1533-1535, 1997.
167. Y. Engel, S. Mannor and R. Meir, "The kernel recursive least-squares algorithm," *IEEE Trans. on Signal Processing*, vol. 52, no. 8, pp. 2275-2285, 2004.
168. I. T. Hettiarachchi, T. T. Nguyen and S. Nahavandi, "Multivariate Adaptive Autoregressive Modeling and Kalman Filtering for Motor Imagery BCI," *In Proc. of IEEE International Conference on Systems, Man, and Cybernetics (SMC)*, pp. 3164-3168, 2015.
169. M. Zeinali and M. Shafiee, "A New Kalman Filter Based 2D AR Model Parameter Estimation Method," *IETE Journal of Research*, pp. 1-9, 2017.
170. D. K. Bhattacharyya and J. K. Kalita, "*Network anomaly detection: A machine learning perspective*," CRC Press, 2013.
171. J. Fan and Y. Fan, "High dimensional classification using features annealed independence rules," *Annals of Statistics*, vol. 36, no. 6, pp. 2605-2637, 2008.
172. J. Tang, S. Alelyani and H. Liu, "Feature selection for classification: A review," *Data Classification: Algorithms and Applications*, pp. 1-33.
173. A. Janecek, W. N. Gansterer, M. Demel and G. Ecker, "On the relationship between feature selection and classification accuracy," *JMLR: Workshop and Conference Proceedings*, vol. 4, pp. 90-105, 2008.
174. M. Dash, and H. Liu, "Feature selection for classification," *Intelligent Data Analysis*, vol. 1, no. 1-4, pp. 131-156, 1997.
175. M. Mandal and A. Mukhopadhyay, "An improved minimum redundancy maximum relevance approach for feature selection in gene expression data," *Procedia Technology*, vol. 10, pp. 20-27, 2013.

176. P. Pudil, J. Novovičová and J. Kittler, "Floating search methods in feature selection," *Pattern Recognition Letters*, vol. 15, no. 11, pp. 1119-1125, 1994.
177. S. Das, A. Abraham and A. Konar, "Automatic clustering using an improved differential evolution algorithm," *IEEE Trans. on Systems, Man, and Cybernetics-Part A: Systems and Humans*, vol. 38, no. 1, pp. 218-237, 2008.
178. S. Das, A. Abraham and A. Konar, "Particle swarm optimization and differential evolution algorithms: technical analysis, applications and hybridization perspectives," *In Advances of Computational Intelligence in Industrial Systems*, Springer Berlin Heidelberg, pp. 1-38, 2008.
179. K. F. Man, K. S. Tang and S. Kwong, "Genetic algorithms: concepts and applications," *IEEE Trans. on Industrial Electronics*, vol. 43, no. 5, pp. 519-534, 1996.
180. D. M. Witten and R. Tibshirani, "Penalized classification using Fisher's linear discriminant," *Journal of the Royal Statistical Society: Series B (Statistical Methodology)*, vol. 73, no. 5, pp. 753-772, 2011.
181. I. Narsky and F. C. Porter, "Linear and Quadratic Discriminant Analysis, Logistic Regression, and Partial Least Squares Regression," *Statistical Analysis Techniques in Particle Physics: Fits, Density Estimation and Supervised Learning*, Willey, pp. 221-249, 2014.
182. D. Ming, C. Sun, L. Cheng, Y. Bai, X. Liu, X. An, H. Qi, B. Wan, Y. Hu and K. D. K. Luk., "ICA-SVM combination algorithm for identification of motor imagery potentials," *In IEEE International Conference on Computational Intelligence for Measurement Systems and Applications (CIMSAs)*, pp. 92-96, 2010.
183. S. Haykin, *Neural Networks-A Comprehensive Foundation (Second Edition)*, Prentice Hall, New Jersey, 1999.
184. Z. Yong, L. Youwen and X. Shixiong, "An improved KNN text classification algorithm based on clustering," *Journal of Computers*, vol. 4, no. 3, pp. 230-237, 2009.
185. N. Kouiroukidis and G. Evangelidis, "The effects of dimensionality curse in high dimensional knn search," *In Proc. of 15th IEEE Panhellenic Conference on Informatics (PCI)*, pp. 41-45, 2011.
186. J. M. Nazzal, I. M. El-Emary and S. A. Najim, "Multilayer Perceptron Neural Network (MLPs) For Analyzing the Properties of Jordan Oil Shale," *World Applied Sciences Journal*, vol. 5, no. 5, pp. 546-552, 2008.
187. R. Palaniappan, "Brain computer interface design using band powers extracted during mental tasks," *In Proc. of 2nd IEEE International Conference on Neural Engineering*, pp. 321-324, 2005.
188. T. Kopinski, S. Magand, U. Handmann and A. Gepperth, "A pragmatic approach to multi-class classification," *In Proc. of IEEE International Joint Conference on Neural Networks (IJCNN)*, pp. 1-8, 2015.



189. C. W. Anderson and Z. Sijercic, "Classification of EEG signals from four subjects during five mental tasks," In *Proc. of the Conference on Engineering Applications in Neural Networks (EANN'96): Solving engineering problems with neural networks*, Turkey, pp. 407-414, 1996.
190. E. Haselsteiner and G. Pfurtscheller, "Using time-dependent neural networks for EEG classification." *IEEE Trans. on Rehabilitation Engineering*, vol. 8, no. 4, pp. 457-463, 2000.
191. S. Chiappa and S. Bengio, *HMM and IOHMM modeling of EEG rhythms for asynchronous BCI systems* (No. EPFL-REPORT-82978). IDIAP, 2003.
192. L. R. Rabiner, "A tutorial on hidden Markov models and selected applications in speech recognition," *Proceedings of the IEEE*, vol. 77, no. 2, pp. 257-286, 1989.
193. E. L. Iglesias, M. L. B. Diz, R. Romero-González and A. S. Vieira, "A HMM text classification model with learning capacity," *Advances in Distributed Computing and Artificial Intelligence Journal*, vol. 3, no. 3, pp. 21-34, 2014.
194. I. Rish, "An empirical study of the naive Bayes classifier," In *IJCAI 2001 Workshop on Empirical Methods in Artificial Intelligence*, IBM New York, vol. 3, no. 22, pp. 41-46, 2001.
195. M. Sokolova and G. Lapalme, "A systematic analysis of performance measures for classification tasks," *Information Processing & Management*, vol. 45, no. 4, pp. 427-437, 2009.
196. M. Hossin and M. N. Sulaiman, "A review on evaluation metrics for data classification evaluations," *International Journal of Data Mining & Knowledge Management Process*, vol. 5, no. 2, pp. 1-11, 2015.
197. B. Blankertz K. Muller, G. Curio, T. M. Vaughan, G. Schalk, J. Wolpaw, A. Schlogl, C. Neuper, G. Pfurtscheller, T. Hinterberger, M. Schroder and N. Birbaumer, "The BCI Competition 2003: progress and perspectives in detection and discrimination of EEG single trials," *IEEE Trans Biomed Eng*, vol. 51, no. 6, pp. 1044-1051, 2004.
198. A. Banerjee, U. B. Chitnis, S. L. Jadhav, J. S. Bhawalkar and S. Chaudhury, "Hypothesis testing, type I and type II errors," *Industrial Psychiatry Journal*, vol. 18, no. 2, pp. 127-131, 2009.
199. J. Wolpaw and H. Ramoser, "EEG-based communication: improved accuracy by response verification," *IEEE Trans Rehabil Eng*, vol. 6, no. 3, pp. 326-333, 1998.
200. D. S. Lee, C. S., Chang and H. N. Chang, "Analyses of the Clustering Coefficient and the Pearson Degree Correlation Coefficient of Chung's Duplication Model," *IEEE Trans. on Network Science and Engineering*, vol. 3, no. 3, pp. 117-131, 2017.
201. H. Fukuda and Y. Ohashi, "A guideline for reporting results of statistical analysis in Japanese Journal of Clinical Oncology," *Japanese Journal of Clinical Oncology*, vol. 27, no. 3, pp. 121-127, 1997.

202. A. Bharathi and A. M. Natarajan, "Cancer Classification of Bioinformatics data using ANOVA," *International Journal of Computer Theory and Engineering*, vol. 2, no. 3, pp. 369-373, 2010.
203. T.G. Dietterich, "Approximate statistical tests for comparing supervised classification learning algorithms," *Neural Computation*, vol. 10, no. 7, pp. 1895-1923, 1998.
204. T. Oda, R. Obukata, M. Yamada, T. Ishitaki, M. Hiyama and L. Barolli, "A Neural Network Based User Identification for Tor Networks: Comparison Analysis of Activation Function Using Friedman Test," *In Proc. of 10th IEEE Conference on Complex, Intelligent, and Software Intensive Systems (CISIS)*, pp. 477-483, 2016.
205. L. Zhang, S. Wang, Q. Sun and A. Li, "Remote sensing image segmentation based on Wilcoxon rank sum test and mean absolute deviation," *In Proc. of IEEE International Geoscience and Remote Sensing Symposium (IGARSS)*, pp. 6340-6343, 2016.
206. D. S. Golenko and O. V. Ampilov, "Unknown Signal Detection Based on Wilcoxon Signed-Rank Test," *In Proc. of IEEE Conference on Engineering and Telecommunication (EnT)*, pp. 72-75, 2016.
207. G. E. Hovland and B. J. McCarragher, "Control of sensory perception using stochastic dynamic programming," *In Proc. of IEEE First Australian Data Fusion Symposium, (ADFS'96)*, pp. 196-201, 1996.
208. G. E. Hovland and B. J. McCarragher, "Control of sensory perception for discrete event systems," *In Proc. of IEEE International Conference on Systems, Man, and Cybernetics*, vol. 1, pp. 776-781, 1998.
209. G. E. Hovland and B. J. McCarragher, "Controlling sensory perception for indoor navigation," *In Proc. of IEEE International Conference on Robotics and Automation*, vol. 3, pp. 2211-2216, 1998.
210. T. Ishikawa, Y. Kaji and T. Nomura, "Sensory perception of unexpected sudden changes in floor level during human gait," *In Proc. of 28th Annual International Conference of the IEEE Engineering in Medicine and Biology Society, (EMBS'06)*, pp. 4474-4477, 2006.
211. A. Kerren, M. Prangova and C. Paradis, "Visualization of sensory perception descriptions," *In Proc. of 15th IEEE International Conference on Information Visualisation (IV)*, pp. 135-144, 2011.
212. A. J. Brockmeier, M. K. Hazrati, W. J. Freeman, L. Li and J. C. Principe, "Locating spatial patterns of waveforms during sensory perception in scalp EEG," *In Proc. of 2012 annual international conference of the IEEE Engineering in medicine and biology society (EMBC)*, pp. 2531-2534, 2012.
213. B. Mathias, B. Tillmann and C. Palmer, "Sensory, cognitive, and sensorimotor learning effects in recognition memory for music," *Journal of Cognitive Neuroscience*, 2016.

214. G. Vecchiato, A. G. Maglione, A. Scorpecci, P. Malerba, P. Marsella, G. Di Francesco, S. Vitiello, A. Colosimo and F. Babiloni, "EEG frontal asymmetry related to pleasantness of music perception in healthy children and cochlear implanted users," *In Proc. of Annual International Conference of the IEEE Engineering in Medicine and Biology Society (EMBC)*, pp. 4740-4743, 2012.
215. A. Khasnobish, S. Datta, A. Konar, D. N. Tibarewala and R. Janarthanan, "Object shape recognition from EEG signals with tactile, visuo-tactile and audio-tactile stimuli," *In Proc. of IEEE International Conference on Communications and Signal Processing (ICCSP)*, pp. 122-126, 2014.
216. L. Twardon, H. Koesling, A. Finke and H. Ritter, "Gaze-contingent audio-visual substitution for the blind and visually impaired," *In Proc. of 7th IEEE International Conference on Pervasive Computing Technologies for Healthcare (PervasiveHealth)*, pp. 129-136, 2013.
217. M. Chaumon and N. A. Busch, "Prestimulus neural oscillations inhibit visual perception via modulation of response gain," *Journal of Cognitive Neuroscience*, vol. 26, no. 11, pp. 2514-2529, 2014.
218. S. Cososchi, R. Strungaru, A. Ungureanu and M. Ungureanu, "EEG features extraction for motor imagery," *In Proc. of 28th Annual International Conference of the IEEE Engineering in Medicine and Biology Society (EMBS'06)* pp. 1142-1145, 2006.
219. Z. Zhou and B. Wan, "Wavelet packet-based independent component analysis for feature extraction from motor imagery EEG of complex movements," *Clinical Neurophysiology*, vol. 123, no. 9, pp. 1779-1788, 2012.
220. R. Corralejo, R. Hornero and D. Alvarez, "Feature selection using a genetic algorithm in a motor imagery-based Brain Computer Interface," *In Proc. of Annual International Conference of the IEEE Engineering in Medicine and Biology Society (EMBC)*, pp. 7703-7706, 2011.
221. Q. Zhao, L. Zhang, A. Cichocki and J. Li, "Incremental common spatial pattern algorithm for BCI," *In Proc. of IEEE International Joint Conference on Neural Networks(IJCNN)*, pp. 2656-2659, 2008.
222. J. S. Kirar and R. K. Agrawal, "Optimal Spatio-spectral Variable Size Subbands Filter for Motor Imagery Brain Computer Interface," *Procedia Computer Science*, vol. 84, pp. 14-21, 2016.
223. S. R. Liyanage, J. X. Xu, C. Guan, K. K. Ang, C. S. Zhang and T. H. Lee, "Classification of self-paced finger movements with EEG signals using neural network and evolutionary approaches," *In Proc. of IEEE International Conference on Control and Automation, (ICCA)*, pp. 1807-1812, 2009.
224. R. N. Khushaba, A. Al-Ani and A. Al-Jumaily, "Feature subset selection using differential evolution and a statistical repair mechanism," *Expert Systems with Applications*, vol. 38, no. 9, pp. 11515-11526, 2011.

225. Y. Wang and S. Makeig, "Decoding Intended Movement from Human EEG in the Posterior Parietal Cortex," *Neuroimage*, vol. 47, pp. 437-446, 2009.
226. G. Pfurtscheller, C. Neuper, A. Schlogl and K. Lugger, "Separability of EEG signals recorded during right and left motor imagery using adaptive autoregressive parameters," *IEEE Trans. on Rehabilitation Engineering*, vol. 6, no. 3, pp. 316-325, 1998.
227. B. Obermaier, C. Guger, C. Neuper and G. Pfurtscheller, "Hidden Markov models for online classification of single trial EEG data," *Pattern Recognition Letters*, vol. 22, no. 12, pp. 1299-1309, 2001.
228. H. Lee and S. Choi, "PCA+HMM+SVM for EEG pattern classification," *In Proc. of Seventh International Symposium on IEEE Signal Processing and Its Applications*, vol. 1, pp. 541-544, 2003.
229. N. Lu, T. Li, X. Ren and H. Miao, "A Deep Learning Scheme for Motor Imagery Classification based on Restricted Boltzmann Machines," *IEEE Trans. on Neural Systems and Rehabilitation Engineering*, no. 99, 2016.
230. T. P. Jung, S. Makeig, M. Stensmo and T. J. Sejnowski, "Estimating alertness from the EEG power spectrum," *IEEE Trans. on Biomedical Engineering*, vol. 44, no. 1, pp. 60-69, 1997.
231. S. Makeig, T. P. Jung and T. J. Sejnowski, "Using feedforward neural networks to monitor alertness from changes in EEG correlation and coherence," *Advances in Neural Information Processing Systems*, pp. 931-937, 1996.
232. D. Begum, K. Ravikumar, J. Mathew, S. Kubakaddi and R. Yadav, "EEG based patient monitoring system for mental alertness using adaptive Neuro-Fuzzy approach," *J. Med. Bioeng*, vol. 4, no. 1, pp. 59-66, 2015.
233. L. Vezard, M. Chavent, P. Legrand, F. Faïta-Aïnseba and L. Trujillo, "Detecting mental states of alertness with genetic algorithm variable selection," *In Proc. of IEEE Congress on Evolutionary Computation (CEC)*, pp. 1247-1254, 2013.
234. A. Sengupta, A. Dasgupta, A. Chaudhuri, A. George, A. Routray and R. Guha, "A Multimodal System for Assessing Alertness Levels due to Cognitive Loading," *IEEE Trans. on Neural Systems and Rehabilitation Engineering*, 2017.
235. C. T. Lin, L. W. Ko, I. F. Chung, T. Y. Huang, Y. C. Chen, T. P. Jung, and S. F. Liang, "Adaptive EEG-based alertness estimation system by using ICA-based fuzzy neural networks," *IEEE Trans. on Circuits and Systems I: Regular Papers*, vol. 53, no. 11, pp. 2469-2476, 2006.
236. B. Biniás, D. Myszor, M. Niezabitowski and K. A. Cyran, "Evaluation of alertness and mental fatigue among participants of simulated flight sessions," *In Proc. of 17th International IEEE Carpathian Control Conference (ICCC)*, pp. 76-81, 2016.

## Chapter 2

# Olfactory Perceptual Ability Measurement Using a Recurrent Neural Classifier

*The chapter introduces a novel approach to measure perceptual-ability of subjects based on their EEG response to olfactory (smell) stimuli. A recurrent neural network model is employed to classify pre-trained base (standard) stimuli and discriminate noisy stimuli for both the olfactory stimuli of similar and different genres, where the noisy stimuli is synthesized by adding impurity to standard stimuli. The primary emphasis of the chapter lies in designing the recurrent neural dynamics with suitable weights, so that for a given base stimulus the convergence of the dynamics to one of several optima (local attractors) on the given Lyapunov energy surface is ensured. Experiments undertaken reveal that for small noise amplitude below a selected threshold, the dynamics essentially converges to fixed stable attractor. However, with a slight increase in noise amplitude above the selected threshold, the local attractor of the dynamics shifts in the neighborhood of the attractor obtained for the noise-free standard stimuli. The other important issues undertaken in the chapter include a novel algorithm for evolutionary feature selection and data-point reduction from multiple experimental EEG trials using principal component analysis. The confusion matrices constructed from the experimental results of olfactory classification justifies the importance of data point reduction. Statistical tests undertaken indicate that the proposed recurrent classifier outperforms its competitors with classification accuracy as the comparator. Lastly, the importance of the chapter is examined on a simulated tea-taster selection problem, where feature level discrimination of both the noisy and standard tea-samples are prominent from the given scatter plot.*

## 2.1 INTRODUCTION

Olfactory perception is the process of understanding and recognizing smell stimuli using previous knowledge/experience about it [1]. A person's ability to recognize and interpret stimuli, hereafter called perceptual-ability, depends on the sensitivity of the participating neurons in the perceptual process [2]. This sensitivity in turn depends on the structural and/or functional behavior of the neurons [3]. Perceptual ability varies widely due to individual differences in neuronal sensitivity [4]. There is no standard approach to measure perceptual-ability based on neuronal participation in the perceptual process. This chapter introduces an approach to measure perceptual-ability using electroencephalographic (EEG) response [5].

Humans process smell stimuli by a sequence of three steps [6]. Aromatic stimuli are perceived by receptors located in the *olfactory epithelium* (inside the nasal cavity) through mucus present in the nostrils. Odor is then sensed by one (or fewer) of several hundred receptor neurons responsible for encoding a particular olfactory stimulus. To synthesize the composite signal for transfer to the olfactory cortex, the fired neuron responses from the stimulus are collected by one of several glomeruli (each reserved for one stimulus) of olfactory bulbs [7]. In humans, pro-cerebral lobes synthesize electrical neuronal spikes while discriminating olfactory stimuli [8]. The pro-cerebral lobe is located half-way within temporal and frontal lobes. The electrical spikes can be acquired as cortical response to olfactory stimuli from appropriate scalp locations.

An EEG machine acquires the cortical current signals from different locations on the scalp using metal electrodes [9] and transforms them into equivalent voltage signals by passing the current through resistive devices. The obtained voltage swings are digitized inside the EEG system for subsequent processing by an attached computer to filter noise and recognize olfactory stimulus. There exist a number of techniques to acquire the brain states involved in perceptual processes. We employed EEG here for its superior temporal resolution [10], noninvasiveness [11], [12], portability and low-price. In addition, EEG signals acquired from the pre-frontal [13], [14] and the temporal lobes [15], have good correlations with olfactory recognition, memory and perception. This work attempts to determine perceptual-ability using EEG response to odor stimuli.

Signal modality selection is an important issue in EEG analysis. Usually, signal modality greatly depends on the cognitive tasks involved, and/or the stimulus type and also the modality of stimulation. In [16], the authors employed olfactory event-related potentials (OERP) to analyze cortical response to olfactory stimuli. OERP offers high sensitivity to olfactory function. The reaction time to odors is typically found to lie in (800-900) millisecond range. Further, the reaction time varies depending on stimulus characteristics [17]. Here, we use OERP particularly for its long persistence to classify smell from EEG response.

The chapter aims at addressing two important aspects concerning olfactory perception. First, it proposes a new technique to recognize olfactory stimuli from the EEG response. The study includes recognizing both pre-trained base (standard) stimuli and noisy stimuli, where the latter is synthesized by injection of noisy aromatic ingredients into a base (standard) stimulus. The other problem addressed in the chapter deals with the measurement of perceptual-ability to recognize pre-trained base stimuli and separating noisy stimuli.

The first problem refers to designing a recurrent neural dynamics, capable of classifying smell stimuli from the EEG signals captured from one's pre-frontal lobe. The initial value of the variables used in the neuronal dynamics here represents the selected features of an olfactory stimulus. The objective of the design lies in identification of a weight vector for the dynamics to ensure its convergence to a given minimum on the selected Lyapunov energy surface, particularly when the dynamics is initialized around the minimum. This is done by designing an optimization problem with an aim to minimize the Lyapunov energy function at selected locations on the energy surface for a unique weight vector. Differential Evolution (DE) [18] algorithm is used to optimize the energy function. Further, we perform feature selection by evolutionary algorithm, and data point reduction by Principal Component Analysis (PCA) [19], [20], [21].

Feature selection of an EEG signal can be performed by attempting to model EEG in different domains to extract necessary domain features [22-24]. For example, the nonlinearity of EEG is captured by time-domain features, while the frequency domain EEG features provide a direct correlation between cognitive tasks and specific frequency bands. The non-stationary characteristic of EEG is captured by time-frequency correlated features, such as wavelet transforms. All the above features together form a very high dimensional feature vector. Selecting fewer features without losing classification accuracy of the underlying cognitive tasks reduces computational overhead of the classifier. The chapter proposes a novel approach to automatic feature selection (from the high dimensional feature space) by an evolutionary algorithm.

Given a set of training instances where each instance includes a set of features with respective class labels. For any integer  $j$ , the  $j$ -th feature of the data points in a given class should differ as little as possible. For each selected feature  $j$ , the difference between the mean-to-standard deviation ratios of the feature of any two classes should be as large as possible. A DE algorithm selects a minimal set of appropriate features that optimizes the above objectives jointly.

Data point reduction is important in EEG-based stimulus classification. The features extracted from multiple trials of the EEG signals, even from the same subject with the same stimulus, are not unique. This requires identifying "ideal" class representative data points, where each point represents a feature vector of a fixed dimension. Here recurrent neural

dynamics is used to map the ideal class representative to an optimum of the Lyapunov energy surface. If instead of mapping the class representatives only, all data points of same class (from the same subject and stimulus) were mapped on to the Lyapunov surface, they would form a small cluster of optima in close vicinity on the energy surface. However, with “poor data points” of a class, the mapped optima may not be close on the energy surface, introducing complexity in the classification of unknown data points. Here instead mapping only uses the “ideal class representatives” on to the energy surface. To find the ideal class representative, we employ PCA to obtain a transformed single data point (class representative) from a set of data points of the smell class of same dimensions.

The second addressed problem deals with perceptual-ability measurement, concerning both recognition-ability of base stimuli and discriminating ability of noisy stimuli. The results of stimuli classification by the proposed recurrent classifier are used to determine (relative) perceptual-ability. The perceptual-ability measurement has been successfully applied in a simulated tea-taster selection problem.

The present chapter extends [25] with a classifier design using a specialized recurrent neural net with Rastrigin function as the Lyapunov surface (Hopfield neural net [26], [27] based classifier was used in [25]). A metric of perceptual-ability is defined herein based on the recognition-ability of base stimuli and discriminating ability of noisy stimuli. An application to determine perceptual-ability of subjects in a tea-taster selection problem is presented.

The chapter is structured as follows. Section 2.2 describes Lyapunov stability analysis. Section 2.3 describes olfactory stimulus classification. Section 2.4 discusses a metric for perceptual-ability measurement. Section 2.5 provides the methods and Section 2.6 provides results of the olfactory classifier validation for odors of both similar and different genres. Section 2.7 demonstrates case study with tea-taster selection. The conclusion is in Section 2.8.

## 2.2 LYAPUNOV STABILITY ANALYSIS

We employ a recurrent neural network classifier, the structural design (connectivity of neurons) of which is determined by Lyapunov stability analysis [28].

*Definition 1:* A scalar function  $V(\vec{U})$  is called a **Lyapunov surface with respect to origin**, if the following three conditions are satisfied:

- i)  $V(\mathbf{0})=0$
- ii)  $V(\vec{U}) > 0$  for  $\vec{U} \neq 0$



iii)  $V(\vec{U})$  has continuous first partial derivatives with respect to all components of  $\vec{U}$ . It means that  $\frac{\partial V}{\partial u_i}$  is a continuous function of  $u_i$ , where  $u_i$  is the  $i$ -th component of  $\vec{U}$  [29].

*Definition 2:* Given the dynamics of a system:

$$\frac{d\vec{U}}{dt} = f(\vec{U}(t)). \quad (2.1)$$

where  $\vec{U}$  is of  $(d \times 1)$  dimension and  $f$  denotes a scalar function of  $\vec{U}(t)$ . The solution  $\vec{U}$  ( $=\vec{U}_{eq}$  say) of  $\frac{d\vec{U}}{dt} = 0$  in (2.1) is called an **equilibrium state/stable point** of the dynamics.

*Definition 3:* Let  $\|\vec{U}\|$  denotes the Euclidean norm of a vector  $\vec{U}$ . For a given dynamics  $\frac{d\vec{U}}{dt} = f(\vec{U}(t))$ , let  $\vec{U}_{eq}$  be the equilibrium point. Then the set of points  $\vec{U}(t)$  for which  $\|\vec{U} - \vec{U}_{eq}\| \leq \epsilon$ , where  $\epsilon$  is positive number, however small, is called the  $\epsilon$ -**neighborhood**  $S(\epsilon)$  of  $\vec{U}(t)$ .

*Definition 4.* A scalar function  $V(\vec{U})$  is called **negative (positive) definite** with respect to the point  $\vec{U}_{eq}$  in the  $\epsilon$ -neighborhood of  $\vec{U}(t)$ , if  $-V(\vec{U}) > 0$  ( $V(\vec{U}) > 0$ ) at all points in the region excluding  $\vec{U}_{eq}$  itself, where it is zero.

*Definition 5.* The necessary conditions for the dynamics  $\frac{d\vec{U}}{dt} = f(\vec{U}(t))$  to be **asymptotically stable** at the equilibrium point  $\vec{U}_{eq}$  are:

- i) there is a region  $S(\delta)$ , where  $\delta < \epsilon$  for any neighborhood  $S(\epsilon)$  surrounding  $\vec{U}_{eq}$ , such that the trajectories of the dynamics would start within  $S(\delta)$  but remains within  $S(\epsilon)$  as time  $t$  approaches infinity, and
- ii) the trajectory of the dynamics would start within  $S(\epsilon)$  and converge to the origin as time  $t$  approaches infinity.

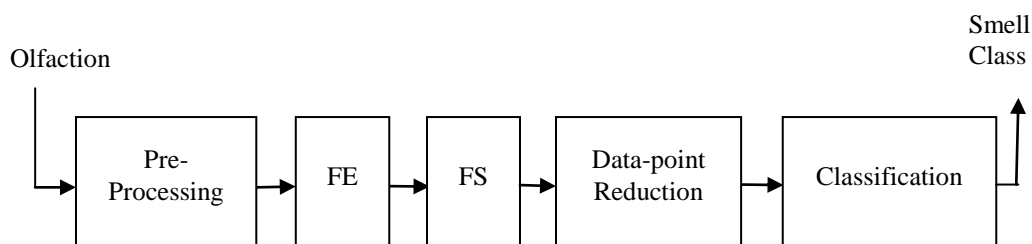
Given a dynamics of the form  $\frac{d\vec{U}}{dt} = f(\vec{U}(t))$  where  $\vec{U}(t)$  is of  $(d \times 1)$  dimension. Let  $V(\vec{U})$  be the Lyapunov surface for the given dynamics. Then the dynamics is **asymptotically stable** in the large, if  $\frac{dV(\vec{U})}{dt}$  is negative definite. This statement is popularly known as **Lyapunov's stability criterion** [29].

## 2.3 SYSTEM OVERVIEW AND DESIGN

This section provides a schematic architecture of smell stimuli classification using the pre-frontal EEG response (Fig. 2.1). Smell stimulus is first processed to keep it free from artifacts due to eye blinking and the power supply. Eye blinking does not predominantly affect the

EEG data as subjects are instructed to keep their eyes closed during the experiments. EEG response to olfactory stimuli is usually confined in (3-13) Hz, i.e., theta (3-7 Hz) and alpha (7-13 Hz) bands [30-33]. Pre-processing in Fig. 2.1, therefore, refers to obtaining the desired frequency band of 3-13 Hz by a band-pass filter.

The next two steps are feature extraction (FE) and feature selection (FS) respectively. While feature extraction involves extraction of features from the EEG signal, feature selection refers to identifying an optimal set of features from the list of extracted features. For EEG feature extraction, researchers usually start with a large set of EEG features and use a feature selection algorithm to down-select features. Here, feature selection (FS) algorithm down-selects the features from a pool containing time-domain, frequency-domain and time-frequency-correlated features. One approach adopted here is to group a few selected features of different domains in different combinations so as to obtain several sets of overlapped features, and later to use a classifier to identify the best feature set. The fourth step is data point reduction, where we obtain a single data point (feature vector) of  $d$ -dimension from a given set of  $t$   $d$ -dimensional data points using the first principal component of the data covariance matrix of  $(t \times d)$  dimension. The last step is classification realized with a recurrent neural network.



**Fig. 2.1** A schematic architecture of smell-stimuli classification

### 2.3.1 Feature Extraction

Existing literature [30], [32], [34] on EEG based brain-computer interfacing (BCI) provides a number of features, which have good correlation with olfactory perception. EEG provides good temporal resolution and therefore temporal features (for example, Hjorth parameters, and autoregressive parameters) carry important information about the mental tasks undertaken by the subject. Further, the neuronal excitations corresponding to a given task are found to have specific narrow frequency bands. Naturally, frequency domain features, such as power spectra at different frequency bands, too are essential attributes to decode brain imagery. Unfortunately, only time- or frequency-domain features are unable to capture the correspondence between time and frequency, i.e., which frequency at a given time. Time-frequency domain features, such as wavelet coefficients, however, capture time-frequency correlations and thus carry more information about the EEG signal corresponding to an imagined task.

The most commonly used features employed in EEG research, irrespective of the cognitive tasks undertaken; include Hjorth parameters [35], [36], power spectral density (PSD) [37], wavelet coefficients [38] and autoregressive (AR) parameters [39]. Each of the above features excluding the Hjorth parameters has a large dimension. The above features yield large feature vectors, adding significant computational overhead to the classifier. One approach to reduce this overhead is to pick up (at least) two types of features of different domains, place them in random proportion in a vector of fixed length, and then select the best among such vectors with respect to classification rate. We consider a mixture of 1) Hjorth plus PSD, 2) wavelet coefficient plus PSD, and 3) AR plus PSD parameters.

### 2.3.2 Feature Selection

Given a set of  $N$  time-domain (fixed duration) EEG signals obtained from multiple subjects, including repeated trials for the same subject, for each EEG signal, we obtain a  $D$ -dimensional data point (also called feature vector containing  $D$  features). Let  $\vec{X}_i = [x_{i,1} \ x_{i,2} \ \dots \ x_{i,D}]$  be the  $i$ -th data point (feature vector), where  $x_{i,j}$  for  $j = 1$  to  $D$  denotes the  $j$ -th feature of the  $i$ -th EEG signal. Each of the  $N$  EEG signals has an assigned (olfactory) class label  $k \in [1, K]$ , where  $K$  denotes the maximum number of classes. The problem in the present context is to optimally select  $d$  out of  $D$  number of features, considering all the  $N$  EEG signals without losing their class identities. Several algorithms for automatic feature selection are available in the current literature [40], [41]. The most popular among them are sequential forward (SF) and sequential backward (SB) selections. The SF (SB) selection starts with an empty (complete) set of features and adds (deletes) one feature at a time with an aim to select the best  $d$  out of  $D$  features. The sequential algorithms suffer from the well-known “nesting effect” [42], which entails that a previously added (deleted) feature cannot be discarded (inserted) later. The drawback of sequential selection can be overcome by formulating the problem using optimization and solving it by a random search/evolutionary algorithm.

Let,

- $x_{i,j}^m$  and  $x_{\ell,j}^m$  be the  $j$ -th feature of the  $i$ -th and  $\ell$ -th EEG time-series respectively belonging to the class  $m$ ;
- $N_m$  be the number of data points in class  $m$ ;
- $\mu_j^m$  and  $\mu_j^n$  are the mean of the  $j$ -th feature respectively in  $m$ -th and  $n$ -th classes;
- $\sigma_j^m$  and  $\sigma_j^n$  be the standard deviation of the  $j$ -th feature in  $m$ -th and  $n$ -th classes respectively.

We now represent feature selection as an optimization problem to satisfy the following two objectives.

The first objective function  $L_1$  aims at minimizing the difference between individual feature values of any two data points within a class. This is ensured by minimization of objective (2.2).

$$L_1 = \sum_{m=1}^K \sum_{j=1}^d \sum_{i=1}^{N_m} \sum_{\substack{\ell=1 \\ \ell \neq i}}^{N_m} |x_{i,j}^m - x_{\ell,j}^m| \quad (2.2)$$

The second objective function  $L_2$  attempts to maximize the *mean to standard deviation* ratio of a feature between any two classes. This is ensured by maximization of (2.3).

$$L_2 = \sum_{m=1}^K \sum_{\substack{n=1 \\ n \neq m}}^K \sum_{j=1}^d |(\mu_j^m / \sigma_j^m) - (\mu_j^n / \sigma_j^n)| \quad (2.3)$$

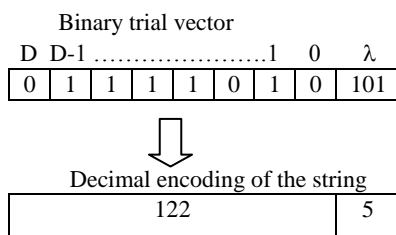
Now, we construct a composite objective function  $L$  given in (2.4), the minimization of which satisfies the above two objectives.

$$L = L_1 - \lambda L_2 \quad (2.4)$$

Here,  $\lambda$  is the scale factor introduced to scale  $L_2$  to maintain uniformity in the order of magnitude between the two terms in the right hand side of (2.4). One approach to optimize (2.4) is to employ any numerical/meta-heuristic optimization algorithm [43-45] to determine the optimal set of features. Several swarm and evolutionary optimization algorithms are available in the current literature [46-49].

We solve the optimization using the Differential Evolution (DE) algorithm. We use DE/rand/1/bin [18] version of DE. The DE used here has four main steps: initialization, mutation, recombination and selection. In the initialization phase, we generate trial solutions (also called parameter vectors) for the optimization problem. Here, the parameter vectors are represented by binary strings consisting of two fields: i) a  $D$ -dimensional sub-string, where a one (zero) in the  $j$ -th component represents inclusion (exclusion) of the  $j$ -th feature, and ii) a choice of  $\lambda$  in  $[0, 10]$ . The above bounds of  $\lambda$  is selected experimentally to maintain a uniformity in the order of magnitude of the two terms in the right-hand side of (2.4). See Fig. 2.2 for an example trial vector.

The rest of the DE algorithm includes mutation, recombination and selection over iterations, until the criteria for convergence is satisfied. See the Appendix A.1 for more details.



**Fig. 2.2** An example trial vector

### 2.3.3 Data Reduction using PCA

Features extracted from EEG signals of the same subject with same stimulus over multiple trials are not unique. We derive a unique set of EEG features by identifying the commonality among the feature vectors, (hereafter called data points) obtained over multiple experimental trials. The derived data point containing commonality (obtained from the same subject with the same stimulus) may be considered as the ‘‘ideal data point’’ for the given class of the stimulus. Here, we use PCA, as many times as the number of stimulus times the number of subjects, to extract the ideal data points from each subject in response to different stimuli.

Let,

$\mathbf{S}_k = \{\overrightarrow{X}_1^k, \overrightarrow{X}_2^k, \dots, \overrightarrow{X}_t^k\}$  be a set of  $t$  extracted feature vectors for the  $k$ -th stimulus, where  $\overrightarrow{X}_i^k = \{x_{i,1}^k, x_{i,2}^k, \dots, x_{i,d}^k\}$  is a  $d$ -dimensional feature vector (data point) obtained after feature selection, and  $k \in [1, K]$  denotes the  $k$ -th stimulus, where  $K$  is maximum number of stimuli used.

The main steps of PCA are briefly outlined below.

1. For each data point  $\overrightarrow{X}_i^k$ , we obtain a new (mean-subtracted) vector

$$\overrightarrow{X}_i'^k = \{x_{i,1}^k - \bar{x}_i^k, x_{i,2}^k - \bar{x}_i^k, \dots, x_{i,d}^k - \bar{x}_i^k\}, \quad (2.5)$$

where  $\bar{x}_i^k$  is the mean of the elements in  $\overrightarrow{X}_i^k$ .

2. Let,  $\mathbf{D}_k = [\overrightarrow{X}_1'^k, \overrightarrow{X}_2'^k, \dots, \overrightarrow{X}_t'^k]^T$  be a matrix of  $(t \times d)$  dimension. We obtain the data covariance matrix  $\mathbf{C}_k = \frac{1}{(d-1)} \mathbf{D}_k \cdot \mathbf{D}_k^T$  and obtain its first principal component  $\overrightarrow{PC}_k$  (i.e.,

Eigen vector corresponding to the largest Eigen value).

3. We project the mean subtracted data points:  $\overrightarrow{X}_i'^k$ ,  $i=1$  to  $t$  along the first principal component to obtain the class representative data point  $\vec{\theta}_k$  by the following transformation:

$$\vec{\theta}_k = (\overrightarrow{PC}_k^T \times \mathbf{D}_k). \quad (2.6)$$

Thus we obtain one class representative data point of  $d$ -dimension from  $t$  data points of  $d$ -dimension of the same class. The process is repeated for each group of  $t$  data points obtained from each subject due to application of each stimulus. Thus for a maximum of  $K$  number of stimuli and  $R$  subjects, the above procedure is repeated  $K \times R$  times.

### 2.3.4 Classification

In classifying the acquired EEG signals corresponding to an unknown smell stimulus into one of several known olfactory classes, we strive to maintain high classification accuracy even when the olfactory stimulus is not free from noise due to aromatic impurities. Recurrent neural topologies [50], for example Hopfield neural net [26], have inherent power to map

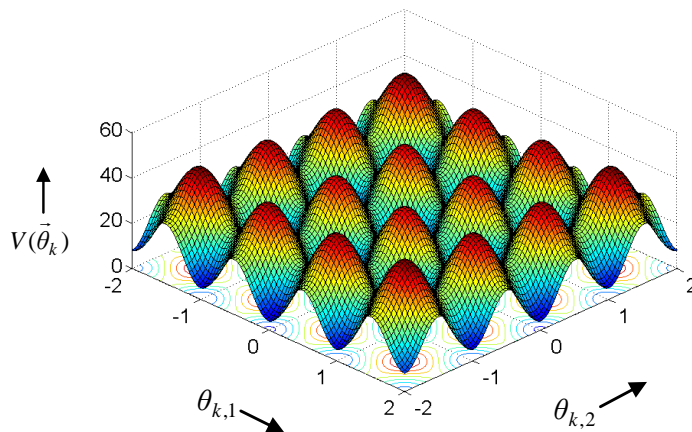
noisy data points into stable classes, represented by the optima on the energy surface constructed for a given Hopfield-like dynamics.

With Hopfield neural nets, researchers generally design an energy function for a given neuronal dynamics of the recurrent network to determine the condition for stability of the dynamics. Instead, we start our design with a given energy function that satisfies the characteristics of a Lyapunov function [28] containing multiple minima. We want the dynamics to settle to one of the available minima depending on the initial parameters. Here, the (reduced) features of an olfactory signal are used as the initial parameters of the dynamics. The dynamics settle to a specific minimum for two or more instances of features corresponding to different smell stimuli when stimuli are similar. Fig. 3.3 provides a plot of two-dimensional Rastrigin function, a smooth (continuous) function with multiple minima, the deepest of which is located at the origin, that satisfy the required criteria of a Lyapunov function with multiple optima (minima). Using the Rastrigin function as the energy function, we determine the neuronal dynamics so as to satisfy the condition of negative definiteness in its time-derivative, ensuring asymptotic stability of the dynamics in the sense of Lyapunov and thus its convergence at one of several minima.

Let  $\vec{\theta}_k = [\theta_{k,1} \ \theta_{k,2} \ \dots \ \theta_{k,d}]_{1 \times d}$  be the  $k$ -th smell class- representative containing  $d$  number of features:  $\theta_{k,j}, j = 1$  to  $d$ , and  $V(\vec{\theta}_k)$  be the Rastrigin-type Lyapunov surface, given by

$$V(\vec{\theta}_k) = \sum_{j=1}^d [\theta_{k,j}^2 - 10w_j \cos(2\pi\theta_{k,j}) + 10] \quad (2.7)$$

for  $k=1$  to  $K$ , involving the weight vector  $\vec{W} = [w_1 \ w_2 \ \dots \ w_d]_{1 \times d}$ . It is also apparent that the function  $V(\vec{\theta}_k)$  in (2.7) satisfies the necessary conditions of Lyapunov function.



**Fig. 2.3** The plot of a two-dimensional Rastrigin function: Equation (7) with dimension=2.

The time-derivative of  $V(\vec{\theta}_k)$  is obtained as

$$\frac{dV(\vec{\theta}_k)}{dt} = \sum_{j=1}^d \frac{\partial V(\theta_{k,j})}{\partial \theta_{k,j}} \cdot \frac{d(\theta_{k,j})}{dt}. \quad (2.8)$$

$$= \sum_{j=1}^d \frac{\partial}{\partial \theta_{k,j}} \left( \sum_{j=1}^d (\theta_{k,j}^2 - 10w_j \cos(2\pi\theta_{k,j}) + 10) \right) \frac{d\theta_{k,j}}{dt}. \quad (2.9)$$

$$= \sum_{j=1}^d (2\theta_{k,j} + 20\pi w_j \sin(2\pi\theta_{k,j})) \frac{d\theta_{k,j}}{dt}. \quad (2.10)$$

Now, the condition for asymptotic stability of the dynamics is given by:

$$\frac{dV(\vec{\theta}_k)}{dt} < 0. \quad (3.11)$$

From (2.10) that the condition stated in (2.11) holds, if

$$\frac{d\theta_{k,j}}{dt} = -2(\theta_{k,j} + 10\pi w_j \sin(2\pi\theta_{k,j})), \forall i,j. \quad (2.12)$$

Equation (2.12) provides a set of dynamics for each smell class  $k$  and feature  $j$ .

We now briefly discuss the encoding and the recall cycles for the proposed recurrent neural network. Encoding refers to identifying the weight vector of the recurrent network, whereas recall refers to determining one of the minima (stable attractor) on the Lyapunov surface for a given initial settings of  $\vec{\theta}_{ij}(t)$ .

*Encoding:* Given  $\vec{\theta}_k = [\theta_{k,1} \ \theta_{k,2} \ \dots \ \theta_{k,d}]_{1 \times d}$  for  $k=1$  to  $K$  smell classes, we now propose a method to determine a unique weight vector  $\vec{W} = [w_1 \ w_2 \ \dots \ w_d]_{1 \times d}$ , such that for each smell class-representative  $\vec{\theta}_k$ ,  $k=1$  to  $K$ , we have a minimum on the energy surface  $V(\vec{\theta}_k)$ . The minimum on the energy surface for a given stimulus is marked as the stable optimum (attractor) for the stimulus class. The weight vector selection is performed using optimization, where the objective is to uniquely determine the weight vector so as to minimize the energy function  $V(\vec{\theta}_k)$  for  $k= 1$  to  $K$  classes. The algorithm to select optimal weight vector for recurrent neural network classifier for a given smell class is given in the Appendix A.2.

*Recall:* To match an unknown input stimulus, we need to take  $t$  instances of the stimulus of uniform durations separated by equal time-delays, and pass the acquired  $t$  instances of EEG signals through pre-processing, feature extraction and feature selection steps as outlined in sections 2.3.1 and 2.3.2, and finally reduce the  $t$  sets of features into one set by data point reduction algorithm, given in section 2.3.3.

Let the assembled  $d$ -dimensional features (data point) obtained following the above steps for an unknown olfactory stimulus be  $\vec{\theta}'(0)$ , representing the initial choice of the parameters

in the neuronal dynamics given in (3.12) with  $\theta_{k,j}$  replaced by  $\theta'_j$  for all  $j$ . Let  $\bar{\theta}_k$  for  $k=1$  to  $K$  be the representative optima for  $K$  distinct smell classes. To identify the nearest known optimum to  $\bar{\theta}'(t)$  at steady-state, we solve the dynamics (2.12) with  $\theta_{k,j} = \theta'_j$  for  $j= 1$  to  $d$ , and identify the optimum stable point (attractor) with the shortest Euclidean distance with steady-state value of  $\bar{\theta}'(t)$ . The class of the unknown stimulus now can be inferred from the pre-defined location of convergence of the each known stimulus class. The algorithm to determine the nearest stable optimum for a given smell class is given in the Appendix A.3.

## 2.4 PERCEPTUAL-ABILITY MEASURE

We propose a novel technique to measure (relative) perceptual-ability based on two parameters. The first parameter, referred to as recognition-ability, represents the ability to recognize pre-trained smell (olfactory) stimuli correctly. The second parameter, called discriminating ability, represents the ability to discriminate two or more noisy smell stimuli, where the noisy smell stimuli are synthesized by adding different aromatic impurities to one base (standard) stimulus. Usually, impurities are added in 100-200 parts per million volumes of the standard stimuli to maintain the traces of the standard stimuli in the noisy stimuli.

Let,  $n_k^s$  be the sample size of the standard olfactory stimulus of class  $k$  presented to subject  $s$  in a random order, where the samples may contain natural impurity due to their collection from diverse sources. Let,  $n'_k{}^s$  be the number of correctly classified stimuli by the same subject. Then the probability that a pre-trained smell stimulus of class  $k$  will be correctly recognized by subject  $s$ , hereafter called  $C_k^s$ , in a single trial is given by

$$P(C_k^s) = \frac{n'_k{}^s}{n_k^s}. \quad (2.13)$$

The average of  $P(C_k^s)$  for a given subject  $s$  for  $k = 1$  to  $K$ , where  $K$  denotes maximum number of classes, is hereafter referred to as the *recognition-ability*, and is given by

$$RA_s = \frac{1}{K} \sum_{k=1}^K P(C_k^s). \quad (2.14)$$

The second parameter,  $DA_s$ , is used to determine the power of discrimination of noisy smell stimuli by the subject  $s$ , based on a measure of similarity of each noisy stimulus with its ideal (noise-free) class centroid and its dissimilarity with the class centroids of other standard stimuli.

Let,

$\bar{X}_c^i$  be the centroid of the noise-free data points of class  $i$  ;

$Q_i$  be the number of noisy data points lying in class  $i$ ;



$\vec{X}_r = [x_{r,j}]_{1 \times d}$  be the  $r$ -th noisy data point lying in class  $i$ ,  $r= 1$  to  $Q_i$ ;

$Dist_i$  be the average of  $Q_i$  city block distances of  $\vec{X}_r = [x_{r,j}]_{1 \times d}$ ,  $r= 1$  to  $Q_i$  from  $\vec{X}_c^i$ .

Let  $Q_i (=4)$  out of  $Q (=14)$  data points for each stimulus be noisy. Thus, we obtain:

$$Dist_i = \frac{1}{Q_i} \sum_{j=1}^d \sum_{r=1}^{Q_i} (|x_{r,j} - x_{c,j}^i|). \quad (2.15)$$

Let,  $Dist'_i$  be the average city block distance of  $(K-1)$  non-noisy class centroids  $\vec{X}_c^k = [x_{c,j}^k]$  for  $k= 1$  to  $K$  classes,  $k \neq i$ , with all noisy data point  $\vec{X}_r = [x_{r,j}]_{1 \times d}$  of class  $i$ . Symbolically,

$$Dist'_i = \frac{1}{(K-1) \times Q_i} \sum_{\substack{k=1 \\ k \neq i}}^K \sum_{r=1}^{Q_i} \sum_{j=1}^d (|x_{c,j}^k - x_{r,j}|) \quad (2.16)$$

Now,  $DA_s$  representing the average discriminating ability, considering all stimuli, is defined as the average of the ratio  $\frac{Dist_i}{Dist'_i}$  for  $i=1$  to  $K$ , i.e.,

$$DA_s = \frac{1}{K} \sum_{i=1}^K \frac{Dist_i}{Dist'_i}. \quad (2.17)$$

The larger is the  $DA_s$ , the higher is the average discriminating ability of subject  $s$ . Usually,  $Dist'_i$  is much larger than  $Dist_i$  for all  $i$ ; consequently  $DA_s$  appears to be much smaller. This motivated us to use a normalized measure of  $DA_s$ , called  $\overline{DA}_s$ , where  $\overline{DA}_s = \frac{DA_s}{\text{Max}_{\forall s}(DA_s)}$ . Now,

treating  $\overline{DA}_s$  like probability and presuming that  $RA_s$  and  $\overline{DA}_s$  are independent, we define Perceptual-ability ( $PA_s$ ) of subject  $s$  as

$$PA_s = RA_s \times \overline{DA}_s. \quad (2.18)$$

The product function introduced in (2.18) reveals that an increase in either  $RA_s$  or  $\overline{DA}_s$  or both cause an increase in  $PA_s$ .

The parameter  $PA_s$  supports comparing the relative perceptual-ability between subjects. We determine the rank of a subject in an experimental group of  $M$  subjects using the index of an array of the total set of sorted  $PA_s$ .

## 2.5 PHYSIOLOGICAL SIGNAL PROCESSING AND CLASSIFICATION EXPERIMENTS

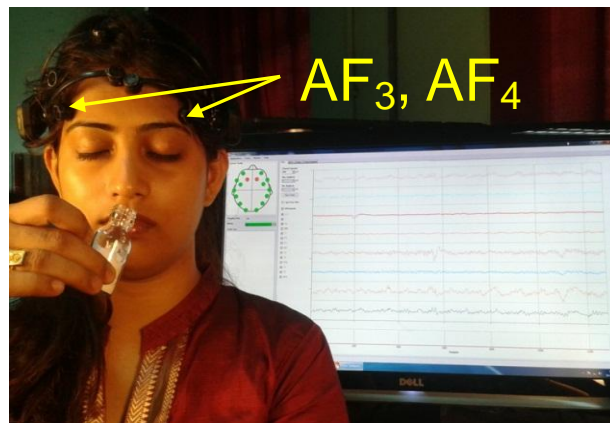
This section describes the methods to identify: i) the active brain regions responsible for olfaction, ii) the necessary frequency spectrum of the EEG associated with olfaction, iii) the

necessary EEG features required for classification of olfactory sources for similar and different genres, and iv) noisy stimulus discrimination.

### 2.5.1 Experimental Framework

The experimental framework includes a wireless 14 channel EEG headset (manufactured by Emotiv) and an Intel i7 desktop computer with 8GB RAM and a CPU clock of 3.4GHz with EEGLAB, MATLAB 2011B with the signal processing toolbox, and EMOTIV Application Processing Interface (API). The EEG Emotiv system has a sampling rate of 128 Hz with a signal resolution of  $100\mu\text{V}$ . EEG signals are picked up from 14 electrodes namely AF<sub>3</sub>, AF<sub>4</sub>, F<sub>7</sub>, F<sub>8</sub>, F<sub>3</sub>, F<sub>4</sub>, P<sub>7</sub>, P<sub>8</sub>, T<sub>7</sub>, T<sub>8</sub>, FC<sub>5</sub>, FC<sub>6</sub>, O<sub>1</sub> and O<sub>2</sub>. Here, odd numbers denote left hemisphere and even numbers denote right hemisphere. Among these, AF<sub>3</sub> and AF<sub>4</sub> are primarily associated for olfactory signal recognition. The experiment includes 17 men and 8 women (subjects) in the age group of 20-28. Fig. 2.4 provides an experimental trial, where a subject is given an unknown smell stimulus to recognize and her EEG signal is captured by Emotiv headset.

Usually, an experiment is composed of ten sessions, with 10 trials per session. Each odorant is presented for 10 seconds with a gap of 5 minutes between consecutive trials. Ten distinct odorants, including naphthalene, odonil (air/room freshener and insect-killer), sandalwood powder, cinnamon, rosewater, male perfume, hydrogen sulphide, ammonia, methane and camphor are used as smell stimuli for the experiments. For classification of odors of similar genre, five distinct stimuli, cumin, coriander, bay leaves, cinnamon and cardamom are used.



**Fig. 2.4** An experimental trial, having a subject experiencing an unknown smell stimulus for olfactory recognition

### 2.5.2 Experiment 1(Selection of Active Brain Regions)

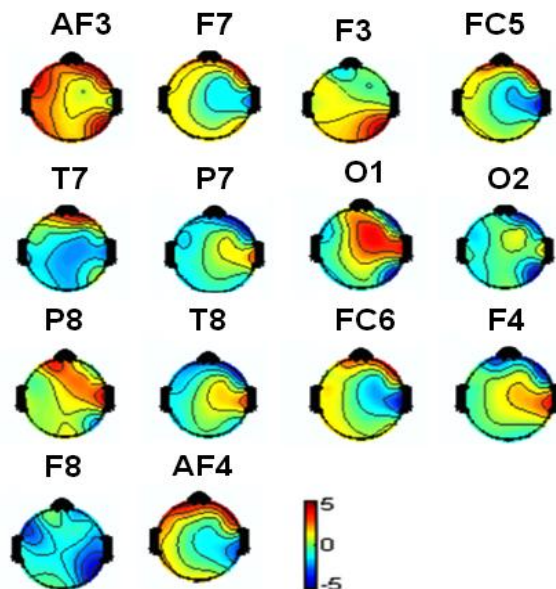
This experiment identifies the active brain regions responsible for sensing and/or processing of olfactory stimuli. Independent Component Analysis (ICA) [51] has been used to localize  $n$  independent sources from  $n$  time-varying EEG signals from different regions on the scalp. For

the present application of olfactory stimuli recognition, fewer locations in the brain are activated (have high signal activation as identified from the component scalp-maps of the ICA response). With  $C=14$  channels, we identify 14 independent sources using ICA, and select fewer than 14 sources having relatively high brain activation due to olfaction.

Fig. 2.5 provides component scalp maps for 14 channels after performing ICA analysis during an experimental trial. The figure demonstrates the high activity (marked in red) in the pre-frontal region, whereas comparatively lower activity (marked in blue) in the remaining regions. Supporting neuro-biological evidence found in [52-56] reveals that olfaction sensing and processing is performed primarily by the pre-frontal cortex.

### 2.5.3 Experiment 2(Frequency Band and Type Selection of Filters in Pre-processing)

We first determine the selective frequency band of the filter and then select the filter type based on the desired characteristics. For filter band selection, we take the Fourier transformation of the EEG signals obtained for different stimuli. The frequency spectra from four distinct stimuli show high amplitude peaks between 3-13 Hz (Fig. 2.6). For all ten samples, the above observation holds for samples from the pre-frontal electrodes. The pass-band of the filters used for pre-processing is 3-13 Hz, covering both theta ( $\theta$ ) and alpha ( $\alpha$ ) bands. The results are supported by [31-32].



**Fig. 2.5** Component epoch maps of 14-channel Emotiv headset. AF3 and AF4 refer to pre-frontal lobe, F3, F4, F7, and F8 refer to frontal lobe, FC5 and FC6 refer to primary motor cortex, T7 and T8 refer to temporal lobe, P7 and P8 refer to parietal lobe, O1 and O2 refer to occipital lobe. Here, blue color in the color bar signifies the lowest activation, whereas the highest activation is denoted by red color.

Next, we select the filter types among the alternatives. Typically, we have four common IIR (infinite impulse response) filter realizations: Butterworth, Chebyshev type-1 and type-2, and elliptic. Filter selection in a given application is usually guided by required filter performance (filter roll-off, ripples in pass and stop band, computational complexity). Since the sampling frequency here is low (128 Hz), we focus on roll-off and ripples in pass/stop bands of the band pass filters in (8-13) Hz band. We varied filter order (i.e., highest degree of the polynomial in the denominator) for different realizations and found the four competitive filters: Butterworth of order 6, Chebyshev type-1 and type-2 of order 4, and elliptic filter of order 4. Fig. 2.7 shows that the sharpest roll-off and good attenuation in both pass/stop band ripples are obtained for the elliptic filter. We selected the elliptic filter of order 4 for the digital band pass filter.

### 2.5.4 Experiment 3(Selection of EEG Features)

Performance of a pattern classifier is determined by the features used for classification and the architectural design of the classifier. Therefore, to attain good classification accuracy, we need to correctly determine the EEG features. However, feature selection is hampered by our inability to reproduce the biological basis of olfaction. One approach is to consider all possible time-, frequency- and time-frequency correlated features, and then identify the discriminating features having a wide margin in their respective spaces for the individual stimulus.

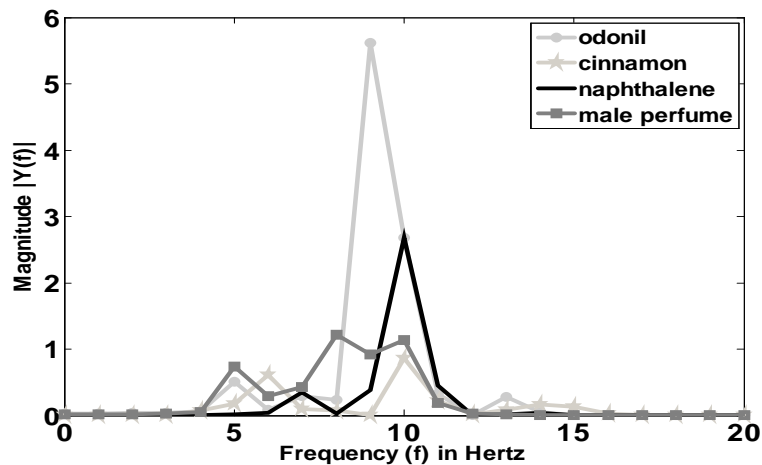
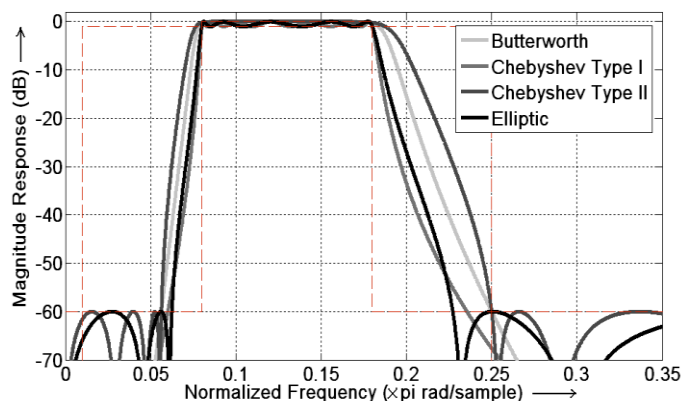


Fig. 2.6 Frequency spectra of four stimuli: the theta (3-7Hz) and alpha (8-13Hz) bands are proven as the desired band of interest.



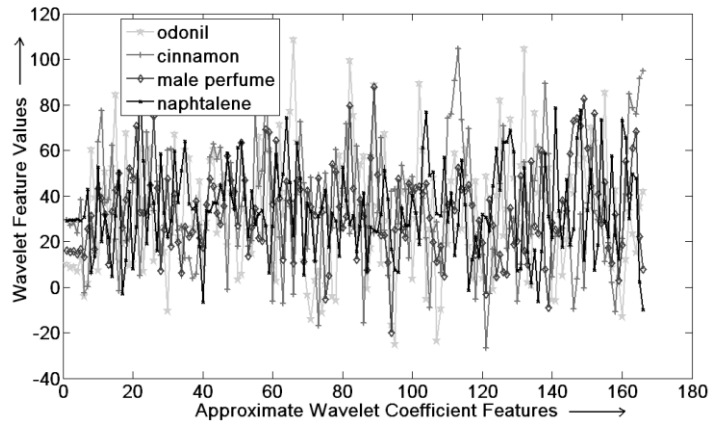
**Fig. 2.7** Frequency response of a Butterworth, Chebyshev-I, Chebyshev-II and Elliptic band pass filter with a pass band and stop band attenuation.

Here, we performed experiments for stimuli within and across different genres. For each subject-stimulus pair, we took 10 EEG signals of 1280 time samples each. We extracted 160 wavelet coefficients, 112 PSDs, 3 Hjorth parameters and 99 AR parameters for each of 10 EEG signals, and constructed 10 feature vectors of each smell class per subject.

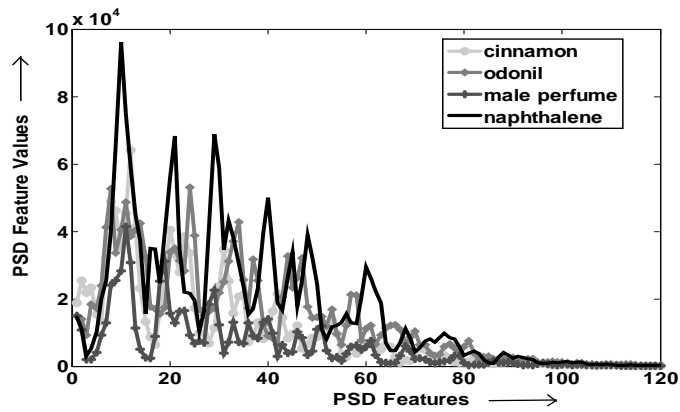
One feature type alone does not yield good classification accuracy. Thus, we group 2 types of features (PSD with wavelet coefficients, PSD with AR parameters, PSD with Hjorth parameters) and separately run the feature selection algorithm with these three groups of features; the optimally reduced dimensions of three feature sets are 30, 27 and 11 respectively.

Fig. 2.8 plots the third level approximated wavelet coefficient ( $A_3$ ) extracted from the  $AF_3$  electrode position. We demonstrate the separation of the wavelet coefficient for four out of ten stimuli. There are fewer features capable of discriminating all four stimuli. For example, the 24<sup>th</sup>, the 64<sup>th</sup> and the 70<sup>th</sup> features can be used jointly to classify the olfactory stimuli. Better olfactory stimuli discrimination is apparent in PSD (Fig. 2.9).

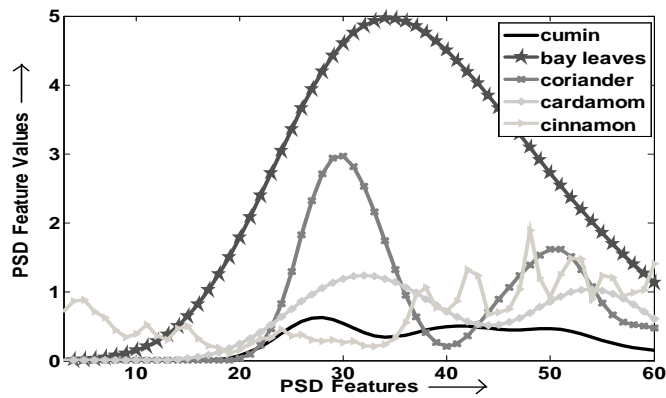
The experiment is repeated for olfactory stimuli of the same genre (Indian spices family) with 10 EEG signals of 1280 time samples each for each of five stimuli. Figures 2.10 and 2.11 plot the first few PSD (out of 120) and wavelet coefficient (out of 126) features respectively extracted from  $AF_3$  electrodes to identify the useful features for discriminating five different Indian spices. The figures show that fewer features, for example, the 28<sup>th</sup>, the 32<sup>nd</sup> and the 47<sup>th</sup> PSD features, are jointly capable of discriminating all five olfactory stimuli. Here, DE optimally selects 18 out of 246 PSD and wavelet coefficient features as the reduced feature set.



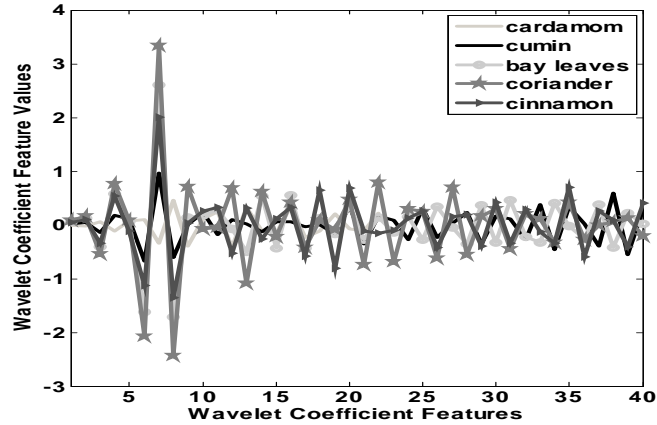
**Fig. 2.8** Approximate wavelet coefficient A3 extracted from AF3 electrode to discriminate four selected stimuli.



**Fig. 2.9** Power spectral density extracted from AF3 electrode to discriminate four selected stimuli.



**Fig. 2.10** Power spectral density extracted from AF3 electrode to discriminate five Indian spices



**Fig. 2.11** Approximate wavelet coefficient  $A_3$  extracted from AF3 electrode to discriminate five Indian spices

### 2.5.5 Experiment 4(Noisy Stimulus Discrimination)

We examine the possible shift in the local (stable) attractors of the recurrent neural dynamics (on the Lyapunov energy surface) with increasing noise in the base stimuli. We inject random noise of small magnitude (varied within  $\pm (10-20)$  % of the instantaneous EEG feature amplitudes over the entire time frame of the EEG trials). Feature-level noise is considered to determine the maximum percentage magnitude of allowable noise to sustain the same stable optimum corresponding to the base stimulus without noise. The experiment is conducted with twenty five subjects with ten repeated trials of varying noise magnitudes for all ten experimental stimuli. For certain stimuli, such as Male perfume and Hydrogen Sulphide, with noise amplitude within 15.6% of the feature values, the dynamics essentially converge to the same optimum with no noise (Fig. 2.12). When the noise amplitude crosses 15.6%, the dynamics converge to one of several optima in the neighborhood of the optimum obtained for the corresponding base stimulus. For certain stimuli, including Cinnamon, Sandalwood powder, Methane, Rosewater, Naphthalene and Camphor, the slope of the curves are more or less uniform, whereas for the others (i.e., for Odonil and Ammonia), the slope changes greatly when the noise amplitude crosses approximately 20%.

## 2.6 CLASSIFIER VALIDATION AND PERFORMANCE

We examine the classification accuracy of the proposed feature selector and classifier combination within a genre and across different genres. We consider a) individual class performance during the classifier training, b) overall performance using confusion matrices, c) performance with/without data point reduction (using PCA), and d) relative performance of the proposed classifier.

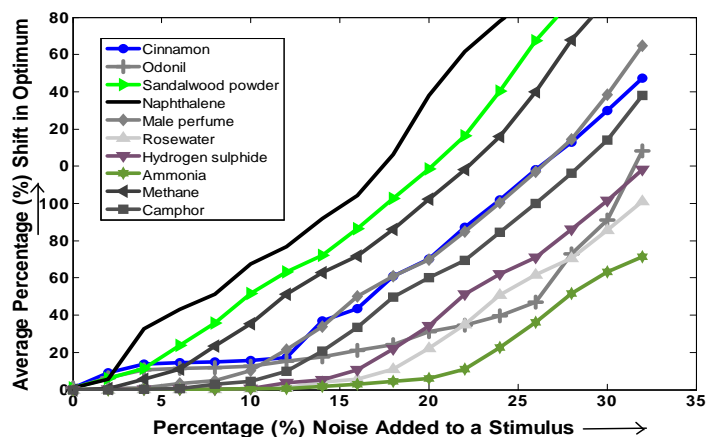


Fig. 2.12 Average percentage shift in optimum versus percentage of noise amplitude injected.

### 2.6.1 Individual Class Performance during Training

For individual class performance of different genres, the recurrent classifier is trained with 2500 trials, one for each stimulus (of different genres), repeated 10 times on each of 25 subjects. For the stimuli of similar genre, the classifier is trained with 1250 trials. A 10-fold cross validation is employed to check the consistency of the data, where 9 out of 10 folds are applied for training purposes and the remaining one fold is used for the validation purposes.

Table-2.1 and 2.2 provide the average classification accuracies of training data across different genres and within a same genre respectively using 68-dimensional and 18-dimensional features averaged over nine folds. The highest classification accuracies for the odorant is marked in bold in both Table 2.1 and 2.2.

### 2.6.2 Overall Performance during Testing Phase

Table 2.3 and Table 2.4 show the individual class performance of different genres and of similar genre, respectively. Table 2.3 indicates that the classification accuracy for the individual class is high, over 97%, for all test stimuli of different genres. Table 2.4 indicates minimum individual classification accuracy over 92%. This latter performance may be due to intra-genre olfactory stimuli having a closer feature space than inter-genre stimuli.

Table 2.1 Average Training Accuracy of 25 Subjects for 10 Stimuli across Different Genres

Stimulus Type	Classification Accuracy (in %)		
	Best	Average	Worst
Naphthalene	<b>99.6</b>	<b>89.8</b>	<b>80.0</b>
Ammonia	97.2	88.4	79.6
Odonil	98.8	87.8	76.8
Cinnamon	98.4	87.6	76.8
Male Perfume	98.0	87.4	76.8
Methane	97.6	87.7	78.0
Camphor	97.6	86.6	75.6
Hydrogen Sulphide	99.2	88.7	78.2
Rosewater	97.6	86.3	74.8
Sandalwood Powder	97.2	85.0	72.8



**Table 2.2** Average Training Accuracy of 25 Subjects for 5 Stimuli within A Same Genre

Stimulus Type	Classification Accuracy (in %)		
	Best	Average	Worst
Naphthalene	99.6	89.8	80.0
Ammonia	97.2	88.4	79.6
Odonil	98.8	87.8	76.8
Cinnamon	98.4	87.6	76.8
Male Perfume	98.0	87.4	76.8

**Table 2.3** Confusion Matrix of Ten Smell Classes of Different genres Using DE-Recurrent NN classifier Along with PSD and Wavelet Coefficient Features

		Predicted Class									
Actual Class		Napthalene	Ammonia	Odonil	Cinnamon	Male Perfume	Methane	Camphor	Hydrogen Sulphide	Rosewater	Sandalwood Powder
	Napthalene	99.6	0.0	0.4	0.0	0.0	0.0	0.0	0.0	0.0	0.0
	Ammonia	0.4	97.2	1.2	0.0	0.8	0.0	0.4	0.0	0.0	0.0
	Odonil	0.4	0.4	98.8	0.0	0.4	0.0	0.0	0.0	0.0	0.0
	Cinnamon	0.0	0.0	0.0	98.4	0.4	0.0	1.2	0.0	0.0	0.0
	Male Perfume	0.4	0.8	0.4	0.4	97.6	0.0	0.4	0.0	0.0	0.0
	Methane	0.0	0.0	0.0	0.4	0.0	97.6	0.0	2.4	0.0	0.0
	Camphor	0.4	0.8	0.4	0.4	0.8	0.0	97.6	0.0	0.0	0.0
	Hydrogen Sulphide	0.0	0.0	0.4	0.4	0.0	0.4	0.0	99.2	0.0	0.0
	Rosewater	0.0	0.0	0.0	0.4	0.8	0.0	0.4	0.0	97.6	1.2
	Sandalwood Powder	0.0	0.0	0.0	0.4	0.8	0.0	0.8	0.0	1.2	97.2

**Table 2.4** Confusion Matrix of Five Intra-genre Smell Classes Using DE-Recurrent NN Classifier Along with PSD and Wavelet Coefficient Features

		Predicted Class				
Actual Class		Cumin	Coriander	Bay leaves	Cinnamon	Cardamom
	Cumin	92.8	4.0	1.2	1.2	0.8
	Coriander	6.4	92.0	1.2	0.4	0.0
	Bay leaves	1.2	2.8	96.0	0.0	0.0
	Cinnamon	0.0	0.0	2.0	94.8	3.2
	Cardamom	0.0	0.0	0.0	5.6	94.4

### 2.6.3 Performance Analysis with/without Data-Point Reduction

We examine data-point reduction using PCA. Since intra-genre classification performance for individual stimulus is relatively worse than inter-genre, we restrict the present analysis to intra-genre (Table 2.5).

The classification performance with the average of the data points within a given stimulus class used to train the recurrent neural net classifier (instead of PCA), appears in Table 2.6. Average classification accuracy decreases by 7% in absence of PCA as the data point selector.

**Table 2.5** Average Classifier Accuracy Along with True Positive, True Negative, False Positive and False Negative Rates Using PCA

Stimulus Types	DE-Recurrent NN Classifier with PSD +Wavelet Coefficients				Average Classifier Accuracy (%)
	True Positive (%)	True Negative (%)	False Positive (%)	False Negative (%)	
Cumin	92.8	98.1	1.9	7.2	94.0
Coriander	92.0	98.3	1.7	8.0	
Bay leaves	96.0	98.9	1.1	4.0	
Cinnamom	94.8	98.2	1.8	5.2	
Cardamom	94.4	99.0	1.0	5.6	

**Table 2.6** Average Classifier Accuracy Along with True Positive, True Negative, False Positive and False Negative Rates Without Using PCA

Stimulus Types	DE-Recurrent NN Classifier with PSD +Wavelet Coefficients				Average Classifier Accuracy (%)
	True Positive (%)	True Negative (%)	False Positive (%)	False Negative (%)	
Cumin	89.2	96.2	3.8	10.8	87.04
Coriander	75.6	96.7	3.3	24.4	
Bay leaves	94.0	96.1	3.9	6.0	
Cinnamom	90.8	96.0	4.0	9.2	
Cardamom	85.6	98.8	1.2	14.4	

#### 2.6.4 Relative Performance Analysis

To study the relative performance, we consider standard PCA based feature selection and the following classifiers: 1) Linear Discriminant Analysis (LDA) [57], 2) k-nearest Neighbor (KNN) [58], 3) Feed-forward Neural Network (FFNN) [59], 4) Linear Support Vector Machine (LSVM) [60], [61], [62], 5) Support Vector Machine with Radial Basis Function (SVM-RBF) [63] kernel, and 6) Naïve Bayes [64], [65] (Table 2.7).

Table 2.7 reveals that the final measure of classification accuracy is the highest for the proposed feature selector-classifier combination. Further, wavelet coefficients and power spectral density together offer the highest overall classification accuracy of 98.08%. The above study is undertaken on inter-genre classification. A paired t-test is used to compare the said classifiers considering DE-Recurrent neural structure as the reference classifier.

McNemar's test [66], [67] compares the relative performance of our proposed DE-Recurrent NN algorithm with six standard techniques (PCA-LDA, PCA-kNN, PCA-FFNN, PCA-LSVM, PCA-Naïve Bayes, and PCA-SVM-RBF) (Table 2.8). McNemar's test has been applied to determine the performance of two classification algorithms for correct classification of the feature vectors. Because of lack in availability of databases, the study is performed with our Indian (Jadavpur University) smell database [68]. It is evident from Table 2.8 that the proposed classifier outperforms all its competitors excluding PCA-Naïve Bayes.

This confirms the fact that PCA-Naïve Bayes perform nearly similar to that of the proposed classifier.

**Table 2.7** Mean Classifier Accuracy and Standard Deviation (within Parenthesis) of Inter-Genre Testing Data Using DE Feature Selection Algorithm along with False Positive Rate ( $\alpha$ ) and False Negative Rate ( $\beta$ )

Features	Percentage Classifier Accuracy (in %)							Statistical Significance
	PCA-LDA	PCA-kNN	PCA-FFNN	PCA-LSVM	PCA-SVM-RBF	PCA-Naïve Bayes	DE-Recurrent NN	
Hjorth + PSD	77.4 (0.0004)	82.08 (0.0100)	83.04 (0.004)	84.44 (0.0212)	85.48 (0.0108)	86.20 (0.0092)	<b>97.8</b> <b>(0.0065)</b>	t=51.4890 std. error of difference= 0.002
$\alpha$	0.1860	0.1500	0.1476	0.1372	0.1364	0.1296	<b>0.0034</b>	
$\beta$	0.2512	0.2090	0.1923	0.1736	0.1539	0.1465	<b>0.0225</b>	
Wavelet + PSD	78.72 (0.0128)	82.52 (0.0144)	83.76 (0.0112)	85.52 (0.0096)	89.92 (0.0336)	90.92 (0.0338)	<b>98.08</b> <b>(0.0121)</b>	t = 9.9720 std. error of difference= 0.007
$\alpha$	0.1805	0.1496	0.1408	0.1359	0.1176	0.1082	<b>0.0022</b>	
$\beta$	0.2408	0.2009	0.1831	0.1537	0.1427	0.1410	<b>0.0192</b>	
AR + PSD	76.2 (0.0124)	78.64 (0.0244)	81.12 (0.0152)	83.72 (0.0084)	84.28 (0.0228)	85.24 (0.0188)	<b>95.08</b> <b>(0.0206)</b>	t = 17.6413 std. error of difference= 0.006
$\alpha$	0.2119	0.1904	0.1604	0.1411	0.1406	0.1395	<b>0.0054</b>	
$\beta$	0.2609	0.2384	0.2161	0.1843	0.1733	0.1557	<b>0.0492</b>	
<b>Mean Classifier Accuracy (in %)</b>	77.44	81.08	82.64	84.56	86.56	87.52	<b>96.98</b>	

## 2.7 APPLICATION IN SIMULATED TEA-TASTER SELECTION

There is no standard technique to automatically determine the perceptual-ability of tea-tasting. Here we examine perceptual-ability in tea-tasting by measuring their EEG response to the aroma of tea-samples. We use 5 different varieties of tea leaves with 14 samples each.

**Table 2.8** Statistical Comparison of Classifiers using McNemar's Test

Reference Algorithm: DE - Recurrent Neural Net				
Classifier algorithm used for comparison using desired features $d=50$	Parameters used for McNemar Test		Z	Comments on acceptance / rejection of hypothesis
	n01	n10		
PCA-LDA	210	354	36.2570	$p < 0.00001$ (Rejected)
PCA-KNN	196	277	13.5306	$p < 0.00001$ (Rejected)
PCA-FFNN	180	254	12.2788	$p < 0.00001$ (Rejected)
PCA-LSVM	160	226	10.9455	$p < 0.00001$ (Rejected)
PCA-SVM-RBF	143	193	7.1458	$p < 0.00001$ (Rejected)
PCA-Naïve-Bayes	142	170	2.3365	$p=0.019465$ (Accepted)

Noise is introduced for four samples of each class by using four different organic solvents (vinegar, rosewater solution, orange juice and pineapple juice). All 70 tea-liquor samples are smelled by 10 subjects. First EEG signals are acquired from AF3 and AF4 channels, and feature extraction, feature selection, data-point reduction and classification (by using recurrent neural net) are performed (Table 2.9). The last column in Table 2.9 provides  $RA_s$  measure of each subject.

**Table 2.9** Recognition-Ability of Subjects Based on Classification Accuracy

Subjects	Percentage Classification accuracy in					RAs
	Class 1	Class 2	Class 3	Class 4	Class 5	
1.	97	80	92	95	77	0.882
2.	85	80	90	77	75	0.814
3.	77	90	85	77	90	0.838
4.	75	82	95	97	85	0.868
5.	95	75	75	82	97	0.848
6.	85	90	95	87	92	0.898
7.	82	85	87	82	77	0.826
8.	92	97	95	90	95	<b>0.938</b>
9.	87	77	97	85	75	0.842
10.	87	82	87	75	80	0.822

We also measure  $DA_s$ . Here, for each of the four noisy stimuli of one class, we perform FE, FS, data-point reduction and classification. We measure the city block distance of the current attractor from the attractor of the corresponding classes, when experimented with standard stimuli. We also measure the city block distance of the current attractor with the attractor for individual class, when experimented with standard stimuli. These distances are used to determine  $DA_s$ ,  $\overline{DA_s}$  and subsequent  $PA_s$  by (2.18). The results of  $DA_s$ ,  $\overline{DA_s}$  and  $PA_s$  are given in Table 2.10. To compute rank, we sorted two entries of the Table 2.10: subject

number, and  $PA_s$  measure, and sort the list of entries in descending order of the  $PA_s$  measure. The last column in Table 2.10 provides the computed rank of individual subjects.

**Table 2.10** Ranking of Perceptual-Ability of 10 Subjects

Subject	RAs	DAs	$\overline{DA}_s$	% PAs	Rank
1.	0.882	0.27	0.5294	46.69	9
2.	0.814	0.31	0.6078	49.47	7
3.	0.838	0.23	0.4509	37.78	10
4.	0.868	0.45	0.8823	76.58	4
5.	0.848	0.38	0.7450	63.17	6
6.	0.898	0.51	1.0000	<b>89.80</b>	<b>1</b>
7.	0.826	0.48	0.9411	77.73	3
8.	0.938	0.44	0.8627	80.92	2
9.	0.842	0.43	0.8431	70.98	5
10.	0.822	0.29	0.5686	46.73	8

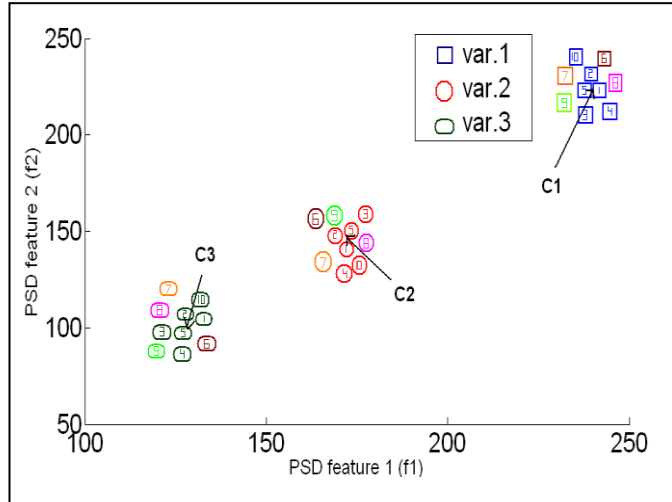
The feature vectors for near-similar stimuli are mapped around the optimum (of the Lyapunov energy surface), identified for the standard (noise-free) base stimuli of the same class. The distance between the locations of any two mapped noisy stimuli on the energy surface represent the dissimilarity between the two stimuli. In the present context, the fine differences among the aroma of noisy tea samples are automatically detected by the natural convergence of the recurrent neural dynamics at local optima around the identified stable optimum of their standard (noise-free) samples.

The feature level discrimination is also prominent from the scatter plot (Fig. 2.13) of the best two selected features for both noisy (four samples of three varieties) and standard stimuli (any six out of ten samples of three varieties). The noise-free samples of different varieties are marked by the corresponding base colors including blue, red and dark green. The noisy tea-samples of each variety e.g., 6<sup>th</sup>, 7<sup>th</sup>, 8<sup>th</sup> and 9<sup>th</sup> are contaminated by vinegar solution, rosewater solution, orange juice and pineapple juice respectively.  $C_1$ ,  $C_2$  and  $C_3$ , in Fig. 2.13 refer to the cluster centres of the standard (noise-free) tea-samples of corresponding varieties. Four noisy samples of a particular tea genre appear closely to the ideal sample of their class, maintaining their identity (discriminating ability among them).

## 2.8 CONCLUSIONS

The chapter introduced a novel approach to classify olfactory stimulus from the EEG response. A recurrent neural network classifier is designed to classify pre-trained stimuli and detect the nearest pre-trained class for noisy stimulus modulated over the selected pre-trained stimulus. A new metric to compute perceptual-ability of subjects based on their recognition-ability of pre-trained stimulus and discriminating ability of noisy stimulus is proposed. This metric has successfully been used to determine the perceptual ability of subjects using a set of standard (pre-trained) stimuli. Among the other approaches introduced in the chapter, design

of new evolutionary technique for feature selection and a novel use of the traditional PCA algorithm in data point reduction need special mention.



**Fig. 2.13** Feature level discrimination of best two selected features for both noisy (contaminated) and noise free (ideal) tea-samples.

Four experiments have been proposed to examine the performance of the system from different perspectives: physiological, signal processing and classification. The physiological issues deal with selection of specific brain regions capable of recognizing olfaction. Signal processing issues include EEG frequency band selection to find the best response for olfactory stimulus. Classifier issues include EEG feature selection for olfactory stimulus and validation of classifier performance.

The proposed scheme has successfully been applied in simulated tea-taster identification and ranking by measuring their perceptual-ability using a few pre-trained stimuli. The suggested scheme of (relative) perceptual-ability measurement of subjects, to the best of the authors' knowledge, is the first successful work of its kind.

## APPENDIX

### A.1 Pseudo code for feature selection using DE

---

**Input:**  $D$  dimensional data points  $\mathbf{X} = \{\vec{X}_1, \vec{X}_2, \dots, \vec{X}_N\}$ , where  $\vec{X}_i = \{x_{i,1}, x_{i,2}, \dots, x_{i,D}\}$ , each having  $D$  features and an assigned class level  $m \in [1, K]$  for  $K$  classes with class labels for each  $\vec{X}_i$ .

**Output:** Selected  $d$ -dimensions of the data points (feature vectors) corresponding to minimal  $J$ .

---

#### Begin

- 1. Initialization:** Initialize  $NP$  number of trial solutions  $\vec{Z}_i$  of the format given in Fig. 2.2 for  $i= 1$  to  $NP$ . Initialize crossover ratio  $Cr=0.7$ .

2. **Mutation:** For each  $\vec{Z}_i$ , pick up 3 companion target vectors:  $\vec{Z}_j, \vec{Z}_k$  and  $\vec{Z}_l$  and compute  $\vec{Z}'_i = \vec{Z}_j + F(\vec{Z}_k - \vec{Z}_l)$ , where,  $F$  is a scale factor in  $[0, 2]$ . Here  $j, k$  and  $l$  are distinct and mutually exclusive to each other.
3. **Recombination:** Now for each pair of  $\vec{Z}_i$  and  $\vec{Z}'_i$ , construct a new trial vector  $\vec{M}_i$ , where  $j$ -th element of  $\vec{M}_i$  is obtained by:
 
$$m_{i,j} \leftarrow z'_{i,j}, \text{ if } r, \text{ a randomly selected number in } [0,1] < Cr.$$

$$m_{i,j} \leftarrow z_{i,j}, \text{ otherwise.}$$
4. **Selection:** For each pair of  $\vec{M}_i$  and  $\vec{Z}_i$ ,  $\vec{Z}_i \leftarrow \vec{M}_i$ , if  $f(\vec{M}_i) < f(\vec{Z}_i)$ , where  $f(\cdot)=L$  (Eqn. (2.4)) is the fitness (objective) function for the minimization problem.
5. Repeat from step 2 until the stopping criterion is not attained.
6. Output the best fit member from the population pool. The components of the best fit parameter vector with one values are the required features.

**End.**

---

## A.2 Pseudo code for optimal weight selection of recurrent neural net classifier

**Input:**  $K$  class representatives  $\Omega = [\vec{\theta}_1, \vec{\theta}_2, \dots, \vec{\theta}_K]$  with each  $\vec{\theta}_k$  ( $k \in [1, K]$ ) of dimension  $d$ , obtained by data reduction using Principal Component Analysis for each of the  $K$  individual classes, each of dimension  $1 \times d$ .

**Output:** Optimal connection vector  $\vec{W}$  of dimension  $1 \times d$ .

---

**Begin**

1. Set the generation number  $t=0$  and randomly initialize a population of NP individuals  $\mathbf{P}_t = \{\vec{W}_1(t), \vec{W}_2(t), \dots, \vec{W}_{NP}(t)\}$  with  $\vec{W}_m(t) = [w_{m,j}(t)]$  for  $j \in [1, d]$ , and  $m = [1, NP]$ .
2. Evaluate the trial vector  $\vec{W}_m(t)$  by measuring its cost function
 
$$f(\vec{W}_m(t)) = \sum_{k=1}^K \sum_{j=1}^d [\theta_{k,j}^2 - 10w_{m,j} \cos(2\pi\theta_{k,j}) + 10] \text{ by (2.7).}$$
3.  $\vec{W}_{best}(t) \leftarrow \arg(\min_{m=[1, NP]} (f(\vec{W}_m(t))))$
4. **While** terminating condition is not reached **do begin**
  - a) **Mutation:** Generate a donor vector  $V_m(t) = [v_{m,j}(t)]$  corresponding to the  $m$ -th target vector  $\vec{W}_m(t)$  via the mutation scheme of DE as mentioned in Appendix-A.1 (Step 2).
  - b) **Recombination:** Generate trial vector  $\vec{U}_m(t) = [u_{m,j}(t)]$  for the  $m$ -th target vector  $\vec{W}_m(t)$  through binomial recombination scheme of DE as mentioned in Appendix-A.1 (Step3).
  - c) **Selection:** Evaluate the trial vector  $\vec{U}_m(t)$  by measuring its cost function  $f(\vec{U}_m(t))$ .

**If**  $f(\vec{U}_m(t)) < f(\vec{W}_m(t))$

$$\vec{W}_m(t+1) = \vec{U}_m(t);$$

Evaluate  $f(\vec{W}_m(t+1))$  and save it for future.

**If**  $f(\vec{U}_m(t)) < f(\vec{W}_{best}(t))$

$$\vec{W}_{best}(t) = \vec{U}_m(t);$$

Evaluate  $f(\vec{W}_{best}(t))$  and save it for future.

**End-if;**

**Else**  $\vec{W}_m(t+1) = \vec{W}_m(t);$

**End-if;**

Increase the counter value  $t=t+1$ .

**End-while;**

Print  $\vec{W}_{best}(t);$

**End.**

---

### A.3 Pseudo code for Recall phase of recurrent neural net classifier

---

**Input:** Optimal connection vector  $\vec{W}$  of dimension  $1 \times d$ .

**Output:** Class  $\ell$  of unknown smell stimulus.

---

**Begin**

1. Initialize  $\vec{\theta}'(0) = [\theta'_j(0)], \forall j$ .
2. Solve the dynamics (12) with  $\theta_{k,j} = \theta'_j$  by Newton-Raphson method presented below.

$$\theta'_j(t+1) = \theta'_j(t) - \frac{f(\theta'_j(t))}{f'(\theta'_j(t))}, \forall j.$$

where,  $f(\theta'_j(t)) = \theta'_j(t) + 10\pi w_j \sin[2\pi\theta'_j(t)]$ , until  $|\theta'_j(t+1) - \theta'_j(t)| < \varepsilon$ , where  $\varepsilon$  is a pre-assigned positive number, however small possible.

3. For known optima  $\vec{\theta}_1, \vec{\theta}_2, \dots, \vec{\theta}_K$ , find  $\vec{\theta}_k$  having the smallest distance with  $\vec{\theta}'(t) = [\theta'_j(t)]$  for  $k=1$  to  $K$ .

Let,  $\|\vec{\theta}_\ell(t) - \vec{\theta}'(t)\| \leq \|\vec{\theta}_k(t) - \vec{\theta}'(t)\|, \forall k;$

then  $\vec{\theta}_\ell(t) \leftarrow \vec{\theta}'(t)$ , i.e.,  $\vec{\theta}'(t)$  falls in  $\ell$ -th class of stimulus.

**End**

---



## REFERENCES

1. D. A. Wilson and R. J. Stevenson, "The fundamental role of memory in olfactory perception," in *Proc. Elsevier conference in TRENDS in Neurosciences*, vol. 26, no. 5, pp. 243-247, Alicante, Spain, May 2003.
2. J. A. Cardin, R. D. Kumbhani, D. Contreras and L. A. Palmer, "Cellular mechanisms of temporal sensitivity in visual cortex neurons," *The Journal of Neuroscience*, vol. 30, no. 10, pp. 3652–3662, March 2010.
3. C. R. Palmer, "Neural correlates of behavior and stimulus sensitivity of individual neurons and population responses in the primary visual cortex," *Dissertation of University of Texas*, Texas, USA, 2009.
4. R. D. Newcomb, M. B. Xia and D. R. Reed, "Heritable differences in chemosensory ability among humans," *Flavour*, vol. 1, no. 1, pp. 1-9, 2012.
5. S. Blanco, R. Q. Quiroga, O. A. Rosso and S. Kochen, "Time-frequency analysis of electroencephalogram series," *Physical Review*, vol. 51, no. 3, pp. 2624-2631, March 1995.
6. I. Gaillard, S. Rouquier and D. Giorgi, "Review: Olfactory receptors," *Cellular and Molecular Life Sciences*, vol. 61, no.4, pp. 456–469, 2004.
7. S. Firestein, "How the olfactory system makes sense of scents," *Nature*, vol. 413, no. 6852, pp. 211–218, 2001.
8. A. L. A. N. Gelperin, "Oscillatory dynamics and information processing in olfactory systems," *Journal of Experimental Biology*, vol. 202, no. 14, pp. 1855-1864, 1999.
9. A. Lymberis and A. Dittmar, "Advanced wearable health systems and applications - research and development efforts in the European union," *IEEE Engineering in Medicine and Biology Magazine*, vol. 26, no. 3, pp. 29-33, May-June 2007.
10. A. M. Dale and M. I. Sereno, "Improved localization of cortical activity by combining EEG and MEG with MRI cortical surface reconstruction: a linear approach," *Journal of cognitive neuroscience*, vol. 5, no. 2, pp. 162-176, 1993.
11. F. Babiloni, D. Mattia, S. Bufalari, F. Aloise, A. Tocci, L. Astolfi, F. D. V. Fallani, S. Gao, S. Salinari, M. G. Marciani and F. Cincotti, "Non invasive EEG-based brain computer interface for communication and control," *International Journal of Bioelectromagnetism*, vol. 9, no. 1, pp. 17-18, 2007.
12. T. Ball, M. Kerna, I. Mutschler, A. Aertsens and A. Schulze-Bonhage, "Signal quality of simultaneously recorded invasive and non-invasive EEG," *Neuroimage*, vol. 46, no. 3, pp. 708-716, 2009.
13. W. L. Zhou, P. Yan, J. P. Wuskell, L. M. Loew and S. D. Antic, "Dynamics of action potential backpropagation in basal dendrites of prefrontal cortical pyramidal neurons," *European Journal of Neuroscience*, vol. 27, no. 4, pp. 923–936, 2008.
14. E. T. Rolls, "The orbitofrontal cortex and reward," *Cerebral cortex*, vol. 10, no. 3, pp. 284-294, 2000.

15. L. A. Dade, R. J. Zatorre and M. J. Gotman, "Olfactory learning: Convergent findings from lesion and brain imaging studies in humans," *Brain*, vol. 125, no. 1, pp. 86–101, 2002.
16. J. Kowalewski and C. Murphy, "Olfactory ERPs in an odor/visual congruency task differentiate ApoE  $\epsilon$ 4 carriers from non-carriers," *Brain research*, vol. 1442, pp. 55-65, 2012.
17. T. S. Lorig, T. S. Mayer, F. H. Moore and S. Warrenburg, "Visual event-related potentials during odor labeling," *Chemical Senses*, vol. 18, no. 4, pp. 379–387, 1993.
18. R. Storn and K. G. Price, "Differential Evolution- a simple and efficient heuristic for global optimization over continuous spaces," *Journal of Global Optimization*, vol. 11, no. 4, pp. 341-359, 1997.
19. B. C. Min, S. H. Jin, I. H. Kang, D. H. Lee, J. K. Kang, S. T. Lee and K. Sakamoto, "Analysis of mutual information content for EEG responses to odor stimulation for subjects classified by occupation," *Chemical Senses*, vol. 28, no. 9, pp. 741–749, 2003.
20. H. Zhao, P. C. Yuen and J. T. Kwok, "A novel incremental principal component analysis and its application for face recognition," *IEEE Transactions on Systems, Man, and Cybernetics, Part B: Cybernetics*, vol. 36, no. 4, pp. 873-886, 2006.
21. C. Fang and A. Ralescu, "2D-PCA vs. PCA applied to pedestrian recognition," in *Proc. 19th Midwest Artificial Intelligence & Cognitive Science Conference (MAICS)*, Cincinnati, OH, April 11-13, 2008.
22. A. Zhang, B. Yang and L. Huang, "Feature extraction of EEG signals using power spectral entropy," in *Proc. International Conference on BioMedical Engineering and Informatics*, vol.2, pp.435-439, Hainan, China, May 2008.
23. C. Vidaurre, N. Krämer, B. Blankertz and A. Schlögl, "Time domain parameters as a feature for EEG-based brain–computer interfaces," *Neural Networks*, vol. 22, no. 9, pp. 1313-1319, 2009.
24. D. Garrett, D. A. Peterson, C. W. Anderson and M. H. Thaut, "Comparison of linear, nonlinear, and feature selection methods for EEG signal classification," *IEEE Transactions on Neural Systems and Rehabilitation Engineering*, vol. 11, no. 2, pp. 141-144, 2003.
25. A. Saha, A. Konar, P. Rakshit, A. L. Ralescu and A. K. Nagar, "Olfaction recognition by EEG analysis using differential evolution induced Hopfield neural net," in *proc. International Joint Conference on Neural Networks (IJCNN)*, pp. 1-8, Dallas, USA, 2013.
26. J. J. Hopfield, "Olfactory computation and object perception," in *proc. National Academy of Sciences of the United States of America*, vol. 88, no. 15, pp. 6462-6466, USA, August 1991.
27. A. Saha, A. Konar, R. Burman and A. K. Nagar, "EEG Analysis for Cognitive Failure Detection in Driving Using Neuro-Evolutionary Synergism," in *proc. International Joint Conference on Neural Networks (IJCNN)*, Beijing, China, 2014.
28. S. Bhattacharya, A. Konar, S. Das and S. Y. Han, "A Lyapunov-based extension to particle swarm dynamics for continuous function optimization," *Sensors*, vol. 9, no. 12, pp. 9977-9997, 2009.
29. I.J. Nagrath and M. Gopal, *Control Systems Engineering (4th Edition)*, New Age International Publishers, New Delhi, India, 2005.

30. A. Yazdani, E. Kroupi, J. M. Vesin and T. Ebrahimi, "Electroencephalogram alterations during perception of pleasant and unpleasant odor," in *Proc Fourth International Workshop on Quality of Multimedia Experience (QoMEX)*, pp. 272–277, Yarra Valley, Australia, 2012.
31. T. S. Lorig, E. Huffman, A. DeMartino and J. DeMarco, "The effects of low concentration odors on EEG activity and behavior," *Journal of Psychophysiology*, 1991.
32. W. R. Klemm, S. D. Lutes, D. V. Hendrix and S. Warrenburg, "Topographical EEG maps of human responses to odors," *Chemical senses*, vol. 17, no. 3, pp. 347-361, 1992.
33. L. M. Kay, "Theta oscillations and sensorimotor performance," in *Proc. National Academy of Sciences of the United States of America*, vol. 102, no. 10, pp. 3863-3868, Shenzhen, China, 2005.
34. B. S. Bhattacharya, Y. Cakir, N. Serap-Sengor, L. Maguire and D. Coyle, "Model-based bifurcation and power spectral analyses of thalamocortical alpha rhythm slowing in alzheimer's disease," *Neurocomputing*, vol. 115, pp. 11-22, 2013.
35. B. Hjorth, "EEG analysis based on time domain properties," *Electroencephalography and Clinical Neurophysiology*, vol. 29, no. 3, pp. 306-310, 1970.
36. R. Kar, A. Konar and A. Chakraborty, "EEG-Analysis for the Detection of True Emotion/Pretension.Synthesizing Human Emotion in Intelligent Systems and Robotics," *IGI Global*, 2014.
37. R. Martin, "Noise power spectral density estimation based on optimal smoothing and minimum statistics," *IEEE Transactions on Speech and Audio Processing*, vol. 9, no. 5, pp. 504-512, July, 2001.
38. L. M. Ai, W. Rui, H. D. Mei and Y. J. Fu, "Feature extraction and classification of mental EEG for motor imagery," in *Proc. IEEE Fifth International Conference on Natural Computation*, vol. 2, pp. 139-143, Tianjian, China, 2009.
39. W. Gersch, "Estimation of the autoregressive parameters of a mixed autoregressive moving-average time series," *IEEE Transactions on Automatic Control*, vol. 15, no. 5, pp. 583-58, 1970.
40. V. S. Devi and M. N. Murty, *Pattern Recognition-An introduction*, University Press, Himayatnagar, Hyderabad, 2011.
41. A. K. Jain, R. P. W. Duin and J. Mao, "Statistical pattern recognition: A review," *IEEE Transactions on Pattern Analysis and Machine Intelligence*, vol. 22, no. 1, pp. 4-37, January 2000.
42. Q. Du, H. Yang and N. H. Younan, "Improved sequential endmember extraction algorithms," in *proc. IEEE conference of Hyperspectral Image and Signal Processing: Evolution in Remote Sensing (WHISPERS)*, pp. 1-4, Lisbon, Portugal, June 2011.
43. A. Konar, *Computational Intelligence: principles, techniques, and applications*, Springer, Berlin, Heidelberg, 2005.
44. S. Durairaj, D. Devaraj and P.S.Kannan, "Improved genetic algorithm approach to line flow constrained reactive power dispatch under both normal and contingent operation states, " in *proc.*

- National Conference on Mathematical and Computational Models (NCMCM)*, pp. 15-16, PSG College of Technology, Coimbatore, December 2005.
45. C. C. Cheng and H. Hexmoor, "Improve Path Planning Performance by Monitoring Human Decisions," *in proc. IC-AI*, pp. 293-297, LasVegas, NV, 2013.
  46. T. A. Reddy, K. R. Dev and S. V. Gangashetty, "Multilayer feedforward neural network models for pattern recognition tasks in earthquake engineering," *in proc. Advanced Computing, Networking and Security*, Springer Berlin Heidelberg, pp. 154-162, 2012.
  47. B. Subudhi and D. Jena, "A differential evolution based neural network approach to nonlinear system identification," *Applied Soft Computing*, vol. 11, no. 1, pp. 861-871, 2011.
  48. S. Das and A. Konar, "A swarm intelligence approach to the synthesis of two-dimensional IIR filters," *Engineering Applications of Artificial Intelligence*, vol. 20, no. 8, pp. 1086-1096, 2007.
  49. P. Bhattacharjee, P. Rakshit, I. Goswami, A. Konar and A. K. Nagar, "Multi-robot path-planning using artificial bee colony optimization algorithm" *in proc. Third World Congress on In Nature and Biologically Inspired Computing (NaBIC)*, pp. 219-224, October 2011.
  50. R. J. Williams and D. Zipser, "A learning algorithm for continually running fully recurrent neural networks," *Neural computation*, vol. 1, no. 2, pp. 270-280, 1989.
  51. T. W. Lee, *Independent component analysis*, Springer US, pp. 27-66, 1998.
  52. D. C. Krawczyk, "Review: Contributions of the prefrontal cortex to the neural basis of human decision making," *Neuroscience and Biobehavioral Review (Elsevier)*, vol. 26, no. 6, pp. 631-664, 2002.
  53. S. Francis, E. T. Rolls, R. Bowtell, F. McGlone, J. O'Doherty, A. Browning, S. Clare and E. Smith, "The representation of pleasant touch in the brain and its relationship with taste and olfactory areas," *Neuroreport*, vol. 10, no. 3, pp. 453-459, 1999.
  54. M. S. Gazzaniga, R. B. Ivry and G. R. Mangun, *Cognitive neuroscience, The biology of the mind (2nd edition)*, W. W. Norton & Co., New York, USA, 2002.
  55. L. A. Dade, R. J. Zattore, A. C. Evans and M. J. Gotman, "Working memory in another dimension: functional imaging of human olfactory working memory," *Neuroimage*, vol. 14, no. 3, pp. 650-660, 2001.
  56. D. H. Zald and C. Andreotti, "Reviews and perspectives: Neuropsychological assessment of the orbital and ventromedial prefrontal cortex", *Neuropsychologia (Elsevier)*, vol. 48, no. 12, pp. 3377-3391, 2010.
  57. R. O. Duda, P. E. Hart and D. G. Stork, *Pattern Recognition (2nd edition)*, Wiley-Interscience, New York, USA, 2001.
  58. Y. Song, J. Huang, D. Zhou, H. Zha and C. L. Giles, *IKNN: Informative k-nearest neighbor pattern classification*, Springer-Verlag Berlin Heidelberg, pp. 248-264, 2007.
  59. M. Leena, K. S. Rao and B. Yegnanarayana, "Neural network classifiers for language identification using phonotactic and prosodic features," *in proc. IEEE Intelligent Sensing and Information Processing*, pp. 404-408, 2005.

60. R. Scherer, G. R. Muller, C. Neuper, B. Graimann and G. Pfurtscheller, "An asynchronously controlled EEG-based virtual keyboard: improvement of the spelling rate," *IEEE Transactions on Biomedical Engineering*, vol. 51, no. 6, pp. 979-984, 2004.
61. C. Distanto, N. Ancona and P. Siciliano, "Support vector machines for olfactory signals recognition," *Sensors and Actuators B: Chemical*, vol. 88, no. 1, pp. 30-39, 2003.
62. R. Kar, A. Konar, A. Chakraborty and A. K. Nagar, "Detection of Signaling Pathways in Human Brain during Arousal of Specific Emotion," in *proc. IEEE International Joint Conference in Neural Networks*, Beijing, China, 2014.
63. Q. Chang, Q. Chen and X. Wang, "Scaling gaussian rbf kernel width to improve svm classification," in *Proc. International Conference on Neural Networks and Brain (ICNN&B)*, vol. 1, pp. 19-22, Beijing, China, 13-15 October, 2005.
64. D. Wei and L. X. Yang, "Weighted naive bayesian classifier model based on information gain," in *Proc. International Conference on Intelligent System Design and Engineering Application (ISDEA)*, vol.2, pp. 819-822, Changsha, China, 13-14 October, 2010.
65. S. Bhattacharyya, A. Khasnobish, A. Konar, D.N. Tibarewala and A.K. Nagar, "Performance analysis of left/right hand movement classification from EEG signal by intelligent algorithm," in *proc. IEEE Symposium on Computational Intelligence, Cognitive Algorithms, Mind and Brain (CCMB)*, Paris, pp. 1-8, 2011.
66. A. Halder, A. Konar, R. Mandal, A. Chakraborty, P. Bhowmik, N. R. Pal and A. K. Nagar, "General and interval type-2 fuzzy face-space approach to emotion recognition," *IEEE Transactions on Systems, Man, and Cybernetics: Systems*, vol. 43, no. 3, pp. 587-605, 2013.
67. T. G. Dietterich, "Approximate statistical tests for comparing supervised classification learning algorithms," *Neural Computation*, vol. 10, no. 7, pp. 1895-1923, 1998.
68. [http://www.computationalintelligence.net/papers/data/excel/olfactory\\_eegdataset/EEG dataset extracted from AF3 electrode for Cinnamon.xls](http://www.computationalintelligence.net/papers/data/excel/olfactory_eegdataset/EEG_dataset_extracted_from_AF3_electrode_for_Cinnamon.xls).

# Chapter 3

## Cognitive Failure Detection in Driving Using Type-2 Fuzzy Classifiers

*The chapter aims at detecting on-line cognitive failures in driving by decoding the EEG signals acquired during visual alertness, motor-planning and motor-execution phases of the driver. Visual alertness of the driver is detected by classifying the pre-processed EEG signals obtained from his pre-frontal and frontal lobes into two classes: alert and non-alert. Motor-planning performed by the driver using the pre-processed parietal signals is classified into four classes: braking, acceleration, steering control and no operation. Cognitive failures in motor-planning are determined by comparing the classified motor-planning class of the driver with the ground truth class obtained from the co-pilot through a hand-held rotary switch. Lastly, failure in motor execution is detected, when the time-delay between the onset of motor imagination and the EMG response exceeds a predefined duration. The most important aspect of the present research lies in cognitive failure classification during the planning phase. The complexity in subjective plan classification arises due to possible overlap of signal features involved in braking, acceleration and steering control. A specialized interval/general type-2 fuzzy set induced neural classifier is employed to eliminate the uncertainty in classification of motor-planning. Experiments undertaken reveal that the proposed neuro-fuzzy classifier outperforms traditional techniques in presence of external disturbances to the driver. Decoding of visual alertness and motor-execution are performed with kernelized support vector machine classifiers. An analysis reveals that at a driving speed of 64 km/hr, the lead-time is over 600 milliseconds, which offer a safe distance of 10.66 meters.*

### 3.1 INTRODUCTION

Driving involves complex cognitive processes, concerning sensory perception, motor-planning and motor-execution. The cognitive failure detection (CFD) problem, introduced here, refers to classifying cognitive failures involved in visual alertness (VA), motor-planning (MP) and motor-execution (ME) phases of driving with a motive to alert the driver by an (audio) alarm before an accident takes place. One approach to solve the above problem is to capture the brain signals of the driver by a non-invasive means for subsequent processing and classification.

Among the well-known brain signal acquisition techniques, electroencephalography (EEG) [1] is most popular for its prompt time-response [2], non-invasive characteristic [3], [4] portability and cost-effectiveness. Because of the above merits, the chapter attempts to employ EEG-signal processing and classification to detect VA failure (VAF), MP failure (MPF) and ME failure (MEF). The VAF is recognized from the acquired P-300 response of the driver in reaction to external stimulation [5]-[8], such as sudden appearance of bumpers, traffic light changes, and the like. MPF and MEF detection, require Event Related Desynchronization/Synchronization (ERD/ERS), which, being spontaneous, requires no external stimulation for its generation [5], [6].

Classification of cognitive tasks from the acquired EEG signals is relatively easier when the tasks involve disjoint brain regions. However, cognitive tasks (braking, acceleration and steering control) involved in MP usually engage the same cortical regions (parietal and motor cortex), with an overlap in their feature space. This overlap acts as a source of uncertainty to the classifier. Traditional classifiers, which usually show promising performance, unfortunately, fail to accurately discriminate pattern classes with overlapped features. The logic of fuzzy sets has an inherent power to handle uncertainty in measurement space. Thus fuzzy logic induced classifiers are a good choice for the present MP classification. Our experience [9]-[12] further reveals that the MP features of the above three cognitive tasks have wider fluctuations over experimental instances of the same subject and across subjects. Type-2 fuzzy set has an added advantage over its type-1 counterpart to handle both intra- and inter-personal level uncertainty [13]. This motivated us to employ Interval type-2 Fuzzy sets/General type-2 Fuzzy sets (IT2FS/GT2FS) [14] to design classifiers for the MP classes.

There exist traces of works on pattern classifiers using type-2 fuzzy sets. Das *et al.* employed projection-based learning techniques to determine optimal weights of a multilayered type-2 neuro-fuzzy classifier [15]. Lee *et al.* introduced a recurrent interval type-2 fuzzy neural net (IT2FNN) for non-linear system identification. They employed asymmetric interval type-2 membership functions for type-2 fuzzy reasoning, and used gradient descent learning for weight adaptation [16]. Lin *et al.* in [17], proposed a self-organizing model of IT2FNN, where the motivation is to employ i) self-organized learning for the determination of

fuzzy rules and ii) parameter learning for the selected fuzzy rules. In the self-organized learning phase, new type-2 rules are added and inefficient rules are pruned out of the IT2FNN. In [18], Park *et al.* introduced a new model of IT2FNN where type-2 fuzzy rules include a function of the linguistic variables in the consequent. The fundamental aspect of their work lies in automatic tuning of parameters of the IT2FNN using real-coded Genetic Algorithm.

Current research on type-2 classifiers is primarily focused around adding sophisticated learning paradigms to improve classifier performance. The new learning paradigms introduced include extreme learning machines [19], active/incremental learning [20], [21], transfer learning [22], [23] and multi-view learning [24] techniques. For example, Deng *et al.* employed extreme learning algorithm to adapt parameters in the consequent of type-2 fuzzy rules to improve generalization performance of the resulting system [19]. Pratama *et al.* also addressed techniques for generalization and summarization capability of IT2FS classifier by introducing learning mechanisms to expand, prune, recall and merge rules [25]. Yang *et al.* utilized transfer learning principles [22] in Takagi-Sugeno fuzzy logic systems for adaptive recognition of epileptic EEG signals [23]. In [20], [21] the authors proposed two interesting works on incremental type-2 meta-cognitive learning machines that autonomously detect what, how and when to learn.

In recent times, an increasing interest to classify brain signals is noticed in research community [26], [27]. For example, Wang *et al.* selected random forest algorithm for epilepsy detection for its superior performance over its three competitors, including decision tree and support vector machine (SVM) based realizations of both decision tree and random forest [28]. Herman *et al.* [29] examined the scope of IT2FS induced classifier in motor imagery related EEG classification task for both off-line and online test cases. In [30], the authors indicated that type-2 fuzzy logic classifier outperforms the traditional linear discriminant analysis (LDA) classifier in terms of classification accuracy in presence of noise. Nguyen *et al.* proposed a novel approach for motor imagery classification using wavelet feature induced interval type-2 fuzzy classifier [31] and demonstrated that the said classifier outperforms traditional statistical, neural and adaptive neuro-fuzzy inference system (ANFIS) classifiers. Andreu-Perez *et al.* proposed a self-adaptive GT2FS-induced inference system for online classification of motor imagery to navigate a bi-pedal humanoid robot [32].

Traditional type-2 fuzzy inference generating systems usually employ rules with type-2 fuzzy propositions in the antecedent and type-2/interval type-1 fuzzy propositions in the consequent [15], [33]-[37]. The classifier rules employed in this chapter are designed with type-2 fuzzy propositions to synthesize the antecedent and a single crisp class label at the consequent. The intra- and inter-subjective variations in the acquired brain signals are accommodated in the construction of type-2 membership functions (MFs) of the antecedent



propositions. The crisp, instead of interval type-2, class label is used in the consequent to describe precise/hard classification of MP tasks in presence of imprecise measurements.

In this chapter, two different proposals for type-2 classifiers are introduced, one synthesized with interval type-2 (IT2) and the other with general type-2 (GT2) fuzzy neural networks. Both the realizations include two layered neural nets with the first layer performing IT2/GT2 fuzzification [13], firing interval computation [15] and Nie-Tan type-reduction [15], [38], [39]. We here do not require defuzzification, as the class label of the input fuzzified features is determined by comparison of the type-reduced outputs of the neurons in the first layer. The second layer selects the neuron with the highest type-reduced output in the first layer and generates a decoded output pattern corresponding to the position of the selected neuron in the first layer. Since defuzzification is avoided and Nie-Tan type-reduction involves only averaging operation, the run-time complexity of the classifiers is reduced significantly, making them amenable for real-time driving application.

In addition, the GT2 classifiers proposed here utilize a novel technique for secondary MF evaluation. Here, the secondary MF at a given value of the linguistic variable  $x = x'$  and primary membership  $\mu_{\tilde{A}}(x)$  in fuzzy set  $\tilde{A}$  is obtained based on the location of the optima of  $\mu_{\tilde{A}}(x)$  over  $x$ , and the distance of  $x'$  from its two neighborhood optima on its both sides. The computation of secondary membership is done offline to reduce run-time complexity of the classifiers. It may be noted that in traditional z-sliced based GT2 system [40], the GT2MF is presumed to have a specific geometry, such as triangle. The proposed method, on the other hand, computes secondary MF from the primary MF and thus is more accurate. Computational complexity of the proposed GT2FS-induced classifier also is nominal as it requires  $m \cdot d$  extra multiplications in comparison to the proposed IT2FS induced classifier, where  $d$  denotes the number of GT2FS used in the antecedent of a rule and  $m$  denotes the number of rules used.

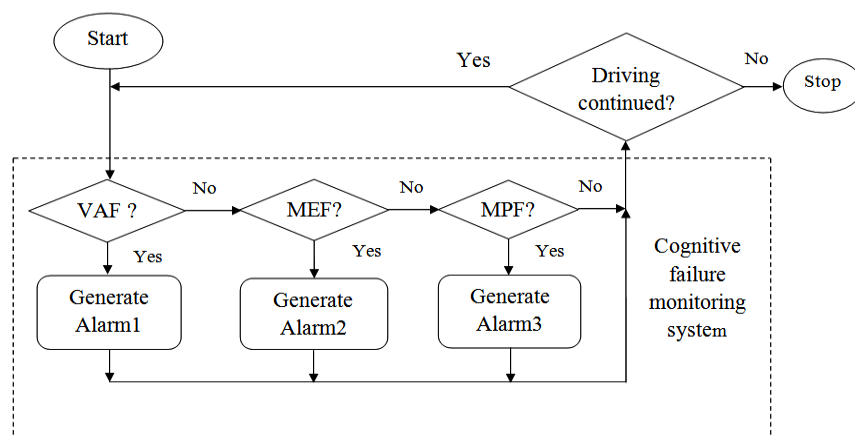
The novelty of the chapter thus lies in the design of an integrated CFD system for driving applications with special emphasis to the design of a fast and accurate type-2 (IT2FS/GT2FS) classifier to classify the MP classes, including braking (BR), acceleration (ACC), steering (STR) control and no operation (NOP). Besides CFD system and type-2 neuro-fuzzy classifier design, the other original contribution of the chapter lies in the design of an evolutionary feature selection algorithm. This algorithm is used to reduce dimension of EEG-features for subsequent classification of MP and ME signals. The work presented here is significantly different from the authors' previous works [9]-[12] with respect to formulation, approach and experiments.

The rest of the chapter is structured as follows. In section 3.2, we propose a psychological model of CFD cycle and present an integrated approach to system design for CFD. Section 3.3 describes evolutionary feature selection algorithm. In section 3.4, we emphasize the

design of the proposed type-2 (IT2FS/GT2FS) classifiers as well as the KSVM classifier. Section 3.5 is developed to deal with psycho-physiological experiments concerning selection of EEG filter bands, active brain regions and EEG features. In Section 3.6, we validate classifier performance, estimate lead-time for different speeds and evaluate objective performance of the proposed CFD system. Concluding remarks are given in section 3.7.

### 3.2 SYSTEM DESIGN AND INTEGRATION

This chapter examines cognitive failures in driving from three important perspectives: visual alertness (VA), MP and ME. VAF, refers to cognitive failures due to lack of visual alertness of the subject (driver). MPF refers to cognitive failures occurring during the phase of translating traffic conditions into necessary plans for ACC, BR and STR control. In presence of correct motor-planning, MEF might occur because of delay in executing the plans due to muscle fatigue/drowsiness and/or poor health of the driver. Fig. 3.1 provides a schematic representation of the cognitive failure detection loop, where VAF, MPF and MEF are monitored sequentially by the proposed system to generate necessary audio alarms to alert the driver. A commonsense thinking reveals that VAF may in turn result in MPF, which subsequently may result in MEF. In Fig. 3.1, we, however, attempt to identify the first occurrence of only one cognitive failure in the loop, rather than generating audio alarms for sequential failures, to avoid confusion of the driver.



**Fig. 3.1** Proposed psychological model of cognitive failure detection in driving to appropriately alert the driver with different audio alarms

In order to detect the above three cognitive failures of the driver, we need to process EEG signals from four distinct brain regions, including pre-frontal and frontal regions for testing VA, parietal lobe for MP and motor cortex region for ME. The acquired EEGs from pre-frontal/frontal, parietal and motor cortex regions are pre-processed using band pass filters (BPFs) of suitable frequency bands. VA being more prominent in alpha band (~8-13 Hz) [41]

and MP/ME being relatively more active in mu- (8-13 Hz) [42] and beta (13-30 Hz) [43] bands, we used BPFs of required pass bands. More review on EEG channel selection and frequency band selection are provided in [44] and [45]. Subsequent steps undertaken on the filtered signals include feature extraction, feature selection and classification.

For VAF, we require feature extraction and classification only as VAF can be characterized by fewer features. The importance of the VAF classifier is to detect the presence/absence of the P300 oddball signal within a finite interval of approximately 350 milliseconds. The classifier should recognize the visual non-alertness of the subject in absence of the P300. For MPF and MEF, we, require all the three steps: FE, FS and classification. Here, the classifier aims at detecting ERD/ERS from the parietal lobe within a specific time-period of approximately 600 milliseconds from the onset of the stimulus. It may be noted that although we count the time-point of ERD/ERS generation from the onset of the stimulus, such generation is spontaneous and is not directly influenced by the stimulus. In addition, MPF detection requires the ground truth (GT) planning decision from a second user, usually the co-pilot.

The response of the MPF classifier is compared with the GT decisions to determine any subjective error of the pilot. Lastly, for the MEF detection, the classifier looks for the presence or absence of an ERD/ERS signal from the motor cortex. If no ERD/ERS is detected within 800 milliseconds from the onset of the stimulus, the classifier declares the failures in motor execution. To confirm the MEF, we also pre-process, filter and classify the electromyogram (EMG) signal acquired from the fore-arms/leg muscles of the subject. If no EMG signal is detected within 1200 milliseconds from the onset of the stimulus, the subject must have committed a fatal execution error. The above measurements are referred to driving speed above 64 km/hour. If driving speed falls off, the subject is relaxed and the above time markers shift right depending on the speed.

Fig. 3.2 includes three classifiers for VAF detection (VAFD), MPF detection (MPFD) and MEF detection (MEFD) and their interconnections. The VAFD classifier has two outputs: visually alert and non-alert. The MPFD classifier classifies planning failures into four classes: BR, ACC, STR and NOP. The MEFD unit includes three classifiers to classify ACC, BR and STR control failures during ME phase. The class labels of BR classifier are BR-pressed (BR-P) and BR-not pressed (BR-NP). Similar nomenclature is used for other two classifier outputs.

The planning classifier is structurally more complex than the rest as it needs to compare the detected class labels of the driver with the GT classes. The GT class labels are obtained from the co-pilot, who continuously feeds his decisions about the requirement of BR, ACC and STR control to the decision logic (Fig. 3.2) using a digital rotary switch. Since there are four possible classes (BR, ACC, STR and NOP), the co-pilot keeps the rotary switch in NOP mode

unless any change is required at any point of time. After the co-pilot informs his planning decisions by pressing the right switch for ACC, BR and STR, it naturally returns to NOP by mechanical spring action. So, each planning decision may be regarded as a short duration pulse. The following two criteria have been used to select the co-pilot to assist a given pilot.

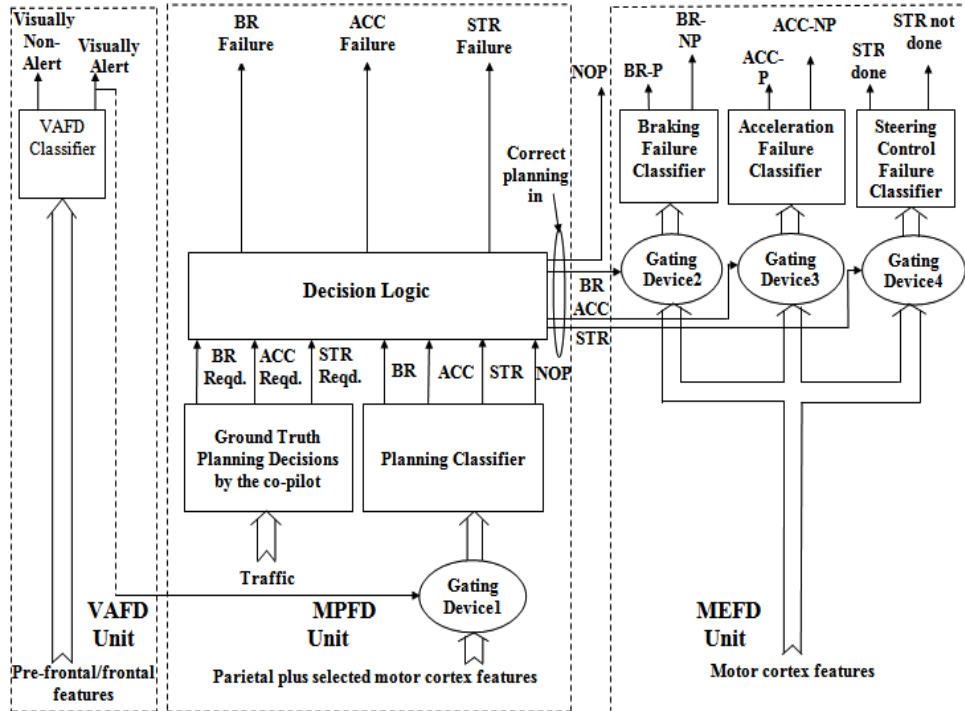


Fig. 3.2 Basic classifier architecture for CFD

- (1) The co-pilot's response time of generating Event Related Potential should be  $\leq$  to that of the main pilot, and
- (2) The co-pilot and the main pilot should be able to receive stimuli concurrently without any interruptions.

The decision logic unit compares the parietal classifier response with the GT classes obtained from the co-pilot and thus determines appropriate planning failures in case there is a mismatch between the two responses (Fig. 3.3). Side connections from one classifier to the next in Fig. 3.2 are used to realize asynchronous operations between two successive classifiers. For example, if the subject is visually alert, we use this signal to act as a control input of a gating device to pass on parietal features to the MPFD classifier. Similarly, if no errors in BR, ACC and STR control signals are detected in MP phase, we use these signals as the control input of respective gating devices for subsequent BR, ACC and STR control classifiers during the ME phase.

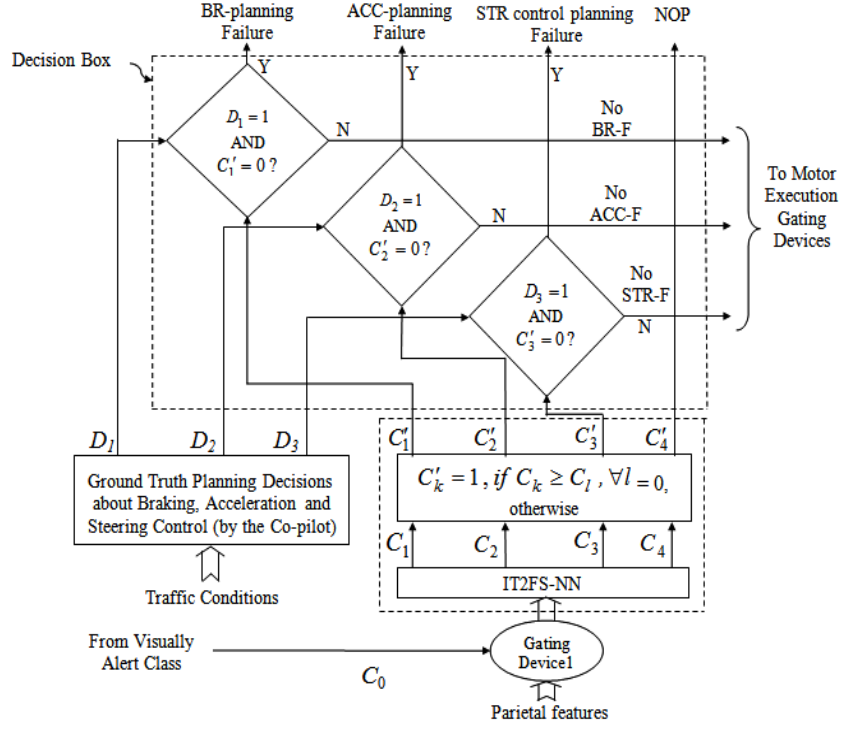


Fig.3.3 Complete architecture of IT2FS induced planning failure detection in driving

### 3.3 FEATURE SELECTION

In the proposed CFD system, we used adaptive autoregressive parameters (AAR) for VAFD, power spectral density (PSD) and db4 wavelet coefficients for MPFD and MEFD. We selected these features based on our previous experience of working with EEG-based driving [9]. The AAR parameters being of low dimensions require no feature selection. However, PSD and DWT [46] features used in MP and ME having large dimensions require reducing features using a feature selection algorithm.

Let,  $\vec{F}_i^k = \{f_{i,1}^k, f_{i,2}^k, \dots, f_{i,D}^k\}$  be the  $i$ -th feature vector with component  $f_{i,j}^k$ ,  $j = 1$  to  $D$  falling in the  $k$ -th class, where,  $i \in [1, n]$  and  $k \in [1, m]$  are positive integers,

$c_j^k$  and  $c_j^l$  be the  $j$ -th component of the cluster centers (geometric centroids) for the classes  $k$  and  $l$  respectively.

Then the aim of the proposed feature selection algorithm is to select  $d \ll D$  number of features in a manner such that it satisfies the following two objectives jointly.

(1) The first objective function  $J_1$  aims at minimizing the city-block distance of all components of the  $i$ -th feature vector,  $i \in [1, n]$  from their respective cluster centers. This is ensured by minimizing (3.1).

$$J_1 = \sum_{k=1}^m \sum_{i=1}^n \sum_{j=1}^D |f_{i,j}^k - c_j^k| \quad (3.1)$$

(2) The second objective function  $J_2$  aims at maximizing the distance between the cluster centers  $c_j^k$  and  $c_j^l$  of two classes  $k$  and  $l$  respectively. This is realized with maximization of (2).

$$J_2 = \sum_{\substack{l=1 \\ l \neq k}}^m \sum_{k=1}^m \sum_{j=1}^D |c_j^k - c_j^l| \quad (3.2)$$

The two objective functions can be jointly represented by a composite objective function, given in (3), which needs to be minimized to attain the above two objectives satisfactorily.

$$J = \frac{J_1}{\delta + J_2}, \quad (3.3)$$

where,  $\delta$  is a small positive number ( $\approx 0.001$  say). The trial solutions here are binary strings of  $D$ -dimension representing presence or absence of a feature in the feature-vector. DE/rand/1/bin variation of Differential evolution (DE) [45] is used to obtain optimal solution (i.e., a binary string of  $D$ -dimension for which  $J$  is minimum) for the given minimization problem. Pseudo code for feature selection using DE is given in Appendix [A.1].

### 3.4 CLASSIFIER SELECTION AND DESIGN

The VAFD and the MEFD classifiers are selected from the standard off-the-shelf classifiers as they have only two class labels. Here, because of superiority of KSVM in classification of non-linearly separable data-points [48], [49], we selected it for VAFD and MEFD classification.

The MPFD classifier has four classes: BR, ACC, STR and NOP, which are often found to have overlaps in feature space because of commonality of signal sources (here, motor cortex). This makes MPFD classification hard, leaving little space for traditional classifiers for the present application. Here, we need to design a suitable classifier, capable of performing classification with high accuracy at low computational overhead for real-time application. Fuzzy classifiers, in particular, type-2 fuzzy classifiers can serve the said purpose for their inherent capability to perform classification with overlapped class boundaries.

The existing IT2FS induced neural classifiers [15]-[18] show good performance with respect to classification accuracy, but their use for the present application is restrictive for their large computational overhead. This motivated us to design a simpler classifier with small computational overhead for real time application, however, without a compromise in their classification accuracy. In this section we would address two such fast classifiers, one realized

with IT2FS- and the other using GT2FS-induced neurons. The proposed GT2FS-induced classifier has relatively better classification accuracy than its IT2FS counterpart, but the computational speed wise IT2FS outperforms all existing and also the proposed GT2FS-NN classifiers.

### 3.4.1 Preliminaries on Interval-Valued, IT2FS and GT2FS

**Definition 1:** Let,  $X$  be the universe of discourse of a linguistic variable  $x$ . A *classical (type-1) fuzzy set*  $A$ , defined on the universe  $X$ , is a two-tuple, given by

$$A = \{(x, \mu_A(x)) \mid \forall x \in X\} \quad (3.4)$$

where,  $\mu_A(x)$ , called membership of  $x$  in  $A$ , is a crisp number in  $[0, 1]$  for any  $x \in X$ . The fuzzy set  $A$  is also expressed as

$$A = \int_{x \in X} \mu_A(x) \mid x \quad (3.5)$$

where  $\int$  represents the union of all feasible  $x \in X$  [50].

**Definition 2:** Given a universe of discourse  $X \neq \emptyset$  for the linguistic variable  $x$ . Let,  $L([0,1])$  denote the set of all closed sub-intervals in  $[0,1]$  and is given by

$$L([0,1]) = \{x = [\underline{x}, \bar{x}] \mid (\underline{x}, \bar{x}) \in [0,1]^2 \text{ and } \underline{x} \leq \bar{x}\}. \quad (3.6)$$

An *interval-valued fuzzy set*  $A$  [51], [52] is given by a mapping

$$A: X \rightarrow L([0,1]), \quad (3.7)$$

and the membership degree of  $x \in X$  is given by  $A(x) = [\underline{A}(x), \bar{A}(x)] \in L([0,1])$ , where  $\underline{A}: X \rightarrow [0,1]$  and  $\bar{A}: X \rightarrow [0,1]$  are mapped as the lower and the upper bound of the membership interval  $A(x)$  respectively.

**Definition 3:** For a given universe of discourse  $X$  for the linguistic variable  $x$ , a type-2, also called *general type-2 fuzzy set (GT2FS)*  $\tilde{A}$  is a two-tuple [14], given by

$$\tilde{A} = \{((x,u), \mu_{\tilde{A}}(x,u)) \mid x \in X, u \in J_x \subseteq [0,1]\} \quad (3.8)$$

where,

$u = \mu_{\tilde{A}}(x)$  (called primary membership) is a crisp number in  $[0, 1]$ ,

$\mu_{\tilde{A}}(x,u) \in [0, 1]$  is the secondary or type-2 membership function (MF).

The fuzzy set  $\tilde{A}$  is also expressed as

$$\tilde{A} = \int_{x \in X} \int_{u \in J_x} \mu_{\tilde{A}}(x,u) \mid (x,u), J_x \subseteq [0,1] \quad (3.9)$$

$$= \int_{x \in X} [ \int_{u \in J_x} f_x(u)/u \mid x, J_x \subseteq [0,1] \quad (3.10)$$

where,  $f_x(u) = \mu_{\tilde{A}}(x, u) \in [0, 1]$ , and  $\coprod$  represents the union over all feasible  $x \in X$  and  $u \in J_x$ .

**Definition 4:** For a given  $x = x'$ , the 2-dimensional plane containing  $u$  and  $\mu(x', u)$  is referred to as *vertical slice* of  $\mu_{\tilde{A}}(x, u)$ . Thus,

$$\mu_{\tilde{A}}(x', u) = \int_{u \in J_x} f_{x'}(u) | u, J_{x'} \subseteq [0, 1], \quad (3.11)$$

here,  $f_{x'}(u)$  lies in  $[0, 1]$ . The amplitude of a secondary MF is referred to as *secondary grade of membership* [13].

**Definition 5:** If  $\mu_{\tilde{A}}(x, u) = 1, \forall x \in X$  and  $\forall u \in J_x \subset [0, 1]$ , then the type-2 fuzzy set  $\tilde{A}$  is called an *interval type-2 fuzzy set (IT2FS)*. In other words, if all the secondary grades of a type-2 fuzzy set are equal to one, it is called as IT2FS [52].

**Definition 6:** An IT2FS contains an infinite number of *embedded type-1 fuzzy sets*. The *upper membership function (UMF)* of an IT2FS is given by

$$\bar{\mu}_{\tilde{A}}(x) = \underset{\forall e}{Max}(\mu_{A_e}(x)), \forall x \quad (3.12)$$

where,  $A_e$  is an embedded fuzzy set in the IT2FS.

Similarly the *lower membership function (LMF)* of an IT2FS is given by

$$\underline{\mu}_{\tilde{A}}(x) = \underset{\forall e}{Min}(\mu_{A_e}(x)), \forall x. \quad (3.13)$$

An IT2FS thus is bounded by an UMF and an LMF. The union of all the embedded fuzzy sets in an IT2FS is called the *footprint of uncertainty (FOU)* [13].

Let,  $f_j$  be a linguistic variable representing an experimental feature and A be a fuzzy set, representing CLOSE-TO-CENTRE-OF-THE-SPAN-OF-  $f_j$ . Because of difference in experimental readings of the feature  $f_j$ , we describe it by a Gaussian MF with mean and variance equal to their respective values of the feature in different experiments for the same subject. Thus, for 10 experimental subjects, we have 10 type-1 Gaussian MFs describing the statement:  $f_j$  is A. We take the maximum and minimum of the 10 type-1 MFs to construct an IT2FS, where the maximum and minimum return the UMF and the LMF respectively (Fig. 3.4).

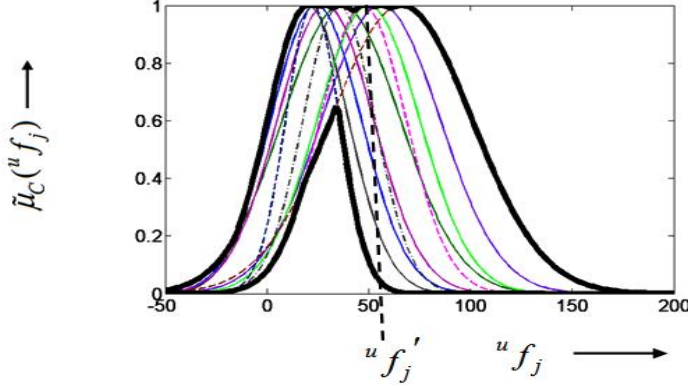
For multi-class classification using IT2FS, we use type-2 classifier rule  $i$  of the form: If  $f_1$  is  $\tilde{A}_1$  and  $f_2$  is  $\tilde{A}_2$  and...and  $f_d$  is  $\tilde{A}_d$ , then class is  $C_i$ , where  $f_1, f_2, \dots, f_d$  are  $d$  features and  $\tilde{A}_j$  for  $j= 1$  to  $d$  are IT2FS. Now, for unknown measurements  $f_1 = f_1'$  and  $f_2 = f_2', \dots, f_d = f_d'$ , we determine the firing strength of the rule  $i$  by taking the average of upper and lower firing strengths  $UFS_i$  and  $LFS_i$ , where

$$UFS_i = \text{Min}(\bar{\mu}_{\tilde{A}_1}(f_1'), \bar{\mu}_{\tilde{A}_2}(f_2'), \dots, \bar{\mu}_{\tilde{A}_d}(f_d')) \quad (3.14)$$



$$\text{and } LFS_i = \text{Min}(\underline{\mu}_{\tilde{A}_1}(f'_1), \underline{\mu}_{\tilde{A}_2}(f'_2), \dots, \underline{\mu}_{\tilde{A}_d}(f'_d)) \quad (3.15)$$

where  $\bar{\mu}_{\tilde{A}_j}$  and  $\underline{\mu}_{\tilde{A}_j}$  are UMF and LMF of IT2FS  $\tilde{A}_j$ .



**Fig. 3.4** Construction of IT2FS<sub>1</sub> for feature  $f_j$  from 10 Gaussians for 10 subjects in braking

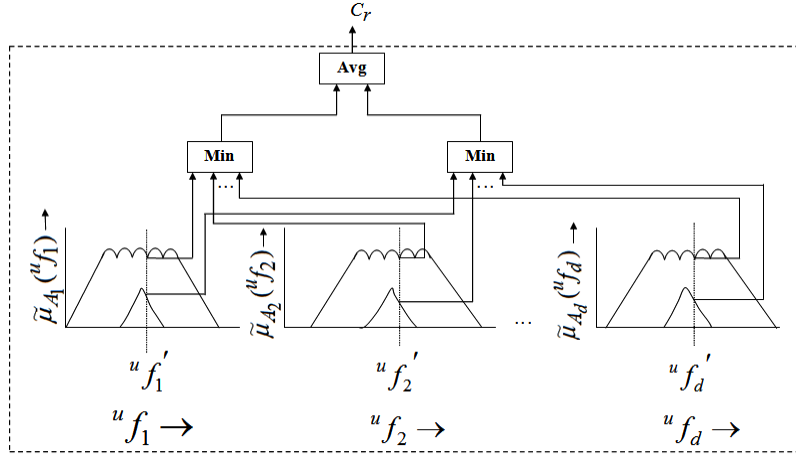
Now, for  $k$  classifier rules, we say that the features:  $f_1 = f'_1, f_2 = f'_2, \dots, f_d = f'_d$  fall in class  $r$  if the average of  $LFS_r$  and  $UFS_r$  exceeds the average of  $LFS_i$  and  $UFS_i, \forall i$ . The justification of the averaging is briefly discussed below.

It is important to note that the actual firing strength of a rule  $i$  lies in  $[LFS_i, UFS_i]$  and is uniformly probable everywhere in the said interval. Thus the expected firing strength of rule  $i$  would be the average of  $LFS_i$  and  $UFS_i$ . The significance of the proposed simple approach is apparent for its low computational overhead and run-time performance over comparable algorithms [15]-[17], [53], [54] for real-time classification of brain signals. The type-2 classifier rule and inference generation using the above rule is represented in the form of a type-2 fuzzy neuron (Fig. 3.5), where the neuron includes  $d$  IT2FS, and for a given set of measurements  ${}^u f_1 = {}^u f'_1, {}^u f_2 = {}^u f'_2, \dots, {}^u f_d = {}^u f'_d$ , we obtain the  $UFS_i$  and  $LFS_i$  to finally obtain their average, representing the degree of the measurements to fall in class  $i$ . The subscript  $u$  above is used to designate the subject.

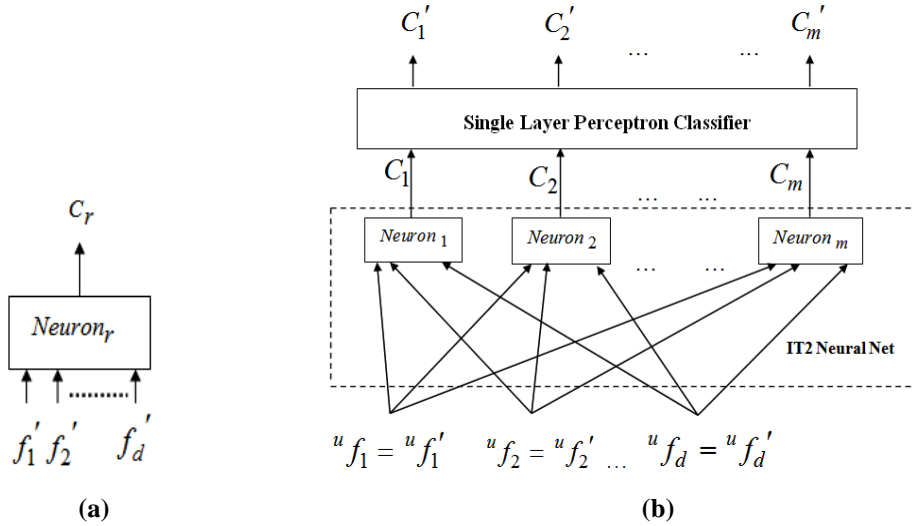
### 3.4.2 IT2FS-Based Classifier Design

The IT2FS-induced planning classifier (Fig. 3.3) determines four class labels including  $C_1$  (braking),  $C_2$  (acceleration),  $C_3$  (steering control) and  $C_4$  (no operation). The small dotted box in Fig. 3.3 describes the MP classifier, comprising two modules, where the first module is an IT2FS neural net with outputs  $C_1, C_2, C_3$  and  $C_4$ . This neural net is realized with IT2FS neurons, the symbol and architecture of which are given Fig. 3.6(a) and 3.6(b) respectively. The next top box within the dotted small box in Fig. 3.3 represents the second module of the MP classifier. This module sets one of its output:  $C'_k = 1$ , if  $C_k \geq C_l \forall l$ , and sets remaining

outputs to zero. In other words, if the IT2FS neural net responds with the largest output at  $C_k$  in comparison to  $C_l, \forall l (\neq k)$ , then the second module sets  $C'_k = 1$  and  $C'_l = 0$ .



**Fig. 3.5** Architecture of the an IT2FS neuron  $r$



**Fig. 3.6(a)** The structure of a neuron, **Fig. 3.6(b)** Architecture of the proposed IT2FS- induced classifier to classify motor-planning classes

The co-pilot, as mentioned earlier, takes binary decisions about  $D_1$  (braking),  $D_2$  (acceleration) and  $D_3$  (steering control) as required during driving. These decisions are considered as ground truth for the driver and consequently a failure occurs when  $D_k = 1$  but  $C'_k = 0$  for any  $k \in [1, 3]$ . This is given in Fig. 3.3 by three decision boxes. It is important to note that  $D_k$  and  $C'_k$  for a given  $k$  respectively represent decision of co-pilot and decoded decision of the driver for the same planning action, say BR.

The two modules representing MP classifier here is realized by a two-layered neural net (Fig. 3.6(b)), where the first layer is constructed with IT2FS neurons and the second layer with perceptron neurons. Suppose, for a given instance of motor-planning by a subject  $s$ , we

have  $d$  features:  ${}^s f_1, {}^s f_2, \dots, {}^s f_d$  after feature selection. Assume that the MP task has  $m$  ( $=4$ ) cognitive classes, such as BR, ACC, STR control and NOP.

The principle of classification by the proposed IT2FS-NN, given in Fig. 3.6(b) is step-wise outlined below for an unknown subject  $u$ .

*Step 1:* Evaluate lower and upper firing strengths:  $LFS_r$  and  $UFS_r$  of the  $r$ -th IT2FS neuron by evaluating the t-norm (here, min) of the embedded type-1 LMFs and UMFs respectively at measurement points  ${}^u f_j', j=1$  to  $d$ , where

$$LFS_r = \underset{j=1}{\overset{d}{\text{Min}}}(LMF({}^u f_j')) \quad (3.16)$$

$$\text{and} \quad UFS_r = \underset{j=1}{\overset{d}{\text{Min}}}(UMF({}^u f_j')) \quad (3.17)$$

where,  $\underset{j=1}{\overset{d}{\text{Min}}}$  is cumulative minimum operator for varying  $j=1$  to  $d$ .

*Step 2:* We next evaluate the average firing strength for the  $r$ -th neuron, given by

$$C_r = \frac{1}{2}(LFS_r + UFS_r), \quad (3.18)$$

for  $r=1$  to  $m$  classes. This has similarity with Nie-Tan type reduction [15], [38].

*Step 3:* For any  $k, l \in [1, m]$ , if  $C_k \geq C_l, k \neq l$ , then the response of proposed neuron  $k$  is given by

$$C'_k = 1 \text{ and } C'_l = 0, \forall l \neq k.$$

By steps 2 and 3, we want to convey that we consider the feature sets to fall in class  $k$  if the average firing strength  $C_k$  (using (3.11)) of the neuron  $k$  exceeds the same of other neurons.

The perceptron learning algorithm used in Fig. 3.6(b) adapts the weights  $w_{kl}, k=1$  to  $m$  and  $l=1$  to  $m$  by using the learning equation:

$$w_{kl}(t+1) = w_{kl}(t) + \eta C_k e_l \quad (3.9)$$

where,

$w_{kl}(t)$  is the weight between  $C_k$  to  $C'_l$  at time  $t$ ,  $e_l = d_l - C'_l =$  error signal corresponding to output  $C'_l$  with reference to pre-defined target value  $d_l$ , and  $\eta$  is the learning rate in  $[0,1]$ .

### 3.4.3 GT2FS-Based Classifier Design

The intra- and inter-personal level uncertainty of individual sources is usually buried in the FOU of an IT2FS. In order to efficiently utilize the above forms of uncertainty, we prefer to use GT2FS-based classifier. A GT2FS, in general, is a 3-tuple given by  $\langle f_j, \mu_{\tilde{C}_k}(f_j), \mu((f_j, \cdot))\mu_{\tilde{C}_k}(f_j) \rangle$ , where  $f_j$  is the  $j$ -th feature,  $\mu_{\tilde{C}_k}(f_j)$  is the type-1 MF and

$\mu(f_j, \mu_{\tilde{C}_k}(f_j))$  is the secondary grade of membership of feature  $f_j$  for a given primary MF  $\mu_{\tilde{C}_k}(f_j)$ .

In this section we propose i) one novel approach to secondary membership evaluation for a given pair of linguistic variable value and corresponding primary membership over each user supplied type-1 MF, and ii) classification of motor imageries using GT2FS-NN.

#### A. Secondary Membership Evaluation

In [55], authors proposed a novel approach for secondary MF evaluation in the settings of an optimization problem. For evaluation of secondary memberships in real-time, we here propose an alternative approach free from optimization using the following assumptions:

1. Suppose in a test, maximum marks=100 and there are 50 students, out of which a few students scored zero and 100 and the rest scored marks in [0, 100]. Now, the examiner is very certain while assigning a marks zero or 100. But he does not have the same degree of certainty while assigning a mark, say 67, to a student.

In the assignment of secondary membership, we adopted a similar policy. The secondary membership should have a maximum value equal to (or close to) 1 at the peaks and minima on the primary MF. The motivation of such selection lies in the phenomenon that the secondary grade representing the degree of primary membership should have the highest value at the peaks and minima (of the type-1 MFs) as the user is confident of assigning maximum and minimum membership values at those selected locations of the type-1 MF. Formally, we write  $\mu(f_j', \mu_{\tilde{C}_k}(f_j')) = 1$ , if  $\mu_{\tilde{C}_k}(f_j)$  has a local peak or minimum at  $f_j = f_j'$ .

2. The secondary membership should decrease as the linguistic variable is away from the location of the peak/minimum of the type-1 primary MF. Presuming an exponential decrease in secondary membership at  $f_j = f_j'$ , when there exists a nearest peak/minimum

at  $f_j = f_j'$ , we obtain  $\mu(f_j', \mu_{\tilde{C}_k}(f_j')) = \mu(f_j', \mu_{\tilde{C}_k}(f_j')) \cdot e^{-|f_j' - f_j'|} = e^{-|f_j' - f_j'|}$  as  $\mu(f_j', \mu_{\tilde{C}_k}(f_j')) = 1$ .

3. When a point  $f_j \in [f_j', f_j'']$  where  $f_j'$  and  $f_j''$  are two nearest peak/minimum on the type-1 MF  $\mu_{\tilde{C}_k}(f_j)$ , we obtain the secondary MF at  $(f_j, \mu_{\tilde{C}_k}(f_j))$  by  $\mu(f_j, \mu_{\tilde{C}_k}(f_j))$

$$= \text{Max}[\mu(f_j', \mu_{\tilde{C}_k}(f_j')) \cdot e^{-|f_j - f_j'|}, \mu(f_j'', \mu_{\tilde{C}_k}(f_j'')) \cdot e^{-|f_j - f_j''|}]$$

$$= \text{Max}[e^{-|f_j - f_j'|}, e^{-|f_j - f_j''|}]$$

as  $\mu(f_j', \mu_{\tilde{C}_k}(f_j')) = 1$  and  $\mu(f_j'', \mu_{\tilde{C}_k}(f_j'')) = 1$

for  $f_j'$  and  $f_j''$  being peak/minimum on the type-1 MF.

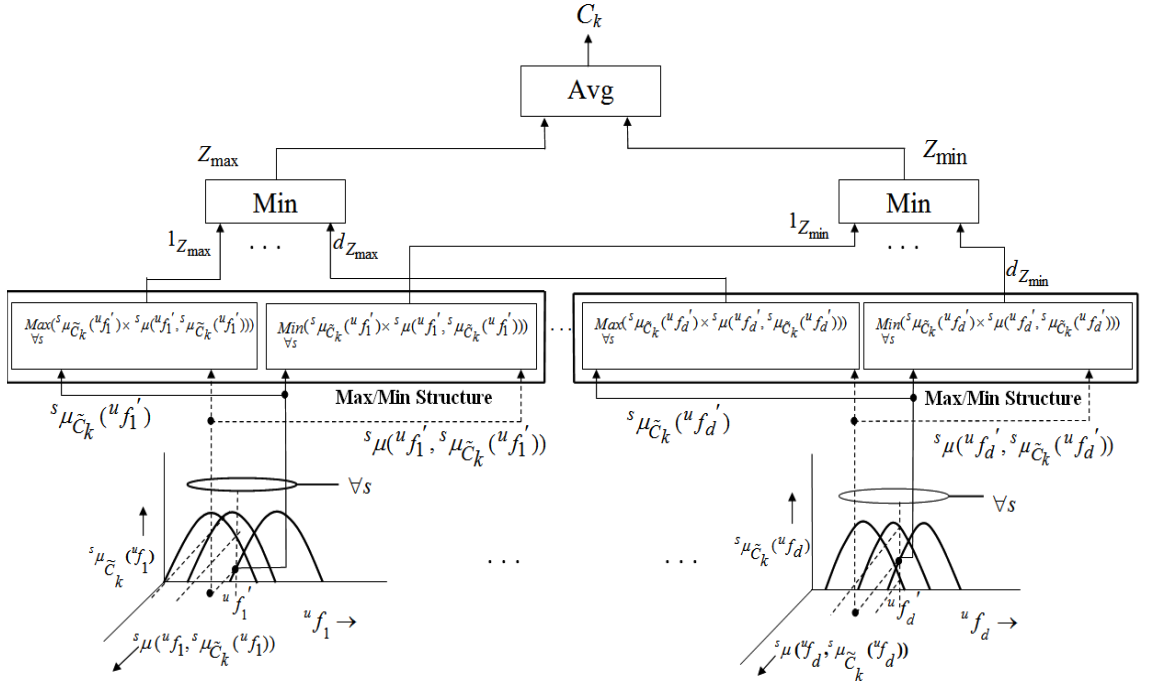
It may be added here that computation of secondary membership has to be performed for the primary MFs obtained from each subject. To represent the subjective primary and

secondary MF for each linguistic variable, we add an extra  $s$  as the left superscript to  $\mu_{\tilde{C}_k}(f_j)$  and  $\mu(f_j, \mu_{\tilde{C}_k}(f_j))$ , which would look like  ${}^s\mu_{\tilde{C}_k}(f_j)$  and  ${}^s\mu(f_j, {}^s\mu_{\tilde{C}_k}(f_j))$  respectively.

### B. GT2FS-NN Based Classification

In GT2FS, we need to consider subjective type-1 MF and their secondary membership values for all possible values of the linguistic variable (here, feature). To represent subjective consideration of type-1 MF, we adopt the old notations like  ${}^s f_j$  to describe  $j$ -th feature for subject  $s$ . Let us assume that we have  $n$  subjects to develop the complete membership space for the entire MP classifier system.

Let,  $\mu_{\tilde{C}_k}({}^s f_j)$  be the primary MF for feature  $f_j$  obtained from experimental data of subject  $s$  for the classifier rule for class  $k$ , and  $\mu({}^s f_j, \mu_{\tilde{C}_k}({}^s f_j))$  be the secondary MF for feature  $f_j$  constructed from primary MF of subject  $s$  for the classifier rule of class  $k$ . Here, we design one GT2FS-neuron to describe the  $k$ -th class classifier rule with features  ${}^u f_1, {}^u f_2, \dots, {}^u f_d$ , where  $u$  denotes the unknown subject. The neuron produces the firing strength  $C_k$  of the  $k$ -th class classifier rule. Thus for  $m$  classes, we have  $m$  such neurons. The neuron with the largest firing strength would describe the right class (classifier output). This is realized by architecture similar to Fig. 3.6(b), where the neurons are of GT2FS type (see Fig. 3.7). The  $k$ -th class neuron works following the principles outlined below.



**Fig. 3.7** Architecture of the proposed GT2FS-induced neuron

1. First, for each type-1 MF  ${}^s\mu_{\tilde{C}_k}({}^u f_j)$  obtained from subject  $s$  for feature  $f_j$ , we evaluate secondary membership  ${}^s\mu({}^u f_j, {}^s\mu_{\tilde{C}_k}({}^u f_j))$  at the measurement point  ${}^u f_j = {}^u f_j'$ ,  $j=1$  to  $d$ .

2. We then submit  ${}^s\mu_{\tilde{c}_k}({}^u f_j')$  and  ${}^s\mu({}^u f_j', \mu_{\tilde{c}_k}({}^u f_j'))$  at the input of Max and Min blocks  $\forall s$ , where we evaluate

$${}^j z_{\max} = \underset{\forall s}{\text{Max}}({}^s\mu_{\tilde{c}_k}({}^u f_j') \times {}^s\mu({}^u f_j', {}^s\mu_{\tilde{c}_k}({}^u f_j')) \text{ and}$$

$${}^j z_{\min} = \underset{\forall s}{\text{Min}}({}^s\mu_{\tilde{c}_k}({}^u f_j') \times {}^s\mu({}^u f_j', {}^s\mu_{\tilde{c}_k}({}^u f_j')) \text{ for } j=1 \text{ to } d.$$

3. Now, we compute  $z_{\max} = \underset{j=1}{\text{Min}}({}^j z_{\max})$  and  $z_{\min} = \underset{j=1}{\text{Min}}({}^j z_{\min})$  by two additional blocks.

4. In the last step, we compute average of  $z_{\max}$  and  $z_{\min}$  to compute  $C_k$ , the class membership (or firing strength) of the fired  $k$ -th classifier rule realized with the neuron.

After  $C_k$ 's are evaluated for  $k = 1$  to  $m$ , we use a figure similar to Fig. 3.6(b) with IT2FS neurons being replaced by GT2FS neurons to identify the class  $p$  where  $C_p' = 1$  for  $C_p > C_r, \forall r$  and  $C_r' = 0$  for  $r \neq p$ .

The GT2FS-induced classifier outperforms both the existing and the proposed IT2FS-induced classifiers because of utilization of secondary memberships in firing strength evaluation of rules. In GT2FS-induced classification, we attempted to obtain an equivalent IT2FS-like representation in the product space of primary and secondary memberships and hence evaluated the UMF and the LMF at a given measurement point. Such product function based UMF and LMF computation improves the qualitative measure of firing strength computation, which in turn enhances the classifier performance in comparison to its IT2FS counterparts. In this chapter, secondary MF computation, however, is done offline.

### 3.4.4 Complexity Analysis

The IT2 classifier includes four main steps: i) Determining the LMF and the UMF at the given measurement points of  $d$  IT2FS present in the antecedent of a classifier rule represented by the IT2 neurons, ii) computing t-norm of the resulting LMFs (and the UMFs) obtained from  $d$  IT2FS to generate LFS and UFS respectively from each neuron, iii) Taking average of the UFS and the LFS from each neuron and iv) a forward pass in the single layer perceptron classifier to produce the desired class of the given measurement space.

The complexity of step (i) is  $O(d)$ . The complexity of step (ii) is also  $O(d)$ . The complexity of step (iii) is  $O(1)$ . The complexity of step (iv) is  $O(m)$ , where  $m$  denotes number of neurons. As we have  $m$  neurons working in parallel, their complexity represented by the first three steps, need to be considered once only. So, the overall time-complexity is  $2O(d) + O(1) + O(m) \approx O(d) + O(m)$ . In uni-processor architecture, the complexity of the individual neurons, however, adds up, yielding an overall complexity of  $O(m.d) + O(m)$ , which approximately is  $O(m.d)$ .

For GT2FS-based classifier, we need extra complexity for secondary membership evaluation plus taking product of primary and secondary MFs at the given measurement points. The secondary membership computation is done offline. So, its complexity does not add to GT2FS classifier-overhead. Now, for  $d$  fuzzy propositions in the antecedent of the

classifier rule, we need to have  $2O(d)$  additional multiplications per neuron with respect to that in IT2FS-induced neurons. So, if the parallel architecture is fully supported, the overall complexity appears to be  $2O(d) + 2O(d) + O(m) + O(1) \approx 4O(d) + O(m)$ . Again, if the computation is performed on a uni-processor architecture, the computational complexity is obtained as  $2m.d + 2m.d + m \approx O(m.d)$ .

### 3.4.5 The KSVM Classifiers

VAFD and MEFD classifiers here are realized with KSVM, for proven performance in two class classification problems and their low computational overhead. In Fig. 3.2, each of the ME tasks: BR, ACC and STR control is classified into two classes, namely BR-P and BR-NP, ACC-pressed (ACC-P) and ACC-not pressed (ACC-NP) and STR-control done and STR-control not done. The VAFD classifier classifies the obtained pre-frontal and frontal feature set into two classes: visually alert and non-alert. A typical SVM classifier aims at designing a hyper-plane that leaves the maximum distance between the hyper-plane and the closest element from the hyper-plane (i.e., margin) from both classes. A linear support vector machine classifier can segregate linearly separable data points by an optimally chosen hyper-plane. KSVM is employed when we do not have knowledge about the linear separable nature of the data points of two classes. One approach to select the right SVM classifier is to consider KSVM with linear, polynomial and radial basis function (RBF) type kernel functions with varied parameters of the kernel and thereby determine the parameters with maximum classification accuracy. Since linear SVM is equivalent to KSVM with linear kernel function, we lose nothing by realizing the latter.

The KSVM attempts to minimize the following cost functional to find an optimal choice of the weight vector  $\mathbf{w}$ .

$$\Phi(\mathbf{w}, \xi, \xi') = \frac{1}{2} \mathbf{w}^T \mathbf{w} + C \sum_{i=1}^N (\xi_i + \xi'_i) \quad (3.19)$$

where, for  $i=1$  to  $N$  the following constraints should hold.

$$\begin{aligned} d_i - \mathbf{w}^T \Phi(\mathbf{x}_i) &\leq \varepsilon + \xi_i, \\ \mathbf{w}^T \Phi(\mathbf{x}_i) - d_i &\leq \varepsilon + \xi'_i, \\ \xi_i &\geq 0 \text{ and } \xi'_i \geq 0, \end{aligned}$$

In the above formulation,  $\{(\mathbf{x}_i, d_i)\}$  for  $i=1, 2, \dots, N$  are the training samples with  $\mathbf{x}_i$  being the input pattern for the  $i$ -th example and  $d_i$  is the target class label +1 or -1. Slack variable  $\xi_i$  and  $\xi'_i$  represent  $\varepsilon$ -insensitive loss function [48] and  $\Phi(\mathbf{x}_i) = [\Phi_0(\mathbf{x}_i) \ \Phi_1(\mathbf{x}_i) \ \dots \ \Phi_{m_1}(\mathbf{x}_i)]$ , whose  $\{\Phi_j(\mathbf{x}_i)\}$  for  $j=0$  to  $m_1$  denote a set of non-linear basis function.  $\mathbf{w}$  is the  $m_1$ -dimensional unknown weight vector, and  $C$  is a user-defined positive parameter. Here,  $K(\mathbf{x}, \mathbf{x}_i) = \Phi^T(\mathbf{x})\Phi(\mathbf{x}_i)$  is an inner product kernel. In our experiment,

we used radial basis function kernel, given by  $K(\mathbf{x}, \mathbf{x}_i) = \exp(-\|\mathbf{x} - \mathbf{x}_i\|^2 / 2\sigma^2)$ , polynomial kernel, given by  $K(\mathbf{x}, \mathbf{x}_i) = (1 + \mathbf{x}^T \mathbf{x}_i)^d$ , and linear kernel  $K(\mathbf{x}, \mathbf{x}_i) = (1 + \mathbf{x}^T \mathbf{x}_i)$ . We adapt C and parameter of the respective kernel function to obtain their settings for maximum classification accuracy. This is discussed in detail in the experiment section.

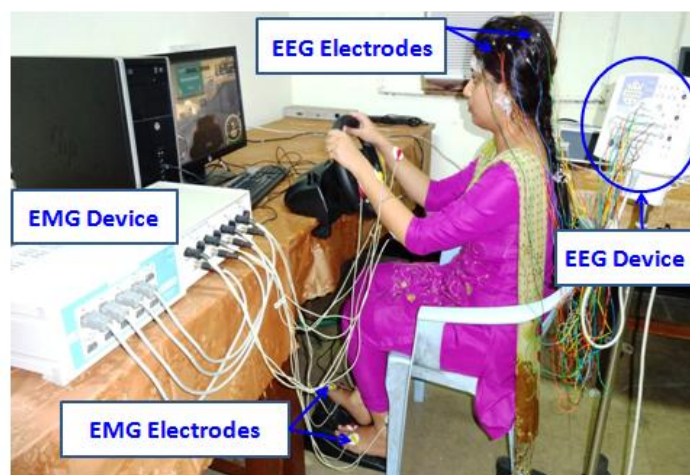
### 3.5 PSYCHO-PHYSIOLOGICAL EXPERIMENTS

This section provides experiments undertaken to determine certain experimental parameters concerning EEG and also to validate the principles outlined in Section 3.2 - 3.4.

#### 3.5.1 Experimental Set-up

EEG is captured from a 21-channel standalone EEG acquisition system with sampling rate of 200 Hz, manufactured by Nihon Kohden while the experiments are performed using a Logitech driving simulator. In addition, four EMG sensors are placed on both hand muscles (extensor carpi radialis longus) and leg muscles (gastrocnemius muscles, often referred to the bulging area of the calf muscle) of the participants to test motor execution failure. The EMG data are recorded at sampling rate of 1 KHz.

The experiments are performed using a Logitech driving simulator (See Fig. 3.8), comprising a steering wheel and a foot rest comprising an accelerator and a brake paddle (from right to left), following configurations for British/Indian cars. The driving simulator is connected to a personal computer using a Universal Serial Bus (USB)-port. The computer is configured with an intel processor with 8GB RAM and a CPU clock of 3.4 GHz. One video display unit (VDU) connected with the computer is used to observe the driving environment, containing the car under reference, roads and other cars and pedestrians.



**Fig. 3.8** Experimental set-up for acquisition of EEG and EMG signals from a subject driving a virtual driving simulator

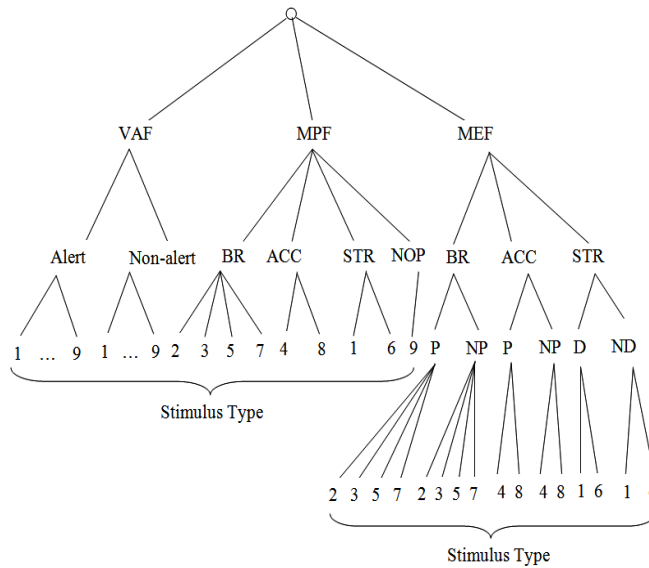


### 3.5.2 Participants

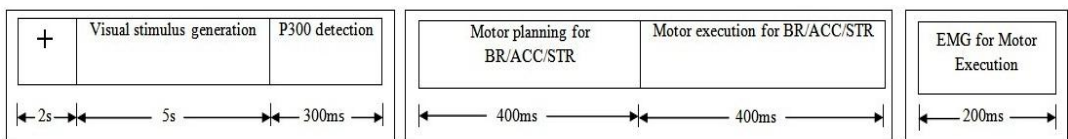
Ten subjects aged 22-30 years are selected for driving experiments, among whom six are healthy (H1-H6) registered drivers, two are fatigued (F1 and F2) due to lack of sleep over last 48 hours, and the rest are driving learners (L1 and L2).

### 3.5.3 The Training Session

At first we prepare the training dataset. The dataset prepared for the CFD problem is presented in the form of a tree (Fig. 3.9). The root node of the tree denotes cognitive failures. At the next level, we present the failure types. At the third level, we list the classes under each failure type. At the lowest level (leaves), we present the stimulus type for each class of the failure. The total number of stimuli/subject/training session is obtained by the count of the leaf nodes, which here is 43. We repeat the experiment 10 times on each of the 10 subjects, thus having an EEG database of  $43 \times 10 \times 10 = 4300$ . The length of the EEG samples collected for each stimulus is  $300\text{ms} + 400\text{ms} + 400\text{ms} = 1100\text{ms}$  (see Fig. 3.10).



**Fig. 3.9** The tree representing 43 EEG data-samples for 43 stimuli per subject per training session



**Fig. 3.10** Structure of the stimulus used and timings

Experimental procedure of the training session is provided in Table 3.1.

**Table 3.1** Experimental Procedure for the Training Session

Steps	Description
Step-I: Stimulus preparation	9 stimuli as indicated in Table-II are submitted to the subject one by one, each for duration of 5 seconds after a uniform interval of 10 seconds between two successive presentations, followed by EEG acquisitions. The 9 stimuli are used to obtain four classes of subjective actions: Braking (by left foot), Acceleration (by right foot), Steering control (by both hands), and No operation/Wait for the next stimulus. The structure of an individual stimulus and timing are given in Fig. 8.
Step-II: EEG and EMG Acquisition	<p>i) P-300 detection from electrodes: <math>Fp_1, Fp_2, F_3, F_4, F_z, F_7, F_8, O_1, O_2, P_z</math> for VAF</p> <p>ii) ERD/ERS detection from electrodes <math>P_3, P_4, C_3, C_4</math> for MP: Steering control (hand-imagery)</p> <p>iii) ERD/ERS detection from electrodes <math>C_2</math> and <math>C_z</math> for MP: Braking (left foot-imagery)</p> <p>iv) ERD/ERS detection from electrodes <math>C_1, C_z, P_3, P_z</math> for MP: Acceleration (right foot-imagery)</p> <p>v) ERD/ERS detection from electrodes <math>C_3</math> and <math>C_4</math> for ME: Steering control (hand-execution)</p> <p>vi) ERD/ERS detection from electrodes <math>C_2</math> and <math>C_z</math> for ME: Braking (left foot-execution)</p> <p>vii) ERD/ERS detection from electrodes <math>C_1</math> and <math>C_z</math> for ME: Acceleration (right foot-execution)</p> <p>viii) PSD detection from EMG electrodes: <math>Ch_1</math> and <math>Ch_2</math> (for hands) and <math>Ch_3</math> and <math>Ch_4</math> (for foot) to check muscle activity</p>
Step-III: Pre-processing and Filtering	<p>Using Elliptic filter of order 4 with pass bands</p> <p>i) <math>\alpha</math>-band (7-13 Hz) for VAF</p> <p>ii) <math>\mu</math> and <math>\beta</math> bands (8-13, 13-30 Hz) for MPF</p> <p>iii) <math>\beta</math> band (13-30 Hz) for MEF</p>
Step-IV: Feature Extraction and Feature Selection	<p>Features extracted for VAF: 11 AAR parameters</p> <p>Features extracted for MPF: 15 PSD + 63 DWT</p> <p>Features extracted for MEF: 15 PSD + 63 DWT</p> <p>Features selected for VAF: All extracted features</p> <p>Features selected for MPF and MEF: 18 out of 78 features by DE-based feature selection</p>
Step-V: MF Construction	<p>IT2FS Construction</p> <ol style="list-style-type: none"> <li>Type-1 MF construction for each feature from multiple trials of the same of the same subject</li> <li>Construction of Mixture of Gaussians by repeating experiments on 10 subjects</li> <li>Taking max and min of the Gaussians to obtain UMF and LMF of IT2FS</li> </ol> <p>GT2FS Construction</p> <ol style="list-style-type: none"> <li>For each Gaussian primary MF obtained in step-2 above, compute secondary MFs at the desired value of linguistic variable <math>x</math> and primary MF: <math>\mu_{\tilde{A}}(x)</math>.</li> </ol>
Step-VI: Classifier Training	<ol style="list-style-type: none"> <li>Define class labels for IT2FS/GT2FS classifiers</li> <li>Feed extracted features to the classifier: (IT2FS/GT2FS) and measure error at the output of layer 2 neurons</li> <li>Adjust the weights of the second layered neurons by Perceptron Learning algorithm.</li> <li>Select KSVM parameters and train the KSVM classifier with the selected parameters.</li> </ol>

### A. Stimuli Preparation

Each subject is instructed to perform driving with a given road map for 10 times, where the road-map includes nine types of visual stimuli. The list of the stimuli along the motor actions required in response to the respective stimulus is given in Table 3.2. The structure of the stimulus is given in Fig. 3.10.

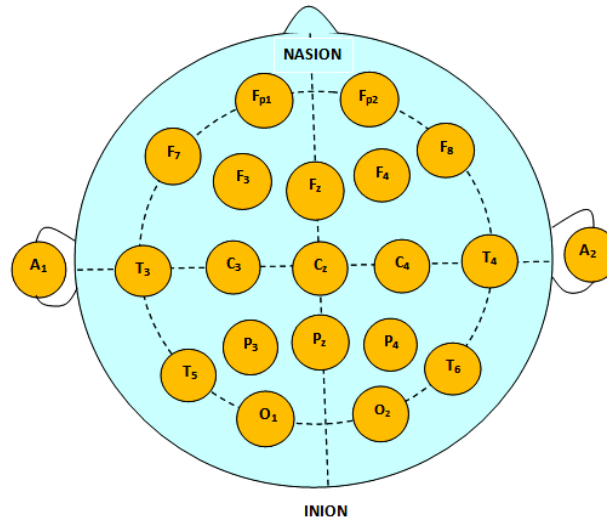
**Table 3.2** List of Stimuli and Required Motor Intension

Stimulus type	Stimulus description	Required motor intension
1	Car moving ahead and side car at either side is too close	Steering (STR) control
2	High bumper	Braking (BR)
3	Car coming from opposite direction at high speed	Braking (BR)
4	Sudden increase in gap between the car moving ahead and the reference car	Acceleration (ACC)
5	Change in traffic light from green to red	Braking (BR)
6	Sharp bending in front	Steering (STR) control
7	Sudden decrease in gap between the car moving ahead and the reference car	Braking (BR)
8	Change in traffic light from red to green	Acceleration (ACC)
9	Cars on road at constant speed and no change in road direction/traffic signal	NOP

### B. EEG Electrodes and Signal Acquisition

We used the standard 10-20 electrode placement technique (Fig. 3.11) to locate the electrodes listed in Table-2.1 for the cognitive tasks associated with VA, MP and ME tasks. 10-20 electrode placement technique is a well-known International standardized method for locating the EEG electrodes on the human scalp. This section includes an outline of 10-20 electrode placement technique using 21-channel EEG acquisition device (Fig. 3.11). The ‘10’ and ‘20’ refer to the fact that the actual distances between adjacent electrodes are either 10% or 20% of the total nasion-inion distance of the skull. Nasion and inion are two anatomical landmarks that are used for the essential positioning of the EEG electrodes. The position of EEG electrodes can be understood from their nomenclature. It is clear from Fig. 3.10 that the first letter of each brain region refers to the location of electrode placement and a number to identify the hemisphere location. Odd numbers (1, 3, 5, 7, 9) refer to electrode positions on the left hemisphere, whereas even numbers (2, 4, 6, 8) refer to those on the right hemisphere.

Here, we selected pre-frontal and frontal electrodes: Fp<sub>1</sub>, Fp<sub>2</sub>, F<sub>3</sub>, F<sub>4</sub>, F<sub>z</sub>, F<sub>7</sub>, F<sub>8</sub> for VA detection as they are usually activated in alertness related brain-activity [56]. In addition, O<sub>1</sub>, O<sub>2</sub> and P<sub>z</sub> electrodes are selected for VA following [57]-[59] for possible engagement of the parietal and the occipital lobes to elicit P300 in the presence of rare/target visual stimuli. It may be noted that usually before motor execution, the subject performs motor imagery for motor planning to mentally prepare for hand or leg movements to perform braking, acceleration and/or steering control.



**Fig. 3.11** 10-20 electrode placement system for 21-channel EEG device.

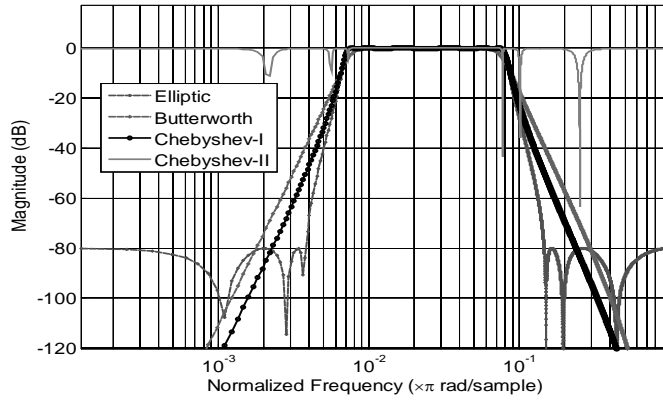
F: Frontal, F<sub>p</sub>: Pre-frontal, C: Motor cortex, T: Temporal, P: Parietal and O: Occipital

When there is no time-pressure, motor imagery and motor execution can be easily recognized from parietal and motor cortex ERD/ERS, particularly for new drivers. But when the subject is under time-pressure, the time-gap between the two ERD/ERS signals is not always visible. For hand motor imagery, the electrodes used are P<sub>3</sub>, P<sub>4</sub>, C<sub>3</sub>, C<sub>4</sub>; for hand motor execution the electrodes used are C<sub>3</sub> and C<sub>4</sub> while for the foot motor imagery and execution, we take the difference signals: P<sub>3</sub> – P<sub>z</sub>, P<sub>4</sub> – P<sub>z</sub> and C<sub>1</sub> – C<sub>z</sub> and C<sub>2</sub> – C<sub>z</sub> to distinguish them from the hand motor imagery/execution [60].

### C. Pre-processing and Filtering

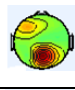
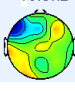
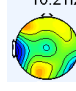
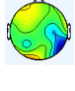
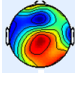

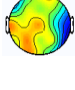
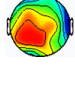
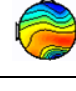
We here select Infinite Impulse Response (IIR) filters over Finite Impulse Response (FIR) filters because of its requirement of fewer filter coefficients with respect to the latter for a given order of the filter.

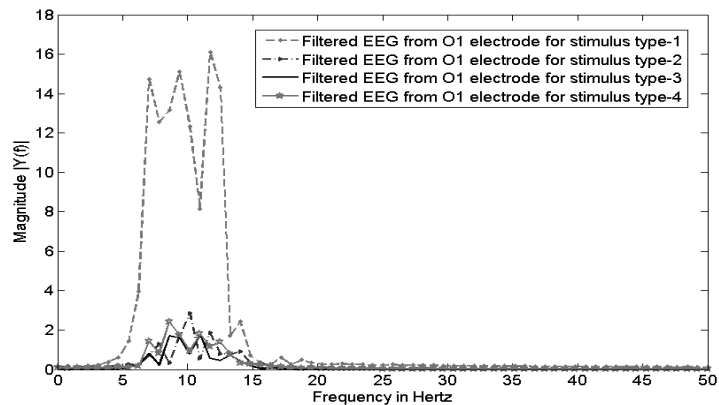
For realization, we select Elliptic filter of order 4 over Butterworth, Chebyshev-I and Chebyshev-II filters for its sharper roll-off around the cut-off frequencies than the rest. (Fig. 3.12). For pass band selection of the elliptic filters, we obtain the centre frequency of the bands for the three cognitive tasks and obtained the scalp maps, given in Table 3.3. The filtered signals in the pass band of the VA and motor imagery classes from occipital and motor cortex regions respectively are given in Fig. 3.13 and 3.14. It is confirmed from both the figures that alpha band (8-13 Hz) is associated during visual alertness and beta (13-30 Hz) band is active during motor execution tasks.



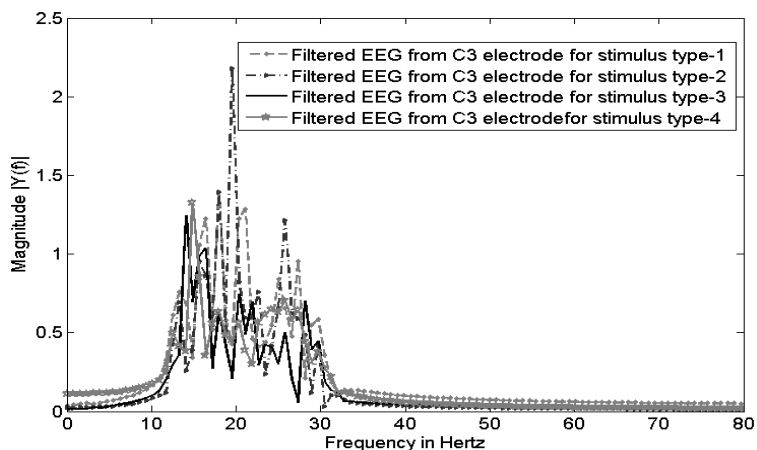
**Fig. 3.12** Frequency response of Filters: Butterworth, Chebyshev-I, Chebyshev-II and Elliptic filters of order 4

**Table 3.3** Activation of Scalp Maps for Different Cognitive Modalities at Different Frequency Bands

Frequency band	Visual alertness phase	Motor-planning phase	Motor-execution phase
Alpha	8 Hz 	10.3 Hz 	10.2 Hz 
Beta	21.9 Hz 	21.9 Hz 	17 Hz 
Mu	10.2 Hz 	11.3 Hz 	10.2 Hz 

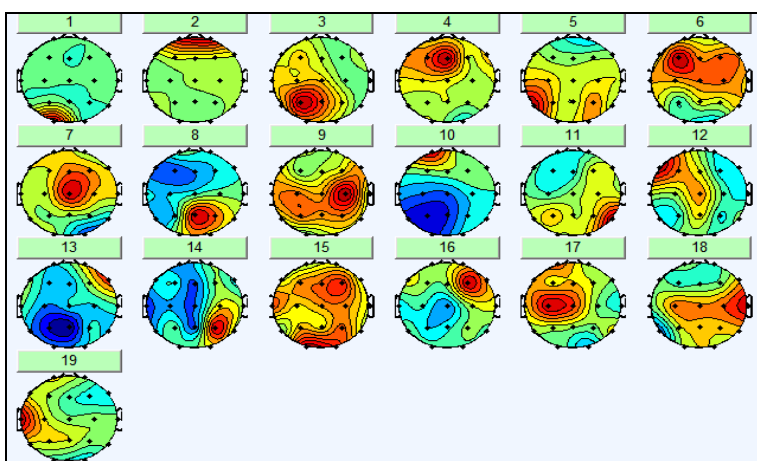


**Fig. 3.13** Pass band (7-13 Hz) selection of the elliptic filter for occipital EEG for four stimuli



**Fig. 3.14** Pass band (13-30 Hz) selection of the elliptic filter during execution of four motor actions for four stimuli

For each driving session, we take ICA of the 19 electrodes and observe that for the independent components 1, 3, 4, 5, 6, 7, 8, 9, 14, 16, 17, we have circular (enclosed) red regions indicating activation of the corresponding brain regions (Fig. 3.15). The remaining components are ignored since these are activated due to eye-blinking and muscle artifacts.

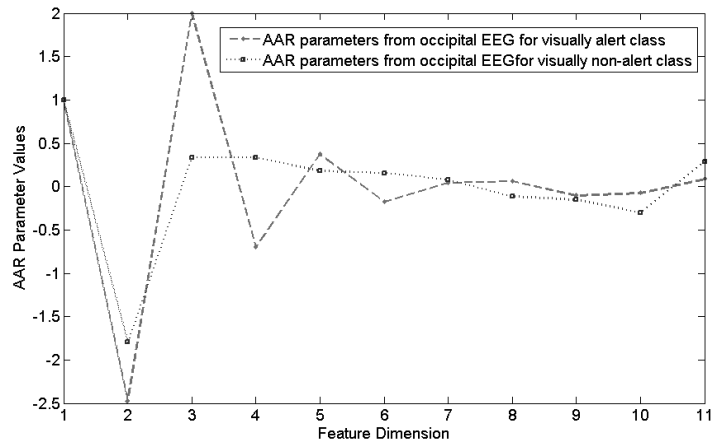


**Fig. 3.15** ICA scalp components from 19 EEG electrodes. Here, red color denotes the highest activation, whereas, blue color represents the lowest activation.

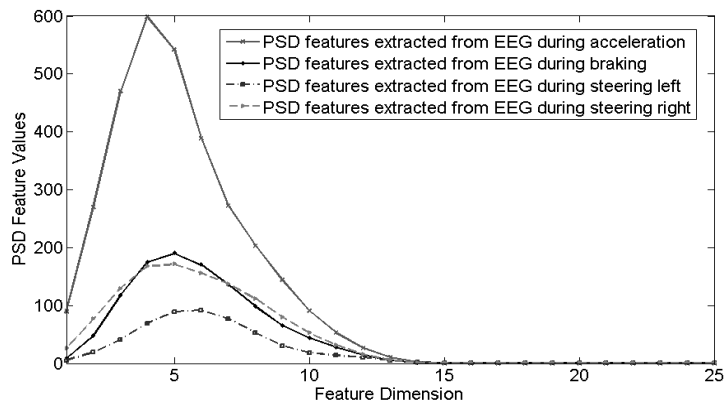
#### *D. EEG Feature Selection*

To select features for a given cognitive task, we plot the feature values against feature-count, and note the discriminating features for the sub-classes (say, BR, ACC, STR and NOP) of the cognitive task (say, MP/ME). We extract AAR parameters for VAFD, and PSDs and DWT coefficients for MPFD and MEFD. To obtain feature sets, the signal is first segmented using a moving window with window size = 500ms, which yields a data array of 10 samples/window at 200 Hz sampling rate. During feature extraction, this sliding window is moved from left-to-right along with each EEG data array and the features: AAR, PSD and DWT coefficients are computed to obtain the required features for VAFD, MPFD and MEFD respectively. Fig. 3.16

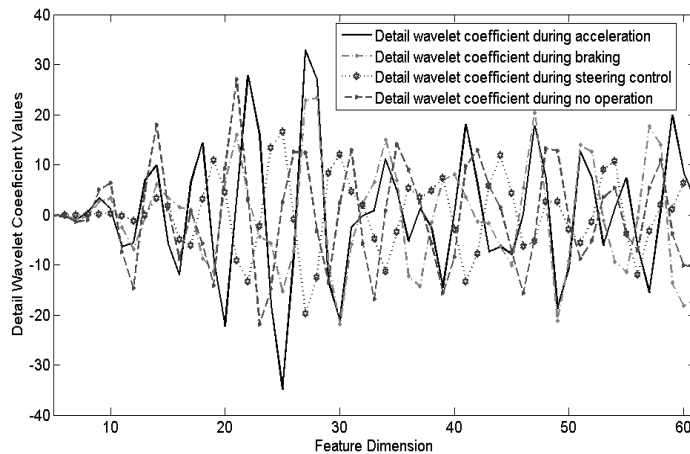
shows AAR feature discrimination during VAFD. Feature discrimination plots for PSD and DWT parameters are given in Fig. 3.17 and 3.18.



**Fig. 3.16** AAR parameter discrimination from occipital EEG of a subject during four different types of stimuli



**Fig. 3.17** PSD feature discriminations from motor imagery response of a subject during ACC, BR, STR control and NOP planning



**Fig. 3.18** DWT feature discriminations from motor imagery response of a subject during ACC, BR, STR control and NOP planning

During visual alertness, we extract 11 AAR features from each of 90 experimental trials for each subject, where each trial represents one visual stimulus. From Fig. 3.16, it is clear that most of the AAR features (i.e., 3<sup>rd</sup>, 4<sup>th</sup>, 5<sup>th</sup>, 6<sup>th</sup>, 8<sup>th</sup> and 10<sup>th</sup>) can successfully discriminate occipital response of a subject between visually alert and non-alert classes. During motor-planning and execution, we extract 15 and 63 dimensional PSD and DWT features respectively, of which all are not equally significant. Fig. 3.17 and 3.18 provide PSD and DWT feature plots during motor-planning. It has been noted from Fig. 3.16 and 3.17 that only a few PSD and DWT features: 8<sup>th</sup>, 9<sup>th</sup>, 11<sup>th</sup> and 12<sup>th</sup> can jointly discriminate 4 motor planning actions.

After feature extraction, we finally obtain 11 AAR, 15 PSD and 63 DWT features. For  $(15 + 63) = 78$  dimensional MPF and MEF feature sets, we require to execute the evolutionary feature selection to select fewer features (here 18) without losing their inherent power of inter-class separation. The superiority of the proposed DE-based feature selection strategy against the traditional principal component analysis (PCA) is validated using confusion matrices (Table 3.4), where, we compare the performance of the proposed DE-based feature selection algorithm with traditional PCA. This is realized by comparing the IT2FS-induced neural classifier performance with *a priori* feature selection by the proposed and PCA techniques. Table 3.4 provides a comparison of classifier performance using confusion matrices. It is apparent from the Table that the proposed feature selection results in better classifier performance in all the four classes with respect to PCA.

**Table 3.4** Confusion Matrices of Four Motor-Planning Classes Using PCA and DE-Induced Feature Selection Algorithm

		Predicted Class using PCA-based Feature Selection				Predicted Class using DE-induced Feature Selection			
		Acceleration	Braking	Steering Control	No action	Acceleration	Braking	Steering Control	No action
Actual Class	Acceleration	<b>0.83</b>	0.015	0.09	0.065	<b>0.95</b>	0.005	0.025	0.02
	Braking	0.0225	<b>0.8775</b>	0.08	0.02	0.0025	<b>0.9675</b>	0.025	0.005
	Steering Control	0.145	0.055	<b>0.795</b>	0.005	0.025	0.01	<b>0.96</b>	0.005
	No operation	0.15	0.05	0.08	<b>0.72</b>	0.04	0.01	0.06	<b>0.93</b>

The rest of the steps in Table 3.1, including MF construction and classifier training are self-explanatory. The classifier performance in the training phase is given in [47]. Only the parameter selection of KSVM with linear, polynomial and RBF Kernels are given in Tables.



It is observed from the Table 3.5 that the KSVM with RBF Kernel yields the best classification accuracy in the training phase with  $C=1$  and  $\sigma=0.75$  (marked in bold). The polynomial kernel (with  $d=2, 3$ ) based KSVM however yields worse classification accuracy than the RBF kernel and the linear kernel ( $d=1$ ) based KSVM (Table 3.6).

**Table 3.5** Classification Accuracy of KSVM-RBF Classifier for Varied  $C$  and  $\sigma$

C	$\sigma$			
	0.01	0.75	1.00	100
0.5	71.44	83.55	80.22	77.33
1	77.22	<b>95.22</b>	88.44	81.55
10	66.55	78.11	73.33	69.11

**Table 3.6** Classification Accuracy of KSVM-Linear and Polynomial Classifier for Varied  $C$  and  $d$

C	$d$		
	1	2	3
0.5	91.33	89.11	87.22
1	95.00	93.11	90.00
10	88.55	86.33	81.33

### 3.5.4 The Test Session

Table 3.7 provides a summary of the main steps undertaken in the test phase. Steps-I to III are similar with those in the training session with the following exception. Although for both the training and the test sessions we used the same driving simulator, the training was performed with presentation of individual stimulus one by one in a discrete sense. However, the test session is performed in a continuous mode. So, any stimulus might appear at any time-point. After the assessment of the classifiers by a team of experts as indicated in Table 3.7, we analyze the classifier performance as given in the next section.

**Table 3.7** Experimental Procedure for the Test Session

<b>Steps</b>	<b>Description</b>
Step-I: Online stimuli presentation	Place the subject along with a co-pilot in a real/emulated driving environment where any one of 9 stimuli may appear at any time-point.
Step-II: EEG acquisition and filtering	Acquire EEG from channels as mentioned in the training session, preprocess and filter them by Elliptic filter of order 4.
Step-III: Feature extraction	Extract AAR, PSD and DWT features and perform DE-based feature selection to obtain 11 AAR for VAF detection and 78 PSD+DWT features for MPF and MEF.
Step-IV: Classification	Feed extracted features to VA, MP and ME classifiers with pre-set weights obtained from the training session
Step-V: Recording	Record VA classifier, MP classifier and ME classifier response over time and save these in a file. Also record a video of the online driving session from the computer screen.
Step-VI: Assessment by experts	<ol style="list-style-type: none"> <li>1. Experts match the recorded co-pilot decision and the traffic instance at the same time-point to detect VAF classifier performance.</li> <li>2. Re-run the video and get the response of three experts at different time-points about MP decisions for alarms. Match the common response of the experts with that of MP alarms recorded earlier and generate classifier performance.</li> <li>3. Experts note the time-delay in EMG response from the time-pint co-pilot points out MP decisions. If the delay exceeds a time limit (600 ms), then MEF is correctly detected.</li> </ol>

### 3.6 PERFORMANCE ANALYSIS

This section provides experimental basis for performance analysis and comparison of the proposed classifiers with traditional/existing ones. It also undertakes experiments for lead-time estimation and objective performance of the proposed CFD system with respect to different stimuli, representative of traffic conditions.

#### 3.6.1 Performance Analysis of VAFD Classifier

Here, we compare the run-time and relative classification accuracy of LDA and KSVM with linear, polynomial and RBF kernels, when experimented over 10 subjects, each experiencing 4 BR, 2 ACC and 2 STR control instances (See Fig. 3.9) for 10 times, and thus yielding altogether 400 BR, 200 ACC and 200 STR control instances. It is observed that the RBF kernel-based KSVM outperforms (marked in bold) its competitors in classification accuracy, whereas LDA offers the least run-time (marked in bold), leaving behind linear, polynomial and RBF kernel-based algorithms in increasing order of their run-times (Table 3.8). The study also compares the classifier performances by taking occipital features only following [57]-

[59] and prefrontal/frontal features following [56]. Table 3.8 reveals that the performances of all classifiers are improved by approximately 2 - 2.5% when prefrontal plus frontal features are used instead of occipital features only.

**Table 3.8** Run-Time and Mean Percentage VAFD Classification Accuracies (standard deviation in percentage) by Different Classifiers

Classifiers	Runtime (in ms)	Brain Regions	Mean percentage classification accuracies in % and (std. deviation in %) for traffic instances		
			BR	ACC	STR control
LDA	8.22 ms	Occipital only	84.00 (0.00413)	87.00 (0.00815)	85.50 (0.00672)
		Pre-frontal + Frontal	86.50 (0.00695)	89.50 (0.00972)	88.00 (0.00879)
Type-1 Fuzzy	9.02 ms	Occipital only	81.25 (0.00134)	83.50 (0.00258)	83.00 (0.00231)
		Pre-frontal + Frontal	82.75 (0.00225)	84.50 (0.00438)	84.0 (0.00378)
ANFIS	11.6 ms	Occipital only	87.50 (0.00847)	88.00 (0.00879)	87.00 (0.00815)
		Pre-frontal + Frontal	89.25 (0.00938)	89.50 (0.00972)	88.50 (0.00891)
SOFNN	10.2 ms	Occipital only	84.75 (0.00454)	86.00 (0.00622)	85.50 (0.00672)
		Pre-frontal + Frontal	85.75 (0.00492)	86.50 (0.00695)	86.00 (0.00622)
KSVM- linear Kernel	12.04 ms	Occipital only	93.75 (0.04543)	93.00 (0.04472)	93.50 (0.04121)
		Pre-frontal + Frontal	95.50 (0.02643)	95.00 (0.02558)	95.50 (0.02643)
KSVM- polynomial Kernel	12.24 ms	Occipital only	91.25 (0.01783)	90.50 (0.00712)	91.00 (0.01429)
		Pre-frontal + Frontal	93.25 (0.02130)	93.00 (0.01907)	94.50 (0.02412)
KSVM-RBF Kernel	13.2 ms	Occipital only	93.33 (0.02289)	92.50 (0.01828)	93.00 (0.01907)
		Pre-frontal + Frontal	<b>95.75 (0.02794)</b>	<b>95.50 (0.02643)</b>	<b>92.00 (0.01864)</b>

### 3.6.2. Performance Analysis of the Type-2 MPFD Classifier

The performance analysis here is undertaken at three levels: i) classification accuracy, ii) run-time complexity and iii) joint occurrence of true/false and positive/negative cases. Table 3.9 includes the result of mean percentage classification accuracies of type-2 fuzzy classifiers against traditional ones, including self-organized fuzzy neural network (SOFNN) [53], artificial neural network fuzzy inference system (ANFIS) [54] and three existing IT2FS-induced models [15]-[17]. The experiment was performed on 10 subjects, each participating in 10 sessions, comprising 9 stimuli, covering  $10 \times 10 \times 9 = 900$  traffic instances. It is observed from Table 3.9 that the proposed IT2FS-NN (GT2FS-NN) classifiers outperform their nearest competitor by an average classification accuracy of  $\sim 3\%$  ( $\sim 5\%$ ) in absence of phone calls, whereas the accuracy changes to  $\sim 5\%$  ( $\sim 8\%$ ) when phone calls are received by the driver.

**Table 3.9** Mean Percentage Classification Accuracy of IT2FS-NN (GT2FS-NN) Against Standard Classifiers for Traffic Instances Plus Without (With) Phone Calls

Classifiers	Mean percentage classification accuracy in % for traffic instance without phone calls (with phone calls)			
	For motor-planning tasks			
	BR	ACC	STR control	NOP
Proposed IT2FS-NN	96.75 (94.25)	95.00 (92.00)	95.50 (91.50)	93.00 (90.0)
Proposed GT2FS-NN	98.75 (97.25)	97.50 (95.50)	98.00 (96.50)	95.00 (93.0)
ANFIS [54]	94.00 (88.75)	92.5 (87.50)	92.0 (85.0)	90.00 (86.00)
IT2FS-NN [15]	92.75 (91.75)	91.50 (90.00)	90.00 (88.50)	89.00 (88.00)
IT2FS-NN [16]	91.25 (89.50)	91.00 (90.00)	89.50 (88.00)	87.00 (86.00)
IT2FS-NN [17]	91.00 (88.75)	89.50 (88.00)	87.50 (85.50)	84.00 (82.00)
SOFNN [53]	85.25 (76.00)	81.00 (73.50)	80.50 (75.50)	79.00 (75.00)
Type-1 Fuzzy NN	89.00 (87.25)	88.00 (86.5)	88.5 (86.5)	86.0 (84.0)
LDA	90.75 (89.25)	90.0 (88.5)	89.5 (87.0)	88.0 (86.0)
LSVM	91.25 (89.75)	90.5 (88.0)	90.0 (88.5)	89.0 (87.0)

In the run-time complexity analysis, given in Table 3.10, we observe that the proposed IT2FS-NN algorithm takes the smallest run-time ( $\sim 38$  milliseconds), when compared with the other classifiers. In addition, the proposed GT2FS-NN, requires 96.02 milliseconds, which is comparable to the run-time of most of the IT2FS-NN [15], [16] classifiers.

**Table 3.10** Run-Time of IT2FS-NN and Other Competitive Classifiers

Motor-Planning Classifier	Run-time in IBM PC Dual-core Machine
IT2FS-NN (proposed)	<b>38.22 milliseconds</b>
IT2FS-NN (Das <i>et al.</i> ) [15]	96.34 milliseconds
IT2FS-NN (Lee <i>et al.</i> ) [16]	98.26 milliseconds
IT2FS-NN (Lin <i>et al.</i> ) [17]	92.42 milliseconds
SVM	38.25 milliseconds
ANFIS [54]	100.02 milliseconds
SOFNN [53]	112.04 milliseconds
GT2FS-NN (proposed)	96.02 milliseconds
Type-1 Fuzzy NN	50.4 milliseconds

Lastly, we consider four distinct performance metrics: True Positive (TP), True Negative (TN), False Positive (FP) and False Negative (FN) to compare the relative performance of all classifiers (Table 3.11), when performed over 6 healthy subjects, yielding 540 traffic instances, where GT2FS is found to outperform all existing and the proposed IT2FS-NN by around 2-3% in TP class.

**Table 3.11** Comparative Studies of Percentage TP, TN, FP and FN Measures (%) of the Proposed Classifiers With Existing IT2FS Classifiers

Classifier	Performance Metrics			
	TP	TN	FP	FN
GT2FS-NN (proposed)	<b>97.96</b>	1.85	0.19	0.00
IT2FS-NN (proposed)	<b>95.92</b>	1.67	1.48	0.93
IT2FS-NN (Das <i>et al.</i> )	95.19	1.48	2.03	1.30
IT2FS-NN [Lee <i>et al.</i> ]	94.81	1.48	1.68	2.03
IT2FS-NN [Lin <i>et al.</i> ]	94.63	1.30	1.85	2.22
Type-1 Fuzzy NN	87.77	3.52	5.74	2.96

Table 3.12 also offers a comparative study of TP, TN, FP and FN measures of the proposed IT2FS-NN (GT2FS-NN) classifier across 10 subjects without/with received phone calls. It is apparent from Table 3.12 that for six healthy subjects (H1-H6), the mean TP and TN measures are almost independent of received phone calls. However, for the fatigued subjects

F1-F2 and Learners L1-L2, the mean TP and TN measures drop by more than 6% while using IT2FS-NN. However, GT2FS-NN provides mean TP and TN measures which almost are independent of received phone calls for all subjects, whereas, FP and FN measures increases by 1-6% in presence of phone calls for fatigued subjects and driving learners, depending on their misclassification in intended motor-planning.

**Table 3.12** Comparative Studies of TP, TN, FP and FN Measures With/Without Phone Calls for IT2FS-NN (GT2FS-NN) Classifier across 10 Subjects

Subject	Stimulus							
	Traffic Instance + Without Phone Calls				Traffic Instance + With Phone Calls			
	TP	TN	FP	FN	TP	TN	FP	FN
H1	97.78 (98.89)	1.11 (1.11)	0.00 (0.00)	1.11 (0.00)	95.56 (96.67)	1.11 (1.11)	0.00 (1.11)	3.33 (1.11)
H2	95.56 (96.67)	2.22 (3.33)	1.11 (0.00)	1.11 (0.00)	93.34 (95.56)	2.22 (2.22)	1.11 (1.11)	3.33 (1.11)
H3	92.23 (94.45)	4.44 (4.44)	1.11 (0.00)	2.22 (1.11)	90.01 (94.45)	2.22 (3.33)	5.55 (1.11)	2.22 (1.11)
H4	94.45 (96.67)	3.33 (3.33)	1.11 (0.00)	1.11 (0.00)	92.23 (95.56)	2.22 (3.33)	3.33 (1.11)	2.22 (0.00)
H5	93.34 (95.56)	3.33 (3.33)	2.22 (1.11)	1.11 (0.00)	91.11 (94.45)	1.11 (3.33)	6.67 (2.22)	1.11 (0.00)
H6	97.78 (98.89)	1.11 (1.11)	0.00 (0.00)	1.11 (0.00)	92.23 (95.56)	1.11 (2.22)	4.44 (1.11)	2.22 (1.11)
<b>Avg. of (H1-H6)</b>	<b>95.19 (96.86)</b>	<b>2.59 (2.77)</b>	<b>0.925 (0.185)</b>	<b>1.295 (0.185)</b>	<b>92.41 (95.375)</b>	<b>1.68 (2.59)</b>	<b>3.51 (1.295)</b>	<b>2.40 (0.74)</b>
F1	87.78 (93.34)	7.78 (5.55)	1.11 (0.00)	3.33 (1.11)	80.00 (87.78)	1.11 (4.44)	7.78 (1.11)	11.11 (6.67)
F2	86.67 (91.11)	8.89 (7.78)	2.22 (1.11)	2.22 (0.00)	80.00 (85.56)	2.22 (5.55)	6.67 (2.22)	11.11 (6.67)
L1	81.12 (87.78)	12.22 (11.11)	2.22 (0.00)	4.44 (1.11)	74.45 (83.34)	5.55 (10.00)	8.89 (2.22)	11.11 (4.44)
L2	83.34 (90.00)	10.00 (10.00)	3.33 (0.00)	3.33 (0.00)	76.67 (84.45)	3.33 (8.89)	6.67 (2.22)	13.33 (4.44)
<b>Avg. of (F1-L2)</b>	<b>84.72 (90.56)</b>	<b>9.73 (8.60)</b>	<b>2.22 (0.28)</b>	<b>3.33 (0.56)</b>	<b>77.78 (85.28)</b>	<b>3.05 (7.22)</b>	<b>7.50 (1.94)</b>	<b>11.67 (5.56)</b>

### 3.6.3 Performance Analysis of MEFD Classifier

Performance of MEFD classifier is determined by classifying EEG acquired from the motor cortex region and EMG acquired from foot and hand muscles into two classes (motor action performed or not performed) for individual actions (BR, ACC and STR control. For both EEG and EMG classification, we use the same set of classifiers as used in VAFD. Table 3.13 and 3.14 provide mean percentage accuracies of KSVM-RBF and other standard classifiers including LDA, KSVM-linear and KSVM polynomial classifiers for EEG and EMG-based MEFD classification respectively. It is apparent from the Tables that for both EEG and EMG-based MEF classification, KSVM-RBF outperform others with a mean percentage classification accuracy of ~91%.

**Table 3.13** Mean Percentage Accuracies of KSVM-RBF and Other Standard Classifiers EEG-Based MEFD Classification

Motor Actions	Mean classifier accuracy in % for Classifiers			
	LDA	SVM-linear	SVM-polynomial	SVM-RBF
Braking	82.50	88.75	86.25	<b>90.25</b>
Acceleration	85.00	89.5	87.50	<b>92.50</b>
Steering contro	82.00	89.5	85.33	<b>90.50</b>
Mean % Acc.	83.167	89.25	86.36	<b>91.083</b>

**Table 3.14** Mean Percentage Accuracies of KSVM-RBF and Other Standard Classifiers for EMG-Based MEFD Classification

Motor Actions	Mean Classifier Accuracy in % for Classifiers			
	LDA	SVM-linear	SVM-polynomial	SVM-RBF
<b>Braking</b>	81.20	88.25	85.25	<b>90.5</b>
<b>Acceleration</b>	82.50	86.50	85.50	<b>91.5</b>
<b>Steering control</b>	80.50	86.66	86.5	<b>91.0</b>
<b>Mean % Acc.</b>	81.40	87.137	85.75	<b>91.0</b>

### 3.6.4 Lead-time Estimation

In this section, we attempt to evaluate the lead-time, determined by the difference between two time estimates, the safety-time to avoid collision and the time point when the alarm for MEF is generated. The safety-time depends on two parameters: the braking distance, i.e., the distance traversed after applying the brake and the speed of the vehicle. When the speed is 64 km/hr (i.e., 40miles/hr), the braking distance is 32 meter, which corresponds to a safety-time of 1.8 seconds.

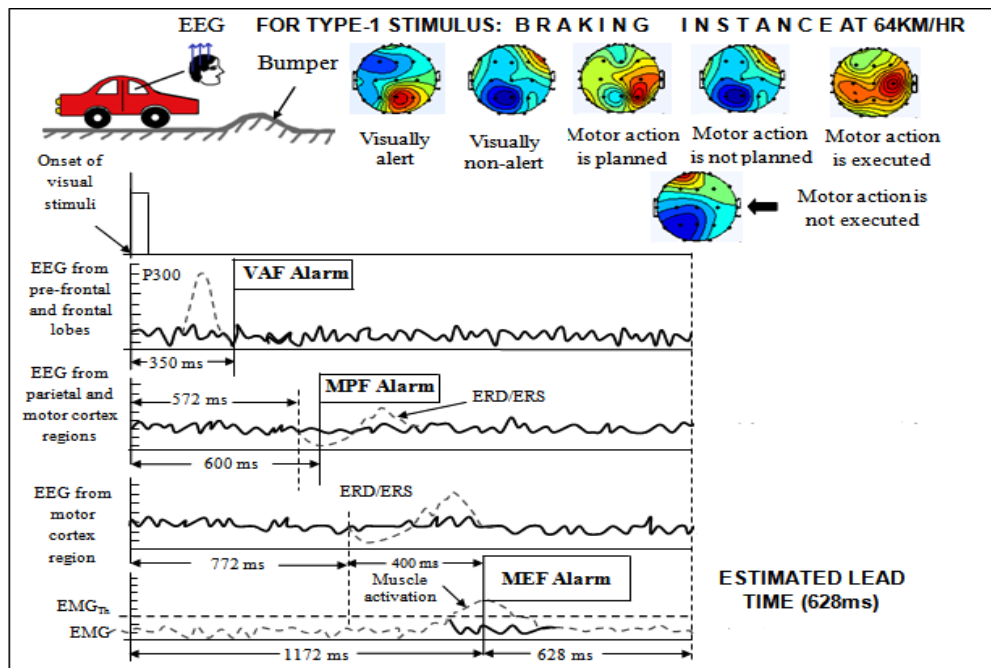
Table 3.15 provides the lead time estimates for seven different stimuli, averaged over 10 subjects, each performing 10 trials of 45 minutes driving session, maintained at 64 km/hour. In the calculation of lead-time, we used the measure of safety-time minus the approximate time for muscle activation, both counted from the onset of the stimuli. The approximate time of muscle activation is computed by time point of the first ERD/ERS generation corresponding to motor planning plus 600 milliseconds. The 600 milliseconds in the calculation are considered for muscle activation after the occurrence of the first ERD/ERS generation.

It is apparent from Table 3.15 that lead time for the seven stimuli usually is over 600 milliseconds for a speed around 64 km/hr. Thus during braking we have a safe distance of  $(64 \times 0.600)/3600 = 10.66$  meter. Figures 3.19, 3.20 and 3.21 present the audio alarm generation and lead time estimation during specific BR, ACC and STR control instances respectively.

Among nine stimuli, as listed in Table 3.2, estimated lead-time are computed for stimulus type-1, type 3 and type 7 and are shown in Figures 3.19, 3.20 and 3.21 respectively. From figures, it has been found that the estimated lead-time being 628 milliseconds, 679 milliseconds and 654 milliseconds respectively, which is acceptable for avoiding traffic accidents if the vehicle runs at a speed of 64km/hr.

**Table 3.15** Average Estimate of Lead-Time for Seven Different Stimuli for Driving Speed=64km/hr

Stimuli Type (Details given in Section V)	Average Time (in ms) counted from the onset of stimuli for the occurrence of			Average Estimate of lead-time (in ms)
	P300 for VA	ERD/ERS for MP	Approximate time for muscle activation/MEF alarm generation	
Type-1	325	572	1172	628
Type-2	322	524	1124	676
Type-3	320	521	1121	679
Type-4	322	524	1124	676
Type-5	342	546	1146	654
Type-6	282	501	1101	699
Type-7	340	570	1170	630



**Fig. 3.19** Audio alarm generation and lead-time for a braking instance



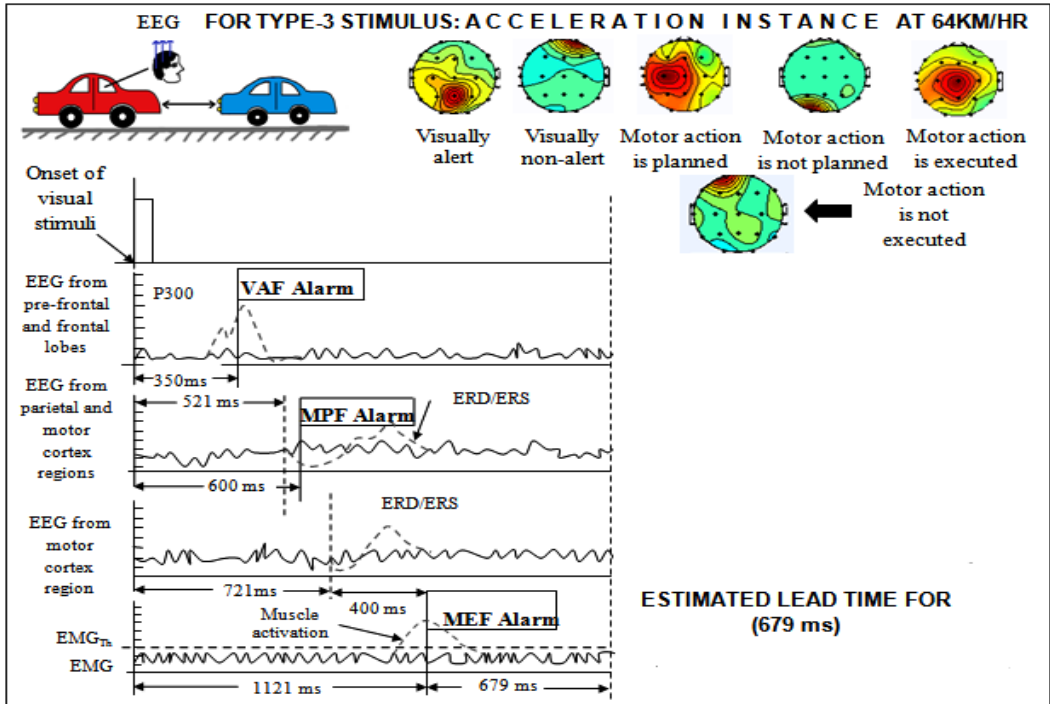


Fig. 3.20 Audio alarm generation and lead-time for an acceleration instance

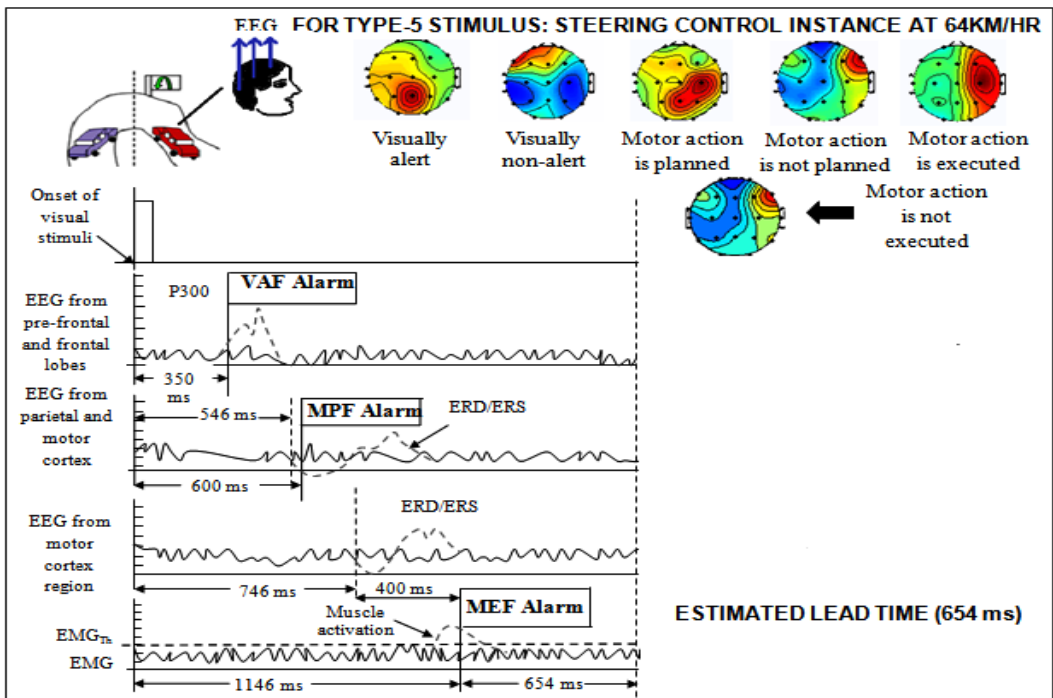


Fig. 3.21 Audio alarm generation and lead-time for a steering control instance

### 3.6.5 Objective Performance of the Proposed CFD System

To evaluate objective performance of the proposed CFD system with respect to 9 different stimuli, describing different traffic instances, we perform driving experiment with ten drivers,

each participating in four simulated driving sessions of 3 hours. The performance analysis given in Table 3.16 indicates significant reduction (by 88% approximately) in failures due to the presence of the proposed CFD system in the simulated environment.

**Table 3.16** Number of Failures Corrected in Presence of the Proposed CFD System

Stimuli	Required motor intension	No. of failures detected in absence of CFD	No. of failures corrected in presence of CFD
Type-1	Braking (BR)	96	85
Type-2	Braking (BR)	42	37
Type-3	Acceleration (ACC)	11	10
Type-4	Braking (BR)	45	40
Type-5	Steering (STR) control	22	19
Type-6	Braking (BR)	68	60
Type-7	Acceleration (ACC)	42	37
Type-8	Steering (STR) control	34	30
Type-9	NOP	06	05

Further, Table 3.17 provides the percentage of FP, FN, TP and TN rates of the proposed CFD system across four motor intensions: BR, ACC, STR control and NOP irrespective of stimulus type. The percentage of true positive cases is found to be around 88% for BR, ACC and STR control, when experimented with 10 drivers, each participating in four driving sessions of 3 hours.

**Table 3.17** Percentages of TP, Tn, FP, FN rates of the proposed CFD system

Required motor intension	Percentage (%) of			
	TP	TN	FP	FN
Braking (BR)	88.44	6.37	3.19	2.00
Acceleration (ACC)	88.68	7.54	1.89	1.89
Steering (STR) control	87.50	3.60	3.60	5.30
No operation (NOP)	83.33	0.00	0.00	16.67

### 3.7 CLASSIFIER VALIDATION USING STATISTICAL TEST

Although several statistical tests to compare relative performance of classifier algorithms are available in the literature [61], most of these require multiple datasets obtained from different sources. At present we undertook experiments with only one database: *Brain-Stimulated Cognitive Failure Detection Database* (BSCFDD), prepared at Jadavpur University. Thus we select McNemar's test [62] for statistical validation of classifiers tested on a single database.

Consider, two algorithms  $A$  and  $B$ , where  $A$  is the reference algorithm. Let,  $f_A$  and  $f_B$  be two classifiers realized with algorithms  $A$  and  $B$  respectively. We define two parameters  $n_{01}$  and  $n_{10}$ , where  $n_{01}$  denotes the number of examples misclassified by  $f_A$  but not by  $f_B$ . On the other hand,  $n_{10}$  denotes the number of examples misclassified by  $f_B$  but not by  $f_A$ . Let the null hypothesis be that both the algorithms have the same error rate [13]. We define a statistic

$$Z = \frac{(|n_{01} - n_{10}| - 1)^2}{n_{01} + n_{10}}. \quad (3.20)$$

In the present circumstance, for MPFD classifier, we consider, A=GT2FS algorithm and B= any one of the 9 algorithms listed in Table 3.2. We compute  $n_{01}$ ,  $n_{10}$  and Z for all the 9 algorithms in Table 3.18. Now, we consult a  $\chi^2$ -distribution table and obtain  $\chi_{1,0.95}^2 = 3.84$ , which represents the value of Chi-square distribution with degree of freedom=1 and probability=0.05. The null hypothesis is accepted, if Z-value evaluated  $< 3.84$ , else the null hypothesis is rejected.

It is apparent from Table 3.18 that McNemar's test reveals that GT2FS-based classifier is comparable with that of IT2FS. However, the rest of the classifiers in the Table are not comparable with the reference algorithm A: GT2FS based classifier.

We also repeat the above procedure for the VAFD and MEFD classification. Here, we use A=KSVM-RBF and B=any one of 6 classifier algorithms listed in Table 3.2. It is apparent from Table 3.19 that the null hypothesis is rejected as the Z-score of all of them exceeds  $\chi_{1,0.95}^2 = 3.84$ .

**Table 3.18** Statistical Validation of Classifiers Using McNemar's Test during MPFD Phase

Reference Algorithm: GT2FS-NN Classifier				
Classifier algorithm used for comparison using desired features d=18	Parameters used for McNemar's Test		Z	Comments on acceptance/rejection of hypothesis
	$n_{01}$	$n_{10}$		
SOFNN	31	77	18.75	Reject
IT2FS-NN (Lin <i>et al.</i> )	23	59	14.93	Reject
LDA	13	37	10.58	Reject
LSVM	13	34	8.510	Reject
IT2FS-NN (Lee <i>et al.</i> )	21	45	8.015	Reject
IT2FS-NN (Das <i>et al.</i> )	6	17	4.348	Reject
TYPE-1 FUZZY-NN	16	31	4.170	Reject
ANFIS	19	35	4.167	Reject
Proposed IT2FS-NN	6	16	3.682	Accept

**Table 3.19** Statistical Validation of Classifiers Using McNemar’s Test during VAFD and MEFD Phase

Reference Algorithm: KSVM-RBF Classifier					
Classifier algorithm used for comparison using desired features d=11 (VAD) and d=18 (MEFD)		Parameters used for McNemar’s Test		Z	Comments on acceptance/rejection of hypothesis
		$n_{01}$	$n_{10}$		
LDA	VAFD:	17	68	29.410	Reject
	MEFD:	31	97	33.008	Reject
Type-1 Fuzzy NN	VAFD:	21	47	9.191	Reject
	MEFD:	24	59	13.927	Reject
SOFNN	VAFD:	16	37	7.547	Reject
	MEFD:	22	49	9.521	Reject
KSVM-linear	VAFD:	8	23	6.322	Reject
	MEFD:	21	44	7.446	Reject
KSVM-polynomial	VAFD:	18	37	5.890	Reject
	MEFD:	23	49	8.680	Reject
ANFIS	VAFD:	15	32	5.446	Reject
	MEFD:	20	39	5.490	Reject

### 3.8 CONCLUSIONS

The chapter proposes a novel approach to CFD in driving at three distinct levels: VA, MP and ME. An IT2FS/GT2FS-induced neural net is used to decode motor imageries and a KSVM classifier has been used to decode VA and ME. Performance analysis of the proposed IT2FS-NN/GT2FS-NN classifier reveals that the said classifier outperforms standard ones by a significant margin of classification accuracy, even in presence of external disturbances, such as attending to phone calls. It is important to mention that GT2FS outperforms all existing and the proposed IT2FS-NN by around 2-3% in TP class. The proposed IT2FS-NN has very good run-time speed with good accuracy and thus useful for the present application. McNemar’s test undertaken reveals that KSVM and the proposed GT2FS-induced classifiers outperform their competitors with respect to classification accuracy.

A lead-time analysis is undertaken to examine the feasibility of the proposed CFD system for field applications. It is observed that for car speed around 64 km/hour lead-time is approximately 600 milliseconds, offering a safe braking distance of 32 meters. An objective performance analysis is also given to demonstrate the reduction in cognitive failures due to incorporation of the proposed CFD system in presence of nine different stimuli. It is observed that on an average there is a decrease in cognitive failures by 88% for BR, ACC and STR control, when experimented with 10 drivers, each participating in 4 simulated driving sessions of 3 hours.

The future work may consider replacing co-pilot by ultrasonic sensor-based CFD system. Among other future works, selection of right features and design of high speed but accurate classifiers also remain an open problem for research.

## APPENDIX

### A.1 Pseudo Code for Feature Selection Using DE

---

**Input:**  $D$  dimensional feature vectors  $\mathbf{F}^k = \{\vec{F}_1^k, \vec{F}_2^k, \dots, \vec{F}_N^k\}$ , where  $\vec{F}_i^k = \{f_{i,1}^k, f_{i,2}^k, \dots, f_{i,D}^k\}$  be the  $i$ -th feature vector having an assigned class level  $k \in [1, m]$  for  $m$  classes.

**Output:** Selected  $d$ -dimensions of the feature vectors corresponding to minimal  $J$ .

---

#### Begin

1. **Initialization:** Initialize  $NP$  number of trial solutions  $\vec{Z}_i$  for  $i = 1$  to  $NP$ . Initialize crossover ratio  $Cr = 0.7$ .
2. **Mutation:** For each  $\vec{Z}_i$ , pick up 3 companion target vectors:  $\vec{Z}_j, \vec{Z}_k$  and  $\vec{Z}_l$  and compute  $\vec{Z}'_i = \vec{Z}_j + F(\vec{Z}_k - \vec{Z}_l)$ , where,  $F$  is a scale factor in  $[0, 2]$ . Here  $j, k$  and  $l$  are distinct and mutually exclusive to each other.
3. **Recombination:** Now for each pair of  $\vec{Z}_i$  and  $\vec{Z}'_i$ , construct a new trial vector  $\vec{M}_i$ , whose  $j$ -th element  $m_{i,j}$  is obtained by:
 
$$m_{i,j} \leftarrow z'_{i,j}, \text{ if } r, \text{ a randomly selected number in } [0,1] < Cr.$$

$$m_{i,j} \leftarrow z_{i,j}, \text{ otherwise.}$$
4. **Selection:** For each pair of  $\vec{M}_i$  and  $\vec{Z}_i$ , we set  $\vec{Z}_i \leftarrow \vec{M}_i$ , if  $f(\vec{M}_i) < f(\vec{Z}_i)$ , where  $f(\cdot) = J$  (Eqn. (3.3)) is the fitness (objective) function for the minimization problem.
5. Repeat from step 2 until the stopping criterion is not attained.
6. Output the best fit member from the population pool. The components of the best fit parameter vector with one value are the required features.

**End.**

---

## REFERENCES

1. C. Y. Fang, S. W. Chen and C. S. Fuh, "Automatic change detection of driving environments in a vision-based driver assistance system," *IEEE Trans. Neural Networks*, vol. 14, no. 3, pp. 646-657, 2003.
2. D. Wen, G. Yan, N. N. Zheng, L. C. Shen and L. Li, "Toward cognitive vehicles," *IEEE Trans. Intelligent Transportation Systems*, vol. 26, no. 3, pp. 76-80, 2011.
3. K. Rezaee, S. R. Alavi, M. Madanian, M. R. Ghezalbash, H. Khavari and J. Haddadnia, "Real-time intelligent alarm system of driver fatigue based on video sequences," *In Proc. of First RSI/ISM IEEE Int. Conf. on Robotics and Mechatronics (ICRoM)*, pp. 378-383, 2013.
4. C. T. Lin, C. J. Chang, B. S. Lin, S. H. Hung, C. F. Chao and I. J. Wang, "A real-time wireless brain-computer interface system for drowsiness detection," *IEEE Trans. Biomedical Circuits and Systems*, vol. 4, no. 4, pp. 214-222, 2010.
5. M. J. Khan and K. S. Hong, "Passive BCI based on drowsiness detection: an fNIRS study," *Biomedical Optics Express*, vol. 6, no. 10, pp. 4063-4078, 2015.
6. M. J. Khan, M. J. Hong and K. S. Hong, "Decoding of four movement directions using hybrid NIRS-EEG brain-computer interface," *Frontiers in Human Neuroscience*, vol. 8, p.244, 2014.
7. A. Turnip and K. S. Hong, "Classifying mental activities from EEG-P300 signals using adaptive neural network," *Int. J. Innov. Comp. Inf. Control*, vol. 8, no. 9, pp. 6429-6443, 2012.
8. A. Turnip, K.S. Hong and M. Y Jeong, "Real-time feature extraction of P300 component using adaptive nonlinear principal component analysis," *Biomedical Engineering Online*, vol. 10, no. 1, p.1, 2011.
9. A. Saha and A. Konar, "A Cyber-Physical System Approach to Cognitive Failure Detection in Driving Using EEG and EMG Artifacts," *Cyber Physical Systems – A Computational Perspective*, CRC Press, Taylor & Francis Group, LLC, Florida, USA, 2016.
10. A. Saha, A. Konar, M. Dan and S. Ghosh, "Decoding of Motor Imagery Potentials in Driving Using DE-Induced Fuzzy-Neural Classifier," *In Proc. of IEEE (RETIS)*, Kolkata, India, pp. 416 – 421, July 9-11, 2015.
11. A. Saha, S. Basu Roy, A. Konar and R. Jonarthanan, "An EEG-based Cognitive Failure Detection in Driving Using Two-stage Motor Intension Classifier", *In Proc. of IEEE International Conference on Control, Instrumentation, Energy & Communication (CIEC)*, pp. 277-281, Kolkata, India, January 31-February 2, 2014.
12. A. Saha, A. Konar, R. Burman and A. K. Nagar, "EEG Analysis for Cognitive Failure Detection in Driving Using Neuro-Evolutionary Synergism," *In Proc. of IEEE International Joint Conference on Neural Networks (IJCNN)*, pp. 2108-2115, Beijing, China, July 7-11, 2014.
13. A. Halder, A. Konar, R. Mandal, A. Chakraborty, P. Bhowmik, N. R. Pal and A. K. Nagar, "General and interval type-2 fuzzy face-space approach to emotion recognition," *IEEE Trans. Systems, Man, and Cybernetics: Systems*, vol. 43, no. 3, pp. 587-605, 2013.

14. J. M. Mendel, R. I. John, and F. Liu, "Interval type-2 fuzzy logic systems made simple," *IEEE Trans. Fuzzy Syst.*, vol. 14, no. 6, pp. 808–821, Dec. 2006.
15. A. K. Das, K. Subramanian and S. Sundaram, "An Evolving Interval Type-2 Neurofuzzy Inference System and Its Metacognitive Sequential Learning Algorithm," *IEEE Trans. Fuzzy Systems*, vol. 23, no. 6, pp. 2080-2093, 2015.
16. C. H. Lee, T. W. Hu, C. T. Lee and Y. C. Lee, "A recurrent interval type-2 fuzzy neural network with asymmetric membership functions for nonlinear system identification," *In Proc. of IEEE Int. Conf. on Fuzzy Systems*, pp. 1496-1502, 2008.
17. C. M. Lin, Y. M. Chen and C. S. Hsueh, "A self-organizing interval type-2 fuzzy neural network for radar emitter identification," *Int. J. Fuzzy Syst*, vol. 16, no. 1 pp. 20-30, 2014.
18. K. J. Park and D. Y. Lee, "Genetic Design of Fuzzy Neural Networks Based on Respective Input Spaces Using Interval Type-2 Fuzzy Set," *Int. J. of Software Engineering and Its Applications*, vol. 7, no. 5, pp. 15-24, 2013.
19. Z. Deng, K. S. Choi, L. Cao and S. Wang, "T2fela: type-2 fuzzy extreme learning algorithm for fast training of interval type-2 TSK fuzzy logic system," *IEEE Trans. Neural Networks and Learning Systems*, vol. 25, no. 4, pp. 664-676, 2014.
20. M. Pratama, G. Zhang, M. J. Er and S. Anavatti, "An incremental type-2 meta-cognitive extreme learning machine," *IEEE Trans. on Cybernetics*, vol. 47, no. 2, pp.339-353, 2017.
21. M. Pratama, J. Lu, E. Lughofer, G. Zhang and S. Anavatti, "Scaffolding type-2 classifier for incremental learning under concept drifts," *Neurocomputing*, vol. 191, pp.304-329, 2016.
22. C. Yang, Z. Deng, K. S. Choi and S. Wang, "Takagi–Sugeno–Kang Transfer Learning Fuzzy Logic System for the Adaptive Recognition of Epileptic Electroencephalogram Signals," *IEEE Trans. on Fuzzy Systems*, vol. 24, no. 5, pp.1079-1094, 2016.
23. C. Yang, Z. Deng, K. S. Choi, Y. Jiang and S. Wang, "Transductive domain adaptive learning for epileptic electroencephalogram recognition," *Artificial Intelligence in Medicine*, vol. 62, no. 3, pp.165-177, 2014.
24. Y. Jiang, Z. Deng, F. L. Chung, G. Wang, P. Qian, K. S. Choi and S. Wang, "Recognition of Epileptic EEG Signals Using a Novel Multiview TSK Fuzzy System," *IEEE Transactions on Fuzzy Systems*, vol. 25, no. 1, pp. 3-20, 2017.
25. M. Pratama, J. Lu and G. Zhang, "Evolving Type-2 Fuzzy Classifier," *IEEE Trans. on Fuzzy Systems*, vol. 24, no. 3, pp. 574-589, 2016.
26. S Bhattacharya, A. Konar and D. N. Tibarewala, "Motor imagery and error-related potential induced position control of a robotic arm," *IEEE CAA Journal of Automatica Sinica*, 2017 (to appear).
27. A. Kahsnobish, A. Konar, D. N. Tibarewala and A. K. Nagar, "Bypassing the natural visual-motor pathway to execute complex movement related tasks using interval type-2 fuzzy sets," *IEEE Trans. on Neural System & Rehabilitation Engineering*, vol. 25, no. 1, January 2017.

28. G. Wang, Z. Deng. and K. S. Choi, "Detection of epilepsy with Electroencephalogram using rule-based classifiers," *Neurocomputing*, vol. 228, pp.283-290, 2017.
29. P. A. Herman, G. Prasad and T. M. McGinnity, " Designing an Interval Type-2 Fuzzy Logic System for Handling Uncertainty Effects in Brain–Computer Interface Classification of Motor Imagery Induced EEG Patterns," *IEEE Transactions on Fuzzy Systems*, vol. 25, no. 1, pp.29-42, 2017.
30. P. Herman, G. Prasad. and T. M. McGinnity, "Investigation of the type-2 fuzzy logic approach to classification in an EEG-based brain-computer interface" *In Proc. of 27th Annual International Conference of the Engineering in Medicine and Biology Society (IEEE-EMBS)*, pp. 5354-5357, 2005.
31. T. Nguyen, A. Khosravi, D. Creighton and S. Nahavandi, "EEG signal classification for BCI applications by wavelets and interval type-2 fuzzy logic systems," *Expert Systems with Applications*, vol. 42, no. 9, pp.4370-4380, 2015.
32. J. Andreu-Perez, F. Cao, H. Hagraas and G. Z. Yang, "A Self-Adaptive Online Brain Machine Interface of a Humanoid Robot through a General Type-2 Fuzzy Inference System," *IEEE Transactions on Fuzzy Systems*, no. 99, 2016.
33. D. Wu, "Approaches for reducing the computational cost of interval type-2 fuzzy logic systems: overview and comparisons," *IEEE Transactions on Fuzzy Systems*, vol. 21, no. 1, pp.80-99, 2013.
34. J. M. Mendel, "General type-2 fuzzy logic systems made simple: a tutorial," *IEEE Transactions on Fuzzy Systems*, vol. 22, no. 5, pp.1162-1182, 2014.
35. S. Chakraborty, A. Konar, A. L. Ralescu and N. R. Pal, "A fast algorithm to compute precise type-2 centroids for real-time control applications," *IEEE Trans. On Cybernetics*, vol. 45, no. 2, pp. 342-353, 2014.
36. D. Bhattacharya, A. Konar and P. Das, "Secondary factor induced stock index time-series prediction using Self-Adaptive Interval Type-2 Fuzzy Sets," *Neurocomputing*, vol. 171, pp. 551-568, 2016.
37. P. Rakshit, S. Saha, A. Konar and S. Saha, "A type-2 fuzzy classifier for gesture induced pathological disorder recognition," *Fuzzy Sets and Systems*, vol. 305, pp. 95-130, 2016.
38. M. Nie, W. Tan, "Towards an efficient type-reduction method for interval type-2 fuzzy logic systems", *Proc. IEEE Int. Conf. Fuzzy Syst.*, pp. 1425-1432, 2008.
39. J. M. Mendel and X. Liu, "Simplified interval type-2 fuzzy logic systems," *IEEE Transactions on Fuzzy Systems*, vol. 21, no. 6, pp.1056-1069, 2013.
40. C. Wagner and H. Hagraas, "Toward general type-2 fuzzy logic systems based on zSlices," *IEEE Transactions on Fuzzy Systems*, vol. 18, no. 4, pp.637-660, 2010.
41. M. S. Worden, J. J. Foxe, N. Wang and G. V. Simpson, "Anticipatory biasing of visuospatial attention indexed by retinotopically specific-band electroencephalography increases over occipital cortex," *Journal of Neuroscience*, vol. 20, no. RC63, pp. 1-6, 2000.



42. G. Pfurtscheller, A. Jr Stancák and C. Neuper, "Event-related synchronization (ERS) in the alpha band an electrophysiological correlate of cortical idling: a review," *International Journal of Psychophysiology*, vol. 24, no. (1-2), pp. 39-46, November, 1996.
43. J. Kamiński, A. Brzezicka, M. Gola and A. Wróbel, "Beta band oscillations engagement in human alertness process," *International Journal of Psychophysiology*, vol. 85, pp. 125–128, 2012.
44. P. M. Lanke, R. K. Shastri and S. D. Biradar, "EEG signal processing techniques for mental task classification," *International Journal of Advanced Computing and Electronics Technology*, vol. 2, no. 1, pp. 66-74, 2015.
45. R. Storn and K. G. Price, "Differential Evolution- a simple and efficient heuristic for global optimization over continuous spaces," *Journal of Global Optimization*, vol. 11, no. 4, pp. 341-359, 1997.
46. M. Arvaneh, C. Guan, K.K. Ang and C. Quek, "Optimizing the channel selection and classification accuracy in EEG-based BCI," *IEEE Transactions on Biomedical Engineering*, vol. 58, no. 6, pp. 1865-1873, 2011.
47. Additional resources available: [http://www.computationalintelligence.net/ieee\\_thms/index\\_cfddriving\\_additional\\_resources.pdf](http://www.computationalintelligence.net/ieee_thms/index_cfddriving_additional_resources.pdf)
48. S. S. Haykin, *Neural Network: A comprehensive foundation*, Upper Saddle River, New Jersey, Prentice Hall, 1999.
49. K. P Soman, R. Loganathan and V. Ajay, *Machine learning with SVM and other kernel methods*, PHI Learning Pvt. Ltd., 2009.
50. J. M. Mendel and R. I. John, "Type-2 fuzzy sets made simple," *IEEE Transactions on Fuzzy Systems*, vol. 10, no. 2, pp. 117–127, Apr. 2002.
51. H. Bustince, "Interval-valued fuzzy sets in soft computing," *International Journal of Computational Intelligence Systems*, vol. 3, no. 2, pp.215-222, 2010.
52. H. B. Sola, J. Fernandez, H. Hagra, F. Herrera, M. Pagola and E. Barrenechea, "Interval type-2 fuzzy sets are generalization of interval-valued fuzzy sets: toward a wider view on their relationship," *IEEE Transactions on Fuzzy Systems*, vol. 23, no. 5, pp.1876-1882, 2015.
53. G. Leng, G. Prasad and T. M. McGinnity, "An on-line algorithm for creating self-organizing fuzzy neural networks," *Neural Networks*, vol. 17, no. 10, pp. 1477-1493, 2004.
54. I. Güler and E. D. Übeyli, "Adaptive neuro-fuzzy inference system for classification of EEG signals using wavelet coefficients," *Journal of Neuroscience Methods*, vol. 148, no. 2, pp. 113-121, 2005.
55. P. Rakshit, A. Chakraborty, A. Konar and A. K. Nagar, "Secondary membership evaluation in Generalized Type-2 Fuzzy Sets by evolutionary optimization algorithm," in *IEEE Int. Conf. on Fuzzy Systems (FUZZ)*, pp.1-8, July 7-10, Hyderabad, India, 2013.

56. H. J. Moller, A. A. Rizzo and D. J. Mikulis, "Prefrontal cortex activation mediates cognitive reserve alertness and attention in the Virtual Classroom: preliminary fMRI findings and clinical implications," *In Proc. Of IEEE Virtual Rehabilitation*, pp. 146-150, 2007.
57. S. Ikegami, K. Takano, M. Wada, N. Saeki and K. Kansaku, "Effect of the green/blue flicker matrix for P300-based brain-computer interface: an EEG-fMRI study," *Frontiers in Neurology*, vol. 3, p. 113, 2012.
58. I. Kiss, R. M. Dashieff and P. Lordeon, "A parieto occipital generator for P300: Evidence from human intracranial recordings," *International Journal of Neuroscience*, vol. 49, no. 1-2, pp. 133-139, 1989.
59. C. Babiloni, F. Vecchio, M. Miriello, G. L. Romani and P. M. Rossini, "Visuo-spatial consciousness and parieto-occipital areas: a high-resolution EEG study," *Cerebral cortex*, vol. 16, no. 1, pp. 37-46, 2006.
60. Y. Hashimoto and J. Ushiba, "EEG-based classification of imaginary left and right foot movements using beta rebound," *Clinical Neurophysiology*, vol. 124, no. 11, pp. 2153-2160, 2013.
61. J. Demšar, "Statistical comparisons of classifiers over multiple data sets," *Journal of Machine Learning Research*, vol. 7, pp.1-30, 2006.
62. T. G. Dierrereich, "Approximate statistical tests for comparing supervised classification learning algorithms," *Neural Comput.*, vol. 10, no. 7, pp. 1895-1923, 1998.

# Chapter 4

## **Tactile Perception of Human Subjects Using Radial Basis Function-Induced Back-Propagation Neural Net Classifier**

*This chapter introduces a novel approach to examine the scope of touch-perception as a possible modality of treatment of patients suffering from certain mental disorder using a Radial Basis function induced Back-propagation Neural Network. Experiments are designed to understand the perceptual difference of schizophrenic patients from normal and healthy subjects with respect to four different touch classes, including soft touch, rubbing, massaging and embracing and their three typical subjective responses (pleasant, acceptable, unpleasant). Experiments undertaken indicate that the frontal part of the scalp map of healthy subjects carry more blood during touch perception than those obtained for the schizophrenic patients. Further, for normal subjects and schizophrenic patients, the average percentage accuracy in classification of all the three classes: pleasant/acceptable/unpleasant is comparable with their respective oral responses. In addition, for schizophrenic patients, the percentage accuracy for acceptable class is very poor of the order of below 10%, which for normal subjects is quite high (46%). Performance analysis reveals that the proposed classifier outperforms its competitors with respect to classification accuracy in all the above three classes.*

## 4.1 INTRODUCTION

Touch refers to physical contact of a person's skin with any non-living substance or living organisms. Perceiving touch usually depends largely on the subjective experience of people. For example, a baby of two months old can recognize his mother by the way she holds the baby. In this way, touch perception can be considered as one of the most important modality during his development stages [1]-[3]. The sense of touch is perceived by various tactile receptors, which in general, utilizes *A-beta* fibers to transmit tactile information with extremely rapid speed. In addition, relatively slower *A-delta* and even slower *C* fibers are also used for signal transmission by free nerve endings. Receptors gather tactile information during various touch nourishments including soft touch, rubbing or massaging from a relatively larger area of the skin, which causes ambiguity in locating the source of the stimulus. Tactile information (sensation) for each touch nourishments are fed to the spine from the receptors by the nerve endings and then ascend to the brain using the spino-thalamic pathway.

This chapter aims at classifying distinctive touch patterns commonly used in hospitals/health centers to treat physio- and psycho-therapeutic patients from their acquired electro-encephalographic (EEG) signals. Experiments have been performed with both normal subjects and physic patients to determine their level of pleasure in four different types of (non-sexual) touch-nourishments offered by nurses or inmates of the subjects from their cortical responses. Later the degree of nourishment perceived is matched with the oral response of the subject to test the validity of the experimental results obtained from cortical responses.

Although there exist traces of works on touch-perception, the objectives and motivation of the present chapter to the best of the authors' knowledge and belief is new. The current literature considers classifying touch perceived by a subject into two classes based on the electroencephalographic (EEG) response [4] of the subject. Multiclass classification and rating of touch sensation has also been examined by Nakamura [5] using factor analysis and artificial neural network (ANN). In a recent work [6], the degree of pleasantness perceived from touch sensation is found to have a positive correlation with the beta power increase in the parietal, temporal and frontal regions whereas mu-band power suppression in the somatosensory cortex of a subject during stimulation [7]-[8]. The research findings about the significant relation between touch sensation and somatosensory cortex are available in [3], [9-14].

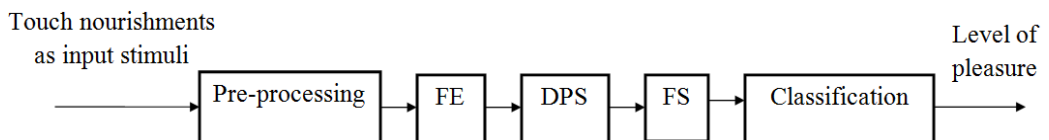
The originality of the present work lies in designing a two-stage classifier, where the first stage employs a Radial Basis Function (RBF) [15] layer to classify EEG features due to different touch modality, and the second stage uses Back-propagation Neural networks to classify detected touch modality into levels of pleasure (Unpleasant, Acceptable and

Pleasant). Besides classifier, other important coverage of the chapter includes defining *degree of pleasure perceived* (DPP) by a subject based on the EEG feature estimates, and comparing the measured DPP with subjective assignments by the patients. Moreover, DPP measure for pleasant touch, as perceived by the subjects, is used to select the best-performing nurse among the group. Lastly, we compare the classification accuracy of the proposed classifier with the listed classifiers after application of touch therapy, and observe that the proposed classifier correctly classifies the touch as Pleasant/Acceptable/Unpleasant.

The rest of the chapter is organized as follows. In section 4.2, we propose a scheme for touch classification. In section 4.3, we offer the relationship between degree of pleasure perceived and its fuzzy ranking as Pleasant / Acceptable / Unpleasant. Experimental details and performance of the proposed classifier are provided in section 4.4. Finally, conclusions are listed in section 4.5.

## 4.2 SYSTEM OVERVIEW AND TOUCH CLASSIFICATION

This section introduces the basic scheme for touch classification from the acquired EEG signals of the subject. We use channels F<sub>3</sub>, F<sub>4</sub>, F<sub>7</sub>, F<sub>8</sub>, P<sub>3</sub>, P<sub>4</sub>, P<sub>z</sub>, C<sub>3</sub> and C<sub>4</sub> channels from frontal, parietal, somato-sensory and motor cortex of the subject’s scalp in conventional 10-20 EEG electrode-placement system. The parietal electrodes offer a good resolution in textural pattern of the touched surface. Pre-frontal and frontal electrodes are responsible for “the emotional (feeling component [5]” of touch. The somato-sensory cortex electrodes offer the tactile sensation as a measure of mu-suppression and beta-band power while touching the subject’s skin [16]-[17]. Fig. 4.1 provides an overview of touch perception by EEG-analysis.



**Fig. 4.1** An overview of touch perception by EEG analysis

FE: Feature extraction, DPS: Data-point selection, FS: Feature selection

Four different touch stimuli, as has been perceived by a subject, are first pre-processed (filtered) to keep it free from artifacts due to eye-blinking and spurious pick-ups of line noise. The filtered data are sent for feature extraction (FE) to extract the basic primitives of the original signal. After FE, it has been found that all the trial instances and the samples for a particular touch stimulus are not equally essential. To identify the right data-point and samples useful for subsequent classification, we here employ Principal Component Analysis (PCA) [18] for performing first data point selection (DPS) followed by feature selection (FS) from the extracted EEG features using FE. Here, we use the standard EEG features, such as

Power Spectral Density (PSD) [19], Discrete Wavelet Transform (DWT) [20] and Approximate Entropy (ApEn) [21] for classifying four different types of touch nourishments. In DPS step, for each touch-nourishment class, PCA selects a single data-point (feature vector) from a set of  $t$  number of  $D$  dimensional data-points and referred as representative data-point of that class. Later in FS step, PCA selects  $d$  number of significant features from the  $D$  dimensional class-representative for each touch-nourishment. Finally, the selected feature vector for each class is applied for classification using radial basis function (RBF) induced back propagation neural network (BPNN).

#### 4.2.1 Feature Extraction

Features of a pattern are best defined by its basic primitives that represent the original pattern in time-, frequenct- and/or time-frequency domain. In the present chapter, frequency domain features including PSD offer information about the power spectrum of an EEG signal during various kinds of touch stimuli. Besides PSD, time-frequency analysis such as DWT and ApEn provides both temporal and spatial information of EEG signals during the experiment.

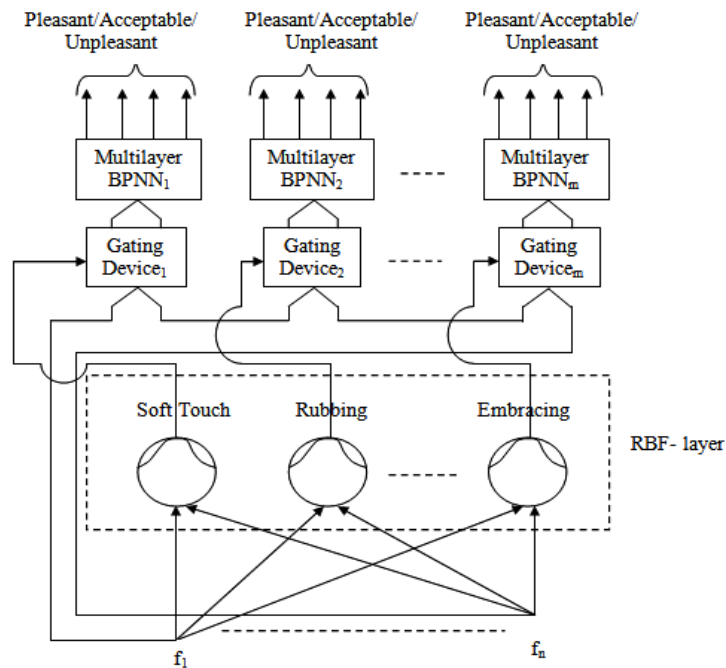
#### 4.2.2 Data-Point Reduction and Feature Selection Using PCA

The present chapter aims at using principal component analysis (PCA) to select EEG data-points as well as EEG features jointly. First, principal component analysis (PCA) derives a unique set of EEG features from a set of data-points for class  $k$ ,  $\mathbf{S}_k = \{\overrightarrow{X}_1^k, \overrightarrow{X}_2^k, \dots, \overrightarrow{X}_t^k\}$  by identifying the commonality among the feature vectors, (hereafter called data points) obtained over multiple experimental trials of the same subject with the same stimulus [22] and refers it 'ideal data point'  $\overrightarrow{X}_1^k$  of that stimulus-class. Second, PCA selects most significant  $d$  features out of  $D$ -dimensional ideal data point  $\overrightarrow{X}_1^k = \{x_{1,1}^k, x_{1,2}^k, \dots, x_{1,D}^k\}$  using the similar procedure. Finally, we obtain  $1 \times d$  dimensional class representative for each touch nourishment. Thus for a maximum of  $K$  number of stimuli and  $R$  subjects, the above procedure is repeated  $K \times R$  times.

#### 4.2.3 Classification

Touch classification, introduced in this chapter, requires designing a suitable classifier capable of classifying touch stimuli into multiple classes with a good level of accuracy. The quality of touch being detrimental to texture of the contact-surface, movement frequency of the touching organ and temperature-rise of the contact area, is an important issue to influence classifier-performance. In addition, physiological parameters of the subject in contact, the personality and relation of the person touching the subject also sometimes influence his/her the cortical responses. Designing a suitable classifier capable of classifying touch into three class labels: unpleasant, acceptable, and pleasant, is an important concern for the present application. In order to accomplish this, we develop a special type feed-forward neural network, comprising two different types of basic neural architecture. The feed-forward

topology employs Radial basis Function (RBF) neurons, which consists of three layers: input, hidden and output layers. Input layer has nodes equal to the number of features used to classify each touch-nourishment, hidden layer comprises  $m$  ( $=4$ ) number of RBF neurons for four different types of touch pattern, including soft touch, rubbing, massaging and embracing. Finally, output layer has three nodes representing three possible classes of pleasure for each touch-nourishment. Each neuron response is used to select a back propagation (BP) neural network [23] through a gating device. A variety of sequential RBF classifiers using minimal resource allocation network (MRAN) and growing and pruning algorithm for radial basis function (GAP-RBF) exist in the literature [24-27]. However, here we restrict the use of traditional RBF only to EEG classification of the pleasure obtained from four touch nourishments. RBF-BPNNs are used to recognize the degree of subjective pleasure, including unpleasant, acceptable, and pleasant, for each basic class/category of touch patterns mentioned above. The gating devices used in Fig. 4.2 are triggered by the RBF neurons to activate the devices in order to transfer the input feature vector indirectly to BPNNs.



**Fig. 4.2** A schematic representation of classification scheme

The RBF neurons used in Fig. 4.2 employ Gaussian type kernel function, where the parameters of the Kernel are obtained by the following procedure. The  $i$ -th component of the mean vector of the Kernel function is obtained by taking average of the  $i$ -th feature of all feature vectors for the given class. The variance of  $i$ -th component of the variance vector is also obtained by taking the variance of  $i$ -th feature of all feature vectors falling under class  $i$ . The BPNNs used employ Sigmoid-type non-linearity for all neurons including those in the last layer.

### 4.3 DEGREE OF PERCEIVED PLEASURE

This section provides a method of calculating the degree of pleasure perceived by a patient in presence of particular touch nourishment to him/her. The degree of pleasure perceived by  $k$ -th patient due to nourishment provided by  $j$ -th nurse is presented in (4.1).

$$Deviation^{j,k} = \sum_{\forall i} \sum_{\forall F_i^j} |F_i^j - F_i^{best}|^k \quad (4.1)$$

Here,  $i$  denotes a particular type of touch and  $F_i^{best}$  is the best feature for a given class of touch nourishment provided to a subject irrespective of any nurses.

The percentage measure of normalized degree of pleasure perceived by  $k$ -th patient due to nourishment provided by  $j$ -th nurse is given by (4.2).

$$DPP = \left( 1 - \frac{Deviation^{j,k}}{\sum_{\forall i} \sum_{\forall features} F_i^{best}} \right) \times 100\% \quad (4.2)$$

The above equation is used in the next section to rank the nurse when they are engaged to provide touch nourishments to the patient.

### 4.4 EXPERIMENTS AND RESULTS

This section includes four experiments: 1) acquisition of filtered EEG signal within bands of interest, 2) selection of EEG features, 3) validation of subject-defined class labels, and 4) ranking of nurses to select best-performing nurse to examine the efficacy of touch perception for possible psycho-therapeutic/remedial applications for patients with left-right asymmetry in alpha-power. The experiments are performed on both normal subjects and schizophrenic patients with alpha-power asymmetry. These patients are selected based on the level of their asymmetry, detected by functional Near Infrared Spectroscopy (f-NIRS) machines in a different experiment. The details of this experiment are dropped here to avoid discussing issues out of the main context.

The experimental framework includes a 21 channel EEG machine (manufactured by Nihon Kohden), 5 nurses and 12 subjects (7 normal healthy subjects and 5 schizophrenic patients) in the age group of 20-32. The EEG system has a sampling rate of 200 Hz with a signal resolution of 100 $\mu$ V. Four distinct touch nourishments, including soft touch, rubbing, massaging and embracing are applied as the stimuli of touch nourishment for the experimental subjects. An experiment comprises 4 trials, where each trial refers to one specific touch nourishment. For touch nourishment classification by a normal healthy person and a schizophrenic patient, both experience 4 different touch stimuli for 40 times, each stimulus being given for 10 times. Since, we have 7 normal healthy persons and



5schizophrenic patients; we altogether obtain as many as 280 and 200 trials respectively. During the experiment, each of four touch nourishments is given to a subject (both normal and patient) for 20 seconds. Being the sampling rate of EEG of 200 Hz, we obtain 4000 samples from 20 seconds. For ranking of nurses, each of 5 nurses provides one specific touch stimulus, such as rubbing to a normal healthy person and a schizophrenic patient both for 10 times, i.e., for all touch nourishments given by a single nurse, total number of input stimuli is 40 for both normal healthy person and a schizophrenic patient. The change in brain-map patterns for each touch class is individually observed and recorded for both the healthy subject and the patient. One such instance for one specific touch class (here, soft touch), as provided by two nurses to a healthy subject and patient is given in Fig. 4.3. Similar figures for other healthy and non-healthy subjects are not included here for lack of space. After a thorough investigation of the scalp maps for all the healthy and schizophrenic patients, it is noted that the frontal part of the scalp map of healthy subjects carry more blood during touch perception than those obtained for the schizophrenic patients. Further, for pleasant feeling the blood concentration at the frontal region is higher than any other parts of the scalp map. This observation also holds for schizophrenic patients.

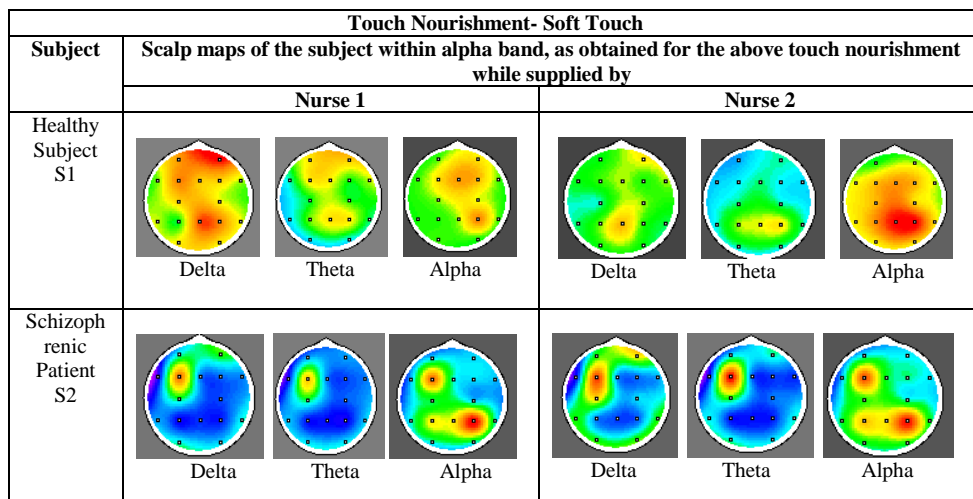
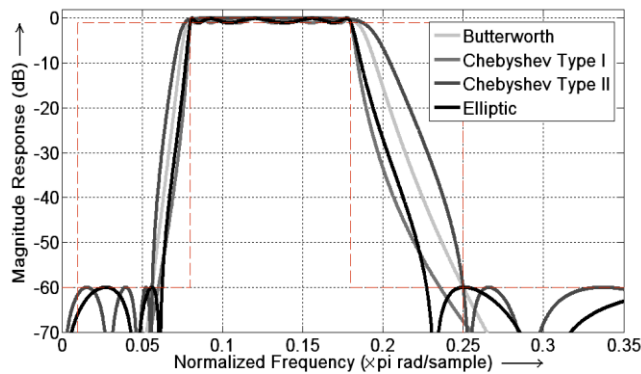


Fig.4.3 Change in brain-map patterns of one healthy subject and one patient for one specific touch class (here, soft touch)

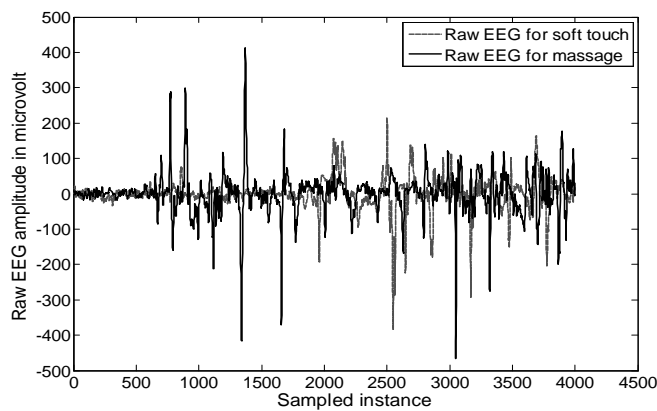
#### 4.4.1 Experiment 1: Acquisition of EEG Signals within Bands of Interest

After data acquisition, noise removal is the next primary concern for classification of different touch nourishments. In order to perform this, filtering of EEG signal within the suitable frequency bands is necessary. The aim of this experiment is two-fold. First is the selection of appropriate filter to clean the raw EEG signal; and second is the selection of pass-band frequency of the chosen filter. The first problem has been taken care by designing four common infinite impulse response (IIR) filter realizations including Butterworth, Chebyshev type-1 and type-2, and elliptic. We here consider four competitive filters: Butterworth of

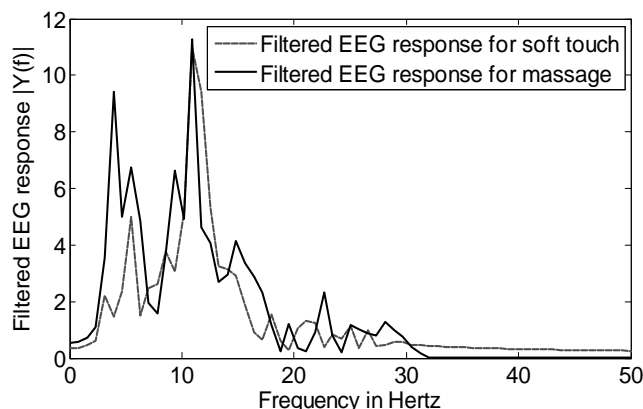
order 6, Chebyshev type-1 and type-2 of order 4, and elliptic filter of order 4 and compare their filter characteristics. Fig. 4.4 presents the frequency response of these four IIR filters, which shows that the sharpest roll-off and good attenuation in stop band ripples are prominent for the elliptic filter for varied filter order. Therefore we selected the elliptic filter of order 4 for our problem. The second problem has been solved by filtering the acquired EEG signals by the selected elliptic band pass filter having a suitable band pass frequencies. Since, the present problem itself has the novelty; we decide to observe the frequency response of the acquired EEG signal from 0.5 to 30 Hz comprising delta (0.5-3 Hz), theta (3-7 Hz), alpha (7-13 Hz) and beta (13-30 Hz). Fig. 4.5 presents raw EEG signals for two touch nourishments: console and massage, whereas Fig. 4.6 provides the filtered EEG response for the above two touch nourishments. It is observed from Fig. 4.6 that filtered EEG signal response possesses its higher magnitude in the frequency range of 3-18 Hz. Hence, we confirm that the prominent features of touch nourishment are present in the EEG signals within the range of 3-18 Hz.



**Fig. 4.4** Frequency response of a Butterworth, Chebyshev-I, Chebyshev-II and Elliptic band pass filter with a pass band and stop band attenuation



**Fig. 4.5** Raw EEG signals for two touch nourishments: soft touch and massage

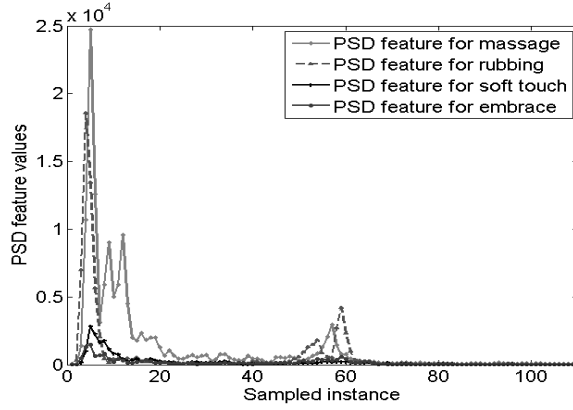


**Fig. 4.6** Filtered EEG response for two touch nourishments: console and massage

#### 4.4.2 Experiment 2: Selection of EEG Features

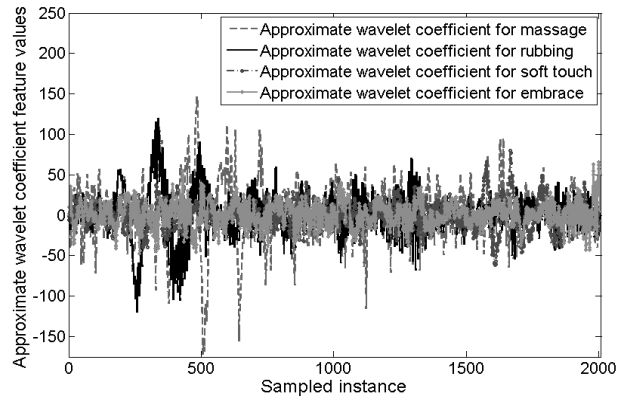
This experiment aims at selecting the most significant features for classifying touch nourishments in two steps. First, EEG features are extracted using well-known feature extraction techniques including power spectral density (PSD), discrete wavelet transform (DWT) and approximate entropy (ApEn). The reason behind using them is to observe the temporal as well as frequency-domain feature discrimination of the recorded EEG signal, since PSD extracts frequency domain features, whereas DWT deals with time-frequency correlated features. In addition, ApEn quantifies the uncertainty of a time series data of physiological signals, and hence can be successfully combined with both PSD and DWT. After feature extraction, we obtain 513 PSD features, 2004 wavelet coefficients (approximate coefficient) and 1 ApEn coefficient.

Fig. 4.7 shows a plot of PSD features and Fig. 4.8 (a)-(b) present two plots of DWT features respectively extracted from a patient for altogether for 50 trials for all kinds of touch nourishments. From Fig. 4.7, it is confirmed that few out of 513 PSD features, such as 5<sup>th</sup>, 12<sup>th</sup>, 55<sup>th</sup> and 58<sup>th</sup> provide prominent feature level discrimination. In case of Fig. 4.8(a) and Fig. 4.8(b), feature level discriminations seem to be difficult only by observing the extracted approximate and detail coefficient, since the dimension of the features are very high, i.e., 2004. To deal with the problem, we need to select only significant features from the high dimensional feature sets. Moreover, to obtain one single data-point as a representative of one specific touch nourishment class and to reduce computational complexity, we perform reduction in data-points (experimental trials). PCA will serve the both problems.

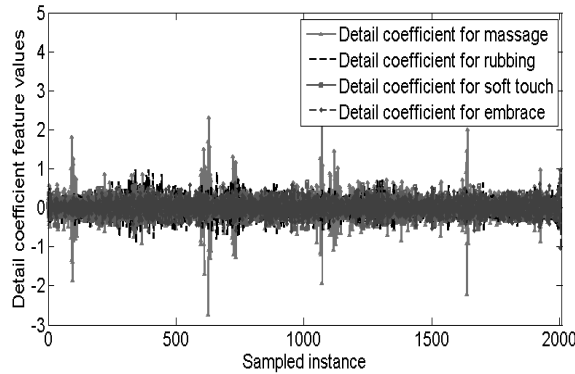


**Fig. 4.7** PSD features extracted for five distinct touch nourishments: console, massage, rubbing, soft touch and embracing

For data-point reduction and feature selection, we form two separate feature sets: 1) PSD plus ApEn comprising 514 features, and 2) Wavelet coefficient plus ApEn comprising 2005 features. PCA first selects one class-representative for each class from 10 experimental trials by reducing redundant data-points, and thus decreases computational overhead. Later, PCA selects 12 PSD plus ApEn, and 24 DWT plus ApEn features from the extracted feature sets.



**Fig. 4.8(a)** Approximate wavelet coefficient features extracted for four distinct touch nourishments: massage, rubbing, soft touch and embracing



**Fig.4.8(b)** Detail wavelet coefficient features extracted for four distinct touch nourishments: massage, rubbing, soft touch and embrace

Table 4.1 and Table 4.2 provide the true positives, true negatives, false positives, and false negatives along with average classification accuracies over 2400 trials of PSD plus ApEn features extracted touch nourishments without using and applying PCA respectively.

**Table 4.1** True Positive, True Negative, False Positive and False Negative rates along with average classification accuracy over 2400 trials without using PCA

Touch Nourishment Types	RBF-BPNN Classifier with PSD +ApEn Coefficients				Average Classification Accuracy (%)
	True Pos. (%)	True Neg. (%)	False Pos. (%)	False Neg. (%)	
Soft touch	53.29	29.16	11.5	6.04	71.54
Massage	65.12	23.91	7.45	3.29	
Rubbing	76.33	20.41	2.5	0.007	
Embracing	91.45	7.08	0.009	0.005	

**Table 4.2** True Positive, True Negative, False Positive and False Negative rates along with average classification accuracy over 2400 trials using PCA

Touch Nourishment Types	RBF-BPNN Classifier with PSD +ApEn Coefficients				Average Classifier Accuracy (%)
	True Pos. (%)	True Neg. (%)	False Pos. (%)	False Neg. (%)	
Soft touch	69.58	24.25	3.79	2.37	84.84
Massage	81.45	15.91	1.54	1.08	
Rubbing	92.29	7.04	0.004	0.002	
Embracing	96.04	3.41	0.003	0.001	

#### 4.4.3 Experiment 3: Validation of Subject-Defined Class Labels

This experiment attempts to validate the subject-defined class labels (unpleasant, acceptable and pleasant) with feature vectors obtained for that class label from multiple experimental instances. This is undertaken by computing the similarity in the patterns of the same class, measured by the Euclidean norm of each feature vector with respect to the class mean, obtained by component-wise averaging of the feature vectors in each class. If the Euclidean norm of the furthest feature vector with respect to the mean is very small (of the order of 0.001 or less), we accept that the class labels have parity with the observed feature distributions.

Table 4.3 offers percentage accuracies of touch nourishments according to the DPP (pleasant/acceptable/unpleasant) from both subjective oral and EEG responses. For lack of space, the following abbreviations have been used in Table 4.3: Soft Touch-ST, Rubbing-R, Massaging-M and Embracing-E. After a careful analysis from Table 4.3, it is observed that for normal subjects and patients, the average percentage accuracy in classification of all the three classes: pleasant/acceptable/unpleasant is comparable with their respective oral responses. In addition, for schizophrenic patients, the percentage accuracy for acceptable class is very poor of the order of below 10%, which for normal subjects is quite high (46%).

**Table 4.3** Touch nourishment classifications by averaging over 5 nurses

Subject	Type of Nourishments	Average Percentage (%) Accuracy of Nourishment Subclass					
		Pleasant		Acceptable		Unpleasant	
		From oral response	From EEG	From oral response	From EEG	From oral response	From EEG
One healthy (normal)	ST/M/R/E	48%	50%	46%	44%	6%	6%
One schizophrenic patient	ST/M/R/E	64%	65%	10%	9%	26%	25%

#### 4.4.4 Experiment 4: Ranking of Nurses Based on EEG Features Performance

This experiment attempts to select the best-performing nurse for the psychotherapeutic (schizophrenic) patients when the patients perceive pleasant touch from any subject. The rank of a nurse is computed from the DPP measure, averaged over all subjects by the pleasant touch.

During this experiment, each nurse is advised to provide all four kinds of pleasant touch nourishments to all schizophrenic patients and  $F_i^{best}$  for a given class of touch nourishment has been calculated irrespective of any nurses. Based on the deviation of the features extracted from the  $k$ -th patient for the nourishments given by  $j$ -th nurse, degree of pleasure perceived by the patient  $k$ , ( $DPP^k$ ) is obtained. Table 4.4 presents deviation,  $DPP^k$  measure and ranking of five nurses for a given subject  $S_k$ . To compute rank, we sorted two entries of the Table 4.4: nurse number, and  $DPP^k$  measure, and sort the list of entries in descending order of the  $DPP^k$  measure. The last column in Table 4.4 provides the computed rank of individual nurse. The best-performing nurse with rank 1 is given in bold.

**Table 4.4** Ranking of nurses based on degree of pleasure perceived from pleasant touch nourishment

Nurse	$F_i^{best}$	$Deviation^k$	$DPP^k$ (%)	Rank
1	7.3256	0.5610	92.34	3
2		0.3285	95.51	2
3		0.9604	86.88	5
4		0.2168	<b>97.04</b>	<b>1</b>
5		0.7157	90.23	4

#### 4.4.5 Experiment 5: Classifier Performance and Validation

The performance of the proposed classifier is compared with a few well-known standard classifiers including linear support vector machines (LSVM) [28], k-nearest neighbor [29] and naïve bayes [30]. For offline training, after PCA, a ten-fold cross-validation technique has been implemented using 480 trials over healthy and schizophrenic patients, where nine-folds are used for training, and the remaining fold is used for validation purpose. The result of the

online testing is tabulated in Table 4.5, where RBF-BPNN outperforms standard classifiers in presence of both feature sets. Last column of Table 4.5 provides the statistical significance of the classifier performance using t-test.

McNemar's test [31] has been applied to validate the classifier performance, where, we define a null hypothesis suggesting that the two algorithms A and B should have same error rate, i.e.,  $n_{01} = n_{10}$ , where  $n_{01}$  denotes the number of examples misclassified by A but not by B and  $n_{10}$  denotes the number of examples misclassified by B but not by A. Let  $f_A$  and  $f_B$  are classifiers' output obtained by algorithms A and B respectively when both the algorithms run on a common training dataset. We now define a statistic as  $\chi^2$  with 1 degree of freedom, called Z scores, which is given by (4.3).

$$Z = \frac{(n_{01} - n_{10} - 1)^2}{n_{01} + n_{10}} \quad (4.3)$$

At the end of the test, the Z scores will indicate whether the null hypothesis is accepted and the alternative hypothesis is rejected or vice-versa.

**Table 4.5** Mean classifier accuracy and statistical significance of testing data using PCA algorithm along with feature sets

Features	Pleasure level	Percentage Classifier Accuracy (in %) for				Statistical Significance
		PCA-LSVM	PCA-k-NN	PCA-Naïve Bayes	PCA-RBF-BPNN	
PSD+ApEn	Pleasant	77.4	76.2	85.48	<b>90.45</b>	t=51.4890 standard error of difference=0.002
	Acceptable	78.64	81.08	86.56	<b>92.29</b>	
	Unpleasant	82.52	81.12	87.52	<b>94.04</b>	
DWT+ApEn	Pleasant	77.44	82.08	86.20	<b>90.92</b>	t = 9.9720 standard error of difference=0.007
	Acceptable	82.08	83.76	87.56	<b>94.08</b>	
	Unpleasant	83.04	84.56	89.92	<b>96.98</b>	

We evaluate Z which represents the comparator statistic of misclassification between the DE-hybridized recurrent network-based classification algorithm (Algorithm: A) and any one of the competitor algorithms (Algorithm: B) for the Indian dataset for desired number of features equal to 36. From Table 4.6, it is confirmed from that the proposed classifier outperforms all its competitors.

## 4.5 CONCLUSIONS

This study offers two interesting outcome for future researchers in brain/cognitive sciences interested to pursue research on touch perception on patients suffering from schizophrenia.

**Table 4.6** Statistical comparison of classifiers using McNemar’s test

REFERENCE ALGORITHM: PCA-RBF-BPNN				
CLASSIFIER ALGORITHM USED FOR COMPARISON USING DESIRED FEATURES D=50	PARAMETERS USED FOR McNEMAR TEST		Z	p
	$n_{01}$	$n_{10}$		
PCA-LSVM	26	49	7.68	p< 0.00001
PCA-k-NN	31	52	5.831	p< 0.00001
PCA-NAÏVE BAYES	21	35	4.0178	p< 0.00001

A thorough investigation undertaken reveals two most fundamental aspects of the present research. The first aspect reveals that the frontal part of the scalp map of healthy subjects carry more blood during touch perception than those obtained for the schizophrenic patients. Further, for pleasant feeling the blood concentration at the frontal region is higher than any other parts of the scalp map. This observation also holds for both schizophrenic patients and normal healthy subjects. The second inference we derive from Table 4.2 includes that for normal subjects and schizophrenic patients, the average percentage accuracy in classification of all the three classes: pleasant/acceptable/unpleasant is comparable with their respective oral responses. In addition, for schizophrenic patients, the percentage accuracy for acceptable class is very poor of the order of below 10%, which for normal subjects is quite high (46%). McNemar’ test confirms that the proposed classifier outperforms all its competitors including PCA-LSVM, PCA-KNN and PCA-Naïve bayes.

## REFERENCES

1. G. K. Essick, F. McGlone, C. Dancer, D. Fabricant, Y. Ragin, N. Phillips, T. Jones and S. Guest, “Quantitative assessment of pleasant touch,” *Neuroscience & Biobehavioral Reviews*, vol. 34, no. 2, pp. 192-203, 2010.
2. A. Gallace and C. Spence, “The science of interpersonal touch: an overview,” *Neuroscience & Biobehavioral Reviews*, vol. 34, no. 2, pp. 246-259, 2010.
3. F. McGlone, J. Wessberg and H. Olausson, “Discriminative and affective touch: sensing and feeling,” *Neuron*, vol. 82, pp. 737–755, 2014.
4. M. Peltoranta and Gert Pfurtscheller, “Neural network based classification of non-averaged event-related EEG responses,” *Medical and Biological Engineering and cComputing*, vol. 32, no. 2, pp. 189-196, 1994.
5. T. Nakamura, Y. Tomita, S. I. Ito and Y. Mitsukura, “A method of obtaining sense of touch by using EEG,” *In RO-MAN*, pp. 276-281, 2010.



6. H. Singh, M. Bauer, W. Chowanski, Y. Sui, D. Atkinson, S. Baurley, M. Fry, J. Evans and N. Bianchi-Berthouze, "The brain's response to pleasant touch: an EEG investigation of tactile caressing," *Frontiers in Human Neuroscience*, vol. 8, 2014.
7. M. Bauer, R. Oostenveld, M. Peeters and P. Fries, "Tactile spatial attention enhances gamma-band activity in somatosensory cortex and reduces low-frequency activity in parieto-occipital areas," *The Journal of Neuroscience*, vol. 26, no. 2, pp. 490-501, 2006.
8. M. Feurra, W. Paulus, V. Walsh and R. Kanai, "Frequency specific modulation of human somatosensory cortex," *Frontiers in Psychology*, vol. 2, 2011.
9. C. E. Chapman, "Active versus passive touch: factors influencing the transmission of somatosensory signals to primary somatosensory cortex," *Canadian Journal of Physiology and Pharmacology*, vol. 72, no. 5, pp. 558-570, 1994.
10. J. E. Huggins, C. Guger, B. Allison, C. W. Anderson, A. Batista, A. M. Brouwer and C. Brunner, "Workshops of the fifth international brain-computer interface meeting: defining the future," *Brain-Computer Interfaces*, vol. 1, no. 1 pp. 27-49, 2014.
11. M. Ploner, J. Gross, L. Timmermann and A. Schnitzler, "Cortical representation of first and second pain sensation in humans," in *Proc. of the National Academy of Sciences*, vol. 99, no. 19, pp. 12444-12448, 2002.
12. E. G. Reed-Geaghan and S. M. Maricich, "Peripheral somatosensation: a touch of genetics," *Current Opinion in Genetics & Development*, vol. 21, no. 3, pp. 240-248, 2011.
13. F. van Ede, F. de Lange, O. Jensen and E. Maris, "Orienting attention to an upcoming tactile event involves a spatially and temporally specific modulation of sensorimotor alpha-and beta-band oscillations," *The Journal of Neuroscience*, vol. 31, no. 6, pp. 2016-2024, 2011.
14. E. Wacker, B. Spitzer, R. Lützkendorf, J. Bernarding and F. Blankenburg, "Tactile motion and pattern processing assessed with high-field fMRI," *PloS One*, vol. 6, no. 9, pp. e24860, 2011.
15. S. Chen, C. FN. Cowan and P. M. Grant, "Orthogonal least squares learning algorithm for radial basis function networks," *IEEE Transactions on Neural Network*, vol. 2, no. 2 pp. 302-309, 1991.
16. N. E. Crone, D. L. Miglioretti, B. Gordon and R. P. Lesser, "Functional mapping of human sensorimotor cortex with electrocorticographic spectral analysis, II. Event-related synchronization in the gamma band," *Brain*, vol. 121, no. 12, pp. 2301-2315, 1998.
17. D. Cheyne, W. Gaetz, L. Garnero, J. P. Lachaux, A. Ducorps, D. Schwartz and F. J. Varela, "Neuromagnetic imaging of cortical oscillations accompanying tactile stimulation," *Cognitive Brain Research*, vol. 17, no. 3, pp. 599-611, 2003.

18. H. Zhao, P. C. Yuen and J. T. Kwok, "A novel incremental principal component analysis and its application for face recognition," *IEEE Transactions on Systems, Man, and Cybernetics, Part B: Cybernetics*, vol. 36, no. 4, pp. 873-886, 2006.
19. R. Martin, "Noise power spectral density estimation based on optimal smoothing and minimum statistics," *IEEE Transactions on Speech and Audio Processing*, vol. 9, no. 5, pp. 504-512, July, 2001.
20. L. M. Ai, W. Rui, H. D. Mei and Y. J. Fu, "Feature extraction and classification of mental EEG for motor imagery," in *Proc. IEEE Fifth International Conference on Natural Computation*, vol. 2, pp. 139-143, Tianjian, China, 2009.
21. S. M. Pincus, "Approximate entropy as a measure of system complexity," in *Proc. of the National Academy of Sciences*, vol. 88, no. 6, pp. 2297-2301, 1991.
22. A. Saha, A. Konar, A. Ralescu and A. K. Nagar, "EEG analysis for classification of Olfactory signals Using a Recurent Neural Classifier," *IEEE Trans. on Human-Machine Systems*, vol. 44, no. 6, pp. 717-730, December, 2014.
23. A. T. C. Goh, "Back-propagation neural networks for modeling complex systems," *Artificial Intelligence in Engineering*, vol. 9, no. 3 pp. 143-151, 1995.
24. K. Salahshoor, Karim and A. S. Kamalabady, "On-line multivariable identification by adaptive RBF neural networks based on UKF learning algorithm," in *Proc. IEEE Control and Decision Conference (CCDC)*, pp. 4754-4759, 2008.
25. G. B. Huang, P. Saratchandran and N. Sundararajan, "An efficient sequential learning algorithm for growing and pruning RBF (GAP-RBF) networks," *IEEE Transactions on Systems, Man, and Cybernetics, Part B: Cybernetics*, vol. 34, no. 6, pp. 284-2292, 2004.
26. R. Zhang, G. B. Huang, N. Sundararajan and P. Saratchandran, "Improved GAP-RBF network for classification problems," *Neurocomputing*, vol. 70, no. 16, pp. 3011-3018, 2007.
27. M. B. Li, G. B. Huang, P. Saratchandran and Narasimhan Sundararajan, "Performance evaluation of gap-rbf network in channel equalization," *Neural Processing Letters*, vol. 22, no. 2, pp. 223-233, 2005.
28. C. Distanto, N. Ancona and P. Siciliano, "Support vector machines for olfactory signals recognition," *Sensors and Actuators B: Chemical*, vol. 88, no. 1, pp. 30-39, 2003.
29. Y. Song, J. Huang, D. Zhou, H. Zha and C. L. Giles, IKNN: Informative k-nearest neighbor pattern classification, *Springer-Verlag Berlin Heidelberg*, pp. 248-264, 2007.

30. D. Wei and L. X. Yang, "Weighted naive bayesian classifier model based on information gain," in *Proc. International Conference on Intelligent System Design and Engineering Application (ISDEA)*, vol.2, pp. 819-822, Changsha, China, 13-14 October, 2010.
31. T. G. Dietterich, "Approximate statistical tests for comparing supervised classification learning algorithms," *Neural Computation*, vol. 10, no. 7, pp. 1895-1923, 1998.

# Chapter 5

## Conclusions and Future Directions

*This is the concluding chapter of the thesis. It provides a self-review of the thesis, highlighting the problems undertaken therein and to what level and to what degree of accuracy the problems have been solved. It also provides an overview of the problems still pending as part of the research works undertaken in the thesis along with a discussion covering the open problems, in general, which may be taken up as future research.*

## 5.1 SELF-REVIEW OF THE THESIS

The thesis addresses three interesting problems concerning perception and motor coordination. The first problem deals with olfactory perceptual-ability measurement of subjects stimulated with aromatic substances. The pertinent features of the problem include large class-size, noisy training instances and real-time computational facility. Traditional supervised learning classifiers usually are not appropriate to handle large class-size. This inspired us to develop a recurrent neural network model, capable of addressing large class-size.

In traditional recurrent neural classifier, the neural dynamics is known, and we need a Lyapunov energy function to determine the condition of stability of the dynamics. Next, we set the condition of stability in the dynamics. In the present context, the dynamics is unknown. We simply had a Rastrigin-like energy function, containing several optima. We associated one smell class to one optimum. In other words, the EEG features of each smell class are assigned to individual optima of the energy surface. The problem here lies with determining the dynamics which is stable with respect to the Rastrigin-like energy function. In the application phase, we initialize the dynamics at a point on the energy surface, the location of which is obtained from the EEG-features extracted for a given cognitive task. The recurrent dynamics is now updated over time repeatedly until it converges to a local optimum, describing a smell class. The optimum where the dynamics converges is the unknown aroma.

The merit of the proposed technique lies in its simplicity. It outperforms traditional algorithms by a large margin with respect classification accuracy as the metric. The method has successfully been applied in tea-taster selection problem, where the basis of selection includes the intra-class and inter-class separation-ability of the subject from their acquired EEG signals during the period of stimulus presentation.

Chapter 3 deals with an interesting problem on cognitive failure detection in driving. Here, the main research goal is to detect three distinct types of cognitive failures, including visual attention failure (VAF), motor-planning failure (MPF) and motor execution failure (MEF) in real time and to generate necessary alarm at the verge of detection of an appropriate fault. For the VAF detection, we simply look for the presence of the P300 signal after 300 ms from the onset of any oddball visual stimulus, such as presence of a bumper or pedestrian on the street. For MEF detection, we look for the presence of the electromyogram (EMG) signal after 650 ms from the onset of the visual stimulus (or 250 ms from the execution of motor planning. The most challenging part of the present research, however, is MPF detection. This is important as there is no reference signal to detect MPF. One approach to overcome the problem is to develop a reference signal using one co-pilot, who is expected to generate the ground-truth of the possible

cognitive failures for on-line comparison with the actual cognitive actions undertaken by the driver. Thus the co-pilot acts as a resource person to the driver, which can be used as the reference for the driver.

The research contribution of the Chapter lies in the design of an interval type-2 fuzzy set (IT2FS) and also a General type-2 fuzzy set (GT2FS) induced design of a classifier, capable of classifying brain signals in presence of noise. It is important to mention here that motor planning instances for the four class problem introduced in the thesis have common signal features, where there exist small variations among the features for two distinct classes. So, apparently motor planning classification is hard. The complexity in motor planning is enhanced in presence of noise. The IT2FS- and GT2FS-induced classifiers have been designed to handle both intra-personal and inter-personal level uncertainty that appears in the system because of the introduction of noise due to parallel thoughts, eye-blinking and others. In the IT2FS classifier, we evaluate the average of Upper and Lower Membership Functions at the measurement point to determine the firing strength of the rule. In the present context, we have four classifier rules, each for one individual class, and we fire the classifier rule having the highest firing strength. It is interesting to note that the averaging process reduces the noise level to half of its strength and thus never overrides over the signal, thereby making it amenable for classification. The GT2FS induced classifiers here offer a higher level of advantage than its IT2FS counterpart for its capability in tuning primary memberships with secondary memberships, resulting in higher classification accuracy.

The type-2 classifiers introduced here offer a lead time of around 600 milliseconds before any emergency situations, such as collision with the car ahead, possible accidents of the pedestrians and traffic signal failures.

Chapter 4 proposes a novel approach to classify touch nourishments of Schizophrenic patients into three classes: pleasant, acceptable and unpleasant. Four different touch nourishments, namely soft touch, rubbing, massaging and embracing are used as stimuli. The experiments are conducted only on women patients and all nurses participated in the experiments are also women. Same gender of both the patients and the nurses are required to keep the experimental results free from gender-related bias. Radial Basis Function (RBF) induced Back-Propagation (BP) neural classifiers have been used to classify the touch nourishments. Here, RBF neural net is used to select one of the four BP neural classifiers reserved for the four touch nourishments indicated above. The classifier has high classification accuracy over 92%. One interesting observation that follows from the experiments include that for healthy/normal subjects, the classification accuracy for unpleasant class label is much lower than the same for schizophrenic patients.

The thesis, to the best of the author's knowledge, is the first of its kind that provides through experiments in both perception and sensory-motor coordination in driving environment. The ideas are original and the realizations too are original, particularly from the design aspects of classifiers and their applications in real-time systems.

## 5.2 FUTURE RESEARCH DIRECTIONS

Olfactory and tactile perceptions are very primitive types of perception, where humans have less sensitivity than many other living organisms, such as lower class mammals like dogs. The thesis proposed solutions to three such interesting problems relating to perception and sensory-motor coordination. In the second problem, while dealing with cognitive failure detection in driving, the thesis slightly touches upon visual perception. There exists ample scope of future research in both extension of the existing work presented in the thesis, and other modalities of perception and sensory-motor coordination. The other modalities include primarily audio and visual perception. The primary focus of the future research thus is two-fold. It includes fundamental research to understand the biological basis of perception in all the basic modalities, and in the other hand to develop engineering systems to supplement where an individual lacks a particular modality. The latest brain-computer interfacing research offers solution to the above problem. A few interesting devices in this regard are artificial implant of retina and cochlea, where the retinal implant helps in transforming images formed on the retinal plane into electrical signals legible to the optic nerve system to recognize the visual stimuli. The implant of cochlea offers in transforming audio sound into electrical signals to be recognized by the human nervous system. There is immense scope of research on further development of artificial implants.

On the signal processing and classification side, there also exists quite a big opportunity to introduce latest technologies of machine learning and pattern classification to improve the performance of the neural classifiers. Recent studies on Deep Learning [1] reveals that classification tasks performed by artificial neural networks can be replaced by multi-layered convolution neural networks, which is expected to offer better performance as the architecture is more relevant to human information processing system.

There also exist immense opportunity to improve GT2FS classifiers by more precise modeling of the secondary membership function and better GT2FS reasoning mechanism. One recent study [2] reveals that a GT2FS can be represented as a collection of vertical slices, where each slice  $\mu(x, u)$  includes a secondary membership function at a given value of the linguistic variable  $x = x_i$  for varied type-1 membership  $u$  in  $[u_1, u_N]$ , where  $u_1 \dots u_N$  lie in  $[0, 1]$ . There exist new

reasoning formalisms with GT2FS [3] and Mendel [2], which, if used, as type-2 classifier might improve classification accuracy further.

## REFERENCES

1. I. Goodfellow, Y. Bengio and A. Courville, "Deep Learning," MIT Press, 2017.
2. J. M. Mendel, "General type-2 fuzzy logic systems made simple: a tutorial," *IEEE Trans. on Fuzzy Systems*, vol. 22, no. 5, pp.1162-1182, 2014.
3. C. Wagner, and H. Hagra, "Toward general type-2 fuzzy logic systems based on zSlices," *IEEE Trans. on fuzzy systems*, vol. 18, no. 4, pp. 637-660, 2010.